

Universidad de Málaga
Escuela Técnica Superior de Ingeniería de Telecomunicación



Tesis Doctoral:

**Mathematical Modelling and Analysis of Spatially
Correlated Heterogeneous and Vehicular Networks -
A Stochastic Geometry Approach**

Autor:

Francisco Javier Martín Vega

Directores:

María del Carmen Aguayo Torres y Gerardo Gómez Paredes

2017



UNIVERSIDAD
DE MÁLAGA

AUTOR: Francisco Javier Martín Vega

 <http://orcid.org/0000-0002-8525-9227>

EDITA: Publicaciones y Divulgación Científica. Universidad de Málaga



Esta obra está bajo una licencia de Creative Commons Reconocimiento-NoComercial-SinObraDerivada 4.0 Internacional:

<http://creativecommons.org/licenses/by-nc-nd/4.0/legalcode>

Cualquier parte de esta obra se puede reproducir sin autorización pero con el reconocimiento y atribución de los autores.

No se puede hacer uso comercial de la obra y no se puede alterar, transformar o hacer obras derivadas.

Esta Tesis Doctoral está depositada en el Repositorio Institucional de la Universidad de Málaga (RIUMA): riuma.uma.es



Por la presente, **Dra. D^a. María del Carmen Aguayo Torres**, y **Dr. D. Gerardo Gómez Paredes**, profesores doctores del *Departamento de Ingeniería de Comunicaciones* de la Universidad de Málaga,

CERTIFICAN:

Que **D. Francisco Javier Martín Vega**, Ingeniero de Telecomunicación, ha realizado en el Departamento de Ingeniería de Comunicaciones de la Universidad de Málaga bajo su dirección, el trabajo de investigación correspondiente a su TESIS DOCTORAL titulada:

“Mathematical Modelling and Analysis of Spatially Correlated Heterogeneous and Vehicular Networks - A Stochastic Geometry Approach”

En dicho trabajo se han propuesto aportaciones originales al problema de modelado y análisis matemático de redes heterogéneas y vehiculares en las que existen correlaciones espaciales. Los resultados expuestos han dado lugar a diversas publicaciones en revistas y aportaciones a congresos internacionales y nacionales.

Por todo ello, considera que esta Tesis es apta para su presentación al Tribunal que ha de juzgarla. Y para que conste a efectos de lo establecido en el Real Decreto 99/2011, de 28 de enero, por el que se regulan las enseñanzas oficiales de Doctorado, AUTORIZA la presentación de esta Tesis en la Universidad de Málaga.

Málaga, a 9 de mayo de 2017.

Fdo: Dra. María del Carmen Aguayo Torres

Fdo: Gerardo Gómez Paredes





UNIVERSIDAD
DE MÁLAGA

UNIVERSIDAD DE MÁLAGA
ESCUELA TÉCNICA SUPERIOR DE INGENIERÍA DE
TELECOMUNICACIÓN

Reunido el tribunal examinador en el día de la fecha, constituido por:

Presidente: Dr. D. _____

Secretario: Dr. D. _____

Vocal: Dr. D. _____

para juzgar la Tesis Doctoral titulada *Mathematical Modelling and Analysis of Spatially Correlated Heterogeneous and Vehicular Networks - A Stochastic Geometry Approach* realizada por D. Francisco Javier Martín Vega y dirigida por los Prof. Dra. María del Carmen Aguayo Torres y Dr. D. Gerardo Gómez Paredes, acordó por

_____ otorgar la calificación de

_____ y para que conste,

se extiende firmada por los componentes del tribunal la presente diligencia.

Málaga a ____ de _____ del ____

El Presidente:

Fdo.: _____

El Secretario:

El Vocal:

Fdo.: _____

Fdo.: _____



UNIVERSIDAD
DE MÁLAGA

A mi familia.



UNIVERSIDAD
DE MÁLAGA

Acknowledgments

I would like to express my full gratitude to my thesis advisors Dr. Gerardo Gómez and Prof. Mari Carmen Aguayo Torres, for their kind guidance, support and encouragement. With their dedication and motivation they have created the perfect environment to research, and they have make me really enjoy researching. I would also like to really thank Prof. José Tomás Entrambasaguas, principal lead of the group of Mobile Communications, Dr. F. Javier López Martínez and Dr. Beatriz Soret for all they have taught me since the very beginning of my research career. I feel very fortunate to have worked with all of them.

Secondly, I am also grateful to all my workmates and all our colleagues from the Department of Ingeniería de Comunicaciones of the University of Málaga for the great atmosphere they create in the lab as well as in the whole department.

The two research stays that has been performed during this PhD have also contributed greatly to the work that it has been done. I wish to express my special gratitude to Prof. Marco Di Renzo, who hosted me at University of Paris-Saclay, for his great guidance over the technical part and all his brilliant comments and feedback about some works analyzed in this thesis. Additionally, I would like to thank Prof. Maged El Kashlan and Dr. Yuanwei Liu for the kind hospitality they gave me at Queen Mary University and their excellent vision about emerging techniques that have improved the work that has been done.

I acknowledge the financial support given by the Spanish Government (Ministerio de Economía y Competitividad) and FEDER under grants TEC2016-80090-C2-1-R and TEC2013-44442-P. This funding has covered all my research stays, the conferences I have attended to and the publication charges. Additionally, I acknowledge the companies Inmarsat Global Limited, Agilent Technologies Spain and AT4 Wireless. Contracts with these companies have covered my living costs and allowed me to do this part-time thesis.

Finally, I would like to acknowledge the most impactful persons in my life, my wife,

my parents and my sister for their unconditional support and love and the example that they represent in my life. Without them this thesis would not have been possible.

Contents

Acknowledgments	9
Abstract	27
Resumen	30
1 Introduction	33
1.1 Scope and Overview	33
1.2 Stochastic Geometry Analysis: state of the art	36
1.3 List of Main Contributions	40
1.4 Author's Publication List	46
1.5 Outline of the dissertation	50
2 Performance Analysis of Interference-Aware Fractional Power Control	51
2.1 Introduction	52
2.1.1 Related Work	53
2.1.2 Contributions	55
2.1.3 chapter Organization and Notations	56
2.2 System Model	57
2.2.1 Channel Model	57
2.2.2 Association and Scheduling	58
2.2.3 Power Control Mechanism	59
2.2.4 SINR	60
2.3 Analysis of Interference Aware Power Control	62
2.4 Approximated Statistical Modeling of the Interference	67
	11



2.4.1	Sigmoidal Approximation	67
2.4.2	Transformed Distribution Approach	68
2.5	Asymptotic Analysis	70
2.5.1	Interference Unaware Power Control ($i_0 \rightarrow \infty$)	70
2.5.2	Low i_0 regime ($i_0 \sim 0$)	73
2.6	Numerical Results	76
2.6.1	Average Transmitted Power, Mean and Variance of the Interference	78
2.6.2	Approximations of the Interference	80
2.6.3	ccdf of the SINR	81
2.6.4	Spectral Efficiency	83
2.7	Discussion	84
2.8	Appendix: Proof of Lemma 1	85
2.9	Appendix: Proof of Lemma 2	85
2.10	Appendix: Proof of Lemma 1	87
3	Performance Analysis of Interference-Aware Muting	88
3.1	Introduction	89
3.1.1	UL Analysis: State-of-the-Art	89
3.1.2	Technical Contribution	91
3.2	System Model	93
3.2.1	Scheduling	95
3.2.2	SINR	97
3.3	General Cell Association Criterion	99
3.4	Smallest Path-Loss Association	105
3.5	Spectral Efficiency and Binary Rate	109
3.5.1	Adaptive Modulation and Coding	110
3.6	Numerical Results	112
3.6.1	Average Transmit Power, Probability of Being Active, Mean & Vari- ance of the Interference	113
3.6.2	Complementary Cumulative Distribution Function of the SINR . .	116
3.6.3	Spectral Efficiency and Binary Rate	118
3.6.4	Impact of the Association Weights: On UL-DL Decoupling	121
3.7	Discussion	125



3.8	Appendix: Proof of Proposition 2	125
3.9	Appendix: Proof of Lemma 5	127
4	Multi-User Coverage Probability in the Uplink of Cellular Systems	129
4.1	Introduction	129
4.2	System Model	132
4.2.1	System Model Description	132
4.2.2	Proposed Analytical Model	133
4.2.3	Simulation Model	135
4.3	Mathematical Results	135
4.3.1	Joint Distribution of Distances	135
4.3.2	Multi-User Coverage Probability	137
4.4	Numerical Results	140
4.4.1	Coverage probability	140
4.4.2	Marginal distributions of distances	143
4.5	Discussion	144
5	Coverage of Cellular Systems Under Hoyt fading	146
5.1	Introduction	146
5.2	System Model	147
5.3	Performance Analysis	148
5.4	Numerical Results	150
5.5	Discussion	151
6	Performance Analysis of Cloud-Radio Access Networks	152
6.1	Introduction	152
6.2	System Model	154
6.2.1	Spatial and Propagation Modeling	154
6.2.2	Proposed CRAN-NOMA Scheme	154
6.2.3	Signal Model	156
6.3	Performance Analysis	157
6.4	Numerical Results	165
6.5	Discussion	167



7	Performance Analysis of Geo-Location Based Access for Vehicular Communications	169
7.1	Introduction	170
7.1.1	Stochastic Geometry Analysis of Vehicular Networks	171
7.1.2	Main Contributions	172
7.2	Related Work	173
7.2.1	MAC schemes for Vehicular Communications	173
7.2.2	Energy Efficiency in Vehicular Communications	175
7.3	System Model	176
7.3.1	Resource Partition Schemes	177
7.3.2	Signal Modeling	181
7.3.3	Key Performance Indicators	183
7.3.4	Broadcast Message Types	183
7.4	Analysis of the Interference and Capture Probability	184
7.4.1	Single-Lane Partition (SLP)	184
7.4.2	Multi-Lane Partition (MLP)	187
7.5	Binary Rate, Energy Efficiency and Optimal Transmit Power	191
7.5.1	Binary Rate and Energy Efficiency	191
7.5.2	Optimal Transmit Power	192
7.6	Numerical Results	194
7.6.1	Impact of the SINR threshold and the traffic activity	195
7.6.2	Impact of the number of Access Resources	198
7.6.3	Impact of the broadcast distance and the segment size: r_{bc} and d_A	201
7.6.4	Transmit Power and Optimum Energy Efficiency	203
7.7	Discussion	205
7.8	Appendix: Proof of Lemma 19	206
7.9	Appendix: Proof of Lemma 21	207
8	Conclusions	209
8.1	Synthesis of the Dissertation	209
8.2	Future Work	211

A	Resumen en castellano	213
A.1	Motivación	213
A.2	Control de Potencia Fraccionado Consciente de la Interferencia	215
A.2.1	Modelo de Sistema	216
A.2.2	Resultados Teóricos	218
A.2.3	Resultados Numéricos	221
A.3	Planificación de Terminales Móviles Consciente de la Interferencia	224
A.3.1	Modelo de Sistema	225
A.3.2	Resultados Teóricos	227
A.3.3	Resultados Numéricos	230
A.4	Probabilidad de Cobertura en Sistemas Multi-Usuario	234
A.4.1	Modelo de Sistema	234
A.4.2	Resultados Teóricos	235
A.4.3	Resultados Numéricos	236
A.5	Probabilidad de Cobertura con Desvanecimiento Hoyt	238
A.5.1	Modelo de Sistema	238
A.5.2	Resultados Teóricos	239
A.5.3	Resultados Numéricos	239
A.6	Acceso Múltiple No Ortogonal para CRANs	240
A.6.1	Modelo de Sistema	241
A.6.2	Resultados Teóricos	243
A.6.3	Resultados Numéricos	244
A.7	Mecanismo de Acceso al Medio Distribuido Basado en la Posición para Redes Vehiculares	244
A.7.1	Modelo de Sistema	245
A.7.2	Resultados Teóricos	248
A.7.3	Resultados Numéricos	250
A.8	Conclusiones	252
	Bibliography	254

List of Figures

1.1	Schematic diagram of the next generation cellular network studied in this dissertation. Blue links represent desired signals whereas red links are related to interfering signals. Synchronization signals are represented in yellow. Low speed backhaul links are represented with orange dashed arrows while high speed fronthaul links that connects BSs with a CU in CRANs are represented with green dotted arrows.	34
2.1	Homogeneous network realization in $[-5000, 5000]^2$ m ² showing with green color the positions related to non truncated MTs. Yellow and blue colors are associated with MTs truncated by i_0 and to p_{\max} , respectively. The simulation parameters are $\lambda^{(1)} = 2$ BS/km ² , $i_0 = -90$ dBm, $p_{\max} = 30$ dBm, $p_0 = -70$ dBm and $\epsilon = 1$	60
2.2	Average transmitted power versus i_0 for IAFPC and non-IA FPC with $\epsilon = 1$, $p_{\max} \rightarrow \infty$ and $p_{\max} = 5$ dBm.	77
2.3	Mean of the interference versus i_0 for IAFPC and non-IA FPC with $\epsilon = 1$, $p_{\max} \rightarrow \infty$ and $p_{\max} = 5$ dBm.	77
2.4	Variance of the interference versus i_0 for IAFPC and non-IA FPC with $\epsilon = 1$, $p_{\max} \rightarrow \infty$ and $p_{\max} = 5$ dBm.	78
2.5	Laplace transform of the analytic interference I in (2.8) conditioned on $\mathcal{X}_{\text{MT}_0}^{(1)}$ and its approximation \hat{I} by using different approaches (IAFPC is assumed). As for the sigmoidal approximation, 8 equally spaced sample points between $s^{(\text{dB})} = 80$ and $s^{(\text{dB})} = 200$ dB are used, in order to obtain its related parameters b_0 and $s_0^{(\text{dB})}$	79



2.6	ccdf of the SINR for the typical MT (IAFPC is assumed) with $\epsilon = 1$ and $i_0 = \{-120, -60\}$ dBm.	80
2.7	ccdf of the SINR in the low i_0 regime given by (2.46) and by using the minimum path loss association.	81
2.8	Average SE versus i_0 (IAFPC is assumed) for $p_{\max} \rightarrow \infty$	82
2.9	Average SE versus p_{\max} (IAFPC is assumed) for $i_0 = -90$ dBm.	82
2.10	Average SE versus ϵ for the IAFPC scheme with $i_0 = -95$ dBm and for the non-IA scheme.	84
3.1	Average transmit power versus i_0 for IAM and IAFPC methods with $\epsilon = 1$, $p_{\max} \rightarrow \infty$ and $p_{\max} = 5$ dBm.	113
3.2	Probability of being active of the typical MT for IAM with $\epsilon = 1$, $p_{\max} \rightarrow \infty$, $p_{\max} = 30$ dBm and $p_{\max} = 5$ dBm.	114
3.3	Mean of the interference versus i_0 for IAM and IAFPC methods with $\epsilon = 1$, $p_{\max} \rightarrow \infty$ and $p_{\max} = 5$ dBm.	115
3.4	Variance of the interference versus i_0 for IAM and IAFPC schemes with $\epsilon = 1$, $p_{\max} \rightarrow \infty$ and $p_{\max} = 5$ dBm.	116
3.5	CCDF of the SINR for the typical MT conditioned on being active for IAM with $\epsilon = 1$, $t^{(1)}/t^{(2)} = 9$ dB, $p_{\max} \rightarrow \infty$ and $i_0 = \{-120, -90, -60\}$ dBm.	117
3.6	CCDF of the SINR for the typical MT conditioned on being active for IAM with $\epsilon = 0.75$, $t^{(1)}/t^{(2)} = 9$ dB, $p_{\max} \rightarrow \infty$ and $i_0 = \{-120, -90, -60\}$ dBm.	118
3.7	Comparison of average SE of IAFPC and IAM for $\epsilon = 1$, $t^{(1)}/t^{(2)} = 9$ dB and $p_{\max} \rightarrow \infty$. As for IAFPC, the average SE based on the Shannon formula is shown as well.	119
3.8	Comparison of average BR of IAFPC and IAM for $\epsilon = 1$, $t^{(1)}/t^{(2)} = 9$ dB and $p_{\max} \rightarrow \infty$. As for IAM, two cases are considered: the typical MT and the typical active MT.	120
3.9	Comparison of average BR of IAFPC and IAM for $\epsilon = 1$, $t^{(1)}/t^{(2)} = 9$ dB and $i_0 = -90$ dBm.	121
3.10	Average BR as a function of the variance of the interference for IAM ($i_0 = -90$ dBm) and IUM ($i_0 \rightarrow \infty$) schemes with $p_{\max} = 5$ dBm and $t^{(1)}/t^{(2)} = 9$ dB.	122

3.11	Probability the typical MT is active as a function of $t^{(1)}/t^{(2)}$ for IUFPFC ($i_0 \rightarrow \infty$) and IAM with $i_0 = \{-90, -80, -70, -60\}$ dBm. $p_{\max} \rightarrow \infty$ for both schemes.	123
3.12	Average BR as a function of $t^{(1)}/t^{(2)}$ for IUFPFC ($i_0 \rightarrow \infty$) and IAM with $i_0 = \{-90, -80, -70, -60\}$ dBm. $p_{\max} \rightarrow \infty$ for both schemes.	124
4.1	System model of multi-user UL cellular system. BSs are represented by triangles (blue: serving BS), scheduled users inside the serving cell are represented by blue dots, interfering users for the l^{th} user transmission are depicted with a red cross. The distance from one interfering user to its serving BS (R_x) and to the target BS (D_x) are represented as an example. Only scheduled users are represented.	132
4.2	Multi-User UL set-up based on conditional thinning for $k = 11$. Interfering users for the l^{th} user transmission are represented with red crosses.	134
4.3	Joint pdf for $l = 2$ and $k = 4$ with $\lambda = 0.24$	137
4.4	Joint pdf for $l = 2$ and $k = 50$ with $\lambda = 0.24$	138
4.5	Coverage probability for $k = \{10, 25, 50\}$ with full power control ($\epsilon = 1$), without noise, $\alpha = 2.5$, $\lambda_b = 0.24$	141
4.6	Coverage probability for cell-interior $l = 1$ and cell-edge $l = k$ with $k = 25$, $\epsilon = 0.75$, without noise, $\alpha = 2.5$, $\lambda_b = 0.24$	141
4.7	Coverage probability for cell-interior $l = 1$ and cell-edge $l = k$ with $k = 25$, without power control $\epsilon = 0$, without noise, $\alpha = 2.5$, $\lambda_b = 0.24$	142
4.8	Empirical and theoretical pdf of R_x	143
4.9	Empirical and theoretical pdfs of R_l , ($l = 1, k = 11$) and ($l = k = 11$)	144
5.1	Coverage probability versus the SINR threshold, t , for $q = 1$ and $q = 0.05$	151
6.1	Illustration of the proposed NOMA-based scheme with coordinated beamforming for CRANs. The probe near MT and probe cell-edge MT are represented as $MT_0^{(n)}$ and $MT_0^{(e)}$, respectively. It is drawn a single interfering cluster, which is centered at x	155
6.2	Comparison of the Laplace transform the normalized transmit power for $n_{BS} = \{2, 5, 8\}$	165

6.3	Comparison of the outage probability for near and cell-edge MTs versus the transmit SNR, ρ_{BS} . The case $a_e = 0.9$ is represented with blue color and circles and the case $a_n = 0.5$ with red color and squares.	166
6.4	Comparison of the outage probability for near and cell-edge MTs versus the number of BSs per cluster, n_{BS} for $a_e = 0.9$. The special case $n_{\text{BS}} = 1$ is added as a reference value for comparison.	167
7.1	Sketch of GLOC based access with SLP for a two-lane road and 3 ARs. Different colors are associated to different ARs. On the bottom it is shown the abstraction model for the study of the road where positions of vehicles are treated as points in the real line.	176
7.2	Sketch of GLOC based access with MLP for a two-lane road and 6 ARs. Different colors are associated to different ARs. On the bottom it is shown the abstraction model for the study of each lane where positions of vehicles are treated as points in the real line.	178
7.3	Illustration of co-channel segments in the abstraction model. The probe transmitter is represented as VT_0 , the probe AR and segment as AR_0 and $\mathcal{A}_0^{(\text{AR}_0)}$ respectively, the probe receiver as a blue x and a single interfering vehicle as VT_i . The length of each segment is represented as $d_{\mathcal{A}}$ and thus $n_{\text{AR}} \cdot d_{\mathcal{A}}$ is the minimum co-channel distance.	181
7.4	Capture probability versus the SINR threshold, γ , for SLP ($d_{\text{safe}} = 0$ m) and for MLP ($d_{\text{safe}} = 42$) with periodic and non-periodic broadcast messages. Analytical results are represented with solid lines whereas simulation results are represented with marks.	195
7.5	Average BR versus the SINR threshold, γ , for SLP ($d_{\text{safe}} = 0$ m) and for MLP ($d_{\text{safe}} = 42$ m) with periodic and non-periodic broadcast messages. . .	196
7.6	Capture probability versus the probability of being active related to non-periodic broadcast messages with SLP and MLP schemes.	197
7.7	Capture probability versus the number of ARs, n_{AR} , for SLP ($d_{\text{safe}} = 0$ m) and for MLP ($d_{\text{safe}} = 42$ m) with periodic and non-periodic broadcast messages.	197

7.8	Maximal capture probability, $c_1^{(\text{MLP})}$, for n_{AR} ranging from 10^2 to 10^4 , under MLP ($d_{\text{safe}} = 42$ m) with periodic and non-periodic broadcast messages with $r_{\text{bc}} = 150$ m, $d_{\text{max}} = 56$ km and $\gamma = 5$ dB.	198
7.9	Average BR versus the number of ARs, n_{AR} , for SLP ($d_{\text{safe}} = 0$ m) and for MLP ($d_{\text{safe}} = 42$ m) with periodic and non-periodic broadcast messages.	199
7.10	Average interference for different locations, $x \in [-105, +105]$ m, for SLP and MLP with $d_{\text{safe}} = \{21, 42\}$ with non-periodic messages, $\lambda = 0.8/84$ vehicles/m and $n_{\text{AR}} = 3$	200
7.11	Capture probability versus the broadcast distance, r_{bc} , for SLP ($d_{\text{safe}} = 0$ m) and for MLP ($d_{\text{safe}} = 42$ m) with periodic and non-periodic broadcast messages.	201
7.12	Capture probability versus the segment size, $d_{\mathcal{A}}$, for SLP ($d_{\text{safe}} = 0$ m) and for MLP ($d_{\text{safe}} = 42$ m) with periodic and non-periodic broadcast messages.	202
7.13	Capture probability versus the transmit power per Hz, ρ_{VT} , for SLP ($d_{\text{safe}} = 0$ m) and for MLP ($d_{\text{safe}} = 42$ m) with periodic and non-periodic broadcast messages.	202
7.14	Average EE versus the transmit power per Hz, ρ_{VT} , for SLP ($d_{\text{safe}} = 0$ m) and for MLP ($d_{\text{safe}} = 42$ m) with periodic and non-periodic broadcast messages.	203
7.15	Optimum EE versus the optimum transmit power per Hz, ρ_{VT}^* , for SLP ($d_{\text{safe}} = 0$ m) and for MLP ($d_{\text{safe}} = 42$ m) with periodic and non-periodic broadcast messages. Each pair of values ($\mathbb{E}[\text{EE}]^*$, ρ_{VT}^*) is obtained for a different SINR threshold, γ , ranging from -5 dB to 20 dB.	204
7.16	Capture probability versus the SINR threshold, γ , associated with the optimum transmit power, ρ_{VT}^* as appear in Fig 7.15.	205
A.1	Potencia media transmitida en función de i_0 para IAFPC y FPC clásico (incosciente de la interferencia) con $\epsilon = 1$, $p_{\text{max}} \rightarrow \infty$ y $p_{\text{max}} = 5$ dBm.	222
A.2	Transformada de Laplace de la interferencia para IAFPC condicionada en el evento $\mathcal{X}_{\text{MT}_0}^{(1)}$ usando diferencias aproximaciones.	223
A.3	Eficiencia espectral media en función de i_0 para IAFPC con $p_{\text{max}} \rightarrow \infty$	223

A.4	Potencia media transmitida en función de i_0 para IAM y IAFPC con $\epsilon = 1$ y dos valores de la potencia máxima de transmisión: $p_{\max} \rightarrow \infty$ y $p_{\max} = 5$ dBm.	231
A.5	BR medio para IAM y IAFPC para $\epsilon = 1$, $t^{(1)}/t^{(2)} = 9$ dB y $p_{\max} \rightarrow \infty$. Para IAM se consideran tanto las prestaciones del MT típico como de los MTs activos.	231
A.6	BR medio como función de $t^{(1)}/t^{(2)}$ para FPC ($i_0 \rightarrow \infty$) y IAM con $i_0 = \{-90, -80, -70, -60\}$ dBm y $p_{\max} \rightarrow \infty$	232
A.7	Probabilidad de estar activo para el MT típico en función de $t^{(1)}/t^{(2)}$ para IAM con $i_0 = \{-90, -80, -70, -60\}$ dBm y $p_{\max} \rightarrow \infty$	233
A.8	Probabilidad de cobertura para $k = \{10, 25, 50\}$ con compensación parical de las pérdidas de propagación ($\epsilon = 0.75$), para el caso sin ruido con $\alpha = 2.5$, $\lambda_b = 0.24$	237
A.9	Probabilidad de cobertura para $k = \{10, 25, 50\}$ con compensación total de las pérdidas de propagación ($\epsilon = 1$), para el caso sin ruido con $\alpha = 2.5$, $\lambda_b = 0.24$	237
A.10	Probabilidad de cobertura en función de la SINR umbral, t , para $q = 1$ y $q = 0.05$	240
A.11	Comparación de la probabilidad de <i>outage</i> para los MTs cercano y lejano en función del número de BSs por cluster, n_{BS} . El caso $n_{\text{BS}} = 1$ se añade como referencia.	244
A.12	Diagrama de GLOC con SLP para una carretera de dos carriles y 3 ARs. Los distintos colores están asociados a distintos ARs. En la parte inferior de la figura se muestra el modelo de abstracción usado para el análisis donde las posiciones de los vehículos son puntos en la recta real.	246
A.13	Diagrama de GLOC con SLP para una carretera de dos carriles y 6 ARs. Los distintos colores están asociados a distintos ARs. En la parte inferior de la figura se muestra el modelo de abstracción usado para el análisis donde las posiciones de los vehículos son puntos en la recta real.	246
A.14	Probabilidad de captura en función del número de ARs, n_{AR} , para SLP y MLP ($d_{\text{safe}} = 42$ m) con mensajes periódicos y no periódicos.	250

-
- A.15 Máxima probabilidad de captura, $c_1^{(\text{MLP})}$, para n_{AR} de 10^2 a 10^4 , con MLP ($d_{\text{safe}} = 42$ m) para mensajes periódicos y no periódicos. $r_{\text{bc}} = 150$ m, $d_{\text{max}} = 56$ km y $\gamma = 5$ dB. 251
- A.16 EE media en función de la potencia de transmisión por Hz, ρ_{VT} , para SLP ($d_{\text{safe}} = 0$ m) y MLP ($d_{\text{safe}} = 42$ m) con mensajes periódicos y no periódicos. 252

List of Tables

2.1	Simulation Parameters	76
3.1	Summary of main symbols and functions used throughout the chapter. . .	94
3.2	SINR thresholds and SE values obtained from the LTE link-level simulator in [1, 2].	112
3.3	Simulation parameters.	112
6.1	Simulation setup.	165
7.1	Summary of main symbols and functions used throughout the chapter. . .	180
7.2	Modeling Differences between SLP and MLP	181
7.3	Summary of mathematical results as functions of ρ_{VT}	191
7.4	Simulation Parameters	194
A.1	Resumen de los principales resultados matemáticos en función de ρ_{VT} . . .	249



acronyms

3GPP	3rd Generation Partnership Project
AMC	Adaptive Modulation and Coding
AR	Access Resource
BBU	Baseband Unit
BR	Binary Rate
BS	Base Station
ccdf	complementary cumulative distribution function
cdf	cumulative distribution function
CRAN	Cloud Radio Access Network
CSMA	Carrier Sense Multiple Access
D2D	Device-to-Device
DL	Downlink
DSRC	Dedicated Short Range Communications
EE	Energy Efficiency
FDD	Frequency Division Duplex
FPC	Fractional Power Control
GCA	General Cell Association
GLOC	Geo-Location Based Access
GPS	Global Positioning System
HCN	Heterogeneous Cellular Network

HCPP	Hard Core Point Process
IA	Interference Aware
IAFPC	Interference Aware Fractional Power Control
IAM	Interference Aware Muting
iid	independent and identically distributed
ITS	Intelligent Transportation System
IUFPC	Interference Unaware Fractional Power Control
IUM	Interference-Unaware Muting
LTE	Long Term Evolution
MAC	Medium Access Control
MBS	Macro cell Base Station
MCS	Modulation and Coding Scheme
MLP	Multi-Lane Partition
MM	Moment Matching
MRC	Maximum Ratio Combining
MT	Mobile Terminals
OC	Optimum Combining
pdf	probability density function
PGFL	Probability Generating Functional
PPP	Poisson Point Process
QoS	Quality of Service

RB	Resource Block
RRH	Radio Remote Head
RV	Random variables
SBS	Small cell Base Station
SDMA	Spatial Division Multiple Access
SE	Spectral Efficiency
SINR	Signal to Interference Plus Noise Ratio
SLP	Single-Lane Partition
SPLA	Smallest Path-Loss Association
TDD	Time Division Duplex
TDMA	Time Division Multiple Access
UL	uplink
V2V	Vehicle-to-Vehicle
VANET	Vehicular Ad Hoc Network

Abstract

Heterogeneous Cellular Networks (HCNs) and vehicular communications are two key ingredients of future 5G communication networks, which aim at providing high data rates on the one former case and high reliability on the latter one. Nevertheless, in these two scenarios, interference is the main limiting factor, which makes achieving the required performance, i.e., data rate or reliability, a challenging task. Hence, in order to cope with such issue, concepts like uplink/downlink (UL/DL) decoupling, Interference-Aware (IA) strategies or cooperative communications with Cloud Radio Access Networks (CRANs) has been introduced for new releases of 4G and future 5G networks. Additionally, for the sake of increasing the data rates, new multiple access schemes like Non-Orthogonal Multiple Access (NOMA) has been proposed for 5G networks.

All these techniques and concepts require accurate and tractable mathematical modelling for performance analysis. This analysis allows us to obtain theoretical insights about key performance indicators leading to a deep understanding about the considered techniques. Additionally, it also allows us to perform optimization, determining the optimal set of system's parameters that maximize a certain metric. Due to the random and irregular nature that exhibits HCNs, as well as vehicular networks, stochastic geometry has appeared recently as a promising tool for system-level modelling and analysis. Nevertheless, some features of HCNs and vehicular networks, like power control, scheduling or frequency planning, impose spatial correlations over the underlying point process that complicates significantly the mathematical analysis. Therefore the main goal of this thesis is to obtain analytic closed-form expressions for key performance indicators in HCNs as well as in vehicular networks. The focus is here on providing simple expression to complex problems where some spatial correlations complicate the tractability of the problem at hand.



Firstly, it is derived a mathematical framework for the analysis of an Interference-Aware Fractional Power Control (IAFPC) for interference mitigation in the UL of HCNs. The analysis reveals that IAFPC outperforms the classical Interference-Unaware Fractional Power control (IUFPC) in terms of Spectral Efficiency (SE), average transmitted power, and mean and variance of the interference. Then, it is investigated the performance of a scheduling algorithm where the Mobile Terminals (MTs) may be turned off if they cause a level of interference greater than a given threshold. To make the results and conclusions closer to real systems, it is proposed a novel framework to obtain the Binary Rate (BR) and SE by using Adaptive Modulation and Coding (AMC), which provides results closer to real implementations.

Secondly, the focus is set on homogeneous networks where the fairness under Rayleigh and coverage under Hoyt fading are investigated. In particular, a multi-user UL model to assess the coverage probability of different MTs in each cell is proposed. This framework allows us to assess the fairness as the difference between the coverage probability of the best and worst MTs. It is proven that with a full channel inversion power control, the fairness of the system is maximal, since all MTs exhibit the same coverage probability. Then, coverage probability of cellular systems under Hoyt fading (Nakagami-q) is studied. This fading model, allows us to consider more severe fading conditions than Rayleigh, which is normally the considered fading model for the sake of tractability. Closed-form expressions are obtained by expressing the fading as a conditional exponential distribution.

Thirdly, a novel NOMA-based scheme for CRANs is proposed, modelled and analyzed. In this scheme, two users are scheduled in the same resources according to NOMA; however the performance of cell-edge users is enhanced by means of coordinated beamforming. To account for the spatial correlation of BSs that belong to the same cooperating cluster, it is considered a cluster point process with a minimum distance between cluster centers to avoid cluster overlapping. Results reveal that the outage probability of cell-edge users greatly improves thanks to coordinated beamforming.

Finally, the performance of a decentralized Medium Access Control (MAC) algorithm for vehicular communications is investigated. With this strategy, the cellular network provides frequency and time synchronization for direct Vehicle to Vehicle (V2V) communication, which is based on its geographical information. This type of communication aims at increasing the safety in the road and hence it imposes severe reliability constraints over

the messages that are exchanged. The analysis demonstrates that there exists an operation regime where the performance is noise-limited. This means that the capture probability, i.e., the probability of successful message reception, can be arbitrary increased by increasing the transmit power. Then, the optimal transmit power that maximizes the Energy Efficiency (EE) of the system subject to a minimum capture probability constraint is derived.

Resumen

Las redes heterogéneas y las comunicaciones vehiculares son dos ingredientes primordiales de las futuras redes de comunicación 5G, que tienen como objetivo proporcionar altas velocidades de transmisión de datos en el primer caso y alta fiabilidad en el segundo. Sin embargo, en estos dos escenarios, la interferencia es el principal factor limitante, lo que hace que alcanzar el rendimiento requerido, es decir, velocidad de datos o fiabilidad, sea una tarea difícil. Por lo tanto, para hacer frente a este factor limitante, se han introducido conceptos como el desacoplamiento de los enlaces ascendente y descendente, estrategias conscientes de la interferencia (IA, Interference-Aware) o las comunicaciones cooperativas con las Redes de Acceso de Radio en la Nube (CRAN, Cloud Radio Access Networks) para las nuevas versiones de redes 4G y las futuras redes 5G. Además, con el fin de aumentar las velocidades de datos, se han propuesto nuevos esquemas de acceso múltiple como NOMA (Non-Orthogonal Multiple Access) para las redes 5G.

Todas estas técnicas y conceptos que se proponen para las futuras redes celulares requieren un modelo matemático preciso y manejable para el análisis de prestaciones. Este análisis nos permite establecer conclusiones teóricas sobre indicadores clave de las prestaciones del sistema que conducen a una comprensión profunda de las técnicas consideradas. Además, también nos permite realizar la optimización, determinando el conjunto óptimo de parámetros del sistema que maximizan una determinada métrica. Debido a la naturaleza aleatoria e irregular que exhiben las redes heterogéneas (HCNs, Heterogeneous Cellular Networks), así como las redes vehiculares, la geometría estocástica ha aparecido recientemente como una herramienta prometedora para el modelado y análisis a nivel de sistema. Sin embargo, algunas características de las HCNs y las redes vehiculares, como el control de potencia, la planificación dinámica de recursos o la planificación de frecuencias, imponen correlaciones espaciales sobre el proceso punto subyacente que complican



significativamente el análisis matemático. Por lo tanto, el objetivo principal de esta tesis es obtener expresiones analíticas cerradas para los indicadores clave de las prestaciones en HCNs, así como en redes vehiculares. El foco está puesto en proporcionar expresiones simples a problemas complejos donde algunas correlaciones espaciales complican el problema a tratar.

En primer lugar, se deriva un marco matemático para el análisis de un mecanismo de control de potencia fraccional consciente de la interferencia (IAFPC, Interference-Aware Power Control) para la mitigación de interferencias en el enlace ascendente (UL, Uplink) de HCNs. El análisis revela que IAFPC supera al control de potencia fraccionado clásico, que es inconsciente de la interferencia, en términos de eficiencia espectral (SE, Spectral Efficiency), potencia media transmitida y media y varianza de la interferencia. A continuación, se investiga el rendimiento de un algoritmo de planificación de recursos en el que los terminales móviles (MTs, Mobile Terminals) se pueden apagar si causan un nivel de interferencia mayor que un umbral dado. Para acercar los resultados y las conclusiones a los sistemas reales, se propone un nuevo marco para obtener el régimen binario (BR, Binary Rate) y la SE mediante la modulación y codificación adaptativas, que proporciona resultados más cercanos a las implementaciones reales.

En segundo lugar se centra el estudio las redes homogéneas, donde se analiza la justicia entre usuarios con desvanecimientos tipo Rayleigh, y la cobertura con desvanecimientos tipo Hoyt. En particular, se propone un modelo multi-usuario del UL para evaluar la probabilidad de cobertura de diferentes MTs en cada celda. Este marco nos permite evaluar la justicia entre usuarios como la diferencia entre la probabilidad de cobertura del mejor y peor MT. Se demuestra que con un control de potencia de inversión de canal completo, la justicia en el sistema es máxima, ya que todos los MTs presentan la misma probabilidad de cobertura. Después se estudia la probabilidad de cobertura de redes celulares con desvanecimientos tipo Hoyt (Nakagami-q). Este modelo de desvanecimientos permite estudiar condiciones de desvanecimiento más severas que las asociadas a un canal Rayleigh, que es el modelo usado normalmente por su sencillez. Se obtienen expresiones cerradas expresando la distribución de Hoyt como una exponencial condicionada.

En tercer lugar, se propone, modela y analiza un nuevo esquema basado en NOMA para CRANs. En este esquema, dos usuarios están planificados en los mismos recursos según NOMA; sin embargo, se mejora el rendimiento de los usuarios de borde mediante

la conformación de haz coordinada. Para tener en cuenta la correlación espacial de las BS que pertenecen al mismo grupo, se considera un proceso punto de tipo cluster con una distancia mínima entre los centros de cada cluster para evitar el solape entre grupos distintos. Los resultados revelan que la probabilidad de interrupción de los usuarios de borde de celda mejora en gran medida gracias a la conformación de haz coordinada.

Finalmente, se investigan las prestaciones de un algoritmo descentralizado de Control de Acceso al Medio (MAC) para comunicaciones vehiculares. Con esta estrategia la red celular proporciona sincronización en tiempo y frecuencia para la comunicación directa Vehículo a Vehículo (V2V), que está basada en su información geográfica. Este tipo de comunicación pretende incrementar la seguridad en la conducción y por tanto se imponen requisitos de fiabilidad muy estrictos sobre los mensajes intercambiados. El análisis demuestra que existe un régimen de operación en el que el rendimiento está limitado por el ruido. Esto significa que la probabilidad de captura, es decir, la probabilidad de recepción de mensajes satisfactoria, puede aumentarse arbitrariamente incrementando la potencia de transmisión. A continuación, se obtiene la potencia óptima de transmisión que maximiza la eficiencia energética (EE) del sistema sujeto a una restricción de probabilidad de captura mínima.

Chapter 1

Introduction

In this chapter it is presented the main motivations and goals of this thesis. The state of the art of system-level analysis by using tools of stochastic geometry is revisited and then, the main contributions are summarized. Finally, the structure and organization of this dissertation is depicted.

1.1 Scope and Overview

With the advent of smart-phones and tablets, demanding higher data rates each year, the cellular network has been rethought. The response of standardization bodies as the 3rd generation partnership project (3GPP) to this demand has led to the fourth generation (4G), which introduces concepts like Heterogeneous Cellular Networks (HCNs), aiming at improving the spectral efficiency per unit area in a cost-effective way. In this approach, there are several tiers of Base Stations (BSs), e.g. Macro BSs (MBSs) and Small-cell BSs (SBSs), that differ in their transmit powers and propagation conditions [3]. This heterogeneity on the access points makes the association between Mobile Terminals (MTs) and BSs a paramount issue. On the one hand, the classical association criteria based on maximal received power from downlink (DL) pilot signals leads to a situation with highly congested MBSs and slightly loaded or even empty SBSs [4]. Adding a cell bias over SBSs and an association criteria based on weighted received power may compensate this issue by shifting MTs to SBSs; however, this cause severe interference to the MTs that are offloaded [5]. As a result of this trade-off between cell offloading and interference, there



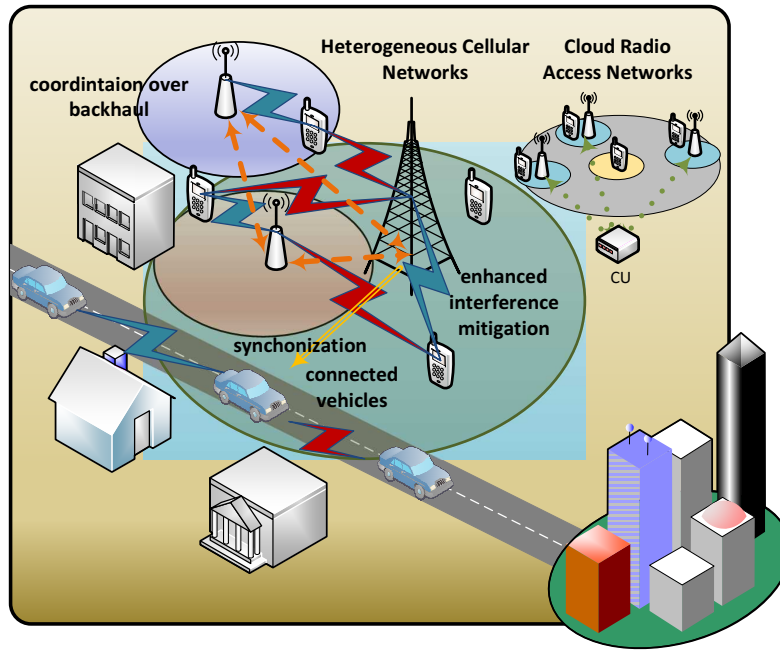


Figure 1.1: Schematic diagram of the next generation cellular network studied in this dissertation. Blue links represent desired signals whereas red links are related to interfering signals. Synchronization signals are represented in yellow. Low speed backhaul links are represented with orange dashed arrows while high speed fronthaul links that connects BSs with a CU in CRANs are represented with green dotted arrows.

exists an optimal biasing factor that maximizes the DL performance in terms of average Binary Rate (BR) [4, 6]. Fig. 3.1 illustrates an sketch of next generation HCNs under study in this dissertation.

Besides, the fact that association is based on received power on the DL, makes the interference even more limiting in the uplink (UL). This is due to the fact that MTs tend to be associated with distant BS, and thanks to power control, they can cause a high interference on neighboring BSs. The root of the problem relays on having MTs connected to the same BS in both DL and UL, despite of the fact that DL and UL are different in many aspects. To overcome this limitation, uplink/downlink (UL/DL) decoupling has been proposed to facilitate joint optimization of both links [7]. Nevertheless, UL/DL also poses additional implementation challenges that complicates the architecture design [8].

To boost the performance, cooperative techniques for enhanced interference mitigation in HCNs needs to be developed and proposed for next generation 4G and 5G networks.

In such context, knowledge about interference is a powerful tool that can be exploited for interference mitigation and performance improvement. In particular, Interference-Awareness (IA) have been recently used for smart association in [9], for Energy Efficiency (EE) maximization in 5G networks in [10] and for rank coordination in 5G MIMO (Multiple-Input-Multiple Output) networks in [11].

Another paramount paradigm for cooperative networks that has been recently introduced is Cloud Radio Access Networks (CRANs). This approach consists on centralizing functionalities by means of a pool of computational resources, which is known as central unit (CU). The CU is connected through high speed links (fronthaul) with several radio remote heads (RRHs) that acts as BSs from the users perspective [12]. Implementing the networks in this manner leads to a cluster of BS, or equivalently RRHs, that can cooperate to perform advanced interference mitigation techniques [13]. Besides this, C-RANs offer numerous advantages like reducing operational costs, facilitating network upgrades and maintenance and leading to a better energy efficiency [14].

Additionally, to increase the data rates in cellular networks, it has been recently proposed the use of Non Orthogonal Multiple Access (NOMA) [15]. This scheme proposes that several MTs are scheduled in the same orthogonal resource block; but the transmission is performed with different power for different MTs. Hence, this allows to perform Successive Interference Cancellation (SIC) at the receiver to detect the intended signal [16].

The evolution of 4G, under commercial standards like Long Term Evolution Advanced (LTE-A) and LTE-A Pro, facilitates the path towards the 5G, which will bring new services and applications and it will improve the overall system's performance. Among the new services that the evolution of 4G (LTE-A Pro) as well as 5G will offer, the direct communication between vehicles is one of the most important proposals. This type of communication aims at increasing the safety on the road and hence it imposes severe reliability constraints over the messages that are exchanged between vehicles. One of the proposals for Vehicle-to-Vehicle (V2V) communications is the IEEE 802.11p standard, which makes use of Carrier Sense Multiple Access (CSMA) as a MAC protocol, since it provides decentralized and ad hoc connectivity.

Nevertheless, 802.11p suffers from the main limitations related to 802.xx standards, such as poor scalability to high traffic density and poor support of high mobility [17].

Hence, solutions based on 4G and 5G cellular networks come to the fore [18]. LTE V2X is the response of the 3GPP standardization body to the high market expectations and will use the same principles as those that are envisioned for Device-to-Device (D2D) communications. Here, instead of the traditional communication through the infrastructure, which may suffer from long delays, the local data exchange through the direct V2V path is preferred. With autonomous mode of operation, it is even possible for the devices to select the transmission resources without network involvement. Yet, the network has a key role in providing time and frequency synchronization as it is sketched in Fig. 3.1.

1.2 Stochastic Geometry Analysis: state of the art

All the aforementioned techniques and concepts that are proposed for future cellular networks require accurate and tractable mathematical modelling for performance analysis. This analysis allows us to obtain theoretical insights about key performance indicators leading to a deep understanding about the considered techniques. Additionally, it also allows us to perform optimization, determining the optimal set of system's parameters that maximize a certain metric.

Due to the random and irregular nature that exhibits HCNs, as well as vehicular networks, stochastic geometry has recently appeared as a promising tool for system-level modelling and analysis. Nevertheless, some features of HCNs and vehicular networks, like power control, scheduling or frequency planning, impose spatial correlations over the underlying point process that complicates significantly the mathematical analysis.

Therefore the main goal of this thesis is to obtain analytic closed-form expressions for key performance indicators in HCN as well as in vehicular networks. The focus is here on providing simple expressions to complex problems where spatial correlations complicate the tractability of the problem at hand. With the derived expressions, interesting insights about system performance has been obtained.

Stochastic geometry analysis normally considers that the positions of BSs (of each tier) and MTs can be modelled as independent and identically distributed (iid) uniform Poisson Point Processes (PPPs) in the entire plane [19, 20]. Several works have recently proved that stochastic geometry provides estimates of key performance indicators that are as accurate as simulation results [21–25]. This approach usually considers the typical link

between a probe MT and its serving BS, where the term *typical* means randomly chosen and foresees that the MT can be placed anywhere within the cell.

In the last few years, stochastic geometry has been extensively used for the analysis of the DL of HCNs. The analysis of the UL, on the other hand, is more involved than that of the DL. This is because the transmission powers of the interferers are coupled with their serving BSs' distances due to power control. Additionally, even if the positions of BSs and MTs follow a PPP, the positions of the interfering MTs do not follow a PPP, making the exact analysis intractable [26].

To understand why the positions of the interfering MTs do not follow a PPP, let us recall that one property of the PPPs is the independence of the number of points falling in disjoint regions. In current networks, orthogonal resource allocation schemes are used, which implies that there is a single interfering MT in any association cell [27]. Thus, given a PPP of BSs, the positions of the interfering MTs are coupled with the positions of BSs due to the cell association criterion being used, and the interfering MTs are not distributed according to a PPP. This can be confirmed by considering two disjoint regions in the same association cell. Having an interfering MT in one of the regions implies that the other region is empty, which contradicts the PPP assumption. The interfering MTs, on the other hand, can be viewed as a stemmed form of Voronoi perturbed lattice process [26, 28], which is not mathematically tractable. This makes the analysis of the UL more complicated than that of the DL.

In spite of its mathematical challenges, there are recent works that analyze the performance of the UL with different power control and association policies. In [29], single tier networks with FPC are analyzed with the aid of stochastic geometry. In order to avoid the intractability of the locations of the interfering MTs, the proposed approach assumes that the MTs that are scheduled in the RB of interest form a Voronoi tessellation and that a single BS is available in each Voronoi cell. In [30], FPC is analyzed by approximating the positions of the interfering MTs as a uniform PPP in the entire plane. With this approach, however, some interfering MTs may undergo, with respect to the probe BS, a smaller path loss than with their serving BS, which is not a realistic situation.

Recently, [26, 31, 32] have proposed accurate frameworks to model the positions of the interfering MTs. These works consider the spatial correlation between the locations of the probe BS and those of the interfering MTs. Such correlation is due to the fact that

the interfering MTs are placed outside the Voronoi cell of the probe BS [27]. The authors of [31] consider a truncated channel inversion power control, where the MTs attempt to fully compensate for the path loss towards their serving BS, provided that they do not have to transmit with more power than p_{\max} . The cell association is based on the smallest path loss. The MTs that necessitate higher power than p_{\max} are kept silent. The case of UL and DL with decoupled access is considered in [26]. The association is based on maximum weighted received powers and FPC is considered in the UL. Here, to account for the spatial correlation a non-homogeneous PPP is considered to model the locations of interfering MTs. A framework for the UL of HCNs with multi-antenna BSs is studied in [32]. In this work it is considered FPC under a generalized association criteria and two extreme detection techniques in terms of complexity and performance: Maximum Ratio Combining (MRC) and Optimum Combining (OC). It is demonstrated that OC greatly outperforms MRC when MTs use aggressive power control, i.e., when the interference is high. The spatial correlation is imposed by means of a conditional thinning that takes into account the generalized cell association procedure.

CRANs are modeled and analyzed with the aid of point process theory in [33] and [34] where it is considered a single cluster of cooperating BSs. In [33] it is obtained an exact expression for the outage probability under dynamic cell selection and an approximated expression in the high SNR regime for coordinated beamforming. [34] focuses on the case of coordinated beamforming and provides an accurate expression for the outage probability, which is valid for any value of SNR. In [35] it is proposed a scheme where b BSs transmits jointly to k users according to NOMA based access. To improve the performance it is proposed an opportunistic algorithm to select the set of cooperating BSs. A NOMA-based scheme with Coordinated Multi-Point (CoMP) transmission is proposed in [36]. Nevertheless, since the scheme is based on Alamuti codes, the number of cooperating BSs is smaller than 3. A common factor of the aforementioned works in [33–36] is that the interference from other clusters, which is the main limiting factor, is not considered. A CoMP scheme is proposed in [37] for HetNets where the k single-antenna BSs, that provides strongest average received power to a given user, transmit jointly to improve its performance. In [38] it is considered a dynamic clustering approach where the k -nearest multiple-antenna BSs transmit to the same user. The cooperating cluster determine the beamforming vector that maximizes the desired signal while nullifying the intra-cluster

interference. Hence, [37] and [38] consider that clusters are formed dynamically for each user, which on the other hand, possesses implementation challenges for real systems.

For tractability, in those aforementioned papers it is assumed Rayleigh distribution for the desired link. Nevertheless, Rayleigh fading is not an appropriate distribution for small scale fading in many scenarios. In this context, Hoyt (Nakagami- q) distribution appears as an interesting tool, since it models fading conditions more severe than Rayleigh, and it includes both Rayleigh fading and one-sided Gaussian fading as special cases [39]. There are some approaches to deal with general fading distributions. In [20] it is proposed to use the Plancherel-Parseval theorem. Gil-Pealez inversion theorem is used in [40] to derive the coverage probability and rate of a cellular network. However, these approaches generally add a single improper integral compared to the case of Rayleigh fading. In [41] it is analyzed the case of η - μ fading. This distribution account for Hoyt fading when $\mu = 0.5$. Nevertheless, with the proposed framework, the coverage probability is obtained as an infinite sum of terms that involve the computation of the k -th derivative of the Laplace transform of the interference, which is numerically complex. Hence, a framework to obtain the coverage for Hoyt fading in cellular systems as a simple closed-form expression is still an open problem.

As for vehicular communications, references in the literature related to performance analysis have mainly focus on decentralized ALOHA and CSMA as MAC protocols. For instance, [42] analyzes, with the aid of stochastic geometry, the capture probability, average throughput and mean density progress of transmitted packets for the case of unicast transmissions with ALOHA. In [43], CSMA for unicast multi-hop communications is considered with several routing strategies. It also considers multi-lane abstraction model which is more accurate than single-lane models for wide roads. The case of a head vehicle that broadcasts info and control messages to a sectorized cluster of client vehicles is considered in [44]. This work models the positions of vehicles as a Cox process whose density follows a Fox distribution; however, the interference caused by other transmitting vehicles is not taken into account. The spatial propagation of broadcast information is tackled in [45]; nevertheless, the signal propagation is neglected and it is assumed that transmission is always successful as long as the distance towards the receiver is smaller than a given distance. The performance of IEEE 802.11p is assessed with the aid of stochastic geometry and queuing theories in [46]. Here it is considered the temporal behavior of CSMA which

adds a delay to access the system by means of a back-off counter. To account for the spatial dependence, which is derived from the carrier sensing, and also for the temporal behavior, which is derived from the back-off counter, a discrete Matérn Hard Core Point Process (HCPP) is proposed to model the locations of concurrent transmitters.

Existing mathematical frameworks, are not enough for the analysis of new interference mitigation techniques in HCNs and vehicular communications, and hence, new frameworks need to be derived.

1.3 List of Main Contributions

In this work, we have addressed mathematical modelling and analysis of different techniques for interference mitigation in HCNs, as well as in vehicular communications, where spatial correlations complicates the tractability of the problem. The focus is on obtaining simple expressions for key performance indicators as average SE, average BR, mean and variance of the interference, average transmitted power, capture probability, and average EE. As stated above, existing mathematical frameworks are not appropriate for analyzing such techniques and hence, new frameworks have been derived.

The interference is the main limiting factor in HCNs and vehicular communications. Hence, in this thesis two mechanisms for interference mitigation has been proposed and analyzed.

Firstly, it is analyzed an Interference-Aware Fractional Power Control (IAFPC) for the UL of HCNs that keeps the generated interference under a given threshold, i_0 . To account for novel concepts in HCNs, like UL/DL decoupling, a generalized cell association has been considered, which includes the coupled and decoupled settings as special cases. The proposed mathematical framework avoids the mathematical intractability of the problem by means of conditional thinning, which adds the necessary correlation that exist between the probe MT, the probe BS and the most interfered BS. More specifically, the contribution of this work can be summarized as follows.

- Analysis and comparison of IA and non-IA FPC schemes. From their numerical comparison, it is shown that interference awareness reduces the mean and the variance of the interference, as well as the average transmitted power. Also, it increases the average spectral efficiency.

- Analysis of several performance metrics that provide better understanding of IA and non-IA FPC schemes. This includes the average transmitted power, the mean and variance of the interference, the coverage probability and the average spectral efficiency.
- Two accurate approximations for the Laplace transform of the interference in the presence of IAFPC. These approximations greatly reduce the computational complexity of the resulting mathematical frameworks.
- Proposal of an asymptotic framework to gain theoretical insight for system design. In particular, it is shown that the statistics of the interference are independent of the BS density in the low i_0 regime and under the smallest path loss cell association criterion.

The contributions mentioned above have been published in [47]. The related work is presented in Chapter 2.

Then, we investigate the performance of a scheduling algorithm where the MTs may be turned off (i.e., muted) if they cause a level of interference greater than a given threshold. This approach, which is referred to as Interference Aware Muting (IAM), may be regarded as an interference-aware scheme that, contrary to IAFPC, is aimed to reduce the level of interference at the MAC layer, instead than in the physical layer. Such a muting procedure introduces further correlations that are appropriately modelled in the developed framework.

Based on these modeling assumptions, which are validated against extensive Monte Carlo simulations, we provide the following contributions.

- We develop a tractable mathematical framework for computing the CCDF of the Signal-to-Interference-plus-Noise-Ratio (SINR), which completely characterizes the performance of the IAM scheduling scheme.
- We study IAM scheme in terms of average transmit power of the MTs, mean and variance of the interference. The mathematical analysis reveals that IAM is capable of reducing the three latter performance metrics compared with IAFPC, which results in several advantages for practical implementations. Reducing the variance

of the interference is beneficial for better estimating the SINR and, thus, for reducing the error probability of practical decoding schemes, e.g., turbo decoding, [48], and for making easier the selection of the most appropriate Modulation and Coding Scheme (MCS) to use in LTE systems [49].

- To make our study and conclusions directly applicable to current communication systems that are based on Adaptive Modulation and Coding (AMC) transmission, we provide tractable expressions of SE and BR based on practical MCSs that are compliant with the LTE standard and whose parameters are obtained from a link-level simulator [1, 2].
- With the aid of the proposed mathematical frameworks, we compare IAFPC and IAM schemes in terms of SE and BR, which provide different information on their strengths and weaknesses. The SE provides information on how well the MTs exploit the available resources (e.g., bandwidth) that are shared among the MTs served by the same BS, whereas the BR accounts for the specific fraction of resources that is allocated to each MT served by a given BS. While the IAFPC scheme is superior in terms of SE, the IAM scheme is superior in terms of RB. This implies that IAM provides service to fewer users, which get better performance compared with IAFPC. To characterize this trade-off, we investigate the resource fairness of both schemes, which is defined here as the probability that a randomly chosen MT gets access to the resources, and provide a tractable frameworks for its analysis.
- In light of the emerging UL-DL decoupling principle, we develop the mathematical framework for a General Cell Association (GCA) criterion, whose association weights may be appropriately optimized for performance enhancement. By direct inspection of the mathematical framework, we prove that three operating regimes can be identified as a function of the interference threshold i_0 : i) the first, where the performance is independent of i_0 , ii) the second, where the performance depends on i_0 but it does not depend on the cell association, and iii) the third, where the performance depends on i_0 and the cell association. Of particular interest in this dissertation is the second regime, which highlights that UL-DL decoupling may not be an issue for some system setups, which in turn simplifies the design of HCNs.
- As for the relevant case study for the UL where the serving BS of the typical MT

is identified based on the Smallest Path-Loss Association (SPLA) criterion with channel-inversion power control [7], we provide simple and closed-form framework for relevant performance indicators and prove that two operating regimes exist: i) the first, where the performance depends on i_0 (interference-aware) and ii) the second, where the performance is independent of i_0 (interference-unaware). We prove, in addition, that i) the scaling law of the average transmit power of the MTs, the mean interference and the probability that a MT gets access to the resources is a polynomial function of i_0 whose exponent depends on the path-loss exponent, ii) the distance towards the serving BS gets smaller as i_0 increases; and iii) the CCDF of the SINR is independent of the density of BSs.

These aforementioned contributions appear in [50], which has been accepted for publication, and [51], which is a work under review. The work associated with these contributions is presented in Chapter 3.

Secondly, we focus on homogeneous networks to assess the fairness under Rayleigh fading and coverage of the typical MT under Hoyt fading. In particular, a multi-user UL model to assess the coverage probability of different MTs in each cell is proposed. Contrary to the resource fairness, which is studied in the above work, this framework allows us to assess the coverage fairness, which is defined here as the difference between the coverage probability of the best and worst MTs. It is proven that with a full channel inversion power control, such fairness is maximal in the system, since all the MTs exhibit the same coverage probability. These aforementioned contributions have been published in [52]. The related work is presented in Chapter 4. Then, we provide a closed-form approximation for the coverage probability of cellular systems under Hoyt (Nakagami-q) fading. The proposed framework express the fading as conditional functions with exponential distribution. The expectation over the distance towards the serving Base Stations (BS) is split in two finite range integrals that can be accurately approximated by means of Gauss-Chebyshev rule. The accuracy of the proposed framework is validated through extensive Monte Carlo simulations. These contributions appear in [53], which is under review. Chapter 5 presents the aforementioned work.

Secondly, a novel NOMA-based scheme for CRANs with coordinated beamforming is proposed and analyzed. On the one hand, this scheme benefits from NOMA in order to increase the spectral efficiency, since two mobile terminals (MTs) are scheduled per

BS. On the other hand, it benefits from cooperation, since each cluster of BSs performs coordinated beamforming to improve the performance of cell-edge MTs. To model the locations of BSs in CRANs, it has been considered a cluster point process (CPP), where a minimum distance over the cluster centers is imposed to avoid spatial overlapping between different clusters. This model involves two sources of spatial correlation: one from the cluster process and another from the minimum distance, that complicate the problem at hand. Besides this, to assess the performance of the system in realistic conditions, both the intra-cluster interference due to NOMA and the inter-cluster interference from other clusters are considered.

Based on this modeling framework, we provide the following contributions, which are validated against extensive Monte Carlo simulations:

- The beamforming gain can be expressed as a mixture Erlang distribution.
- The moments of the beamforming gain are linear functions with respect to the number of BSs per cluster.
- The outage probability for cell-edge MTs can be expressed as a sum of the k -th derivative of the Laplace transform of the inter-cluster interference.
- The proposed scheme greatly improves the performance of the cell-edge MT, which increases with the cluster size.

These contributions appear in [54], which is under review. Chapter 6 presents the aforementioned work.

Finally, the performance of a MAC algorithm for vehicular communications is analyzed taking into account the velocity-dependent safe distance, d_{safe} , between vehicles of the same lane. With the proposed MAC algorithm, the vehicles access the resources for direct V2V communication based on its geographical information. Here, the road is divided in segments and orthogonal Access Resources (ARs) are allocated to consecutive segments. The mapping is made aiming to maximize the co-channel distance.

The aforementioned safe distance imposes some correlation between locations of the vehicles, since the case of two neighboring being closer than d_{safe} is not feasible. Hence, the location of vehicles in this work is modeled by means of a Matérn HCPP of type II. However, such a point process is generally intractable, and only some moments of

the interference can be obtained without resorting to approximations [55]. To overcome such an intractability, we will use conditional thinning. In simple terms, the locations of vehicles are first assumed to be placed according to a PPP of a given density. Then, spatial constraints (correlation) in the form of a minimum distance between points are imposed by means of an indicator function, but only in the proximity of the transmitter and the receiver. Additionally, it is considered that the length of the road is much higher than its width, and hence it is assumed that locations of the vehicles in each lane can be modeled as points in the real line. Based on these modeling assumptions, which are validated against extensive Monte Carlo simulations, the following contributions are provided:

- We propose a mathematical framework for the analysis of GLOC considering a minimum distance between vehicles of the same lane. Two kind of resource allocation schemes are considered: Single-Lane Partition (SLP) and Multi-Lane Partition (MLP), which have different trade-offs and mainly differ on whether lane-finding is required or not. With SLP, the road is divided into different segments, whereas with MLP, each lane is divided into segments. Both broadcast messages, i.e., periodic and non-periodic, are modeled to obtain a complete understanding about the capabilities of GLOC as a MAC for ITS. Additionally, system-level parameters like message size, reporting rate, broadcast distance, etc. are taken from recommendations of the 3GPP Work Items [56] and [57] to study the support of LTE for V2V services. The path loss slope and path loss exponent is taken from [58] where it has been performed a vast V2V channel measurement campaign conducted in Sweden over a carrier frequency of 5.2 GHz. Interestingly, the path loss exponent in V2V channels, α , is normally smaller than 2 [58–60]. This means that only one-dimensional PPPs can be considered¹. Finally, mathematical expressions for a wide variety of performance indicators have been obtained, leading to a deep understanding of the studied techniques. In particular, the capture probability, the average interference, the average Binary Rate (BR) and the average Energy Efficiency (EE) are derived.
- Many useful insights have been obtained from the derived expressions. Interestingly, it has been shown that: (i) the capture probability is an increasing function with

¹As it is mentioned in [61], the Probability Generating Functional of the PPP in \mathbb{R}^d , with $d \in \mathbb{N}^+$, only exists for a path loss exponent, $\alpha > d$. Hence, if we consider two-dimensional PPPs, the mathematical analysis is restricted to the case $\alpha > 2$.

respect to the transmit power with exponential dependence; (ii) the system is noise-limited for MLP when the number of ARs is high enough whereas it is interference-limited in case of SLP; (iii) the average interference diverges when it is evaluated in co-channel segments with SLP, whereas it always converges for the case of MLP. The fact that with MLP the system is noise-limited for a given number of ARs means that it is possible to achieve an arbitrary high capture probability by increasing the transmit power.

- The optimum transmit power that achieves maximal EE subject to a minimum capture probability is obtained. Such a minimum value is expressed as a percentage, δ , of the maximum capture probability that can be achieved. Interestingly, the same optimal transmit power is obtained for SLP and MLP.

These aforementioned contributions appear in [62], which has been accepted for publication, and [63], which is a work under second round of reviews. The work associated with these contributions is presented in Chapter 7.

1.4 Author's Publication List

The research conducted during this thesis resulted in the following publications:

Journal papers:

1. [64] **F. J. Martin-Vega**, Y. Liu, G. Gomez, M. ElKashlan and M.C. Aguayo, “*Coordinated Beamforming with Non Orthogonal Multiple Access for 5G Cloud Radio Access Networks*”, in elaboration to be submitted to IEEE Transactions on Wireless Communication.
2. [53] **F. J. Martin-Vega**, G. Gomez, F. J. Lopez-Martinez and M.C. Aguayo, “*A Closed-Form Expression for the Coverage of Cellular Systems under Hoyt (Nakagami- q) Fading*”, submitted to IEEE Electronic Letters.
3. [51] **F. J. Martin-Vega**, M. C. Aguayo-Torres, G. Gomez and M. Di Renzo, “*On Muting Mobile Terminals for Uplink Interference Mitigation in HetNets - System-Level Analysis via Stochastic Geometry*”, submitted to IEEE Transactions on Communications.

4. [63] **F. J. Martin-Vega**, B. Soret, M. C. Aguayo-Torres, I. Z. Kovacs and G. Gomez, “*Geo-Location Based Access for Vehicular Ad Hoc Networks: Analysis and Optimization via Stochastic Geometry*”, under review (*2nd round of reviews*) in IEEE Transactions on Vehicular Technology.
5. [47] **F. J. Martin-Vega**, G. Gomez, M. C. Aguayo-Torres and M. Di Renzo, “*Analytical Modeling of Interference Aware Power Control for the Uplink of Heterogeneous Cellular Networks*”, in IEEE Transactions on Wireless Communications, vol. 15, no. 10, pp. 6742-6757, Oct. 2016.

Conference papers:

6. [54] **F. J. Martin-Vega**, Y. Liu, G. Gomez, M. Elkashlan and M.C. Aguayo “*Modeling and Analysis of NOMA Enabled CRAN with Cluster Point Process*”, submitted to IEEE Global Communications Conference (GLOBECOM) 2017.
7. [50] **F. J. Martin-Vega**, M. C. Aguayo-Torres, G. Gomez and M. Di Renzo, “*Interference-Aware Muting for the Uplink of Heterogeneous Cellular Networks: A Stochastic Geometry Approach*”, accepted in IEEE International Conference on Communications (ICC) 2017.
8. [62] **F. J. Martin-Vega**, B. Soret, M. C. Aguayo-Torres, I. Z. Kovacs and G. Gomez, “*On Stochastic Geometry Modeling of Distributed Location Access for Vehicular Ad Hoc Networks*”, accepted in IEEE Vehicular Technology Conference (VTC) spring 2017.
9. [52] **F. J. Martin-Vega**, F. J. Lopez-Martinez, G. Gomez and M. C. Aguayo-Torres, “*Multi-user coverage probability of uplink cellular systems: A stochastic geometry approach*”, 2014 IEEE Global Communications Conference, Austin, TX, 2014, pp. 3989-3994.

Other works of the author, which are related to the fields of Mobile Communications and Communication Theory, are listed below:

Patents:

10. **F.J. Martin-Vega**, F. Blaquez-Casado, F. J. Lopez-Martinez, G. Gomez, J. T. Entrambasaguas, “*Systems and Methods for High Throughput, Low Error, Low Complexity Iterative Turbo Decoding*”, Spanish Patent and Brand Office (OEPM), patent number, P201400890.
11. **F.J. Martin-Vega**, F. Blaquez-Casado, F. J. Lopez-Martinez, G. Gomez, J. T. Entrambasaguas, “*Systems and Methods for a Low Error Rate Low Complexity Iterative Turbo Decoding*”, Spanish Patent and Brand Office (OEPM), patent number, P201400891.

Journal papers:

12. A. Carreras, M. C. Aguayo-Torres, **F. J. Martin-Vega**, G. Gomez, F. Blaquez, I. M. Delgado-Luque, J. T. Entrambasaguas, “*Link Abstraction Models for Multicarrier Systems - A Logistic Regression Approach*”, submitted to International Journal of Communication Systems.
13. **F.J. Martin-Vega**, F. Blaquez-Casado, F. J. Lopez-Martinez, G. Gomez, J. T. Entrambasaguas, “*Further Improvements in SOVA for High-Throughput Parallel Turbo Decoding*”, IEEE Communications Letters, vol.19, no.1, pp.6,9, Jan. 2015.

International conference papers:

14. **F. J. Martin-Vega**, I. M. Delgado-Luque, G. Gomez, M. C. Aguayo-Torres and J. T. Entrambasaguas, “*Downlink power setting for energy efficient Heterogeneous Cellular Networks*”, 2016 8th International Congress on Ultra Modern Telecommunications and Control Systems and Workshops (ICUMT), Lisbon, 2016, pp. 147-151.
15. **F. J. Martin-Vega**, M. Di Renzo, M. C. Aguayo-Torres, G. Gomez and T. Q. Duong, “*Stochastic geometry modeling and analysis of backhaul-constrained Hyper-Dense Heterogeneous cellular networks*”, 2015 17th International Conference on Transparent Optical Networks (ICTON), Budapest, 2015, pp. 1-4.
16. I. M. Delgado-Luque, F. Blaquez-Casado, **F. J. Martin-Vega**, M. Fuertes, G. Gomez, M. C. Aguayo-Torres, J. T. Entrambasaguas, J. Baños, “*Performance evaluation of cooperation-based techniques for M2M traffic over LTE*”, 2013 IEEE 24th

Annual International Symposium on Personal, Indoor, and Mobile Radio Communications (PIMRC), London, 2013, pp. 144-148.

17. **F. J. Martin-Vega**, I. M. Delgado-Luque, F. Blaquez-Casado, G. Gomez, M. C. Aguayo-Torres and J. T. Entrambasaguas, “*LTE Performance over High Speed Railway Channel*”, 2013 IEEE 78th Vehicular Technology Conference (VTC Fall), Las Vegas, NV, 2013, pp. 1-5.

National conference papers:

18. S. Montesinos-Barrios M. C. Aguayo-Torres and **F. J. Martin-Vega**, “*Selección Dinámica de Celda en los Enlaces Ascendente y Descendente de Redes Heterogéneas: Estudio de las Estrategias Acoplada y Desacoplada*”, submitted to XXXII National Symposium of the International Radio Union,(URSI) 2017, September 2017, Cartagena (Spain).
19. J. C. Marin-Barranquero, G. Gomez and **F. J. Martin-Vega**, “*Análisis de la Reutilización Fraccional de Frecuencia con Sectorización sobre Redes Celulares*”, submitted to XXXII National Symposium of the International Radio Union,(URSI) 2017, September 2017, Cartagena (Spain).
20. **F. J. Martin-Vega**, G. Gomez, M. C. Aguayo-Torres and J. T. Entrambasaguas, “*A New Tractable Model to Estimate the Uplink Inter-Cell Interference in LTE*”, XXX National Symposium of the International Radio Union,(URSI) 2015, September 2015, Pamplona (Spain).
21. **F. J. Martin-Vega**, G. Gomez, M. C. Aguayo-Torres, “*A New Frequency Planning for Improved Capacity and Coverage in Sectorized OFDMA Cellular Networks*”, XXX National Symposium of the International Radio Union,(URSI) 2015, September 2015, Pamplona (Spain).
22. **F. J. Martin-Vega**, G. Gomez, M. C. Aguayo-Torres and Carlos Mosquera, “*Prestaciones de LTE sobre el canal aeronáutico*”, XXIX National Symposium of the International Radio Union,(URSI) 2014, September 2014, Valencia (Spain).
23. **F. J. Martin-Vega**, F. J. Lopez-Martinez, J. T. Entrambasaguas Muoz, “*Arquitectura HW para decodificador Two-Step SOVA con recorridos hacia atrás sistólicos*”,

XXVII National Symposium of the International Radio Union,(URSI) 2012, September 2012, Elche (Spain).

1.5 Outline of the dissertation

This dissertation is structured as follows. The proposed framework for analysis and modelling of IAFPC for the UL of HCNs is presented in Chapter 2. Then, the performance of IAM is investigated in Chapter 3. A model to assess the coverage probability of different MTs within the same cell is proposed in Chapter 4. The performance of cellular systems under Hoyt fading is investigated in Chapter 5. A novel NOMA-based scheme for CRANs is proposed and analyzed in Chapter 6. Finally, the focus is placed on vehicular communications with Chapter 7. To conclude this dissertation, main conclusions derived with this work are presented in Chapter 8 whereas a summary (in Spanish) of this thesis is provided in Appendix A.

Chapter 2

Performance Analysis of Interference-Aware Fractional Power Control

Inter-cell interference is one of the main limiting factors in current Heterogeneous Cellular Networks (HCNs). Uplink Fractional Power Control (FPC) is a well known method that aims to cope with such a limiting factor and to save the battery life of the Mobile Terminals (MTs). In order to do that, the transmit power of each MT is adjusted as a function of a set of parameters that usually depend only on the link between MTs and serving Base Station (BS), such as the desired received power at the serving BS or the path loss between the MT and its serving BS. Contrary to these classical FPC schemes, in this chapter we use stochastic geometry to analyze a power control mechanism that keeps the interference generated by each MT under a given threshold. We also consider a maximum transmitted power and a partial compensation of the path loss. Our analysis reveals that such Interference Aware (IA) method can reduce the average power consumption and increase the average spectral efficiency at once. Additionally, the variance of the interference is reduced, thus improving the performance of Adaptive Modulation and Coding (AMC) schemes since the interference can be better estimated.



2.1 Introduction

Since the early deployments of cellular systems, interference has been the main limiting factor. This is due, in part, to its highly indeterministic nature and its sensitivity to network conditions. This situation is even aggravated in the uplink, since the interfering set of Mobile Terminals (MTs) depends on the scheduling policies of other cells (that may change from one sub-frame to another), on their channel states, on their locations and on their transmission powers. In irregular networks, in addition, interfering MTs can be closer to the serving BS than its intended MT.

In order to cope with interference, Fractional Power Control (FPC) schemes are considered to be essential components of the uplink (UL) of Long Term Evolution (LTE) and LTE-Advanced communication standards [65]. Essentially, FPC partially compensates for the path loss and allows cell-interior MTs to save battery while ensuring that cell-edge MTs do not cause excessive interference to neighboring cells [66–68]. Such an approach, however, still generates an undesired level of interference that reduces the UL performance. Beside this, the highly indeterministic nature of UL interference poses additional challenges for interference estimation, which degrades the performance of Adaptive Modulation and Coding (AMC) schemes [69].

To solve these issues, an Interference Aware Fractional Power Control (IAFPC) scheme, which is compliant with LTE specifications, was proposed in [49]. This power control mechanism establishes a maximum interference level, i_0 , that each MT is allowed to cause to the most interfered BS. As discussed in [49], both open and closed loop implementations are possible. In the open loop case, each MT estimates the path loss and shadowing towards its serving and the most interfered BS. In the LTE standard, this can be done thanks to the orthogonality of the reference signals from nearby BSs [70]. Hence, the open loop implementation has the benefit that it does not require control overhead between MTs and BSs. The channel reciprocity between UL and Downlink (DL) transmissions, however, must be fulfilled, or, at least, UL and DL links need to have similar path loss and shadowing. Typically this holds in Time Division Duplex (TDD) implementations, but it may not always be true in Frequency Division Duplex (FDD) implementations [71]. To overcome this limitation, closed loop schemes can be used. In this case, each BS measures the received interference in each Resource Block (RB) and then shares this information with its neighboring BSs via the X2 interface [72]. Subsequently, each BS determines the

most interfered BS for each of its served MTs and applies power control. This is done by sending power control messages that increase or reduce the transmitted power of each MT. Based on [49], closed loop schemes can achieve similar performance as their open loop counterparts.

There are several works that have studied IA power control methods [49, 73–75]. However, they are based on simulations and are applicable to single tier network deployments. These studies have demonstrated that IAFPC leads to significant performance improvement, by reducing the variance of the interference, increasing the average rate and decreasing the power consumption. This holds for both open or closed loop schemes. Motivated by these potential gains of IAFPC, there is the compelling need for tractable analytical approaches that enable their analysis and optimization, as well as lead to a better understanding of power control and cell association strategies in the UL. In addition, analytical models are always beneficial as they enable quick evaluation of large sets of candidate solutions.

2.1.1 Related Work

The increasing demand of capacity across service areas and the associated deployment of Heterogeneous Cellular Networks (HCNs) are changing the topology of cellular networks, from a regular grid to a more irregular and random deployment of BSs. In this context, stochastic geometry is considered to be a powerful mathematical tool that enables the tractable analysis of cellular systems where the positions of the BSs are distributed according to a uniform Poisson Point Process (PPP) [20]. Several works have recently proved that stochastic geometry provides estimates of key performance indicators that are as accurate as simulation results [21, 24]. This approach usually considers the typical link between a probe MT and its serving BS, where the term *typical*, means randomly chosen and foresees that the MT can be placed anywhere within the cell.

In the last few years, stochastic geometry has been extensively used for the analysis of the DL of HCNs. The analysis of the UL, on the other hand, is more involved than that of the DL. This is because the transmission powers of the interferers are coupled with their serving BSs' distances due to power control, as well as, even if the positions of BSs and MTs follow a PPP, the positions of the interfering MTs do not follow a PPP, making the exact analysis intractable [26]. To understand why the positions of the interfering MTs

do not follow a PPP, let us recall that one property of the PPPs is the independence of the number of points falling in disjoint regions. In current networks, orthogonal resource allocation schemes are used, which implies that there is a single interfering MT in any association cell [27]. Thus, given a PPP of BSs, the positions of the interfering MTs are coupled with the positions of BSs due to the cell association criterion being used, and the interfering MTs are not distributed according to a PPP. This can be confirmed by considering two disjoint regions in the same association cell. Having an interfering MT in one of the regions implies that the other region is empty, which contradicts the PPP assumption. The interfering MTs, on the other hand, can be viewed as a stemmed form of Voronoi perturbed lattice process [26, 28], which is not mathematically tractable. This makes the analysis of the UL more complicated than that of the DL.

In spite of its mathematical challenges, there are recent works that analyze the performance of the UL with different power control and association policies. In [29], single tier networks with FPC are analyzed with the aid of stochastic geometry. In order to avoid the intractability of the locations of the interfering MTs, the proposed approach assumes that the MTs that are scheduled in the RB of interest form a Voronoi tessellation and that a single BS is available in each Voronoi cell. In [30], FPC is analyzed by approximating the positions of the interfering MTs as a uniform PPP in the entire plane. With this approach, however, some interfering MTs may undergo, with respect to the probe BS, a smaller path loss than with their serving BS, which is not a realistic situation. Recently, [26, 31, 32] have proposed accurate frameworks to model the positions of the interfering MTs. These works consider the spatial correlation between the locations of the probe BS and those of the interfering MTs. Such correlation is due to the fact that the interfering MTs are placed outside the Voronoi cell of the probe BS [27]. The authors of [31] consider a truncated channel inversion power control, where the MTs attempt to fully compensate for the path loss towards their serving BS, provided that they do not have to transmit with more power than p_{\max} . The cell association is based on the smallest path loss. The MTs that necessitate higher power than p_{\max} are kept silent. In the UL, traditionally, the association between MTs and BSs has been coupled with the association in the DL. This is due to technical reasons that are related to network implementation. However, it has been recently proposed to split UL and DL associations (decoupled access), by performing the association in the UL based on a minimum path loss criterion [26]. This approach re-

duces the UL interference as well, since the MTs are associated with the BSs providing the minimum path loss, and, thus, their transmit power is reduced. A generalized weighted association for both coupled and decoupled access with FPC is considered in [26] and the joint DL/UL rate is analyzed.

2.1.2 Contributions

In this chapter, a novel framework for the modeling and analysis of uplink HCNs with IAFPC is presented. The proposed model is general, since interference unaware (non-IA) power control methods can be viewed as particular instances of our analysis when the maximum allowed interference level i_0 tends to infinity. The proposed framework is based on a *conditional thinning* modeling approach, in order to appropriately model the positions of the interfering MTs and to account for the spatial correlation with the location of the probe BS. Compared with previous studies that consider FPC but are not IA, the mathematical modeling is more challenging since the spatial correlation with the most interfered BS need to be considered as well. In addition, it is necessary to deal with non linear functions that depend on the distances towards the serving BS and towards the most interfered BS. All these issues make the computation of the distribution of the Signal to Interference Plus Noise Ratio (SINR) not an easy task. To overcome the mathematical complexity of the problem at hand, we propose two approximations for the Laplace transform of the aggregate interference: i) it is approximated by using a sigmoid function and then logistic regression is applied [76], in order to obtain its parameters and ii) it is approximated by using a suitable function via Moment Matching (MM) methods. In addition, asymptotic analysis is performed to identify performance trends as i_0 becomes low or tends to infinity. The resulting framework avoids the need of approximating the interference and results in lower computational complexity. More specifically, the contribution of the chapter can be summarized as follows.

- Analysis and comparison of IA and non-IA FPC schemes. From their numerical comparison, it is shown that interference awareness reduces the mean and the variance of the interference, as well as the average transmitted power. Also, it increases the average spectral efficiency.
- Analysis of several performance metrics that provide better understanding of IA

and non-IA FPC schemes. This includes the average transmitted power, the mean and variance of the interference, the coverage probability and the average spectral efficiency.

- Two accurate approximations for the Laplace transform of the interference in the presence of IAFPC. These approximations greatly reduce the computational complexity of the resulting mathematical frameworks.
- Proposal of asymptotic frameworks to gain theoretical insight for system design. In particular, it is shown that the statistics of the interference are independent of the BS density in the low i_0 regime and under the smallest path loss cell association criterion.

2.1.3 chapter Organization and Notations

The rest of the chapter is organized as follows. Section 2.2 describes the system model and the proposed approach. In Section 2.3, the analysis of IAFPC is presented. Two approximations of the interference in the presence of IAFPC are proposed in Section 2.4. Section 2.5 introduces asymptotic frameworks for the analysis of IAFPC. They are applicable to non-IA FPC schemes when i_0 tends to ∞ and to IAFPC schemes in the low i_0 regime. In Section 2.6, numerical results are illustrated to validate our approach and findings. Finally, Section 2.7 concludes this chapter.

Notation: $\mathbb{E}[\cdot]$ stands for the expectation operator and $\Pr(\cdot)$ for the probability measure. $\mathbf{1}(\cdot)$ is the indicator function. The first and second derivatives of $f(x)$ evaluated at x_0 are represented as $f'(x_0)$ and $f''(x_0)$. Random variables (RV) and events are represented with capital letters whereas the lower letter case is used for deterministic values and parameters. If X is a RV, $f_X(\cdot)$, $F_X(\cdot)$, $\bar{F}_X(\cdot)$ and $\mathcal{L}_X(\cdot)$ represent its probability density function (pdf), cumulative distribution function (cdf), complementary cdf (ccdf) and Laplace transform of its pdf respectively. $\Gamma(z) = \int_0^\infty t^{z-1} e^{-t} dt$ stands for the Euler gamma function whereas ${}_2F_1(\cdot, \cdot, \cdot, \cdot)$ is the Gauss hypergeometric function defined in [77] (Ch. 15). Given the function $f(x, y)$, we write the limit when $x \rightarrow a$ as $f(y)^{(x \rightarrow a)} = \lim_{x \rightarrow a} f(x, y)$. Finally, a function $f(x)$ can be approximated by another function $f^{(x \sim a)}(x)$ when x is close to a if the following equality holds $\lim_{x \rightarrow a} \frac{f(x)}{f^{(x \sim a)}(x)} = 1$. In this case, we say that $f(x)$ and $f^{(x \sim a)}(x)$ are asymptotically similar when x is close to a .

2.2 System Model

We consider a two-tier HCN, i.e., Macro cell BSs (MBSs) and Small cell (BSs) SBSs, where the BSs of tier $j \in \mathcal{K} = \{1, 2\}$ are spatially distributed in \mathbb{R}^2 according to a uniform PPP, $\Phi^{(j)} = \{\text{BS}_0^{(j)}, \text{BS}_1^{(j)}, \dots\}$, of density $\lambda^{(j)}$ where $\text{BS}_i^{(j)}$ is the location of the i th BS in the j th tier. The positions of all BSs are represented by the PPP $\Phi = \cup_{j \in \mathcal{K}} \Phi^{(j)}$. The MTs are spatially distributed according to another independent and uniform PPP, $\Phi_{\text{MT}} = \{\text{MT}_0, \text{MT}_1, \dots\}$, of density λ_{MT} . It is assumed that the density of MTs is high enough to consider full loaded conditions, i.e., each BS has at least one MT to serve and all the Resource Blocks (RBs) are used. Hence, the density of interfering MTs is the same as the density of BSs and there is a single scheduled MT per BS. If saturated conditions do not hold, the density of interfering MTs is lower than the density of BSs, which leads to lower interference than with full loaded conditions. Nevertheless, a general load model could be taken into account by using the approach recently introduced in [32]. The analysis is performed for the typical MT, i.e., a randomly chosen MT with $\text{MT} \in \Phi_{\text{MT}}$. Since uniform PPPs are translation invariant, such typical MT can be considered to be placed at the origin (without loss of generality) thanks to the Slivnyak's theorem [61]. In this chapter, the typical MT is referred to as the probe MT and is denoted by MT_0 . Likewise, its serving BS is referred to as the probe BS and is denoted by BS_0 .

2.2.1 Channel Model

The transmitted signal undergoes both shadowing and multi-path fading. For different locations, fading is modeled as independent and identically distributed (iid) exponential RVs with unit mean, whereas shadowing is modeled as iid Log-normal RVs with standard deviation σ_s and mean μ_s . A unit mean squared value is assumed, and hence $\mu_s = -\ln(10)\sigma_s^2/20$ [78]. We use equivalent distances that include shadowing as in [79], i.e., $\dot{R}_{x,y} = S_{x,y}^{-1/\alpha} R_{x,y}$, where $S_{x,y}$ is the shadowing between locations x and y and $R_{x,y} = \|x-y\|$ is the Euclidean distance. Hence shadowing can be considered as a random displacement over $\Phi^{(j)}$ [24, 61], where the density of the displaced PPP is $\dot{\lambda}^{(j)} = \lambda^{(j)}\mathbb{E}[S^{-1/\alpha}]$ and $\mathbb{E}[S^{-1/\alpha}] = \exp\left(\frac{\ln(10)\mu_s}{5\alpha} + \frac{1}{2}\left(\frac{\ln(10)\sigma_s}{5\alpha}\right)^2\right)$. In the rest of the chapter, for simplicity, all the distances and PPPs are assumed to include shadowing.

The path loss models proposed in 3GPP are typically formulated as $L(\text{dB}) = a_L +$

$b_L \log_{10}(R_{x,y}(\text{km}))$, where $R_{x,y}$ is the distance between locations x and y expressed in km, and a_L and b_L depend on several radio frequency parameters. In this chapter, we consider a similar path loss law, which can be expressed as $L = (\tau R_{x,y}(m))^\alpha$, where $\tau = 10^{(a_L - 3b_L)/b_L}$ is the path loss slope and $\alpha = b_L/10$ is the path loss exponent. In Section 2.6, in particular, the path loss model adopted in 3GPP ([80], Sec. 4.5.2) is used. It can be formulated as follows:

$$a_L = 80 - 18 \log_{10}(h_{\text{BS}}(\text{m})) + 21 \log_{10}(f_c(\text{MHz})); b_L = 40(1 - 4 \cdot 10^{-3} h_{\text{BS}}(\text{m})) \quad (2.1)$$

where f_c is the carrier frequency in MHz and $h_{\text{BS}}(\text{m})$ is the BS's antenna height in m. Every tier is assumed to have the same path loss exponent and the same path loss slope.

2.2.2 Association and Scheduling

The cell association criterion among MTs and BSs is based on the weighted average received power [26]. The association weights are denoted by $t^{(j)}$ for each tier $j \in \mathcal{K}$.

Let us introduce the event $\mathcal{X}_{\text{MT}_i}^{(j)}$ as: *MT_i is associated with tier j*. More formally, it can be defined as follows

$$\mathcal{X}_{\text{MT}_i}^{(j)} = \left\{ t^{(j)} \left(\tau R_{\text{MT}_i, (1)}^{(j)} \right)^{-\alpha} > t^{(\tilde{j})} \left(\tau R_{\text{MT}_i, (1)}^{(\tilde{j})} \right)^{-\alpha} \right\} \quad (2.2)$$

where $(\tau R_{\text{MT}})^{-\alpha}$ represents the path loss at a distance R_{MT} from the transmitter; $\tilde{j} = \{x \in \mathcal{K} : x \neq j\}$ is the complementary tier of tier j and $R_{x, (q)}^{(\tilde{j})}$ is the distance from x to the q th nearest BS of tier \tilde{j} , i.e. $R_{x, (1)}^{(\tilde{j})}$ is the distance to the nearest BS. The association weights allow us to model the minimum path loss cell association criterion as a special case, by setting $t^{(j)} = 1$, as well as the association criterion based on DL received power.

Full frequency reuse is considered and all the BSs share the same bandwidth, which is divided in RBs for scheduling purposes. A single RB is the minimum amount of bandwidth that can be allocated to a transmission. In LTE and LTE-A, each RB is divided into 12 Resource Elements (REs) of 15 kHz. The RB where the probe MT is scheduled for transmission is referred to as the probe RB. Hence, the set of interfering MTs from tier k , which is denoted by $\Psi^{(k)}$, is the set of MTs that has been scheduled in the probe RB. Each BS chooses at random the MT that is scheduled in each RB.

2.2.3 Power Control Mechanism

We consider an IAFPC mechanism [49], where each MT causes less interference than i_0 to its most interfered BS and transmits with less power than p_{\max} . It is assumed that power control can be adapted to slow variations of the received power, hence it can only compensate for path loss and shadowing. The transmit power can be expressed as follows

$$p_{\text{MT}}(R_{\text{MT}_0}, U_{\text{MT}_0}) = \min(p_0 (\tau R_{\text{MT}_0})^{\alpha\epsilon}, i_0 (\tau U_{\text{MT}_0})^\alpha, p_{\max}) \quad (2.3)$$

where R_{MT_0} is the distance between the probe MT and its serving BS, U_{MT_0} the distance between the probe MT and its most interfered BS, p_0 is the target received signal power at the serving BS and ϵ is the FPC compensation factor. All the MTs use the same set of power control parameters $(p_0, \epsilon, p_{\max}, i_0)$. If the transmit power is equal to $p_{\text{MT}}(R_{\text{MT}_0}, U_{\text{MT}_0}) = p_{\max}$, the transmission is truncated by p_{\max} . If $p_{\text{MT}}(R_{\text{MT}_0}, U_{\text{MT}_0}) = i_0 (\tau U_{\text{MT}_0})^\alpha$, the transmission is truncated by i_0 .

Let us define the event $\mathcal{Q}_{\text{MT}_i}^{(m)}$ as: *the most interfered BS of the transmissions of MT_i belongs to tier m* . Hence, we can define the event $\mathcal{X}_{\text{MT}_i}^{(j,m)} = \mathcal{X}_{\text{MT}_i}^{(j)} \cap \mathcal{Q}_{\text{MT}_i}^{(m)}$ as follows: *MT_i is associated with tier j and its most interfered BS belongs to tier m* . Mathematically this event can be expressed as

$$\begin{aligned} \mathcal{X}_{\text{MT}_i}^{(j,m)} &= \mathcal{X}_{\text{MT}_i}^{(j)} \cap \overbrace{\left\{ R_{\text{MT}_i,(2)}^{(j)} > R_{\text{MT}_i,(1)}^{(m)} \right\}}^{\mathcal{Q}_{\text{MT}_i}^{(m)}}, \text{ if } j \neq m \\ \mathcal{X}_{\text{MT}_i}^{(j,j)} &= \mathcal{X}_{\text{MT}_i}^{(j)} \cap \overbrace{\left\{ R_{\text{MT}_i,(2)}^{(j)} < R_{\text{MT}_i,(1)}^{(j)} \right\}}^{\mathcal{Q}_{\text{MT}_i}^{(j)}}, \text{ if } j = m \end{aligned} \quad (2.4)$$

Fig. 2.1 provides an illustration of the network topology under analysis with IAFPC. It shows that the locations of the non-truncated MTs are different for each BS. This is due to the fact that their locations depend on the positions of the neighboring BSs. It can be noted that the MTs truncated by i_0 tend to be placed in positions close to a victim BS, whereas the MTs truncated by p_{\max} tend to be placed far from their serving BSs but also far from any other BSs. Intuitively, this mechanism allows the network to reach a balance between interference and desired received power, which increases the SINR. In our system model, it is important to note that the MTs that tend to cause more interference than i_0

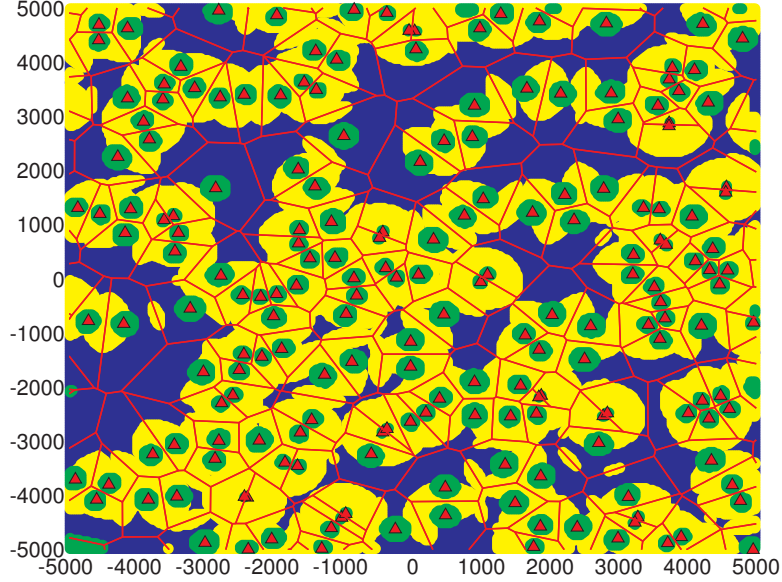


Figure 2.1: Homogeneous network realization in $[-5000, 5000]^2$ m² showing with green color the positions related to non truncated MTs. Yellow and blue colors are associated with MTs truncated by i_0 and to p_{\max} , respectively. The simulation parameters are $\lambda^{(1)} = 2$ BS/km², $i_0 = -90$ dBm, $p_{\max} = 30$ dBm, $p_0 = -70$ dBm and $\epsilon = 1$.

or those that attempt to transmit with more power than p_{\max} are not kept silent. They transmit at a maximum power, instead, that do not violate the aforementioned constraints (i_0 and p_{\max}).

2.2.4 SINR

The SINR of the typical MT, MT_0 , can be expressed as

$$\text{SINR}_{MT_0} = \frac{H_{MT_0} (\tau R_{MT_0})^{-\alpha} p_{MT} (R_{MT_0}, U_{MT_0})}{I_{\text{exact}} + \sigma_n^2} \quad (2.5)$$

where H_{MT_0} is the multi-path fading power of the desired link, R_{MT_0} and U_{MT_0} are the distances towards the serving and the most interfered BSs including shadowing, I_{exact} is the aggregate interference and σ_n^2 is the noise power.

In the UL, as mentioned in Section 2.1, the interfering MTs do not follow a PPP even if the positions of BSs and MTs are distributed according to a PPP. The nature of such point process, which depends on the scheduling and association criteria, makes the analysis

intractable. In this chapter, thus, we assume that the interfering MTs constitute a PPP. However, it is necessary to take into account appropriate spatial correlation constraints between the probe BS and the interfering MTs, in order to improve the accuracy of the analysis [26, 31]. In the UL, in addition, an interfering MT can be located closer to the probe BS than the probe MT. Nevertheless, the interfering MT has always higher weighted received power from its serving BS than from the probe BS thanks to the adopted association criterion. We use this fact, which has been previously used in [31] and [26], to accurately modeling the locations of the interfering MTs. To this end, we perform a conditional thinning over the event $\mathcal{O}_{\text{MT}_i}^{(j,k)}$ defined as: *the interfering MT_i belonging to tier k receives higher weighted power from its serving BS than from the probe BS that belongs to tier j*. In mathematical terms, this can be formulated as follows

$$\mathcal{O}_{\text{MT}_i}^{(j,k)} = \{t^{(k)} (\tau R_{\text{MT}_i})^{-\alpha} > t^{(j)} (\tau D_{\text{MT}_i})^{-\alpha}\} \quad (2.6)$$

where R_{MT_i} is the distance between the interfering MT_i and its serving BS and D_{MT_i} is the distance between MT_i and the probe BS.

Additionally, interference awareness imposes that MT_i cannot cause an interference level higher than i_0 . This introduces additional spatial correlation constraints. This correlation, which exists in the *exact* model, is taken into account by introducing a dependent thinning with the aid of the event $\mathcal{Z}_{\text{MT}_i}$ defined as: *the interfering MT_i causes less interference to BS₀ than i_0* . In mathematical terms, this can be formulated as follows

$$\mathcal{Z}_{\text{MT}_i} = \{p_{\text{MT}} (R_{\text{MT}_i}, U_{\text{MT}_i}) (\tau D_{\text{MT}_i})^{-\alpha} < i_0\} \quad (2.7)$$

where R_{MT_i} and U_{MT_i} represent the distance between MT_i and its serving and most interfering BS, respectively. It is assumed that, for each MT_i, the RVs $\{R_{\text{MT}_i}, U_{\text{MT}_i}\}$ are iid.

Finally, the exact interference term I_{exact} , which is mathematically intractable, is approximated as $I_{\text{exact}} \simeq I$. If the probe MT is associated with tier j , it can be expressed as

$$I = \sum_{k \in \mathcal{K}} \sum_{\text{MT}_i \in \Psi^{(k)}} H_{\text{MT}_i} (\tau D_{\text{MT}_i})^{-\alpha} p_{\text{MT}} (R_{\text{MT}_i}, U_{\text{MT}_i}) \mathbf{1} \left(\mathcal{O}_{\text{MT}_i}^{(j,k)} \right) \mathbf{1} \left(\mathcal{Z}_{\text{MT}_i} \right) \quad (2.8)$$

where $\Psi^{(k)}$ is the PPP of the interfering MTs scheduled in the RB of interest and whose density is $\lambda^{(k)}$. From (2.8), it can be observed that the locations of the interfering MTs of tier k are obtained by applying a conditional thinning over $\Psi^{(k)}$ with the aid of the event $\mathcal{O}_{\text{MT}_i}^{(j,k)}$ that discards all the locations that would result associated with the probe BS and with the aid of the event $\mathcal{Z}_{\text{MT}_i}$ that discards all the locations that would cause higher interference than i_0 . In the exact interference term, every interfering MT causes equal or less interference than i_0 to the probe BS, thanks to the power control rule in (2.3). In the proposed approximated interference model, however, we assume, for tractability, that the RVs $\{R_{\text{MT}_i}, U_{\text{MT}_i}\}$ are iid. This implies that some interfering MTs may cause more interference than i_0 . Since this situation does not happen in the exact model, we impose this constraint by means of a thinning with the aid of the event $\mathcal{Z}_{\text{MT}_i}$.

The benefit of the approximated interference model given by (2.8), I , is that it allows us to model the positions of the interfering MTs as a PPP, $\Psi^{(k)}$, which yields mathematical tractability. On the other hand, the exact interference model, I_{exact} , which originates from the association and scheduling criteria, considers that the positions of the interfering MTs follow a Voronoi perturbed lattice process [26, 28], which is not mathematically tractable and can only be simulated. In the following section, hence, the analysis is carried out based on the approximation I . In the numerical results section, the analytical results based on (2.8) are compared against simulation results based on I_{exact} , in order to assess how accurate the proposed analytical model for the interference is.

2.3 Analysis of Interference Aware Power Control

In this section, the average transmit power, the mean and variance of the interference, the cdf of the SINR, and the average Spectral Efficiency (SE) are studied. The probability of being associated with tier j has been previously obtained in [26] and is reproduced here for convenience $\Pr\left(\mathcal{X}_{\text{MT}_0}^{(j)}\right) = \lambda^{(j)} / \sum_{k \in \mathcal{K}} \left(\frac{t^{(k)}}{t^{(j)}}\right)^{\frac{2}{\alpha}} \lambda^{(k)}$.

The probability of being associated with tier j and being the most interfered BS for tier m is provided in the following lemma.

Lemma 1. *Assume that the probe MT employs IAFPC. The probability of the event $\mathcal{X}_{\text{MT}_0}^{(j,m)}$*

with $j \neq m$ is

$$\Pr \left(\mathcal{X}_{\text{MT}_0}^{(j,m)} \right) = \frac{\lambda^{(j)} \lambda^{(m)} \left(\frac{t^{(j)}}{t^{(m)}} \right)^{\frac{2}{\alpha}}}{(\lambda^{(j)} + \lambda^{(m)})^2} \mathbf{1} \left(\left(\frac{t^{(m)}}{t^{(j)}} \right) > 1 \right) + \left(\frac{\lambda^{(m)} (2\lambda^{(j)} + \lambda^{(m)})}{(\lambda^{(j)} + \lambda^{(m)})^2} - \frac{\lambda^{(m)}}{\lambda^{(j)} \left(\frac{t^{(j)}}{t^{(m)}} \right)^{\frac{2}{\alpha}} + \lambda^{(m)}} \right) \times \mathbf{1} \left(\left(\frac{t^{(m)}}{t^{(j)}} \right) \leq 1 \right) \quad (2.9)$$

If $j = m$, on the other hand, the probability is

$$\Pr \left(\mathcal{X}_{\text{MT}_0}^{(j,j)} \right) = \frac{(\lambda^{(j)})^2}{(\lambda^{(j)} + \lambda^{(j)})^2} \mathbf{1} \left(\left(\frac{t^{(j)}}{t^{(j)}} \right) \leq 1 \right) + \frac{(\lambda^{(j)})^2 \left(\frac{t^{(j)}}{t^{(j)}} \right)^{\frac{2}{\alpha}} \left(\lambda^{(j)} - \lambda^{(j)} \left(\left(\frac{t^{(j)}}{t^{(j)}} \right)^{\frac{2}{\alpha}} - 2 \right) \right)}{(\lambda^{(j)} + \lambda^{(j)})^2 \left(\lambda^{(j)} + \lambda^{(j)} \left(\frac{t^{(j)}}{t^{(j)}} \right)^{\frac{2}{\alpha}} \right)} \times \mathbf{1} \left(\left(\frac{t^{(j)}}{t^{(j)}} \right) > 1 \right) \quad (2.10)$$

Proof. See Appendix 2.8. □

The computation of the transmit power (see (2.3)) requires knowledge of the joint pdf of the distances towards the serving and most interfering BSs. This fact complicates the analysis even further, since it requires a joint pdf of distances as well as the need of dealing with the nonlinear function $\min(\cdot)$. The next lemma provides the joint pdf of the distances of interest.

Lemma 2. Assume that the probe MT employs IAFPC. The joint pdf of the distances towards the serving and most interfered BSs conditioned on the event $\mathcal{X}_{\text{MT}_0}^{(j,m)}$ is

$$f_{R_{\text{MT}_0}, U_{\text{MT}_0}} \left(v, w | \mathcal{X}_{\text{MT}_0}^{(j,m)} \right) = \frac{f_{R_{\text{MT}_0}, (1)}^{(m)}(w) \zeta^{(j)}(v, w)}{\Pr \left(\mathcal{X}_{\text{MT}_0}^{(j,m)} \right)} \mathbf{1} \left(w > \left(\frac{t^{(m)}}{t^{(j)}} \right)^{\frac{1}{\alpha}} v \right) \quad (2.11)$$

if $j \neq m$, and it is

$$f_{R_{\text{MT}_0}, U_{\text{MT}_0}}(v, w | \mathcal{X}_{\text{MT}_0}^{(j,m)}) = \frac{\bar{F}_{R_{\text{MT}_0},(1)}^{(j)} \left(\max \left(\left(\frac{t^{(j)}}{t^{(j)}} \right)^{\frac{1}{\alpha}} v, w \right) \right)}{\Pr \left(\mathcal{X}_{\text{MT}_0}^{(j,j)} \right)} f_{R_{\text{MT}_0},(1), R_{\text{MT}_0},(2)}^{(j)}(v, w) \mathbf{1}(w > v) \quad (2.12)$$

if $j = m$, where

$$\zeta^{(j)}(v, w) = 2\pi\lambda^{(j)} v e^{-\pi\lambda^{(j)} \max^2(v, w)} \quad (2.13)$$

The joint pdf of the nearest and second nearest point was computed in [52] and is

$$f_{R_{\text{MT}_0},(1), R_{\text{MT}_0},(2)}^{(j)}(r_1, r_2) = 4(\pi\lambda^{(j)})^2 r_1 r_2 e^{-\pi\lambda^{(j)} r_2^2}, r_1 < r_2 \quad (2.14)$$

Proof. See Appendix 2.9. □

The joint pdf of the distances provided in **Lemma 2** allows us to compute the average transmitted power. More specifically, it can be formulated as

$$\mathbb{E}[P_{\text{MT}_0}] = \sum_{j \in \mathcal{K}} \sum_{m \in \mathcal{K}} \Pr \left(\mathcal{X}_{\text{MT}_0}^{(j,m)} \right) \times \mathbb{E}_{R_{\text{MT}_0}, U_{\text{MT}_0}} \left[p_{\text{MT}}(R_{\text{MT}_0}, U_{\text{MT}_0}) | \mathcal{X}_{\text{MT}_0}^{(j,m)} \right] \quad (2.15)$$

where $p_{\text{MT}}(R_{\text{MT}_0}, U_{\text{MT}_0})$ is given in (2.3).

The Laplace transform of the aggregate interference is provided in the following proposition.

Proposition 1. *Assume that the probe MT employs IAFPC. The Laplace transform of the aggregate interference is*

$$\mathcal{L}_I(s | \mathcal{X}_{\text{MT}_0}^{(j)}) = \exp(\beta^{(j)}(s)) \quad (2.16)$$

where

$$\begin{aligned} \beta^{(j)}(s) &= - \sum_{k \in \mathcal{K}} 2\pi \lambda^{(k)} \sum_{n \in \mathcal{K}} \Pr \left(\mathcal{Q}_{\text{MT}_i}^{(n)} | \mathcal{X}_{\text{MT}_i}^{(k)} \right) \\ &\times \int_{r=0}^{\infty} \int_{u=\left(\frac{t^{(n)}}{t^{(k)}}\right)^{\frac{1}{\alpha}} r}^{\infty} f_{R_{\text{MT}_i}, U_{\text{MT}_i}} \left(r, u | \mathcal{X}_{\text{MT}_i}^{(k,n)} \right) \chi(s, r, u) dr du \end{aligned} \quad (2.17)$$

and

$$\begin{aligned} \chi(s, r, u) &= \frac{sp_{\text{MT}}(r, u) \tau^{-\alpha} \max^{2-\alpha} \left(\left(\frac{t^{(j)}}{t^{(k)}} \right)^{\frac{1}{\alpha}} r, \frac{1}{\tau} \left(\frac{p_{\text{MT}}(r, u)}{i_0} \right)^{\frac{1}{\alpha}} \right)}{\alpha - 2} \\ &{}_2F_1 \left(1, \frac{\alpha - 2}{\alpha}; 2 - \frac{2}{\alpha}; -sp_{\text{MT}}(r, u) \tau^{-\alpha} \max^{-\alpha} \left(\left(\frac{t^{(j)}}{t^{(k)}} \right)^{\frac{1}{\alpha}} r, \frac{1}{\tau} \left(\frac{p_{\text{MT}}(r, u)}{i_0} \right)^{\frac{1}{\alpha}} \right) \right) \end{aligned} \quad (2.18)$$

and $p_{\text{MT}}(r, u)$ is given in (2.3).

Proof. See Appendix 2.10. □

From the Laplace transform of the interference, the mean and the variance of the interference can be obtained by computing the first and second derivatives of $\beta^{(j)}(s)$. Mean and variance of the interference are provided in the following corollary.

Corollary 1. *Assume that the probe MT employs IAFPC. The mean and variance of the aggregate interference are as follows*

$$\mathbb{E}[I] = - \sum_{j \in \mathcal{K}} \Pr \left(\mathcal{X}_{\text{MT}_0}^{(j)} \right) \beta'^{(j)}(0) \quad (2.19)$$

$$\text{var}(I) = - \sum_{j \in \mathcal{K}} \Pr \left(\mathcal{X}_{\text{MT}_0}^{(j)} \right) \left(\beta''^{(j)}(0) + (\beta'^{(j)}(0))^2 - (\mathbb{E}[I])^2 \right) \quad (2.20)$$

where

$$\begin{aligned} \beta^{(j)}(0) &= - \sum_{k \in \mathcal{K}} 2\pi \lambda^{(k)} \sum_{n \in \mathcal{K}} \Pr \left(\mathcal{Q}_{\text{MT}_i}^{(n)} | \mathcal{X}_{\text{MT}_i}^{(k)} \right) \int_{r=0}^{\infty} \int_{u=\left(\frac{t^{(n)}}{t^{(k)}}\right)^{\frac{1}{\alpha}} r}^{\infty} f_{R_{\text{MT}_i}, U_{\text{MT}_i}} \left(r, u | \mathcal{X}_{\text{MT}_i}^{(k,n)} \right) \\ &\quad \frac{\tau^{-\alpha} p_{\text{MT}}(r, u)}{\alpha - 2} \max^{2-\alpha} \left(\left(\frac{t^{(j)}}{t^{(k)}} \right)^{\frac{1}{\alpha}} r, \frac{1}{\tau} \left(\frac{p_{\text{MT}}(r, u)}{i_0} \right)^{\frac{1}{\alpha}} \right) dudr \end{aligned} \quad (2.21)$$

$$\begin{aligned} \beta^{''(j)}(0) &= - \sum_{k \in \mathcal{K}} 2\pi \lambda^{(k)} \sum_{n \in \mathcal{K}} \Pr \left(\mathcal{Q}_{\text{MT}_i}^{(n)} | \mathcal{X}_{\text{MT}_i}^{(k)} \right) \times \int_{r=0}^{\infty} \int_{u=\left(\frac{t^{(n)}}{t^{(k)}}\right)^{\frac{1}{\alpha}} r}^{\infty} f_{R_{\text{MT}_i}, U_{\text{MT}_i}} \left(r, u | \mathcal{X}_{\text{MT}_i}^{(k,n)} \right) \\ &\quad \frac{(\tau^{-\alpha} p_{\text{MT}}(r, u))^2}{1 - \alpha} \max^{2(1-\alpha)} \left(\left(\frac{t^{(j)}}{t^{(k)}} \right)^{\frac{1}{\alpha}} r, \frac{1}{\tau} \left(\frac{p_{\text{MT}}(r, u)}{i_0} \right)^{\frac{1}{\alpha}} \right) dudr \end{aligned} \quad (2.22)$$

Proof. The proof consists of expressing the mean and variance by conditioning on $\mathcal{X}_{\text{MT}_0}^{(j)}$, computing the first and second derivatives of the Laplace transform, and evaluating it at $s = 0$. \square

The cdf of the SINR is provided in (2.23). In order to obtain it, we have used the total probability theorem over the event $\mathcal{X}_{\text{MT}_0}^{(j,m)}$, by first conditioning on R_{MT_0} , U_{MT_0} and I .

$$\begin{aligned} \bar{F}_{\text{SINR}}(\gamma) &= \sum_{j \in \mathcal{K}} \sum_{m \in \mathcal{K}} \Pr \left(\mathcal{X}_{\text{MT}_0}^{(j,m)} \right) \int_{v=0}^{\infty} \int_{w=\left(\frac{t^{(m)}}{t^{(j)}}\right)^{\frac{1}{\alpha}} v}^{\infty} f_{R_{\text{MT}_0}, U_{\text{MT}_0}} \left(v, w | \mathcal{X}_{\text{MT}_0}^{(j,m)} \right) e^{-\frac{\gamma \sigma_n^2 (\tau v)^\alpha}{p_{\text{MT}}(v, w)}} \\ &\quad \times \mathcal{L}_I \left(\frac{\gamma (\tau v)^\alpha}{p_{\text{MT}}(v, w)} | \mathcal{X}_{\text{MT}_0}^{(j)} \right) dv dw \end{aligned} \quad (2.23)$$

The SE of the typical MT is usually expressed in bits per second per Hertz (bps/Hz). It is directly related to the SINR via the Shannon formula $\text{SE}_{\text{MT}_0} = \log_2(1 + \text{SINR}_{\text{MT}_0})$.

The ccdf of the SE of the probe MT can be expressed as

$$\bar{F}_{\text{SE}}(\xi) = \sum_{j \in \mathcal{K}} \sum_{m \in \mathcal{K}} \Pr\left(\mathcal{X}_{\text{MT}_0}^{(j,m)}\right) \bar{F}_{\text{SINR}}\left(2^\xi - 1 | \mathcal{X}_{\text{MT}_0}^{(j,m)}\right) \quad (2.24)$$

where we have applied the total probability theorem. Since the SE is a positive RV, the average SE can be obtained from its ccdf as $\mathbb{E}[\text{SE}] = \int_{\xi > 0} \bar{F}_{\text{SE}}(\xi) d\xi$. So, it can be directly computed from (A.8).

We note that the ccdf of the SINR in (2.23) requires the computation of four nested integrals, since the Laplace transform of the interference given in (2.17) is formulated in terms of two nested integrals. Hence tractable approximations for the Laplace transform of the interference are essential in order to make the proposed approach mathematically tractable. In the next section, we propose approximations of the form $\mathcal{L}_I\left(s | \mathcal{X}_{\text{MT}_0}^{(j)}\right) \simeq \mathcal{L}_f\left(s | \mathcal{X}_{\text{MT}_0}^{(j)}\right)$, where $\mathcal{L}_f\left(s | \mathcal{X}_{\text{MT}_0}^{(j)}\right)$ has a closed form expression. In addition, asymptotic analysis is performed in Section 2.5. This latter approach avoids the need of approximating the interference.

2.4 Approximated Statistical Modeling of the Interference

In this section two approaches for approximating the Laplace transform of the interference are proposed and investigated: i) approximations based on a sigmoidal logistic function whose parameters are obtained by means of logistic regression and ii) approximations through known distribution functions via the MM approach.

2.4.1 Sigmoidal Approximation

The Laplace transform of the interference in (2.16) has a S-shape, if the s-axis is expressed in dB. Sigmoidal logistic functions, are aimed to fit data that exhibits a S-shape [81]. This is because sigmoidal functions emerge if a logit transformation [76] is applied to the data, which *linearizes* S-shaped data and allows one to perform linear regression based on the least mean square criteria [82]. Based on this observation, an approximation based on a

sigmoidal logistic function is proposed as follows

$$\mathcal{L}_I \left(s^{(\text{dB})} | \mathcal{X}_{\text{MT}_0}^{(j)} \right) \simeq g_I \left(s^{(\text{dB})} \right) = \frac{1}{1 + e^{b_0 \left(s^{(\text{dB})} - s_0^{(\text{dB})} \right)}} \quad (2.25)$$

where $s^{(\text{dB})} = 10 \log_{10}(s)$ and $g_I(s^{(\text{dB})})$ is a sigmoidal function of two parameters b_0 and $s_0^{(\text{dB})}$, which satisfies the following properties

$$\begin{aligned} \lim_{s^{(\text{dB})} \rightarrow -\infty} g_I \left(s^{(\text{dB})} \right) &= 1; \quad \lim_{s^{(\text{dB})} \rightarrow +\infty} g_I \left(s^{(\text{dB})} \right) = 0; \\ g_I \left(s_0^{(\text{dB})} \right) &= \frac{1}{2}; \quad \left. \frac{dg_I \left(s^{(\text{dB})} \right)}{ds^{(\text{dB})}} \right|_{s^{(\text{dB})} = s_0^{(\text{dB})}} = -b_0/4 \end{aligned} \quad (2.26)$$

The parameters b_0 and $s_0^{(\text{dB})}$, which are related to the inflection point and to the slope around the inflection point, respectively, can be easily obtained from the properties of the sigmoidal logistic function and by solving the following equation $\mathcal{L}_I \left(s_0^{(\text{dB})} | \mathcal{X}_{\text{MT}_0}^{(j)} \right) = 1/2$, which gives $s_0^{(\text{dB})}$. Then, b_0 can be computed as $b_0 = -4d/ds^{(\text{dB})} \mathcal{L}_I \left(s^{(\text{dB})} | \mathcal{X}_{\text{MT}_0}^{(j)} \right) |_{s^{(\text{dB})} = s_0^{(\text{dB})}}$.

In particular, these parameters can be efficiently obtained by applying logistic regression [82]. To this end, it is sufficient to evaluate the Laplace transform of the interference given in Lemma 1 only at a few sample values $\{s_1^{(\text{dB})}, s_2^{(\text{dB})}, \dots, s_{n_{\text{sig}}}^{(\text{dB})}\}$ and then to perform logistic regression, which is a built-in function available in common mathematical software packages like Mathematica or Matlab. This allows one to obtain the fitting parameters $s_0^{(\text{dB})}$ and b_0 without the need of solving the aforementioned equations. In summary, the numerical evaluation of (2.23) consists of the following steps: i) compute (2.16) for n_{sig} sample points (good results are obtained with $n_{\text{sig}} \sim 8$), ii) perform logistic regression based on the obtained sample points, so as to obtain b_0 and $s_0^{(\text{dB})}$ and iii) evaluate (2.23). Finally, expressing s in linear scale, the Laplace transform of the aggregate interference is approximated as

$$\mathcal{L}_I \left(s | \mathcal{X}_{\text{MT}_0}^{(j)} \right) = \frac{1}{1 + e^{b_0 \left(10 \log_{10}(s) - s_0^{(\text{dB})} \right)}} \quad (2.27)$$

2.4.2 Transformed Distribution Approach

The second approach that we study for approximating the Laplace transform of the interference consists of identifying a suitable approximation function $f(s, \underline{\theta}^{(j)})$, which depends

on the n approximating parameters $\underline{\theta}^{(j)} = \{\theta_0^{(j)}, \dots, \theta_{n-1}^{(j)}\}$. The n parameters of the approximation are computed with the aid of the MM approach, which consists of enforcing that the exact and the approximated Laplace transforms have the same n moments. We refer to this method as the Transformed Distribution Approach (TDA). The matching between the proposed function and the exact Laplace transform of the interference needs to be accurate only for $s \in \mathbb{R}^+$, since only this range of values is needed to obtain the ccdf of the SINR. The Laplace transform of the interference satisfies two conditions $\mathcal{L}_I(0|\mathcal{X}_{\text{MT}_0}^{(j)}) = 1$ and $\mathcal{L}_I(\infty|\mathcal{X}_{\text{MT}_0}^{(j)}) = 0$. Hence, suitable approximating functions must satisfy the following conditions

$$\lim_{s \rightarrow 0} f(s, \underline{\theta}^{(j)}) = 1; \quad \lim_{s \rightarrow \infty} f(s, \underline{\theta}^{(j)}) = 0; \quad 0 < \left| \frac{d^r}{ds^r} f(s, \underline{\theta}^{(j)}) \Big|_{s=0} \right| < \infty, \quad r \in [1, n] \quad (2.28)$$

where the two limits in (2.28) are necessary in order to obtain the Laplace transform of a pdf and the inequality is necessary to perform MM over n moments¹, since the moments are obtained from the derivatives of the Laplace transform evaluated at the origin. Hence, we approximate the interference $I|\mathcal{X}_{\text{MT}_0}^{(j)}$ as $\hat{I}|\mathcal{X}_{\text{MT}_0}^{(j)}$, where $\mathcal{L}_{\hat{I}}(s|\mathcal{X}_{\text{MT}_0}^{(j)}) = f(s, \underline{\theta}^{(j)})$.

Based on this approach, we propose two functions to approximate the Laplace transform of the interference.

Exponential Function

The first option consists of using an exponential function

$$f(s, \theta_0^{(j)}) = e^{-\theta_0^{(j)} s} \mathbf{1}(s \geq 0) \quad (2.29)$$

It satisfies the conditions given in (2.28). Applying the MM approach yields $\theta_0^{(j)} = -\beta'^{(j)}(0)$.

¹We have assumed that the n first moments are finite. However, it is sufficient that n moments, not necessarily the first, are finite to apply MM.

Algebraic Function

The second option consists of using an algebraic function

$$f\left(s, \theta_0^{(j)}\right) = \frac{1}{1 + s\theta_0^{(j)}} \quad (2.30)$$

It satisfies the conditions given in (2.28). Applying the MM approach yields $\theta_0^{(j)} = -\beta^{(j)}(0)$.

Approximating the Laplace transform of the interference with the approaches proposed in this section allows us to formulate the ccdf of the SINR in terms of two nested integrals instead of four. Hence, the reduction in computational complexity is considerable. The sigmoidal approximation needs the evaluation of the equation in (2.16) n_{sig} times, where n_{sig} is the number of sample points of $\mathcal{L}_I\left(s|\mathcal{X}_{\text{MT}_0}^{(1)}\right)$ used to perform logistic regression and to obtain b_0 and $s_0^{(\text{dB})}$. Each evaluation of (2.16) involves two nested integrals. The TDA, either using an algebraic or an exponential function, requires the evaluation of (2.21) only once, which is still formulated in terms of a two-fold integral similar to (2.16). Although the sigmoidal approximation is numerically more complex than the TDA, it allows one to obtain a better fitting by increasing the number of sample values, n_{sig} , used to perform logistic regression.

2.5 Asymptotic Analysis

In this section, we study the asymptotic performance of IAFPC in two limiting regimes: i) when i_0 tends to ∞ and ii) when i_0 is small. The first case study is interesting since it corresponds to the non-IA FPC. The second case of study allows us to gain insight into the average transmitted power and average interference for small values of i_0 .

2.5.1 Interference Unaware Power Control ($i_0 \rightarrow \infty$)

From the expression of the transmitted power in (2.3), we note that interference awareness is lost if i_0 tends to ∞ . Hence, studying the performance in the limiting regime $i_0 \rightarrow \infty$ provides insight on non-IA FPC setups. In this regime, the transmit power is

$p_{\text{MT}}^{(i_0 \rightarrow \infty)}(R_{\text{MT}_0}) = \min(p_0(\tau R_{\text{MT}_0})^{\alpha \varepsilon}, p_{\text{max}})$. The following corollary provides a mathematical expression for it.

Corollary 2. *The average transmitted power with non-IA FPC is as follows*

$$P_{\text{MT}_0}^{(i_0 \rightarrow \infty)} = \lim_{i_0 \rightarrow \infty} \mathbb{E}[P_{\text{MT}_0}] = \sum_{j \in \mathcal{K}} \Pr(\mathcal{X}_{\text{MT}_0}^{(j)}) \mathbb{E}_{R_{\text{MT}_0}} [p_{\text{MT}}(R_{\text{MT}_0}) | \mathcal{X}_{\text{MT}_0}^{(j)}] \quad (2.31)$$

$$f_{R_{\text{MT}_0}}(v | \mathcal{X}_{\text{MT}_0}^{(j)}) = \frac{f_{R_{\text{MT}_0, (1)}^{(j)}}(v) \cdot \bar{F}_{R_{\text{MT}_0, (1)}^{(j)}}\left(\left(\frac{t^{(j)}}{t^{(j)}}\right)^{\frac{1}{\alpha}} v\right)}{\Pr(\mathcal{X}_{\text{MT}_0}^{(j)})} \quad (2.32)$$

Proof. Taking the limit $i_0 \rightarrow \infty$, the transmit power does not depend on U_{MT_0} . Hence, we have

$$\begin{aligned} \mathbb{E}[P_{\text{MT}_0}^{(i_0 \rightarrow \infty)}] &= \sum_{j \in \mathcal{K}} \int_{v=0}^{\infty} \sum_{m \in \mathcal{K}} \Pr(\mathcal{X}_{\text{MT}_0}^{(j,m)}) \int_{w=0}^{\infty} p_{\text{MT}}(R_{\text{MT}_0}) f_{R_{\text{MT}_0, U_{\text{MT}_0}}}(v, w | \mathcal{X}_{\text{MT}_0}^{(j,m)}) dw \\ &= \sum_{j \in \mathcal{K}} \Pr(\mathcal{X}_{\text{MT}_0}^{(j)}) \mathbb{E}_{R_{\text{MT}_0}} [p_{\text{MT}}(R_{\text{MT}_0}) | \mathcal{X}_{\text{MT}_0}^{(j)}] \end{aligned} \quad (2.33)$$

which is obtained with the aid of the following identity (total probability theorem)

$$\sum_{m \in \mathcal{K}} \Pr(\mathcal{X}_{\text{MT}_0}^{(j,m)}) \int_{w=0}^{\infty} f_{R_{\text{MT}_0, U_{\text{MT}_0}}}(v, w | \mathcal{X}_{\text{MT}_0}^{(j,m)}) dw = \Pr(\mathcal{X}_{\text{MT}_0}^{(j)}) f_{R_{\text{MT}_0}}(v | \mathcal{X}_{\text{MT}_0}^{(j)}) \quad (2.34)$$

The proof follows by integrating over w , which yields the marginal pdf in (2.32). \square

Lemma 3. *The Laplace transform of the interference when $i_0 \rightarrow \infty$ is*

$$\mathcal{L}_I^{(i_0 \rightarrow \infty)}(s | \mathcal{X}_{\text{MT}_0}^{(j)}) = \exp\left(-\sum_{k \in \mathcal{K}} 2\pi \lambda^{(k)} \times \int_{r=0}^{\infty} \chi^{(i_0 \rightarrow \infty)}(s, r) f_{R_{\text{MT}_i}}(r | \mathcal{X}_{\text{MT}_i}^{(k)}) dr\right) \quad (2.35)$$

where

$$\begin{aligned} \chi^{(i_0 \rightarrow \infty)}(s, r) &= \frac{r^{2-\alpha} sp_{\text{MT}}^{(i_0 \rightarrow \infty)}(r) \tau^{-\alpha} \left(\frac{t^{(j)}}{t^{(k)}}\right)^{\frac{2-\alpha}{\alpha}}}{\alpha - 2} \\ &\times {}_2F_1\left(1, \frac{\alpha - 2}{\alpha}; 2 - \frac{2}{\alpha}; -\frac{sp_{\text{MT}}^{(i_0 \rightarrow \infty)}(r) \tau^{-\alpha} \left(\frac{t^{(j)}}{t^{(k)}}\right)^{-1}}{r}\right) \end{aligned} \quad (2.36)$$

Proof. The limit of the Laplace transform can be expressed as $\mathcal{L}_I^{(i_0 \rightarrow \infty)}(s | \mathcal{X}_{\text{MT}_0}^{(j)}) = e^{(\beta^{(i_0 \rightarrow \infty)}(j)(s))}$. In particular, the limit of $\beta^{(j)}(s)$ is

$$\begin{aligned} \beta^{(i_0 \rightarrow \infty)}(j)(s) &= - \sum_{k \in \mathcal{K}} 2\pi\lambda^{(k)} \times \int_{r=0}^{\infty} \chi^{(i_0 \rightarrow \infty)}(s, r) \\ &\cdot \sum_{n \in \mathcal{K}} \frac{\Pr(\mathcal{X}_{\text{MT}_i}^{(k,n)})}{\Pr(\mathcal{X}_{\text{MT}_i}^{(k)})} \int_{u=\left(\frac{t^{(n)}}{t^{(k)}}\right)^{\frac{1}{\alpha}} r}^{\infty} f_{R_{\text{MT}_i}, U_{\text{MT}_i}}(r, u | \mathcal{X}_{\text{MT}_i}^{(k,n)}) dr du \end{aligned} \quad (2.37)$$

where the equality in (2.34) is used. \square

In the non-IA system setup, the cdf of the SINR can be obtained by directly computing the limit for $i_0 \rightarrow \infty$ of the cdf of the SINR in (2.23). The resulting expression is as follows

$$\begin{aligned} \bar{F}_{\text{SINR}}^{(i_0 \rightarrow \infty)}(\gamma) &= \sum_{j \in \mathcal{K}} \int_{v=0}^{\infty} e^{-\frac{\gamma \sigma_n^2(\tau v)^\alpha}{p_{\text{MT}}(v)}} f_{R_{\text{MT}_0}}(v | \mathcal{X}_{\text{MT}_0}^{(j)}) \exp\left(-\sum_{k \in \mathcal{K}} 2\pi\lambda^{(k)} \int_{r=0}^{\infty} f_{R_{\text{MT}_i}}(r | \mathcal{X}_{\text{MT}_i}^{(k)}) \right. \\ &\left. \chi^{(i_0 \rightarrow \infty)}\left(\frac{\gamma \sigma_n^2(\tau v)^\alpha}{p_{\text{MT}}(v)}, r\right) dr\right) dv \end{aligned} \quad (2.38)$$

The latter formulas are obtained by taking into account that, for $i_0 \rightarrow \infty$, the dependence on the distance towards the most interfered BS, which is represented by w , disappears in both the Laplace transform and in transmit power $p_{\text{MT}}(v, w)$. Hence, it is possible to apply the equality given in (2.34) and to simplify the expression by removing

the integral over w . In the non-IA setup, it can be observed that the cdf of the SINR is formulated in terms of a two-fold integral.

2.5.2 Low i_0 regime ($i_0 \sim 0$)

In this section, we study the asymptotic regime when i_0 is small and simplified expressions of key performance indicators are provided. Our approach is based on the observation that, if i_0 is small enough, the transmitted power in (2.3) is well approximated as $p_{\text{MT}}(R_{\text{MT}_0}, U_{\text{MT}_0}) \simeq i_0 (\tau U_{\text{MT}_0})^\alpha$. To understand this approximation, let us recall that the transmitted power in (3) is expressed as the minimum of three terms: $p_0 (\tau R_{\text{MT}_0})^{\alpha\epsilon}$, $i_0 (\tau U_{\text{MT}_0})^\alpha$ and p_{max} . If i_0 is small enough, the term $i_0 (\tau U_{\text{MT}_0})^\alpha$ is smaller than the others, in statistical sense, and hence the transmitted power tends to be equal to $i_0 (\tau U_{\text{MT}_0})^\alpha$. In mathematical terms, this implies that the two functions $p_{\text{MT}}(R_{\text{MT}_0}, U_{\text{MT}_0})$ and $p_{\text{MT}}^{(i_0 \sim 0)}(U_{\text{MT}_0}) = i_0 (\tau U_{\text{MT}_0})^\alpha$ are asymptotically similar when i_0 is small. In other words, they tend to the same value as i_0 tend to 0, i.e. $\lim_{i_0 \rightarrow 0} \frac{p_{\text{MT}}(R_{\text{MT}_0}, U_{\text{MT}_0})}{p_{\text{MT}}^{(i_0 \sim 0)}(U_{\text{MT}_0})} = 1$. It is important to remark that, despite the fact that in the definition of asymptotically similar we have used the limit for $i_0 \rightarrow 0$, the proposed approximation of the transmitted power is valid for i_0 small but not necessarily equal to 0.

Average Transmit Power

The average transmit power in the low i_0 regime can be expressed as follows

$$\mathbb{E} \left[P_{\text{MT}_0}^{(i_0 \sim 0)} \right] = \sum_{m \in \mathcal{K}} \Pr \left(\mathcal{Q}_{\text{MT}_0}^{(m)} \right) \mathbb{E}_{U_{\text{MT}_0}} \left[i_0 (\tau U_{\text{MT}_0})^\alpha \mid \mathcal{Q}_{\text{MT}_0}^{(m)} \right] \quad (2.39)$$

since, in this case, the transmit power only depends on U_{MT_0} . The marginal pdf of U_{MT_0} can be obtained from (2) and it is equal to

$$f_{U_{\text{MT}_0}} \left(w \mid \mathcal{Q}_{\text{MT}_0}^{(m)} \right) = \frac{\sum_{j \in \mathcal{K}} \Pr \left(\mathcal{X}_{\text{MT}_0}^{(j,m)} \right)}{\Pr \left(\mathcal{Q}_{\text{MT}_0}^{(m)} \right)} \int_{v=0}^{\infty} f_{R_{\text{MT}_0}, U_{\text{MT}_0}} \left(v, w \mid \mathcal{X}_{\text{MT}_0}^{(j,m)} \right) dv \quad (2.40)$$

Special case: cell association based on the smallest path loss. If a cell association based

on the smallest path loss is assumed, the association weights $t^{(j)}$ are all equal to one. Since we assume the same path loss exponents and slope for every tier, this case study boils down to a single tier cellular network [26, Corollary 6], where the density of the single tier of BSs is $\lambda = \sum_{j \in \mathcal{K}} \lambda^{(j)}$. Accordingly, the distance towards the serving BS turns out to be the distance towards the nearest BS and the distance towards the most interfered BS is the distance towards the second nearest BS. Hence, the joint pdf of these distances is $f_{R_{\text{MT}_0}, U_{\text{MT}_0}}(v, w) = 4(\pi\lambda)^2 v w e^{-\pi\lambda w^2} \mathbf{1}(v < w)$. In this case, the average transmit power can be further simplified to

$$\mathbb{E} \left[P_{\text{MT}_0}^{(i_0 \sim 0)} \right] = i_0 \left(\frac{\tau}{\sqrt{\pi\lambda}} \right)^\alpha \Gamma \left(2 + \frac{\alpha}{2} \right) \quad (2.41)$$

Laplace Transform of the Interference

The Laplace transform of the interference can be expressed as

$$\begin{aligned} \mathcal{L}_I^{(i_0 \sim 0)} \left(s | \mathcal{X}_{\text{MT}_0}^{(j)} \right) &= \exp \left(- \sum_{k \in \mathcal{K}} 2\pi\lambda^{(k)} \sum_{n \in \mathcal{K}} \Pr \left(\mathcal{Q}_{\text{MT}_i}^{(n)} | \mathcal{X}_{\text{MT}_i}^{(k)} \right) \int_{r=0}^{\infty} \int_{u=\left(\frac{t^{(n)}}{t^{(k)}}\right)^{\frac{1}{\alpha}} r}^{\infty} \right. \\ &\left. f_{R_{\text{MT}_i}, U_{\text{MT}_i}} \left(r, u | \mathcal{X}_{\text{MT}_i}^{(k,n)} \right) \chi^{(i_0 \sim 0)}(s, r, u) \, dr du \right) \end{aligned} \quad (2.42)$$

where $\chi^{(i_0 \sim 0)}(s, r, u)$ is defined as follows

$$\begin{aligned} \chi^{(i_0 \sim 0)}(s, r, u) &= \frac{s i_0 (\tau u)^\alpha \tau^{-\alpha}}{\alpha - 2} \max^{2-\alpha} \left(\left(\frac{t^{(j)}}{t^{(k)}} \right)^{\frac{1}{\alpha}} r, u \right) \\ &\times {}_2F_1 \left(1, \frac{\alpha - 2}{\alpha}; 2 - \frac{2}{\alpha}; \frac{-s i_0 (\tau u)^\alpha \tau^{-\alpha}}{\max^\alpha \left(\left(\frac{t^{(j)}}{t^{(k)}} \right)^{\frac{1}{\alpha}} r, u \right)} \right) \end{aligned} \quad (2.43)$$

Special case: cell association based on the smallest path loss. In this case, $\chi^{(i_0 \sim 0)}(s, r, u)$

can be simplified as follows

$$\begin{aligned} \chi^{(i_0 \sim 0)}(s, r, u) &= \frac{\mathbf{1}(r \leq u) si_0 u^2}{\alpha - 2} {}_2F_1\left(1, \frac{\alpha - 2}{\alpha}; 2 - \frac{2}{\alpha}; -si_0\right) + \frac{\mathbf{1}(r > u) si_0 u^\alpha r^{2-\alpha}}{\alpha - 2} \\ &{}_2F_1\left(1, \frac{\alpha - 2}{\alpha}; 2 - \frac{2}{\alpha}; -si_0 \left(\frac{u}{r}\right)^\alpha\right) \end{aligned} \quad (2.44)$$

which is obtained by setting the association weights in (2.44) equal to one and by re-writing the $\max(\cdot)$ function as the sum of two indicator functions. From the integration limits in (2.43), we note that, if the smallest path loss association is used, the second term is canceled out. Finally, integrating the resulting expression over r and u in (2.43) yields

$$\mathcal{L}_I^{(i_0 \sim 0)}(s) = \exp\left(-\frac{4si_0}{\alpha - 2} F_1\left(1, \frac{\alpha - 2}{\alpha}; 2 - \frac{2}{\alpha}; -si_0\right)\right) \quad (2.45)$$

which is a closed form expression.

Remark 1. By direct inspection of (2.45), we note that the Laplace transform of the interference does not depend on the BS density in the low i_0 regime. Hence all statistics of the interference like mean and variance do not depend on λ .

By using (2.45), the cdf of the SINR, by assuming a minimum path loss cell association, can be expressed as follows

$$\begin{aligned} \bar{F}_{\text{SINR}}^{(i_0 \sim 0)}(\gamma) &= \int_{v=0}^{\infty} \int_{w=v}^{\infty} f_{R_{\text{MT}_0}, U_{\text{MT}_0}}(v, w) \cdot e^{-\frac{\gamma \sigma_n^2}{i_0} \left(\frac{v}{w}\right)^\alpha} \exp\left(-{}_2F_1\left(1, \frac{\alpha - 2}{\alpha}; 2 - \frac{2}{\alpha}; -\gamma \left(\frac{v}{w}\right)^\alpha\right)\right) \\ &\frac{4\gamma}{\alpha - 2} \left(\frac{v}{w}\right)^\alpha \Big) dv dw \end{aligned} \quad (2.46)$$

Remark 2. By inspection of (2.46), we evince that, although the Laplace transform of the interference does not depend on λ , the cdf of the SINR does depend on λ . This originates from the joint pdf of the distances. The dependence on i_0 , in particular, only appears in the term $e^{-\frac{\gamma \sigma_n^2}{i_0} \left(\frac{v}{w}\right)^\alpha}$. Since this term disappears in the absence of noise ($\sigma_n^2 = 0$), we conclude that interference-limited HCNs become independent of i_0 when such parameter is small enough (low i_0 regime).

Table 2.1: Simulation Parameters

Parameter	Value	Parameter	Value
f_c (MHz)	2×10^3	h_{BS} (m)	10
b_w (MHz)	9	$t^{(1)}/t^{(2)}$ (dB)	9
$\lambda^{(1)}$ (points/m ²)	2×10^{-6}	$\lambda^{(2)}$ (points/m ²)	4×10^{-6}
λ_{MT} (points/m ²)	80×10^{-6}	n_{thermal} (dBm/Hz)	-174
n_{F} (dB)	9	σ_s (dB)	4
p_0 (dBm)	-70	p_{max} (dBm)	$\{\infty, 5\}$
i_0 (dBm)	$[-120, -60]$	ϵ	$[0, 1]$

2.6 Numerical Results

In this section, the proposed mathematical frameworks are evaluated numerically and compared against Monte Carlo results. The thermal noise power spectral density is set equal to $n_{\text{thermal}} = -174$ dBm/Hz and the noise figure at the receiver is set equal to $n_{\text{F}} = 9$ dB. The main simulation parameters are presented in Table 2.1. It is considered association weights $t^{(1)}/t^{(2)} = 9$ dB, which accounts for transmission powers of 46 and 30 dBm for MBSs and SBSs respectively, where SBSs use a bias of 7 dB so as to offload MBSs.

Monte Carlo results are obtained by simulating 10^4 spatial realizations. In the simulations, first we place the BSs of the two tiers according to two uniform PPPs of densities $\lambda^{(1)}$ and $\lambda^{(2)}$. Then, we distribute the MTs according to another PPP of density λ_{MT} . Finally, we perform cell association for each MT. The probe MT is selected randomly, and then the interfering set of MTs is obtained by randomly choosing one MT per interfering BS. This method allows one to simulate the exact interference, I_{exact} , which is not mathematically tractable.

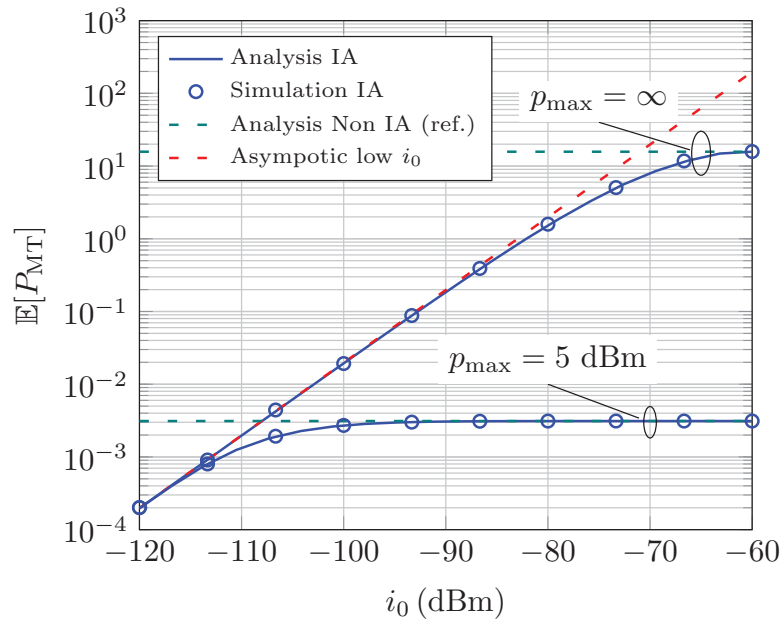


Figure 2.2: Average transmitted power versus i_0 for IAFPC and non-IA FPC with $\epsilon = 1$, $p_{max} \rightarrow \infty$ and $p_{max} = 5$ dBm.

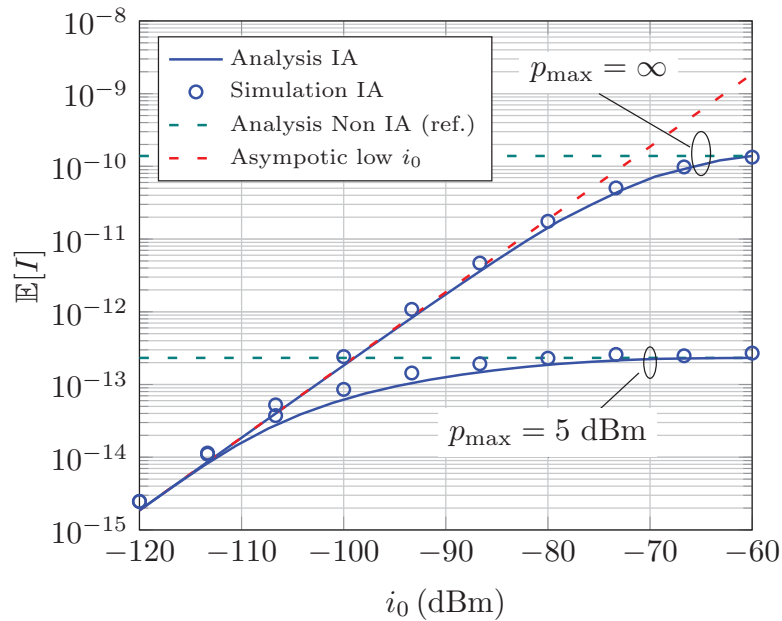


Figure 2.3: Mean of the interference versus i_0 for IAFPC and non-IA FPC with $\epsilon = 1$, $p_{max} \rightarrow \infty$ and $p_{max} = 5$ dBm.

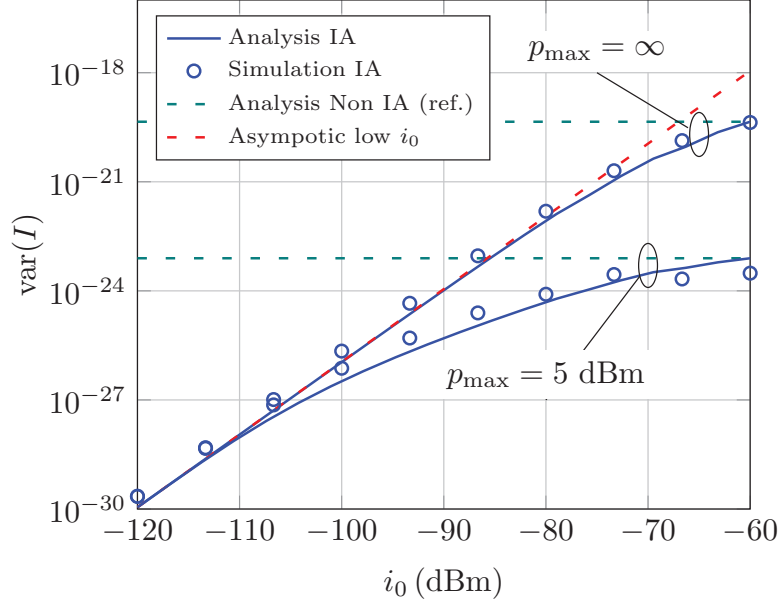


Figure 2.4: Variance of the interference versus i_0 for IAFPC and non-IA FPC with $\epsilon = 1$, $p_{\max} \rightarrow \infty$ and $p_{\max} = 5$ dBm.

2.6.1 Average Transmitted Power, Mean and Variance of the Interference

In this section, the average transmitted power, the average interference and the variance of the interference are obtained and compared against simulations. It is important to remark that the locations of the interfering MTs does not follow a PPP [26] and hence the interference in (2.8) is an approximation that aims to capture some spatial correlations among the locations of interfering MT and probe BS. Therefore, the performance indicators related to the interference (the mean and variance of the interference or the ccdf of the SINR) are approximations. On the other hand, theoretical results that do not involve the interference (the average transmitted power) are exact. This can be observed from Fig. 2.2 and Fig. 2.3 and Fig. 2.4

In Fig. 2.2, the average transmitted power versus i_0 for IAFPC and non-IA FPC schemes is presented, by assuming $p_{\max} \rightarrow \infty$ and $p_{\max} = 5$ dBm. Since i_0 plays no role in non-IA FPC case, the related curve is drawn only to facilitate the comparison. It can be observed that both IA and non-IA FPC methods provide the same average transmitted power for $i_0 = -60$ dBm. This is reasonable, since almost all the MTs do not truncate

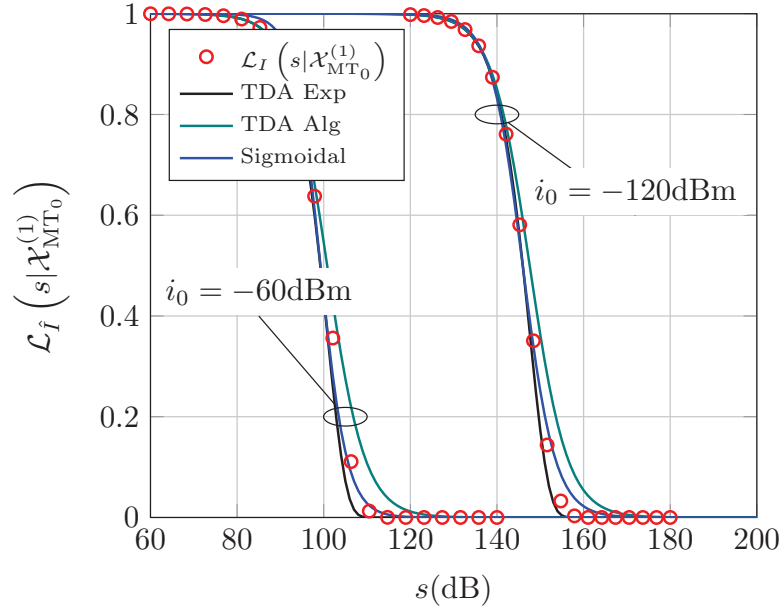


Figure 2.5: Laplace transform of the analytic interference I in (2.8) conditioned on $\mathcal{X}_{\text{MT}_0}^{(1)}$ and its approximation \hat{I} by using different approaches (IAFPC is assumed). As for the sigmoidal approximation, 8 equally spaced sample points between $s^{(\text{dB})} = 80$ and $s^{(\text{dB})} = 200$ dB are used, in order to obtain its related parameters b_0 and $s_0^{(\text{dB})}$.

their transmit power due to i_0 if i_0 is sufficiently high.

Let us consider the asymptotic analysis (red curve). It increases unboundedly with i_0 , and hence the proposed approximation of the transmitted power is accurate only for small values of i_0 . This is in agreement with the assumption of our analysis, i.e., i_0 needs to be small enough as discussed in Section 2.5. The same holds for the mean and the variance of the interference that are illustrated in Fig. 2.3 and Fig. 2.4. A high value of the variance of the interference degrades the estimation of the SINR, which, in turn, negatively affects the performance of AMC schemes in real implementations [49]. Hence, methods that reduce the variance of the interference are important. From the figures illustrated in this section, we evince that IAFPC reduces both the mean and the variance of the interference, as well as the average transmitted power when it is compared to non-IA FPC methods. This is the beneficial impact of IA.

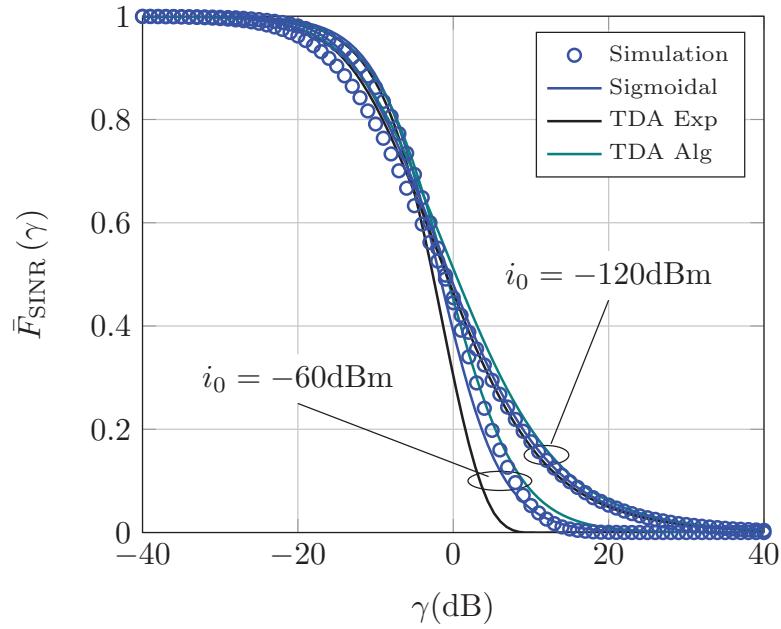


Figure 2.6: cdf of the SINR for the typical MT (IAFPC is assumed) with $\epsilon = 1$ and $i_0 = \{-120, -60\}$ dBm.

2.6.2 Approximations of the Interference

From Sections 2.2 and 2.4, we know that the exact interference is intractable, since the positions of the interfering MTs do not follow a PPP. Thus, approximations for the interference are proposed (2.8). Although the proposed approximation of the interference, I , leads to tractable expressions, the numerical complexity of the obtained expressions require further approximations if IAFPC schemes are used. Hence, in Section 2.4 two approaches to approximate the interference I with \hat{I} were proposed. The aim of this section is to compare such approaches in terms of the Laplace transform of its pdf. Fig. 2.5 illustrates the Laplace transform of \hat{I} for the sigmoidal and the TDA approximations, by conditioning on the event that the probe MT is associated with tier 1. The s-axis is expressed in dB and hence it is possible to observe the s-shape of the Laplace transform. The logistic regression of the sigmoidal approximation is obtained by assuming 8 equally spaced points that lie in the range $s = 60$ dB and $s = 200$ dB. It can be noted that the difference in the Laplace transform of the interference in the range $i_0 = -60$ dBm and $i_0 = -120$ dBm is large and such difference tends to increase for values larger than $i_0 = -60$ dBm. All

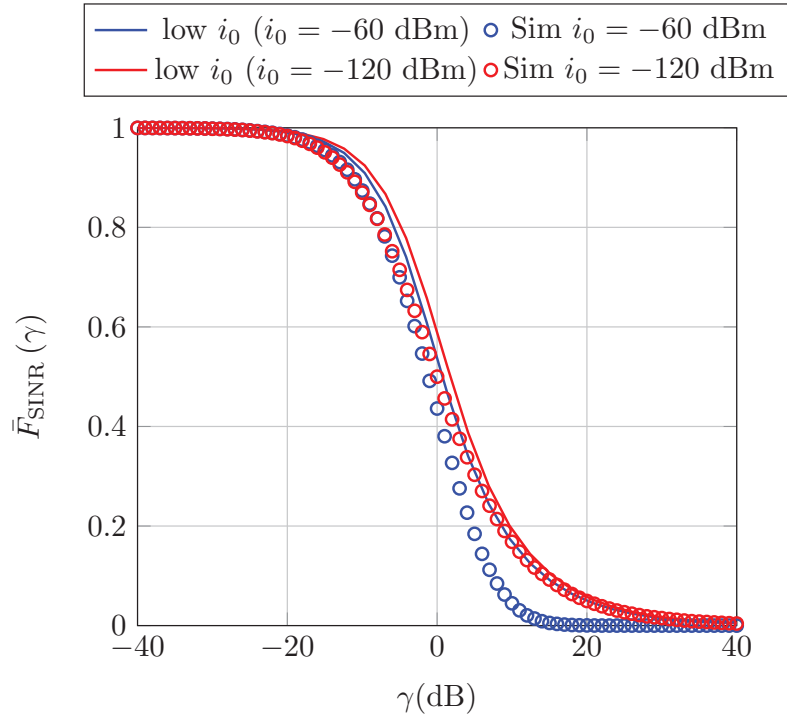


Figure 2.7: cdf of the SINR in the low i_0 regime given by (2.46) and by using the minimum path loss association.

approximations, however, follow the same trend as the Laplace transform of the analytical interference I and are sufficiently accurate for a large set of parameters.

2.6.3 cdf of the SINR

In this section, numerical illustrations for the cdf of the SINR are provided and analytical and simulation results are compared by considering $p_{\max} \rightarrow \infty$. Fig. 2.6 illustrates the cdf of the SINR, by assuming IAFPC with $\epsilon = 1$. It can be observed that the sigmoidal and the TDA approximations based on an algebraic function provides a better approximation of the cdf than those provided by the TDA approximation based on the exponential function. This is especially true if $i_0 = -120$ and $i_0 = -60$ dBm.

Finally, Fig. 2.7 compares the cdf of the SINR in the low i_0 regime, which is available in (2.46), and that obtained from simulation results. The minimum path loss cell association and $\epsilon = 1$ are assumed. As mentioned in Section 2.5, the proposed asymptotic analysis in the low i_0 regime provides performance results that are accurate only if i_0

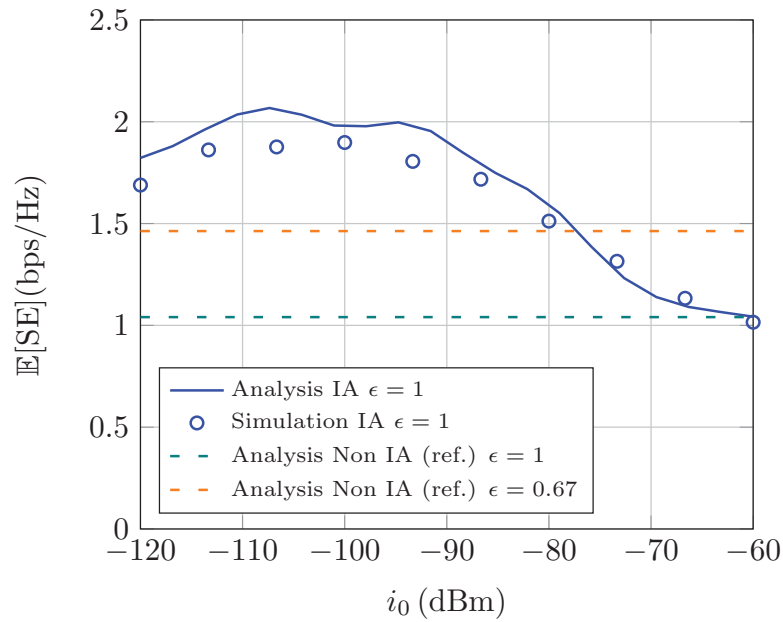


Figure 2.8: Average SE versus i_0 (IAFPC is assumed) for $p_{\max} \rightarrow \infty$.

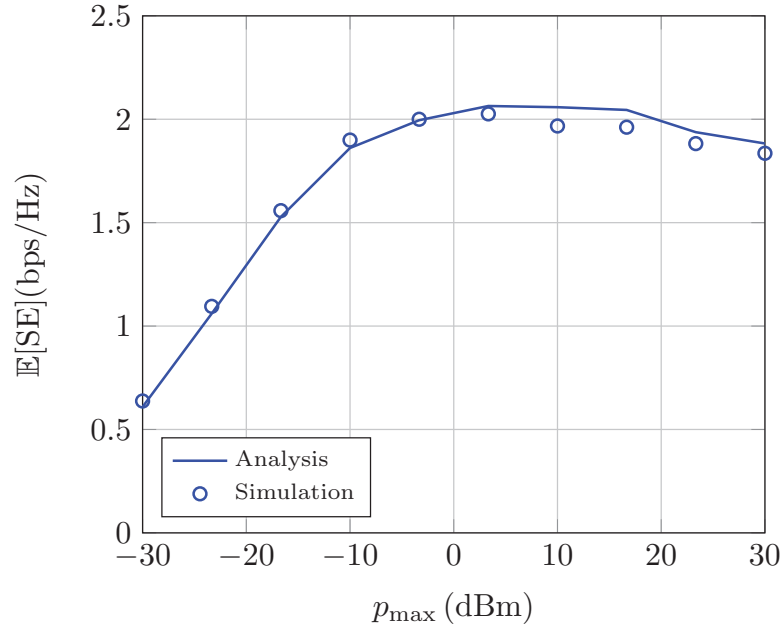


Figure 2.9: Average SE versus p_{\max} (IAFPC is assumed) for $i_0 = -90$ dBm.

is small. Hence, it can be observed a good match between simulation and analysis for

$i_0 = -120$ dBm. The accuracy is, on the other hand, reduced if $i_0 = -60$ dBm as it was expected, since in this case i_0 is not sufficiently small.

2.6.4 Spectral Efficiency

In this section, the average SE of IA and non-IA schemes is studied and compared. Such metric represents how well a MT exploits the available bandwidth and it is expressed in terms of bits per second per Hertz (bps/Hz). As far as the IAFPC setup is considered, the sigmoidal approximation of the interference is considered. In particular, 8 equally spaced sample points in the range $s^{(\text{dB})} = 60$ dB and $s^{(\text{dB})} = 200$ dB are considered.

Fig. 2.8 illustrates the average SE versus i_0 for the IAFPC scheme with $\epsilon = 1$ and for the non-IA FPC scheme with $\epsilon = 1$ and $\epsilon = 0.67$. It is observed that IA outperforms non-IA, in terms of average SE as well. The reason is that only the transmit power of the MTs that cause strong interference is truncated by i_0 , while the rest of the transmissions of the MTs are not truncated. This keeps under control the interference and the average SE improves. It is worth noting that there exist an optimal value for i_0 .

Fig. 2.9 illustrates the average SE versus p_{\max} with $\epsilon = 1$. It can be observed that reducing p_{\max} causes a performance loss since the MTs cannot compensate for the associated path losses.

Finally, Fig. 2.10 illustrates the average SE versus ϵ for IA and non-IA FPC schemes. As far as the non-IA FPC scheme is concerned, there exists an optimal value (around $\epsilon = 0.67$) that maximizes the SE. This is due to the fact that the total compensation of the path loss and shadowing ($\epsilon = 1$) causes strong interference to neighboring cells. Hence, partial compensation provides a better balance between interference and desired power that maximizes the average SE. As far as the IAFPC scheme is concerned, on the other hand, the maximum SE is reached by applying the total compensation of the path loss, i.e. for $\epsilon = 1$. This is due to the fact that IAFPC reaches a good balance between interference and desired power by means of the maximum allowed interference level i_0 . Hence, it can be observed that IAFPC outperforms non-IA FPC if i_0 lies in between -80 and -120 dBm.

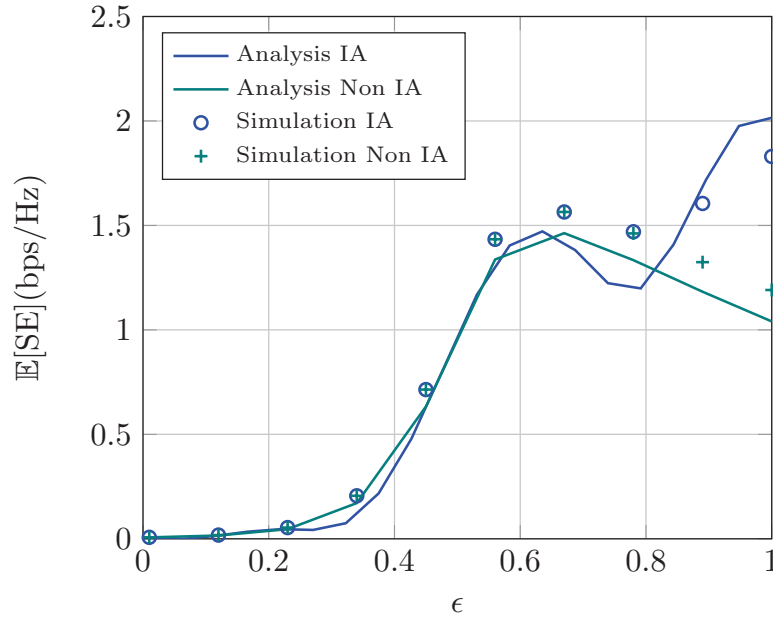


Figure 2.10: Average SE versus ϵ for the IAFPC scheme with $i_0 = -95$ dBm and for the non-IA scheme.

2.7 Discussion

In this chapter, a general framework to analyze IAFPC for the UL of HCNs is presented. For mathematical tractability, we model the locations of the interfering MTs as a PPP by enforcing some spatial correlation constraints between the probe BS and the interfering MTs. By using the proposed approach, we provide mathematical expressions for several performance metrics, including the average transmitted power, the mean and variance of the interference and the average SE. With the objective to reduce the computational complexity of the resulting mathematical frameworks, two approximations of the interference are proposed as well. Finally, asymptotic results are presented which provide further insight into fundamental performance trends in the presence of IAFPC. The accuracy of the proposed approach is assessed via Monte Carlo simulations, and it is shown that IAFPC is capable of reducing the transmitted power, of reducing the mean and the variance of the interference as well as of increasing the average SE.

The contributions mentioned above have been published in [47].

2.8 Appendix: Proof of Lemma 1

If $j \neq m$, the probability of $\mathcal{X}_{\text{MT}_0}^{(j,m)}$ can be written as

$$\begin{aligned} \Pr \left(\mathcal{X}_{\text{MT}_0}^{(j,m)} \right) &= \mathbb{E}_{R_{\text{MT}_0,(1)}^{(j)}, R_{\text{MT}_0,(2)}^{(j)}} \left[\mathbf{1} \left(R_{\text{MT}_0,(2)}^{(j)} > \left(\frac{t^{(m)}}{t^{(j)}} \right)^{\frac{1}{\alpha}} R_{\text{MT}_0,(1)}^{(j)} \right) \right. \\ &\times \left. \left(\bar{F}_{R_{\text{MT}_0,(1)}^{(m)}} \left(\left(\frac{t^{(m)}}{t^{(j)}} \right)^{\frac{1}{\alpha}} R_{\text{MT}_0,(1)}^{(j)} \right) - \bar{F}_{R_{\text{MT}_0,(1)}^{(m)}} \left(R_{\text{MT}_0,(2)}^{(j)} \right) \right) \right] \end{aligned} \quad (2.47)$$

In the above expression, we have used the fact that $R_{\text{MT}_0,(1)}^{(m)}$ and the two correlated RVs $\{R_{\text{MT}_0,(1)}^{(j)}, R_{\text{MT}_0,(2)}^{(j)}\}$ are statistically independent. The proof follows by computing the expectation using the joint pdf of $\{R_{\text{MT}_0,(1)}, R_{\text{MT}_0,(2)}\}$ given in (2.14).

Likewise, if $j = m$ we have

$$\Pr \left(\mathcal{X}_{\text{MT}_0}^{(j,j)} \right) = \mathbb{E}_{R_{\text{MT}_0,(1)}^{(j)}, R_{\text{MT}_0,(2)}^{(j)}} \left[\bar{F}_{R_{\text{MT}_0,(1)}^{(j)}} \left(\max \left(\left(\frac{t^{(j)}}{t^{(j)}} \right)^{\frac{1}{\alpha}} R_{\text{MT}_0,(1)}^{(j)}, R_{\text{MT}_0,(2)}^{(j)} \right) \right) \right] \quad (2.48)$$

The computation of the expectation with respect to $R_{\text{MT}_0,(1)}^{(j)}, R_{\text{MT}_0,(2)}^{(j)}$ completes the proof.

2.9 Appendix: Proof of Lemma 2

If $j \neq m$, the joint pdf of the distances towards the serving BS and the most interfered BS can be expressed as

$$f_{R_{\text{MT}_0}, U_{\text{MT}_0}} \left(v, w | \mathcal{X}_{\text{MT}_0}^{(j,m)} \right) = \frac{d^2}{dvdw} \frac{\Pr \left(R_{\text{MT}_0,(1)}^{(j)} \leq v, R_{\text{MT}_0,(1)}^{(m)} \leq w, \mathcal{X}_{\text{MT}_0}^{(j,m)} \right)}{\Pr \left(\mathcal{X}_{\text{MT}_0}^{(j,m)}, \mathcal{A}_{\text{MT}_0} \right)} \quad (2.49)$$

The numerator of the previous expression can be formulated as

$$\begin{aligned} \Pr \left(R_{\text{MT}_0,(1)}^{(j)} \leq v, R_{\text{MT}_0,(1)}^{(m)} \leq w, \mathcal{X}_{\text{MT}_0}^{(j,m)} \right) &= \mathbb{E}_{R_{\text{MT}_0,(1)}^{(j)}, R_{\text{MT}_0,(2)}^{(j)}} \mathbb{E}_{R_{\text{MT}_0,(1)}^{(m)}} \left[\right. \\ &\mathbf{1} \left(R_{\text{MT}_0,(1)}^{(m)} > \left(\frac{t^{(m)}}{t^{(j)}} \right)^{\frac{1}{\alpha}} R_{\text{MT}_0,(1)}^{(j)} \right) \\ &\left. \mathbf{1} \left(R_{\text{MT}_0,(1)}^{(m)} < R_{\text{MT}_0,(2)}^{(j)} \right) \mathbf{1} \left(R_{\text{MT}_0,(1)}^{(j)} \leq v \right) \mathbf{1} \left(R_{\text{MT}_0,(1)}^{(m)} \leq w \right) \right] \end{aligned} \quad (2.50)$$

The above expression can be expressed as the following triple integral

$$\begin{aligned} &\int_{r_1^{(m)}=0}^w \int_{r_1^{(j)}=0}^v \int_{r_2^{(j)}=1}^{\infty} f_{R_{\text{MT}_0,(1)}^{(j)}, R_{\text{MT}_0,(2)}^{(j)}} \left(r_1^{(j)}, r_2^{(j)} \right) f_{R_{\text{MT}_0,(1)}^{(m)}} \left(r_1^{(m)} \right) \mathbf{1} \left(R_{\text{MT}_0,(1)}^{(m)} < R_{\text{MT}_0,(2)}^{(j)} \right) \\ &\mathbf{1} \left(r_2^{(j)} > \left(\frac{t^{(m)}}{t^{(j)}} \right)^{\frac{1}{\alpha}} r_1^{(j)} \right) dr_2^{(j)} dr_1^{(j)} dr_1^{(m)} \end{aligned} \quad (2.51)$$

The proof follows by computing the inner integral with respect to $r_2^{(j)}$ and then applying the Leibniz integration rule.

Likewise, if $j = m$ the numerator can be expressed as

$$\int_{r_1^{(j)}=0}^v \int_{r_2^{(j)}=1}^w f_{R_{\text{MT}_0,(1)}^{(j)}, R_{\text{MT}_0,(2)}^{(j)}} \left(r_1^{(j)}, r_2^{(j)} \right) \bar{F}_{R_{\text{MT}_0,(1)}^{(j)}} \left(\max \left(\left(\frac{t^{(j)}}{t^{(j)}} \right)^{\frac{1}{\alpha}} r_1^{(j)}, r_2^{(j)} \right) \right) dr_2^{(j)} dr_1^{(j)} \quad (2.52)$$

The proof follows from the Leibniz integration rule.

2.10 Appendix: Proof of Lemma 1

The Laplace transform of the interference can be expressed as

$$\begin{aligned}
 \mathcal{L}_I \left(s | \mathcal{X}_{\text{MT}_0}^{(j)} \right) &= \mathbb{E}_I \left[e^{-sI} | \mathcal{X}_{\text{MT}_0}^{(j)} \right] = \prod_{k \in \mathcal{K}} \mathbb{E}_{\Psi^{(k)}} \\
 &\prod_{\text{MT}_i \in \Psi^{(k)}} \mathbb{E}_{R_{\text{MT}_i}, U_{\text{MT}_i}} \left[\mathbb{E}_{H_{\text{MT}_i}} \exp \left(-s H_{\text{MT}_i} (\tau D_{\text{MT}_i})^{-\alpha} \right. \right. \\
 &\left. \left. p_{\text{MT}} (R_{\text{MT}_i}, U_{\text{MT}_i}) \mathbf{1} \left(\mathcal{O}_{\text{MT}_i}^{(j,k)} \right) \mathbf{1} \left(\mathcal{Z}_{\text{MT}_i} \right) \right) | \mathcal{X}_{\text{MT}_i}^{(k)} \right] \quad (2.53)
 \end{aligned}$$

The RVs $\{R_{\text{MT}_i}, U_{\text{MT}_i}\}$ are iid and their joint pdf is given in Lemma 2. Applying the Probability Generating Function theorem, computing the expectation over the fading and by conditioning over the event $\mathcal{Q}_{\text{MT}_i}^{(n)}$ yields

$$\begin{aligned}
 \mathcal{L}_I \left(s | \mathcal{X}_{\text{MT}_0}^{(j)} \right) &= \exp \left(- \sum_{k \in \mathcal{K}} 2\pi \lambda^{(k)} \sum_{n \in \mathcal{K}} \Pr \left(\mathcal{Q}_{\text{MT}_i}^{(n)} | \mathcal{X}_{\text{MT}_i}^{(k)} \right) \times \int_{r=0}^{\infty} \int_{u=\left(\frac{t^{(n)}}{t^{(k)}}\right)^{\frac{1}{\alpha}} r}^{\infty} \right. \\
 &\left. f_{R_{\text{MT}_i}, U_{\text{MT}_i}} \left(r, u | \mathcal{X}_{\text{MT}_i}^{(k,n)} \right) \int_{\rho=\max\left(\left(\frac{t^{(j)}}{t^{(k)}}\right)^{\frac{1}{\alpha}} r, \frac{1}{\tau} \left(\frac{p_{\text{MT}}(r,u)}{i_0}\right)^{\frac{1}{\alpha}}\right)}^{\infty} \frac{s (\tau \rho)^{-\alpha} p_{\text{MT}}(r, u) \rho d\rho dr}{1 + s (\tau \rho)^{-\alpha} p_{\text{MT}}(r, u)} \right) \quad (2.54)
 \end{aligned}$$

Computing the integration with respect to ρ completes the proof.

Chapter 3

Performance Analysis of Interference-Aware Muting

We investigate the performance of a scheduling algorithm where the Mobile Terminals (MTs) may be turned off if they cause a level of interference greater than a given threshold. This approach, which is referred to as Interference Aware Muting (IAM), may be regarded as an interference-aware scheme that is aimed to reduce the level of interference. We analyze its performance with the aid of stochastic geometry and compare it against other interference-unaware and interference-aware schemes, where the level of interference is kept under control in the power control scheme itself rather than in the scheduling process. IAM is studied in terms of average transmit power, mean and variance of the interference, coverage probability, Spectral Efficiency (SE), and Binary Rate (BR), which accounts for the amount of resources allocated to the typical MT. Simplified expressions of SE and BR for adaptive modulation and coding schemes are proposed, which better characterize practical communication systems. Our system-level analysis unveils that IAM increases the BR and reduces the mean and variance of the interference. It is proved that an operating regime exists, where the performance of IAM is independent of the cell association criterion, which simplifies the joint design of uplink and downlink transmissions.



3.1 Introduction

Interference awareness can be exploited at both the physical and Medium Access Control (MAC) layers to boost the performance of mobile networks. It is especially useful in the Uplink (UL) of Heterogeneous Cellular Networks (HCNs) for interference mitigation and performance enhancement. In current HCNs, the Mobile Terminals (MTs) are associated with the same Base Station (BS) in the UL and Downlink (DL) [7]. The cell association is performed based on DL pilot signals and the serving BS is chosen based on a given criterion, e.g., the highest average received power in the DL. In the UL, the same BS is used [7] which leads to a situation where MTs are associated with distant BSs. In this context, the use of Fractional Power Control (FPC) accentuates the detrimental effect of the MTs that cause strong interference to neighboring BSs.

3.1.1 UL Analysis: State-of-the-Art

The complex aforementioned interactions between power control and association in the UL require accurate mathematical frameworks to gain insights about the performance trends and limits of existing and future networks. Unfortunately, the mathematical analysis of the UL of HCNs is more involved than the analysis of the DL for two main reasons: i) due to the use of power control, the transmit power of the MTs depends on the distance to their serving BSs and ii) even though the locations of BSs and MTs are drawn from two independent Poisson Point Processes (PPPs), the locations of the interfering MTs scheduled in a given orthogonal Resource Block (RB) do not follow a PPP. These two peculiarities as compared to the DL make the mathematical analysis of the UL intractable without resorting to approximations [26]. In [29] it is studied the case of homogeneous cellular networks with FPC. To avoid such a mathematical intractability, it is assumed that the MTs that are scheduled in a given RB form a Voronoi tessellation and a single BS is available in each Voronoi cell. However, such an approach does not consider HCNs. The case of the UL of HCNs is accurately modeled in recent works like [26, 31, 32, 47], where it is considered the spatial correlation between the location of the probe BS and those of the interfering MTs. In [31], is studied a framework to model HCNs with a truncated channel inversion power control under smallest path loss association. In this work it is considered an homogeneous PPP as a generative process for the locations

of interfering MTs, but then, the spatial correlation is added by means of an indicator function that discards interfering MTs' locations based on their received powers. The case of UL and DL with decoupled access is considered in [26]. The association is based on maximum weighted received powers and FPC is considered in the UL. Here, to account for the spatial correlation a non-homogeneous PPP is considered to model the locations of interfering MTs. A framework for the UL of HCNs with multi-antenna BSs is studied in [32]. In this work it is considered FPC under a generalized association criteria and two extreme detection techniques in terms of complexity and performance: Maximum Ratio Combining (MRC) and Optimum Combining (OC). It is demonstrated that OC, which can be regarded as an interference-aware detection technique for multi-antenna receivers, greatly outperforms MRC when MTs use aggressive power control, i.e., when the interference is high. The spatial correlation is imposed by means of a conditional thinning that takes into account the generalized cell association procedure. Interference-awareness is also studied in [47], which considers HCNs with single-antenna BSs. In this work, it is studied a power control mechanism [49], which is referred to as Interference Aware Fractional Power Control (IAFPC). This approach consists of introducing a maximum interference level, i_0 , that the transmission of each MT is allowed to cause to its most interfered BS. In simple terms, the MTs adjust their transmit power in order to cause a maximum interference level of i_0 to their most interfered BS.

In the present chapter, we investigate another option for interference mitigation in the UL and compare it with previously reported schemes. The approach consists of exploiting interference-awareness when scheduling the transmission of the MTs, rather than in the power control scheme itself (IAFPC) or in the detection process of the receiver (OC). As a result, interference management is conducted at the MAC layer rather than at the physical layer. The considered approach is referred to as Interference Aware Muting (IAM) and consists of turning off, i.e., muting, the MTs whose interference towards the most interfered BS is above a given threshold. The main difference between IAFPC and IAM can be summarized as follows. In IAFPC, all the MTs are active and adjust their transmit power for interference mitigation. In IAM, on the other hand, the transmit power of the MTs does not account for any interference constraints but some MTs may not be allowed to transmit if they produce too much interference. As a result, IAM has the potential of reducing the aggregate interference in the UL and of enabling the active

MTs to better use the available resources, i.e., the transmission bandwidth. On the other hand, it reduces the fairness of allocating the resources among the MTs, since some of them may be turned off. Nevertheless, thanks to mobility and shadowing, muted MTs are only inactive for a given period of time. Hence, from the perspective of MTs the question to answer is whether this muting increases its achievable Binary Rate (BR), taking into account both the active and inactive periods. The main objective of the present chapter is to quantify the advantages and the limitations of IAM and compare it against the IAFPC scheme.

3.1.2 Technical Contribution

In this chapter, we overcome this mathematical intractability by using an approach similar to [32] and [47], which is referred to as *conditional thinning*. In simple terms, the locations of the active MTs are assumed to be drawn from a PPP but spatial constraints (correlations) are introduced, which account for the location of the serving BS, for the location of the most interfered BS, and for the maximum level of interference allowed. Based on these modeling assumptions, which are validated against extensive Monte Carlo simulations, we provide the following contributions.

- We study IAM scheme in terms of average transmit power of the MTs, mean and variance of the interference. The mathematical analysis reveals that IAM is capable of reducing the three latter performance metrics compared with IAFPC, which results in several advantages for practical implementations. Reducing the variance of the interference, e.g., is beneficial for better estimating the SINR and, thus, for reducing the error probability of practical decoding schemes, e.g., turbo decoding, [48], and for making easier the selection of the most appropriate Modulation and Coding Scheme (MCS) to use in LTE systems [49].
- To make our study and conclusions directly applicable to current communication systems that are based on Adaptive Modulation and Coding (AMC) transmission, we provide tractable expressions of SE and BR based on practical MCSs that are compliant with the LTE standard and whose parameters are obtained from a link-level simulator [1, 2].

- With the aid of the proposed mathematical frameworks, we compare IAFPC and IAM schemes in terms of SE and BR, which provide different information on their strengths and weaknesses. The SE provides information on how well the MTs exploit the available resources (e.g., bandwidth) that are shared among the MTs served by the same BS, whereas the BR accounts for the specific fraction of resources that is allocated to each MT served by a given BS. While the IAFPC scheme is superior in terms of SE, the IAM scheme is superior in terms of RB. This implies that IAM provides service to fewer users, which get better performance compared with IAFPC. To characterize this trade-off, we investigate the fairness of both schemes, which is defined as the probability that a randomly chosen MT gets access to the resources, and provide a tractable frameworks for its analysis.
- In light of the emerging UL-DL decoupling principle, we develop the mathematical frameworks for a General Cell Association (GCA) criterion, whose association weights may be appropriately optimized for performance enhancement. By direct inspection of the mathematical frameworks, we prove that three operating regimes can be identified as a function of the interference threshold i_0 : i) the first, where the performance is independent of i_0 , ii) the second, where the performance depends on i_0 but it does not depend on the cell association, and iii) the third, where the performance depends on i_0 and the cell association. Of particular interest in this chapter is the second regime, which highlights that UL-DL decoupling may not be an issue for some system setups, which in turn simplifies the design of HCNs.
- As for the relevant case study for the UL where the serving BS of the typical MT is identified based on the Smallest Path-Loss Association (SPLA) criterion with channel-inversion power control [7], we provide simple and closed-form frameworks for relevant performance indicators and prove that two operating regimes exist: i) the first, where the performance depends on i_0 (interference-aware) and ii) the second, where the performance is independent of i_0 (interference-unaware). We prove, in addition, that i) the scaling law of the average transmit power of the MTs, the mean interference and the probability that a MT gets access to the resources is a polynomial function of i_0 whose exponent depends on the path-loss exponent, ii) the distance towards the serving BS gets smaller as i_0 increases; and iii) the CCDF of the SINR is independent of the density of BSs.

To the best of authors knowledge, all these contributions are new in the literature and are not included in previous works. For instance, the muting mechanism introduces further correlations that do not exist in [47] and need to be taken into account. This muting differentiates the whole analysis. New metrics like the BR, which accounts for the amount of resources allocated by the scheduler, are obtained and it is also introduced a new framework to compute the SE and BR with AMC, which is closer to real systems than Shannon formula. Finally, a lot of closed-form expressions and remarks are obtained which provide important insights about system performance, fairness and cell association.

The remainder of this chapter is organized as follows. Section 3.2 introduces the system model and the approach for system-level analysis. In Sections 3.3 and 3.4, the analysis of IAM is presented for GCA and SPLA criteria, respectively. The BR of AMC schemes is analyzed and discussed in Section 3.5. In Section 3.6, IAM and IAFPC schemes are compared against each other via numerical simulations and the main findings and performance trends derived in the chapter are substantiated with the aid of Monte Carlo simulations. Finally, Section 3.7 concludes this chapter.

Notation: A summary of the main symbols and functions used throughout the present chapter is provided in Table 3.1 for the convenience of the readers.

3.2 System Model

We consider the UL of a HCN composed of two tiers, $j \in \mathcal{K} = \{1, 2\}$, e.g., macro and small-cell BSs, which are spatially distributed according to two independent PPPs, $\Phi^{(j)}$, of intensities $\lambda^{(j)}$. Each transmitted signal goes through an independent multi-path fading channel with Rayleigh fading and log-normal shadowing. The path-loss is modeled by using a path-loss slope τ and a path-loss exponent $\alpha > 2$ ¹. The cell association among MTs and BSs is based on the weighted average received power criterion, similar to [26], where the association weights are denoted by $t^{(j)}$ for tier $j \in \mathcal{K}$. Hence, the i th MT is associated with the n th BS of tier j if the MT is in the weighted Voronoi cell of $\text{BS}_n^{(j)}$ with respect to $\Phi = \bigcup_{j \in \mathcal{K}} \Phi^{(j)}$. With these assumptions, shadowing can be modeled as a random displacement [61] of $\Phi^{(j)}$ [47, 79].

¹ The proposed framework can be generalized to account for a bounded path loss model; however, an unbounded path loss model has been used for the sake of mathematical tractability.

Table 3.1: Summary of main symbols and functions used throughout the chapter.

Symbol/function	Definition
$\Gamma(z)$, $\Gamma(a, z)$	Euler gamma function and incomplete gamma function
$f_X(\cdot)$, $F_X(\cdot)$, $\mathcal{L}_X(\cdot)$	PDF, CCDF and Laplace transform of a random variable X
$f'(x_0)$, $f''(x_0)$	First and second derivatives of $f(x)$ evaluated at $x = x_0$
$\mathbb{E}[\cdot]$, $\Pr(\cdot)$, $\mathbf{1}(\cdot)$	Expectation operator, probability measure and indicator function
${}_2F_1(\cdot, \cdot, \cdot, \cdot)$	Gauss Hypergeometric function
$\mathcal{K} = \{1, 2\}$	Tier set: tier 1 is related to macro BSs and tier 2 is related to small cell BSs
$\tilde{j} = \{k \in \mathcal{K} : k \neq j\}$	Complementary tier, i.e. $\tilde{1} = 2$ and $\tilde{2} = 1$
$\Phi^{(j)}$, $\lambda^{(j)}$	PPP and its density related to the locations of macro ($j = 1$) and small cell BSs ($j = 2$)
λ_{MT}	Density of the PPP of MTs' positions
Φ , λ	PPP and its density related to the locations of all BSs
$t^{(j)}$	Association weight for tier j
$i_0, p_0, \epsilon, p_{\max}$	Interference threshold, target receive power, partial compensation factor, and maximum transmit power
τ, α	Path loss slope and path loss exponent
MT_0, MT_i	Position of the probe MT and position of a generic MT, e.g., an interfering MT
$\Psi^{(k)}$	PPP of interfering MTs' locations
$R_{x,(q)}^{(j)}$	Distance (including shadowing) between location x and the q th nearest BS from tier j
$R_{\text{MT}_i}, U_{\text{MT}_i}, D_{\text{MT}_i}$	Distances (including shadowing) between MT_i and its serving BS, its most interfered BS and the probe BS
H_{MT_i}	Power gain of the fading which is exponentially distributed
$p_{\text{MT}}(r) = p_0 (\tau r)^{\alpha\epsilon}$	Transmit power, for a given distance r , towards the serving BS for active MTs. Muted MTs has 0 transmit power
σ_n^2, I	Noise power and interference according to Assumption 1
$\mathcal{X}_{\text{MT}_i}^{(j)}$	Event defined as: MT_i is associated with tier j
$\mathcal{Q}_{\text{MT}_i}^{(m)}$	Event defined as: the most interfered BS of MT_i belongs to tier m
$\mathcal{X}_{\text{MT}_i}^{(j,m)}$	Event defined as: MT_i is associated with tier j and the most interfered BS of MT_i belongs to tier m
$\mathcal{A}_{\text{MT}_i}$	Event defined as: MT_i is active, i.e., non-muted
$\mathcal{O}_{\text{MT}_i}^{(j,k)}$	Event defined as: the interfering MT_i of tier k receives higher weighted average power from its serving BS than from the probe BS that belong to tier j
$\mathcal{Z}_{\text{MT}_i}$	Event defined as: the interfering MT_i causes a level of interference less than i_0 to the probe BS

For ease of writing, we introduce the event $\mathcal{X}_{\text{MT}_i}^{(j)}$ as follows.

Definition 1. The event $\mathcal{X}_{\text{MT}_i}^{(j)}$ is defined as “ MT_i is associated with tier j ”.

In mathematical terms, therefore, the association criterion can be formulated as follows:

$$\mathcal{X}_{\text{MT}_i}^{(j)} = \left\{ t^{(j)} \left(\tau R_{\text{MT}_i, (1)}^{(j)} \right)^{-\alpha} > t^{(\tilde{j})} \left(\tau R_{\text{MT}_i, (1)}^{(\tilde{j})} \right)^{-\alpha} \right\} \quad (3.1)$$

where $(\tau R_{\text{MT}})^{-\alpha}$ is the path-loss at a distance² R_{MT} from the transmitter, $\tilde{j} = \{k \in \mathcal{K} : k \neq j\}$ is the complementary tier of j , i.e., $\tilde{1} = 2$ and $\tilde{2} = 1$, $R_{x, (q)}^{(\tilde{j})}$ is the distance from x to the q th nearest BS of tier \tilde{j} , i.e., $R_{x, (1)}^{(\tilde{j})}$ is the distance to the nearest BS. The association weights $t^{(1)}$ and $t^{(2)}$ allow us to model the GCA criterion, which encompasses the SPLA criterion for $t^{(1)} = t^{(2)}$.

Throughout this chapter, the analysis is performed for the probe or typical MT, i.e., for a randomly chosen MT, which is denoted by MT_0 . Its serving BS is referred to as the probe BS.

3.2.1 Scheduling

We consider full-frequency reuse, where all the BSs share the same bandwidth. Each BS has available a bandwidth of b_w Hz that is shared among the MTs that are in its Voronoi cell. In practice, b_w is divided in orthogonal RBs and each scheduled MT in each cell transmits in one (or several) of these RBs. Thus, no intra-cell interference is available. This implies that a single MT per BS can interfere with the probe MT. The set of active interfering MTs of tier k that are scheduled for transmission in a given RB is denoted by $\Psi^{(k)}$. For tractability, we assume that the number of RBs is large enough to be regarded as a continuous resource by the scheduler.

Based on these assumptions, the scheduling process of every BS consists of two steps:

1. To determine the set of active MTs. The active transmitters are the MTs that, simultaneously, cause less interference than i_0 to any BSs and that transmit with less power than p_{max} . The MTs that do not fulfill these two constraints are turned off (muted).

²Throughout this chapter, all the distances implicitly include shadowing.

2. Resource allocation. Once the active MTs in each cell are identified, the bandwidth of each BS is equally divided among the active MTs associated with it. Let $N_{\text{BS}_n^{(j)}}^{\mathcal{A}}$ be the number of MTs associated with BS $\text{BS}_n^{(j)}$. Each of them is allocated a bandwidth $b_w/N_{\text{BS}_n^{(j)}}^{\mathcal{A}}$ ³ Hz.

This scheduling process characterizes the IAM scheme and makes it different from the IAFPC scheme in [47]. In [47], all the MTs are active and power control is responsible for controlling the level of interference, by making sure that the interference level at any BS is less than i_0 .

To better understand the implications of interference awareness on turning off (muting) some MTs, we analyze the case study $i_0 \rightarrow \infty$ as well, which is referred to as Interference-Unaware Muting (IUM)⁴. For ease of writing, we introduce some definitions that are useful for mathematical analysis.

Definition 2. The event $\mathcal{Q}_{\text{MT}_i}^{(m)}$ is defined as “the most interfered BS of MT_i belongs to tier m ”.

Definition 3. The event $\mathcal{X}_{\text{MT}_i}^{(j,m)} = \mathcal{X}_{\text{MT}_i}^{(j)} \cap \mathcal{Q}_{\text{MT}_i}^{(m)}$ is defined as “ MT_i is associated with tier j and the most interfered BS of MT_i belongs to tier m ”.

In mathematical terms, $\mathcal{X}_{\text{MT}_i}^{(j,m)}$ can be formulated as follows:

$$\begin{aligned} \mathcal{X}_{\text{MT}_i}^{(j,m)} &= \mathcal{X}_{\text{MT}_i}^{(j)} \cap \overbrace{\left\{ R_{\text{MT}_i,(2)}^{(j)} > R_{\text{MT}_i,(1)}^{(m)} \right\}}^{\mathcal{Q}_{\text{MT}_i}^{(m)}}, \text{ if } j \neq m \\ \mathcal{X}_{\text{MT}_i}^{(j,m)} &= \mathcal{X}_{\text{MT}_i}^{(j)} \cap \overbrace{\left\{ R_{\text{MT}_i,(2)}^{(j)} < R_{\text{MT}_i,(1)}^{(j)} \right\}}^{\mathcal{Q}_{\text{MT}_i}^{(m)}}, \text{ if } j = m \end{aligned} \quad (3.2)$$

According to IAM, the MTs that either cause higher interference than i_0 or transmit with higher power than p_{\max} are kept silent. The set of active MTs is defined as follows.

³Although, in practice, the bandwidth is divided in RBs, we assume that it can be treated as a continuous resource and hence that it can be equally divided among the active MTs. This is assumed in [26] as well.

⁴In the present chapter, IUM and Interference Unaware FPC (IUFPC) schemes are similar but slightly different. IUM is referred to a setup where $i_0 \rightarrow \infty$ and $p_{\max} < \infty$. IUFPC is referred to a setup where $i_0 \rightarrow \infty$ and $p_{\max} \rightarrow \infty$. As for IUM, only the constraint on the maximum transmit power exists. As for IUFPC, there is no constraint on either the maximum transmit power or the maximum interference.

Definition 4. The event $\mathcal{A}_{\text{MT}_i}$ is defined as “ MT_i is active”.

In mathematical terms, $\mathcal{A}_{\text{MT}_i}$ can be formulated as follows:

$$\mathcal{A}_{\text{MT}_i} = \{(p_{\text{MT}}(R_{\text{MT}_i}) < i_0 (\tau U_{\text{MT}_i})^\alpha) \cap (p_{\text{MT}}(R_{\text{MT}_i}) < p_{\text{max}})\} \quad (3.3)$$

where $p_{\text{MT}}(r)$, p_0 and ϵ are related to power control and they are described in Table 3.1, R_{MT_i} is the distance between MT_i and its serving BS, and U_{MT_i} is the distance between MT_i and its most interfered BS. If the probe MT is associated with tier j , i.e., the event $\mathcal{X}_{\text{MT}_i}^{(j)}$ is true, then $R_{\text{MT}_i} = R_{\text{MT}_i,(1)}^{(j)}$. The distance U_{MT_i} depends, on the other hand, on the event $\mathcal{X}_{\text{MT}_i}^{(j,m)}$. Accordingly, $U_{\text{MT}_i} = R_{\text{MT}_i,(1)}^{(m)}$ if $j \neq m$ and $U_{\text{MT}_i} = R_{\text{MT}_i,(2)}^{(j)}$ if $j = m$. The aim of event $\mathcal{A}_{\text{MT}_i}$ is to capture the spatial correlation between the position of a given MT, its serving BS and its most interfered BS, which follows from the muting process.

As far as IAM is concerned, fractional power control is applied at the physical layer and is interference-unaware, i.e., the transmit power of the MTs that are not turned off depends only on path-loss and shadowing and it can be expressed as $p_{\text{MT}}(R_{\text{MT}_0})$. If the MTs are muted, on the other hand, their transmit power is equal to zero. This implies that their associated SINR, BR, etc. are, by definition, equal to zero as well.

3.2.2 SINR

The SINR of the typical active MT that is measured at the probe BS can be formulated as:

$$\text{SINR}_{\text{MT}_0} = \frac{H_{\text{MT}_0} (\tau R_{\text{MT}_0})^{-\alpha} p_{\text{MT}}(R_{\text{MT}_0})}{I + \sigma_n^2} \quad (3.4)$$

where H_{MT_0} is the channel gain, R_{MT_0} is the distance from the serving BS, $p_{\text{MT}}(R_{\text{MT}_0})$ is the transmit power, I is the other-cell interference, and σ_n^2 is the noise power.

In the UL, as discussed in Section 3.1, the set of interfering MTs does not constitute a PPP, even though the MTs and BSs are distributed according to a PPP. Further details can be found in [32] and [47]. This makes the mathematical analysis intractable. In the present chapter, the distinctive scheduling process of IAM negatively affects the mathematical tractability of the problem at hand even further. To make the analysis tractable, some approximations for modeling the set of active MTs are needed. In [32] and [47], it is shown that a tractable approximation consists of assuming that the set of active MTs can

still be modeled as a PPP, provided that appropriate spatial constraints on the locations of the MTs are introduced. Stated differently, the set of active MTs is modeled as a spatially-thinned PPP or equivalently as a non-homogeneous PPP.

Before introducing the approach to model interfering MTs' locations, the following events need to be defined:

Definition 5. The event $\mathcal{O}_{\text{MT}_i}^{(j,k)}$ is defined as “the interfering MT_i of tier k receives higher weighted average power from its serving BS than from the probe BS that belongs to tier j ”.

In mathematical terms, $\mathcal{O}_{\text{MT}_i}^{(j,k)}$ can be formulated as follows:

$$\mathcal{O}_{\text{MT}_i}^{(j,k)} = \{t^{(k)} (\tau R_{\text{MT}_i})^{-\alpha} > t^{(j)} (\tau D_{\text{MT}_i})^{-\alpha}\} \quad (3.5)$$

Definition 6. The event $\mathcal{Z}_{\text{MT}_i}$ is defined as “the interfering MT_i causes a level of interference less than i_0 to the probe BS”.

In mathematical terms, $\mathcal{Z}_{\text{MT}_i}$ can be formulated as follows:

$$\mathcal{Z}_{\text{MT}_i} = \{p_{\text{MT}} (R_{\text{MT}_i}) (\tau D_{\text{MT}_i})^{-\alpha} < i_0\} \quad (3.6)$$

Hence, inspired by [32] and [47], our mathematical framework is based on the following approximation.

Assumption 1. The other-cell interference of the typical active MT is approximated as [47]:

$$I \approx \sum_{k \in \mathcal{K}} \sum_{\text{MT}_i \in \Psi^{(k)}} \frac{H_{\text{MT}_i} p_{\text{MT}} (R_{\text{MT}_i})}{(\tau D_{\text{MT}_i})^\alpha} \mathbf{1}(\mathcal{O}_{\text{MT}_i}^{(j,k)}) \mathbf{1}(\mathcal{Z}_{\text{MT}_i}) \quad (3.7)$$

where $\Psi^{(k)}$ is a PPP of intensity $\lambda^{(k)}$ whose points constitute the locations of the interfering MTs that are scheduled for transmission in the same RB as that of the typical MT, the events $\mathcal{O}_{\text{MT}_i}^{(j,k)}$ and $\mathcal{Z}_{\text{MT}_i}$ take into account the necessary spatial constraints imposed by the cell association criterion and the maximum interference and power constraints, respectively, R_{MT_i} and D_{MT_i} are the distances from MT_i to its own serving BS and to the probe BS, respectively.

More specifically, i) the event $\mathcal{O}_{\text{MT}_i}^{(j,k)}$ is necessary to account for the spatial correlation that exists between the locations of the probe BS, the interfering MTs and their serving

BSs, since the interfering MTs must lie outside the Voronoi cell of the probe BS by definition of cell association, and ii) the event $\mathcal{Z}_{\text{MT}_i}$ is necessary to account for the fact that the interfering MTs need to cause less interference than i_0 according to the IAM scheduling process.

The next two sections provide mathematical expressions of the CCDF of the SINR and of the mean and variance of the other-cell interference for GCA and SPLA cell association criteria respectively.

3.3 General Cell Association Criterion

We start introducing some enabling results for proving the main theorems of this section.

Proposition 2. *The probability that the typical MT is active and is associated with tier j is:*

$$\Pr(\mathcal{A}_{\text{MT}_0}) = \sum_{j \in \mathcal{K}_{v>0}} \int \mathbf{1} \left(v < \frac{1}{\tau} \left(\frac{p_{\max}}{p_0} \right)^{\frac{1}{\alpha}} \right) (\nu^{(j)}(v) + \eta^{(j)}(v)) dv \quad (3.8)$$

where $\nu^{(j)}(v)$ and $\eta^{(j)}(v)$ are defined in (3.9) and (3.10), respectively.

$$\begin{aligned} \nu^{(j)}(v) = & 2\pi v \lambda^{(j)} \left(e^{-\pi \lambda^{(j)} v^2} \times \left(e^{-\pi \lambda^{(\tilde{j})} \max^2 \left(\left(\frac{p_0}{i_0} \right)^{\frac{1}{\alpha}} \frac{(\tau v)^\epsilon}{\tau}, \left(\frac{t^{(\tilde{j})}}{t^{(j)}} \right)^{\frac{1}{\alpha}} v \right)} - e^{-\pi \lambda^{(\tilde{j})} v^2} \right) \times \right. \\ & \mathbf{1} \left(v > \max \left(\left(\frac{p_0}{i_0} \right)^{\frac{1}{\alpha}} \frac{(\tau v)^\epsilon}{\tau}, \left(\frac{t^{(\tilde{j})}}{t^{(j)}} \right)^{\frac{1}{\alpha}} v \right) \right) \\ & \left. + \frac{\lambda^{(\tilde{j})}}{\lambda^{(j)} + \lambda^{(\tilde{j})}} e^{-\pi (\lambda^{(j)} + \lambda^{(\tilde{j})}) \max^2 \left(\left(\frac{p_0}{i_0} \right)^{\frac{1}{\alpha}} \frac{(\tau v)^\epsilon}{\tau}, \left(\frac{t^{(\tilde{j})}}{t^{(j)}} \right)^{\frac{1}{\alpha}} v, v \right)} \right) \end{aligned} \quad (3.9)$$

$$\begin{aligned}
\eta^{(j)}(v) &= 2\pi v \lambda^{(j)} \left(e^{-\pi \lambda^{(\tilde{j})} \left(\frac{t^{(\tilde{j})}}{t^{(j)}}\right)^{\frac{2}{\alpha}} v^2} \times \left(e^{-\pi \lambda^{(j)} \max^2 \left(\left(\frac{p_0}{i_0}\right)^{\frac{1}{\alpha}} \frac{(\tau v)^\epsilon}{\tau}, v \right)} - e^{-\pi \lambda^{(j)} \left(\frac{t^{(\tilde{j})}}{t^{(j)}}\right)^{\frac{2}{\alpha}} v^2} \right) \times \right. \\
&\quad \left. \mathbf{1} \left(v > \left(\frac{t^{(j)}}{t^{(\tilde{j})}}\right)^{\frac{1}{\alpha}} \max \left(\left(\frac{p_0}{i_0}\right)^{\frac{1}{\alpha}} \frac{(\tau v)^\epsilon}{\tau}, v \right) \right) \right. \\
&\quad \left. + \frac{\lambda^{(j)}}{\lambda^{(j)} + \lambda^{(\tilde{j})}} e^{-\pi(\lambda^{(j)} + \lambda^{(\tilde{j})}) \max^2 \left(\left(\frac{p_0}{i_0}\right)^{\frac{1}{\alpha}} \frac{(\tau v)^\epsilon}{\tau}, v, \left(\frac{t^{(\tilde{j})}}{t^{(j)}}\right)^{\frac{1}{\alpha}} v \right)} \right) \quad (3.10)
\end{aligned}$$

Proof. See Appendix 3.8. □

Proposition 2 is useful for understanding and quantifying the fairness of the IAM scheme. The higher $\Pr(\mathcal{A}_{\text{MT}_0})$ is, in fact, the higher the probability that a randomly chosen MT is served in a given RB and, thus, the higher the fairness that it gets access to the available resources is⁵.

Lemma 4. *The Probability Density Function (PDF) of the distance between the typical MT and its serving BS by conditioning on the event $\mathcal{X}_{\text{MT}_0}^{(j,m)} \cap \mathcal{A}_{\text{MT}_0}$ can be formulated as follows:*

$$f_{R_{\text{MT}_0}} \left(v | \mathcal{X}_{\text{MT}_0}^{(j,m)}, \mathcal{A}_{\text{MT}_0} \right) = \begin{cases} \frac{\nu^{(j)}(v)}{\Pr(\mathcal{X}_{\text{MT}_0}^{(j,m)}, \mathcal{A}_{\text{MT}_0})} & \text{for } 0 < v < \frac{1}{\tau} \left(\frac{p_{\max}}{p_0} \right)^{\frac{1}{\alpha\epsilon}} \text{ and } j \neq m \\ \frac{\eta^{(j)}(v)}{\Pr(\mathcal{X}_{\text{MT}_0}^{(j,j)}, \mathcal{A}_{\text{MT}_0})} & \text{for } 0 < v < \frac{1}{\tau} \left(\frac{p_{\max}}{p_0} \right)^{\frac{1}{\alpha\epsilon}} \text{ and } j = m \end{cases} \quad (3.11)$$

where $\nu^{(j)}(v)$ and $\eta^{(j)}(v)$ are defined in (3.9) and (3.10), respectively.

Proof. The Cumulative Distribution Function (CDF) of the distance between the typical MT and its serving BS by conditioning on the MT being active and on $\mathcal{X}_{\text{MT}_0}^{(j,m)}$ is obtained by using steps similar to Appendix 3.8. The PDF is obtained from the CDF by computing the derivative. □

⁵The system fairness can be defined in different ways. In [83], e.g., it is defined based on the proportionally fair criterion and is obtained by computing the logarithm of the average rate. Our framework could be generalized for analyzing the system fairness based on this definition, but this study is outside the scope of the current chapter and is postponed to future research.

In the UL, an important performance metric to study is the average transmit power of the typical MT, which is related to its power consumption. Since some MTs may be turned off in the IAM scheme, this implies that some MTs may transmit zero power, which results in reducing their power consumption. The following proposition provides the average transmit power of the typical MT, by taking into account that the *typical* MT may be a MT that is turned off as it does not fulfill either the maximum power constraint or the maximum interference constraint.

Proposition 3. *The average transmit power of the typical MT can be formulated as follows:*

$$\mathbb{E}[P_{\text{MT}_0}] = \sum_{j \in \mathcal{K}} \sum_{m \in \mathcal{K}} \Pr\left(\mathcal{X}_{\text{MT}_0}^{(j,m)}, \mathcal{A}_{\text{MT}_0}\right) \int_0^\infty \frac{p}{\tau p_0 \alpha \epsilon} \left(\frac{p}{p_0}\right)^{\frac{1}{\alpha \epsilon} - 1} f_{R_{\text{MT}_0}}\left(\frac{1}{\tau} \left(\frac{p}{p_0}\right)^{\frac{1}{\alpha \epsilon}} \mid \mathcal{X}_{\text{MT}_0}^{(j,m)}, \mathcal{A}_{\text{MT}_0}\right) dp \quad (3.12)$$

where $f_{R_{\text{MT}_0}}\left(v \mid \mathcal{X}_{\text{MT}_0}^{(j,m)}, \mathcal{A}_{\text{MT}_0}\right)$ is in (3.11) and $\Pr\left(\mathcal{X}_{\text{MT}_0}^{(j,m)}, \mathcal{A}_{\text{MT}_0}\right)$ is defined in Appendix A.

Proof. It follows by computing the average transmit power by conditioning on the events $\mathcal{A}_{\text{MT}_0}$ and $\mathcal{X}_{\text{MT}_0}^{(j,m)}$. The final result is obtained from the total probability theorem. \square

Remark 3 (Exact analysis). *The previous propositions and lemmas are exact, since they do not depend on the set of active interfering MTs but depend only on the locations of the BSs, which constitute a PPP, and on the typical MT. In other words, **Assumption 1** is not applied.*

The next lemma provides the Laplace transform of the other-cell interference based on its mathematical formulation in (3.7), which exploits **Assumption 1**.

Lemma 5. *Assume that the typical MT is associated with a BS of tier j . The Laplace transform of the (conditional) interference in (3.7) can be formulated as follows:*

$$\mathcal{L}_I\left(s \mid \mathcal{X}_{\text{MT}_0}^{(j)}\right) = \exp\left(\beta^{(j)}(s)\right) \quad (3.13)$$

where $\beta^{(j)}(s)$ is defined as follows:

$$\beta^{(j)}(s) = - \sum_{k \in \mathcal{K}} 2\pi \lambda^{(k)} \sum_{n \in \mathcal{K}} \Pr \left(\mathcal{Q}_{\text{MT}_i}^{(n)} | \mathcal{X}_{\text{MT}_i}^{(k)}, \mathcal{A}_{\text{MT}_i} \right) \int_0^\infty f_{R_{\text{MT}_i}} \left(r | \mathcal{X}_{\text{MT}_i}^{(k,n)}, \mathcal{A}_{\text{MT}_i} \right) \chi(s, r) dr, \quad (3.14)$$

$f_{R_{\text{MT}_i}} \left(r | \mathcal{X}_{\text{MT}_i}^{(k,n)}, \mathcal{A}_{\text{MT}_i} \right)$ is the PDF of the distance between the i th interfering MT and its serving BS, which is provided in Lemma 4, $\chi(s, r)$ is defined as follows:

$$\begin{aligned} \chi(s, r) = & \frac{p_0 s (\tau r)^{\alpha\epsilon} \tau^{-\alpha}}{\alpha - 2} \max^{2-\alpha} \left(\left(\frac{t^{(j)}}{t^{(k)}} \right)^{\frac{1}{\alpha}} r, \left(\frac{p_0}{i_0} \right)^{\frac{1}{\alpha}} \frac{(\tau r)^\epsilon}{\tau} \right) \\ & \times {}_2F_1 \left(1, \frac{\alpha - 2}{\alpha}, 2 - \frac{2}{\alpha}, -p_0 s (\tau r)^{\alpha\epsilon} \tau^{-\alpha} \max^{-\alpha} \left(\left(\frac{t^{(j)}}{t^{(k)}} \right)^{\frac{1}{\alpha}} r, \left(\frac{p_0}{i_0} \right)^{\frac{1}{\alpha}} \frac{(\tau r)^\epsilon}{\tau} \right) \right) \end{aligned} \quad (3.15)$$

and $\Pr \left(\mathcal{Q}_{\text{MT}_i}^{(n)} | \mathcal{X}_{\text{MT}_i}^{(k)}, \mathcal{A}_{\text{MT}_i} \right)$ is defined as follows:

$$\Pr \left(\mathcal{Q}_{\text{MT}_i}^{(n)} | \mathcal{X}_{\text{MT}_i}^{(k)}, \mathcal{A}_{\text{MT}_i} \right) = \frac{\Pr \left(\mathcal{X}_{\text{MT}_i}^{(k,n)}, \mathcal{A}_{\text{MT}_i} \right)}{\Pr \left(\mathcal{X}_{\text{MT}_i}^{(k)}, \mathcal{A}_{\text{MT}_i} \right)} = \frac{\Pr \left(\mathcal{X}_{\text{MT}_i}^{(k,n)}, \mathcal{A}_{\text{MT}_i} \right)}{\sum_{q \in \mathcal{K}} \Pr \left(\mathcal{X}_{\text{MT}_i}^{(k,q)}, \mathcal{A}_{\text{MT}_i} \right)} \quad (3.16)$$

Proof. See Appendix 3.9. □

From the Laplace transform in (3.13), the moments of the interference can be obtained as shown in the next proposition. Of particular interest is the variance of the interference, since it affects the performance of AMC schemes [49]: the smaller the variance is, the more robust and accurate the estimation of the SINR is, which makes easier the choice of the best MCS to use.

Proposition 4. *The mean and variance of the interference can be formulated as follows:*

$$\mathbb{E} [I] = - \sum_{j \in \mathcal{K}} \Pr \left(\mathcal{X}_{\text{MT}_0}^{(j)} \right) \beta^{(j)}(0); \quad \text{var} (I) = - \sum_{j \in \mathcal{K}} \Pr \left(\mathcal{X}_{\text{MT}_0}^{(j)} \right) \left(\beta^{(j)''}(0) + (\beta^{(j)'}(0))^2 - (\mathbb{E} [I])^2 \right) \quad (3.17)$$

where the following definitions hold:

$$\begin{aligned} \beta^{(j)}(0) &= - \sum_{k \in \mathcal{K}} 2\pi\lambda^{(k)} \sum_{n \in \mathcal{K}} \Pr \left(\mathcal{Q}_{\text{MT}_i}^{(n)} | \mathcal{X}_{\text{MT}_i}^{(k)}, \mathcal{A}_{\text{MT}_i} \right) \\ &\times \int_0^\infty f_{R_{\text{MT}_i}} \left(r | \mathcal{X}_{\text{MT}_i}^{(k,n)}, \mathcal{A}_{\text{MT}_i} \right) \frac{p_0 (\tau r)^{\alpha\epsilon} \tau^{-\alpha}}{\alpha - 2} \max^{2-\alpha} \left(\left(\frac{t^{(j)}}{t^{(k)}} \right)^{\frac{1}{\alpha}} r, \left(\frac{p_0}{i_0} \right)^{\frac{1}{\alpha}} \frac{(\tau r)^\epsilon}{\tau} \right) dr \end{aligned} \quad (3.18)$$

$$\begin{aligned} \beta''^{(j)}(0) &= - \sum_{k \in \mathcal{K}} 2\pi\lambda^{(k)} \sum_{n \in \mathcal{K}} \Pr \left(\mathcal{Q}_{\text{MT}_i}^{(n)} | \mathcal{X}_{\text{MT}_i}^{(k)}, \mathcal{A}_{\text{MT}_i} \right) \\ &\times \int_0^\infty f_{R_{\text{MT}_i}} \left(r | \mathcal{X}_{\text{MT}_i}^{(k,n)}, \mathcal{A}_{\text{MT}_i} \right) \frac{p_0^2 (\tau r)^{2\alpha\epsilon} \tau^{-2\alpha}}{1 - \alpha} \max^{2(1-\alpha)} \left(\left(\frac{t^{(j)}}{t^{(k)}} \right)^{\frac{1}{\alpha}} r, \left(\frac{p_0}{i_0} \right)^{\frac{1}{\alpha}} \frac{(\tau r)^\epsilon}{\tau} \right) dr \end{aligned} \quad (3.19)$$

Proof. It directly follows from the first and second derivative of (3.13) evaluated at $s = 0$. \square

Remark 4 (Impact of i_0). *By inspection of **Propositions 3** and **4**, we evince that the average transmit power, the mean and variance of the interference decrease by decreasing i_0 . Since the interference-unaware setup is obtained by setting $i_0 \rightarrow \infty$, this implies that IAM is beneficial in terms of reducing the power consumption of the MTs and of implementing AMC schemes. The system fairness may, however, be negatively affected if i_0 decreases, as more MTs are muted.*

The next theorem provides a tractable expression of the coverage probability of HCNs.

Theorem 1. *The CCDF of the SINR of the typical MT can be formulated as follows:*

$$\begin{aligned} \bar{F}_{\text{SINR}}(\gamma) &= \sum_{j \in \mathcal{K}} \sum_{m \in \mathcal{K}} \Pr \left(\mathcal{X}_{\text{MT}_0}^{(j,m)}, \mathcal{A}_{\text{MT}_0} \right) \\ &\times \int_0^\infty f_{R_{\text{MT}_0}} \left(v | \mathcal{X}_{\text{MT}_0}^{(j,m)}, \mathcal{A}_{\text{MT}_0} \right) e^{-\gamma \sigma_n^2 (\tau v)^{\alpha(1-\epsilon)} p_0^{-1}} \mathcal{L}_I \left(\gamma (\tau v)^{\alpha(1-\epsilon)} p_0^{-1} | \mathcal{X}_{\text{MT}_0}^{(j)} \right) dv \end{aligned} \quad (3.20)$$

Proof. With the aid of the total probability theorem, we have:

$$\begin{aligned}
\bar{F}_{\text{SINR}}(\gamma) &= \bar{F}_{\text{SINR}}(\gamma | \mathcal{A}_{\text{MT}_0}) \Pr(\mathcal{A}_{\text{MT}_0}) + 0 \times \Pr(\overline{\mathcal{A}_{\text{MT}_0}}) \\
&= \sum_{j \in \mathcal{K}} \sum_{m \in \mathcal{K}} \Pr(\mathcal{X}_{\text{MT}_0}^{(j,m)}, \mathcal{A}_{\text{MT}_0}) \bar{F}_{\text{SINR}}(\gamma | \mathcal{X}_{\text{MT}_0}^{(j,m)}, \mathcal{A}_{\text{MT}_0}) = \sum_{j \in \mathcal{K}} \sum_{m \in \mathcal{K}} \Pr(\mathcal{X}_{\text{MT}_0}^{(j,m)}, \mathcal{A}_{\text{MT}_0}) \\
&\quad \times \mathbb{E}_{R_{\text{MT}_0}} \mathbb{E}_I \left[\Pr \left(H_{\text{MT}_0} > \frac{\gamma}{p_0} (I + \sigma_n^2) (\tau R_{\text{MT}_0})^{\alpha(1-\epsilon)} | \mathcal{X}_{\text{MT}_0}^{(j,m)}, \mathcal{A}_{\text{MT}_0} \right) \right] \quad (3.21)
\end{aligned}$$

The proof follows by computing the two remaining expectations. \square

Corollary 3. Assume $\epsilon = 1$, i.e., the active MTs apply a power control scheme based on full channel inversion. The CCDF in **Theorem 1** simplifies as follows:

$$\bar{F}_{\text{SINR}}(\gamma) = \sum_{j \in \mathcal{K}} \sum_{m \in \mathcal{K}} \Pr(\mathcal{X}_{\text{MT}_0}^{(j,m)}, \mathcal{A}_{\text{MT}_0}) e^{-\gamma \sigma_n^2 / p_0} \mathcal{L}_I(\gamma / p_0 | \mathcal{X}_{\text{MT}_0}^{(j)}) \quad (3.22)$$

Proof. It follows from (3.20) by setting $\epsilon = 1$ and some algebra. \square

Remark 5 (Operating regimes as a function of i_0). By direct inspection of **Corollary 3**, three operating regimes as a function of i_0 can be identified: i) interference-unaware, where the CCDF of the SINR is independent of i_0 . This occurs if $i_0 > p_0$ and $p_0/i_0 < \min(t^{(1)}/t^{(2)}, t^{(2)}/t^{(1)})$, ii) interference-aware and cell association independent, where the CCDF of the SINR depends on i_0 but does not depend on the cell association weights $t^{(1)}$ and $t^{(2)}$. This occurs if $i_0 < p_0$ and $p_0/i_0 > \max(t^{(1)}/t^{(2)}, t^{(2)}/t^{(1)})$, iii) interference-aware and cell association dependent, where the CCDF of the SINR depends on i_0 and $t^{(j)}/t^{(i)}, \forall j \in \mathcal{K}$. This occurs if the conditions above are not satisfied. The same operating regimes can be identified from **Propositions 4** and **3**.

Proof. It follows by direct inspection of $\Pr(\mathcal{X}_{\text{MT}_0}^{(j,m)}, \mathcal{A}_{\text{MT}_0})$, $\nu^{(j)}(v)$ and $\eta^{(j)}(v)$. \square

The second operating regime, i.e., the performance is independent of the cell association weights, is of particular interest for making the design of HCNs easier: it implies that, for some system parameters, optimizing the DL results in optimizing the UL as well.

It is worth mentioning, in addition, that the conditions that identify the three operating regimes in **Remark 5** can be conveniently formulated in dB as well, which provides further information for system design. More precisely, regime i) emerges if $i_0 > p_0$ dB

and $t^{(1)}/t^{(2)} \in [-i_0/p_0, i_0/p_0]$ dB and regime ii) emerges if $i_0 < p_0$ dB and $t^{(1)}/t^{(2)} \in [-p_0/i_0, p_0/i_0]$ dB.

3.4 Smallest Path-Loss Association

In this section, tractable mathematical frameworks under the SPLA scheme are provided. In this case, the condition $t^{(1)} = t^{(2)}$ holds and simplified formulas can be obtained. Under the assumption that the path-loss exponents of all the tiers of BSs are the same, in fact, multi-tier HCNs reduce to an equivalent single-tier cellular network of intensity $\lambda = \sum_{j \in \mathcal{K}} \lambda^{(j)}$ [26].

Proposition 5. *The probability that the typical MT is active can be formulated as follows:*

$$\Pr(\mathcal{A}_{\text{MT}_0}) = \int_{r_1=0}^{\frac{1}{\tau} \left(\frac{p_{\max}}{p_0} \right)^{\frac{1}{\alpha}}} 2\pi\lambda r_1 e^{-\pi\lambda \max^2 \left(r_1, \left(\frac{p_0}{i_0} \right)^{\frac{1}{\alpha}} \frac{(\tau r_1)^\epsilon}{\tau} \right)} dr_1 \quad (3.23)$$

Proof. The proof is similar to that of **Proposition 2**. The difference is that only the joint PDF of the distance of nearest and second nearest BSs needs to be used (see Appendix A). \square

Corollary 4. *If $\epsilon = 1$, $\Pr(\mathcal{A}_{\text{MT}_0})$ in (3.23) simplifies as follows:*

$$\Pr(\mathcal{A}_{\text{MT}_0}) = \left(1 - e^{-\frac{\pi}{\tau^2} \left(\frac{p_{\max}}{p_0} \right)^{\frac{2}{\alpha}} \lambda \max \left(1, \left(\frac{p_0}{i_0} \right)^{\frac{2}{\alpha}} \right)} \right) / \max \left(1, \left(\frac{p_0}{i_0} \right)^{\frac{2}{\alpha}} \right) \quad (3.24)$$

Proof. It directly follows from (3.23) by setting $\epsilon = 1$ and computing the integral. \square

Remark 6 (Operating regimes as a function of i_0). *From (3.24), two operating regimes can be identified: i) interference-unaware, i.e., $\Pr(\mathcal{A}_{\text{MT}_0})$ is independent of i_0 , which occurs if $i_0 > p_0$ and ii) interference-aware, i.e., $\Pr(\mathcal{A}_{\text{MT}_0})$ depends on i_0 , which occurs if $i_0 < p_0$.*

Remark 7 (Unlimited transmit power of the MTs). *Assume $p_{\max} \rightarrow \infty$, i.e., the MTs have no maximum transmit power constraint. From (3.24), the following holds: i) under*

the interference-unaware regime ($i_0 > p_0$), $\Pr(\mathcal{A}_{\text{MT}_0}) \rightarrow 1$, and ii) under the interference-aware regime ($i_0 < p_0$), $\Pr(\mathcal{A}_{\text{MT}_0}) = (i_0/p_0)^{\frac{2}{\alpha}}$. In both regimes, $\Pr(\mathcal{A}_{\text{MT}_0})$ is independent of the density of BSs λ .

Lemma 6. *The PDF of the distance between the typical MT and its serving BS is as follows:*

$$f_{R_{\text{MT}_0}}(v|\mathcal{A}_{\text{MT}_0}) = \frac{2\pi\lambda v e^{-\pi\lambda \max^2\left(v, \left(\frac{p_0}{i_0}\right)^{\frac{1}{\alpha}} \left(\frac{\tau v \epsilon}{\tau}\right)\right)}}{\Pr(\mathcal{A}_{\text{MT}_0})} \mathbf{1}\left(0 < v < \frac{1}{\tau} \left(\frac{p_{\max}}{p_0}\right)^{\frac{1}{\alpha}}\right) \quad (3.25)$$

Proof. The proof is similar to that of **Lemma 4**. The difference is that only the joint PDF of the distance of nearest and second nearest BSs needs to be used (see Appendix A). \square

Remark 8 (Interference-awareness is equivalent to network densification if $p_{\max} \rightarrow \infty$). *If the system operates in the interference-aware regime ($i_0 < p_0$) and $p_{\max} \rightarrow \infty$, (3.25) reduces to:*

$$f_{R_{\text{MT}_0}}(v|\mathcal{A}_{\text{MT}_0}) = 2\pi\lambda \left(\frac{p_0}{i_0}\right)^{\frac{2}{\alpha}} v e^{-\pi\lambda \left(\frac{p_0}{i_0}\right)^{\frac{2}{\alpha}} v^2} \quad (3.26)$$

This implies that IAM's impact is equivalent to increasing the density of BSs from λ to $\lambda(p_0/i_0)^{\frac{2}{\alpha}}$, since the PDF of the distance from the nearest BS in Poisson cellular networks is $2\pi\lambda v e^{-\pi\lambda v^2}$. Hence, the distance between probe MT and probe BS is reduced, resulting in better performance.

Proposition 6. *If $\epsilon = 1$, the average transmit power of the typical MT is as follows:*

$$\mathbb{E}[p_{\text{MT}}(R_{\text{MT}_0})] = \frac{p_0\tau^\alpha \left(\Gamma\left(1 + \frac{\alpha}{2}\right) - \Gamma\left(\frac{2+\alpha}{2}, \frac{\lambda\pi}{\tau^2} \left(\frac{p_{\max}}{p_0}\right)^{\frac{2}{\alpha}} \max\left(1, \left(\frac{p_0}{i_0}\right)^{\frac{2}{\alpha}}\right)\right) \right)}{(\pi\lambda)^{\frac{\alpha}{2}} \max\left(1, \left(\frac{p_0}{i_0}\right)^{\frac{2}{\alpha}+1}\right)} \quad (3.27)$$

Proof. It follows from **Proposition 3**, by setting $\epsilon = 1$ and computing the integral. \square

Remark 9 (Impact of interference-awareness). *If $p_{\max} \rightarrow \infty$ and $i_0 < p_0$ (interference-*

aware regime), (3.27) simplifies as follows:

$$\mathbb{E} [p_{\text{MT}} (R_{\text{MT}_0})] = \frac{\tau^\alpha \Gamma \left(1 + \frac{\alpha}{2}\right)}{(\pi \lambda)^{\frac{\alpha}{2}} p_0^{\frac{2}{\alpha}}} i_0^{\frac{2}{\alpha} + 1} \quad (3.28)$$

which implies that the average power consumption of the MTs scales polynomially with exponent $2/\alpha + 1$, as a function of the maximum interference constraint i_0 .

Lemma 7. Assume $\epsilon = 1$. The Laplace transform of the aggregate interference can be formulated as $\mathcal{L}_I(s) = \exp(\beta(s))$, where $\beta(s) = -2\pi\lambda\theta\mu(s)$ and the following holds:

$$\theta = \left(1 - \left(1 + \frac{\pi}{\tau^2} \lambda \left(\frac{p_{\text{max}}}{p_0}\right)^{\frac{2}{\alpha}}\right) e^{-\frac{\pi}{\tau^2} \lambda \left(\frac{p_{\text{max}}}{p_0}\right)^{\frac{2}{\alpha}} \max\left(1, \left(\frac{p_0}{i_0}\right)^{\frac{2}{\alpha}}\right)}\right) \left(\pi \lambda \max\left(1, \left(\frac{p_0}{i_0}\right)^{\frac{2}{\alpha}}\right)\right)^{-1} \quad (3.29)$$

$$\mu(s) = \frac{p_0 s}{\alpha - 2} \max^{2-\alpha} \left(1, \left(\frac{p_0}{i_0}\right)^{\frac{1}{\alpha}}\right) {}_2F_1 \left(1, \frac{\alpha - 2}{\alpha}, 2 - \frac{2}{\alpha}, -p_0 s \max^{-\alpha} \left(1, \left(\frac{p_0}{i_0}\right)^{\frac{1}{\alpha}}\right)\right) \quad (3.30)$$

Proof. The proof follows from $\chi(s, r)$ in (3.15), by setting $t^{(1)} = t^{(2)}$ and formulating it as $\chi(s, r) = r^2 \mu(s)$. Hence, $\beta(s) = -2\pi\lambda\mu(s)\theta$, where $\theta = \mathbb{E} [R_{\text{MT}_i}^2 | A_{\text{MT}_0}]$. \square

Proposition 7. Assume $\epsilon = 1$. The mean and variance of the interference can be expressed as:

$$\mathbb{E} [I] = 2\pi\lambda\theta \frac{p_0 \max^{2-\alpha} \left(1, \left(\frac{p_0}{i_0}\right)^{\frac{1}{\alpha}}\right)}{\alpha - 2}; \quad \text{var} (I) = 2\pi\lambda\theta \frac{p_0^2 \max^{2-2\alpha} \left(1, \left(\frac{p_0}{i_0}\right)^{\frac{1}{\alpha}}\right)}{\alpha - 1} \quad (3.31)$$

Proof. It follows from **Lemma 7** evaluating the derivatives of the Laplace transform at zero. \square

Remark 10 (Trends of mean and variance of the interference as a function of i_0). Assume $p_{\text{max}} \rightarrow \infty$ and consider the interference-aware regime, i.e., $i_0 < p_0$. Then, (3.29) simplifies to $\theta = \frac{1}{\pi\lambda} \left(\frac{i_0}{p_0}\right)^{\frac{4}{\alpha}}$ and the mean and variance of the interference can be formulated as

follows:

$$\mathbb{E}[I] = \frac{2}{\alpha - 2} (p_0)^{-\frac{2}{\alpha}} (i_0)^{\frac{\alpha+2}{\alpha}}; \quad \text{var}(I) = \frac{2}{\alpha - 1} (p_0)^{-\frac{2}{\alpha}} (i_0)^{\frac{2(\alpha+1)}{\alpha}} \quad (3.32)$$

which implies that the mean and variance of the interference scale polynomially with exponents $\alpha + 2/\alpha$ and $2(\alpha + 1)/\alpha$ as a function of i_0 , respectively, and they do not depend on the BSs' density.

Finally, the following theorem provides the coverage probability under the SPLA criterion.

Theorem 2. Assume $\epsilon = 1$, $p_{\max} \rightarrow \infty$ and that the system operates in the interference-aware regime ($i_0 < p_0$). The CCDF of the SINR can be formulated as follows:

$$\bar{F}_{\text{SINR}}(\gamma | \mathcal{A}_{\text{MT}_0}) = \exp\left(-\frac{\gamma \sigma_n^2}{p_0} - 2\frac{\gamma}{\alpha - 2} \left(\frac{i_0}{p_0}\right)^{\frac{\alpha+2}{\alpha}} {}_2F_1\left(1, \frac{\alpha - 2}{\alpha}, 2 - \frac{2}{\alpha}, -\gamma \left(\frac{i_0}{p_0}\right)\right)\right) \quad (3.33)$$

Proof. The proof follows from **Theorem 1** by setting $t^{(1)} = t^{(2)}$ and $\epsilon = 1$, and from **Lemma 7** by letting $p_{\max} \rightarrow \infty$ and considering $i_0 < p_0$. \square

Remark 11 (SINR invariance as a function of λ). From (3.33), we evince that the CCDF of the SINR is independent of λ , but it depends on the ratio i_0/p_0 and the path-loss exponent α .

Interestingly the SINR in such a setup is invariant with the BSs' density. Intuitively, this means that both the desired received power and the interference does not vary with the BSs' density. On the one hand, the desired power does not vary thanks to full channel inversion power control ($\epsilon = 1$, $p_{\max} \rightarrow \infty$). On the other hand, although the distances towards nearest interfering MTs decrease with λ , their transmit power also decrease with λ , making received interference invariant with λ , as it can be observed from its moments in eq. (3.32). This density invariance has been also reported in [21, 26] for the case of the SIR.

3.5 Spectral Efficiency and Binary Rate

This section is focused on the analysis of SE and BR. Unlike the vast majority of papers on stochastic geometry modeling of HCNs that evaluate these key performance indicators based on the Shannon formula, we provide a mathematical formulation that is more useful for current cellular deployments based on practical AMC schemes and, thus, provides estimates of SE and BR that can be achieved at a finite target value of the Block Error Rate (BLER) rather than their theoretically achievable counterparts under the assumptions of unlimited decoding complexity and arbitrarily small BLER. We show, remarkably, that more tractable expressions of SE and BR can be provided, compared to those that can be obtained based on the Shannon definition. As mentioned in Section I, the BR accounts for the amount of bandwidth allocated to the typical MT by the scheduler and, thus, accounts for the BS's load, i.e., the number of MTs that need to be simultaneously served in the cell to which the typical MT belongs to. Accordingly, SE and BR provide different information on the advantages and limitations of transmission schemes and, as such, are both employed for assessing the performance of practical LTE systems [84].

SE and BR, however, are related to each other and, in mathematical terms, we have:

$$\text{BR}_{\text{MT}_0} = \frac{b_w}{N_{\mathcal{B}_{\text{MT}_0}}^A} \text{SE}_{\text{MT}_0} \quad (\text{bps}) \quad (3.34)$$

where b_w is the available bandwidth per BS and $N_{\mathcal{B}_{\text{MT}_0}}^A$ denotes the number of active MTs associated with the probe BS, which is commonly referred to as the cell load [85].

As extensively discussed in, e.g., [85], [27] [86], the distribution of $N_{\mathcal{B}_{\text{MT}_0}}^A$ is not available for cell association criteria that are not based on the shortest distance, and, thus approximations need to be used. For mathematical tractability, but without losing in accuracy, we exploit the approximation in [27] which, for the convenience of the readers, is reported in what follows.

Assumption 2. *The Probability Mass Function (PMF) of the number of active MTs,*

$N_{\mathcal{B}_{\text{MT}_0}}^{\mathcal{A}}$, associated with a BS of tier j is approximated as follows:

$$\Pr\left(N_{\mathcal{B}_{\text{MT}_0}}^{\mathcal{A}} = n | \mathcal{X}_{\text{MT}_0}^{(j)}, \mathcal{A}_{\text{MT}_0}\right) \approx \frac{3.5^{3.5}}{(n-1)!} \frac{\Gamma(n+3.5)}{\Gamma(3.5)} \left(\frac{\lambda_{\text{MT}} \cdot p}{\lambda^{(j)}}\right)^{n-1} \left(3.5 + \frac{\lambda_{\text{MT}} \cdot p}{\lambda^{(j)}}\right) \quad (3.35)$$

where, for notational simplicity, the short-hand $p = \Pr(\mathcal{X}_{\text{MT}_0}^{(j)}, \mathcal{A}_{\text{MT}_0})$ is used.

3.5.1 Adaptive Modulation and Coding

In modern cellular systems [84], AMC is aimed to adapt the MCS to be used to the channel conditions. This is needed for maximizing the BR while providing a BLER below a desired threshold BLER_T . In practice, AMC is implemented as follows. In the UL, the MTs transmit sounding reference signals that are used by the BSs for estimating the SINR. Based on these estimates, the BSs choose the MCS to use (usually identified by an index), which corresponds to a given Channel Quality Indicator (CQI), $i_{\text{CQI}} \in [1, n_{\text{CQI}}]$, that maximizes the SE while maintaining the BLER below BLER_T . The choice of the best MCS to use is made based on lookup tables that provide the SINR thresholds, $\gamma_{i_{\text{CQI}}}$, associated to each value of CQI. Finally, the BSs inform each scheduled MT of the MCS index to use for its subsequent transmission. To reduce the reporting overhead associated with the CQIs, the LTE standard assumes that the number of bits used for reporting the CQI is equal to 4, which implies $n_{\text{CQI}} = 15$.

Based on this working principle, the BR can be obtained from (3.34) and the SE is as follows:

$$\text{SE}_{\text{MT}_0} = \sum_{i_{\text{CQI}}=1}^{n_{\text{CQI}}} \text{SE}_{i_{\text{CQI}}} \mathbf{1}(\text{SINR}_{\text{MT}_0} \in [\gamma_{i_{\text{CQI}}}, \gamma_{i_{\text{CQI}+1}})) \quad (3.36)$$

where $\gamma_1 < \dots < \gamma_{n_{\text{CQI}}}$, $i_{\text{CQI}} = 0$ if no transmission, $\bigcap_{i_{\text{CQI}}=1}^{n_{\text{CQI}}} [\gamma_{i_{\text{CQI}}}, \gamma_{i_{\text{CQI}+1}}) = \emptyset$, $\gamma_{n_{\text{CQI}+1}} \rightarrow \infty$.

Based on (A.11), the spatially-average SE can be obtained from the CCDF of the SINR provided in Sections III and IV for GCA and SPLA criteria, respectively. More precisely,

we have:

$$\begin{aligned} \mathbb{E} [\text{SE}_{\text{MT}_0}] &= \sum_{j \in \mathcal{K}} \sum_{m \in \mathcal{K}} \Pr \left(\mathcal{X}_{\text{MT}_0}^{(j,m)}, \mathcal{A}_{\text{MT}_0} \right) \\ &\quad \times \sum_{i_{\text{CQI}}=1}^{n_{\text{CQI}}} \text{SE}_{i_{\text{CQI}}} \left(\bar{F}_{\text{SINR}} \left(\gamma_{i_{\text{CQI}}} | \mathcal{X}_{\text{MT}_0}^{(j,m)}, \mathcal{A}_{\text{MT}_0} \right) - \bar{F}_{\text{SINR}} \left(\gamma_{i_{\text{CQI}}+1} | \mathcal{X}_{\text{MT}_0}^{(j,m)}, \mathcal{A}_{\text{MT}_0} \right) \right) \end{aligned} \quad (3.37)$$

With similar arguments, the average BR of the probe MT can be written as follows:

$$\begin{aligned} \mathbb{E} [\text{BR}_{\text{MT}_0}] &= \sum_{j \in \mathcal{K}} \sum_{m \in \mathcal{K}} \sum_{n > 0} \Pr \left(\mathcal{X}_{\text{MT}_0}^{(j,m)}, \mathcal{A}_{\text{MT}_0} \right) \Pr \left(N_{\mathcal{B}_{\text{MT}_0}}^{\mathcal{A}} = n | \mathcal{X}_{\text{MT}_0}^{(j)}, \mathcal{A}_{\text{MT}_0} \right) \\ &\quad \times \sum_{i_{\text{CQI}}=1}^{n_{\text{CQI}}} \frac{b_w}{n} \text{SE}_{i_{\text{CQI}}} \left(\bar{F}_{\text{SINR}} \left(\gamma_{i_{\text{CQI}}} | \mathcal{X}_{\text{MT}_0}^{(j,m)}, \mathcal{A}_{\text{MT}_0} \right) - \bar{F}_{\text{SINR}} \left(\gamma_{i_{\text{CQI}}+1} | \mathcal{X}_{\text{MT}_0}^{(j,m)}, \mathcal{A}_{\text{MT}_0} \right) \right) \\ &\stackrel{(a)}{=} \sum_{j \in \mathcal{K}} \sum_{m \in \mathcal{K}} \sum_{i_{\text{CQI}}=1}^{n_{\text{CQI}}} \Pr \left(\mathcal{X}_{\text{MT}_0}^{(j,m)}, \mathcal{A}_{\text{MT}_0} \right) \text{SE}_{i_{\text{CQI}}} \frac{3.5^{3.5} b_w (3.5 \lambda^{(j)} + \lambda_{\text{MTP}}) \left(1 - \left(1 - \frac{\lambda_{\text{MTP}}}{\lambda^{(j)}} \right)^{3.5} \right)}{\lambda_{\text{MTP}} \left(1 - \frac{\lambda_{\text{MTP}}}{\lambda^{(j)}} \right)^{3.5}} \\ &\quad \times \left(\bar{F}_{\text{SINR}} \left(\gamma_{i_{\text{CQI}}} | \mathcal{X}_{\text{MT}_0}^{(j,m)}, \mathcal{A}_{\text{MT}_0} \right) - \bar{F}_{\text{SINR}} \left(\gamma_{i_{\text{CQI}}+1} | \mathcal{X}_{\text{MT}_0}^{(j,m)}, \mathcal{A}_{\text{MT}_0} \right) \right) \end{aligned} \quad (3.38)$$

where (a) is obtained by computing the summation over $n = N_{\mathcal{B}_{\text{MT}_0}}^{\mathcal{A}}$ in closed-form with the aid of the PMF in (3.35).

The mathematical expressions of SE and BR of AMC schemes are easier to compute than the corresponding formulas obtained from the Shannon definition of SE, since the latter definition requires an extra integral to be computed [85]. This is remarkable, since the SE and BR in (3.37) and (3.38) account for feedback's overhead and limited-complexity receivers.

In the present chapter, as a sensible case study, we consider the range of CQI values and a target BLER equal to 10%, as recommended by LTE specifications [84]. The SINR thresholds $\gamma_{i_{\text{CQI}}}$ are obtained from link-level simulations conducted with an accurate LTE simulator [1, 2]. More precisely, the considered simulator assumes MTs of limited computational complexity, where decoding is performed by using a 1-tap zero forcing equalizer and a turbo decoder based on the soft output Viterbi algorithm. Numerical illustrations are reported in Section 3.6. For completeness, Table 3.2 reports the input

Table 3.2: SINR thresholds and SE values obtained from the LTE link-level simulator in [1, 2].

i_{CQI}	1	2	3	4	5	6	7	8	9	10
$\text{SE}_{i_{\text{CQI}}} [\text{bps/Hz}]$	0.15	0.23	0.38	0.60	0.88	1.18	1.48	1.91	2.41	2.73
$\gamma_{i_{\text{CQI}}} [\text{dB}]$	-3.65	-1.60	0.00	2.25	3.75	4.75	9.00	10.50	12.35	15.40
i_{CQI}	11		12	13	14	15				
$\text{SE}_{i_{\text{CQI}}} [\text{bps/Hz}]$	3.32		3.90	4.52	5.11	5.55				
$\gamma_{i_{\text{CQI}}} [\text{dB}]$	17.18		18.85	20.70	24.0	25.0				

Table 3.3: Simulation parameters.

Parameter	Value	Parameter	Value
$\{\tau, \alpha\}$ (MHz)	$\{2.6, 3.8\}$	n_{thermal} (dBm/Hz)	-174
i_0 (dBm)	$[-120, -60]$	ϵ	$[0, 1]$
b_w (MHz)	9	$t^{(1)}/t^{(2)}$ (dB)	$\{9, 0\}$
p_0 (dBm)	-70	p_{max} (dBm)	$\{\infty, 5\}$
$\{\lambda^{(1)}, \lambda^{(2)}\}$ (points/km ²)	$\{2, 4\}$	λ_{MT} (points/km ²)	80
n_{F} (dB)	9	σ_s (dB)	4

parameters that are needed for computing the SE and BR in (3.37) and (3.38). It is worth emphasizing, however, that (3.37) and (3.38) are general enough for being used for analyzing different wireless standards and receiver implementations.

3.6 Numerical Results

In this section, we validate the mathematical frameworks and findings derived in the previous sections with the aid of Monte Carlo simulations, as well as compare the IAM scheme against IAFPC and IUFPSC schemes. The following setup compliant with LTE specifications is considered. The bandwidth is equal to 10 MHz, which implies $b_w = 9$ MHz by excluding the guard bands. The noise power spectral density is $n_{\text{thermal}} = -174$ dBm/Hz and the noise figure of the receiver is $n_{\text{F}} = 9$ dB. Both GCA and SPLA criteria are studied, and the association weights are, unless otherwise stated, $t^{(1)}/t^{(2)} = 9$ dB and $t^{(1)}/t^{(2)} = 0$ dB, respectively. The case study $t^{(1)}/t^{(2)} = 9$ dB is related to a cell association

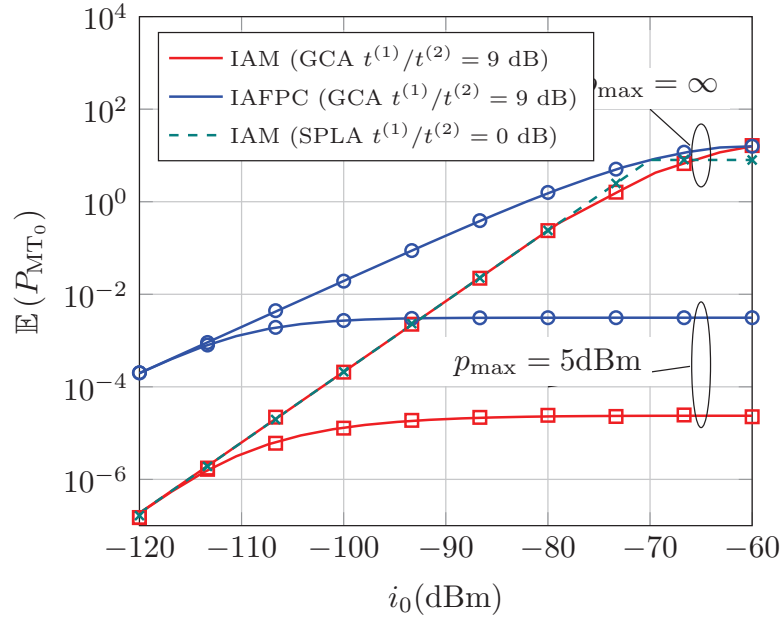


Figure 3.1: Average transmit power versus i_0 for IAM and IAFPC methods with $\epsilon = 1$, $p_{\max} \rightarrow \infty$ and $p_{\max} = 5$ dBm.

based on the average DL received power criterion, where the first tier of BSs (macro) has transmit power equal to 46 dBm and the second tier of BSs (small-cell) has transmit power equal to 37 dBm, which agrees with [87, Annex A: Simulation Model]. Other simulation parameters are provided in Table 3.3. As far as Monte Carlo simulations are concerned, they are obtained by considering 10^4 realizations of channels and network topologies. In all the figures, analytical and Monte Carlo simulation results are represented with solid lines and markers, respectively.

3.6.1 Average Transmit Power, Probability of Being Active, Mean & Variance of the Interference

In this section, we analyze the average transmit power of the MTs, the probability that the typical MT is active, which provides information on the system fairness, and the mean and variance of the interference. As reported in [49], [48], reducing the variance of the interference is beneficial for reducing the error probability of practical decoding schemes, e.g., turbo decoding, and improving the selection of the most appropriate Modulation and

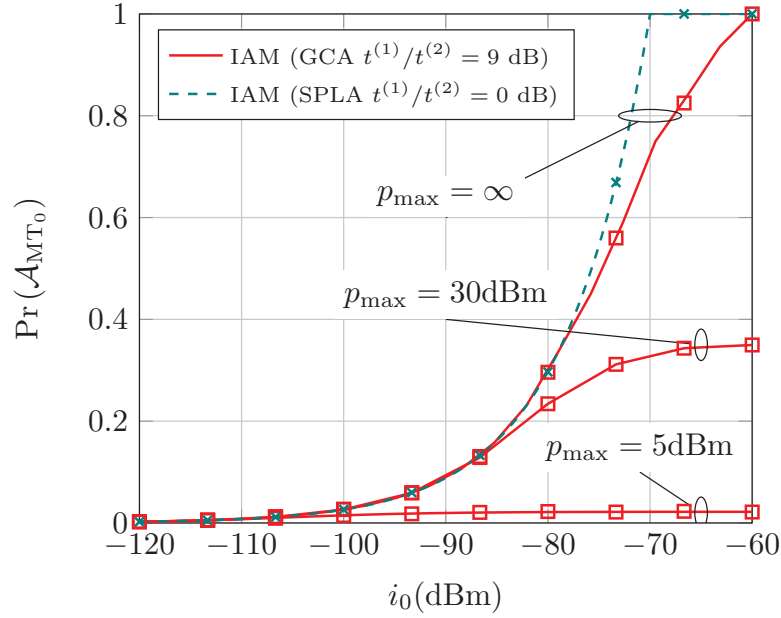


Figure 3.2: Probability of being active of the typical MT for IAM with $\epsilon = 1$, $p_{\max} \rightarrow \infty$, $p_{\max} = 30$ dBm and $p_{\max} = 5$ dBm.

Coding Scheme (MCS) to use in LTE systems.

Figures 3.1-3.4 confirm the conclusions drawn in **Remark 3**, i.e., the mathematical frameworks of average transmit power and probability of being active are exact while those of mean and variance of the interference are approximations that exploit **Assumption 1**. Such an assumption considers that the position of interfering MTs can be modeled as a conditionally thinned (i.e., non-homogeneous) PPP. The difference between such a non-homogeneous PPP, and the actual point process, which is on the other hand not tractable, explains also the difference between simulation and analytical results in all the metrics that depend on the interference (SINR, SE, BR).

The conclusions drawn in **Remark 4** are confirmed as well: the mean and variance of the interference decrease by decreasing i_0 , which provide important advantages for implementing AMC schemes. The price to pay is, however, a decrease of the probability that a MT is active. The proposed mathematical frameworks can be used to find a suitable trade-off that provides an acceptable user fairness while simplifying the implementation of AMC schemes.

In the figures, IAM and IAFPC are compared as well. We observe that IAM reduces

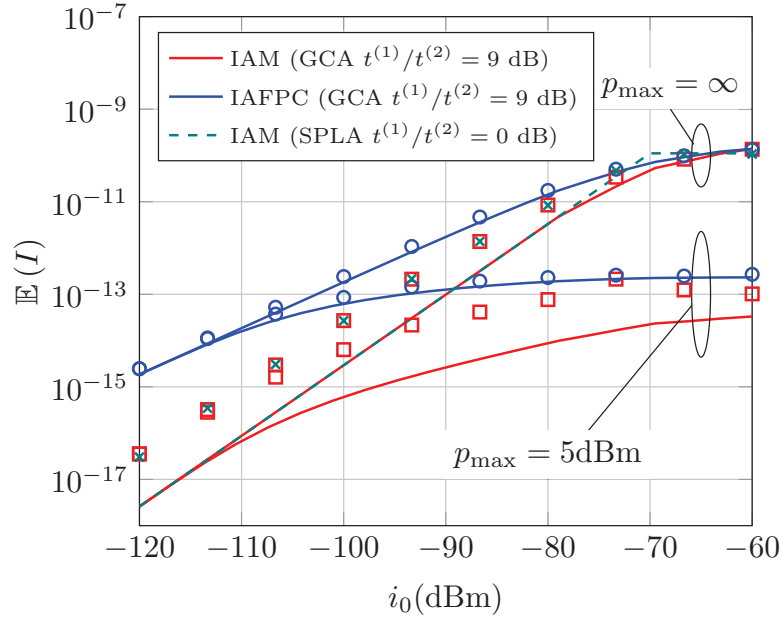


Figure 3.3: Mean of the interference versus i_0 for IAM and IAFPC methods with $\epsilon = 1$, $p_{\max} \rightarrow \infty$ and $p_{\max} = 5$ dBm.

the average transmit power and the mean and variance of the interference. Consider, for example, the case study $p_{\max} \rightarrow \infty$. IAM and IAFPC converge to the same performance for $i_0 \geq -60$ dBm. This behavior is expected, since both schemes tend to be equivalent if p_{\max} and i_0 are large enough. This occurs, in particular, if all the MTs can apply power control without causing more interference than i_0 and without necessitating a transmit power higher than p_{\max} . In this case, both IAM and IAFPC provide the same performance as the IUFPC scheme.

Consider the SPLA criterion, which is illustrated with dashed lines in the figures. We observe that the findings in **Remark 6** are confirmed: the system is interference-aware and interference-unaware if $i_0 < p_0$ and $i_0 > p_0$, respectively. As expected, the crossing point occurs at $p_0 = -70$ dBm based on the simulation parameters used. In addition, the scaling laws of average transmit power and average interference are in agreement with the findings in **Remark 9**, **Remark 10**.

All in all, the numerical illustrations reported in Figs. 3.1-3.4 confirm all the conclusions and performance trends discussed in the previous sections and highlight the advantages of IAM.

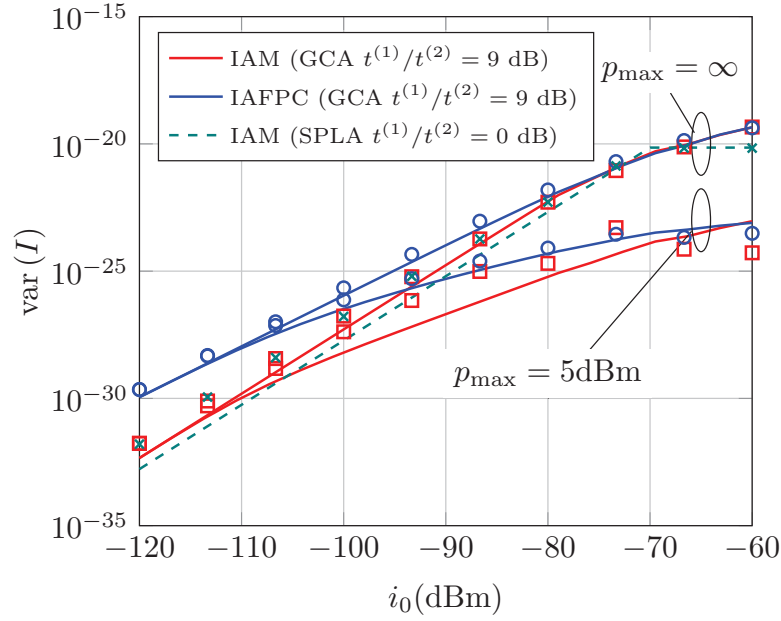


Figure 3.4: Variance of the interference versus i_0 for IAM and IAFPC schemes with $\epsilon = 1$, $p_{\max} \rightarrow \infty$ and $p_{\max} = 5$ dBm.

With SPLA, MTs associate with their nearest BS whereas for the case of GA with $t^{(1)}/t^{(2)} \neq 0$ dB, MTs associate with the BS that provides more received weighted power in the DL, and hence such BS is not necessary the closest BS. This involves that in the interference unaware case the transmit power with SPLA is smaller than in the coupled case as it can be observed in Fig. 3.1. In the GA case with $t^{(1)}/t^{(2)} \neq 0$ dB, MTs are not associated with their closest BS, and hence they tend to cause higher interference than in case of SPLA, where $t^{(1)}/t^{(2)} = 0$ dB. This can be also observed from Fig. 3.2 where it is shown that the probability to be active is higher in case of SPLA.

3.6.2 Complementary Cumulative Distribution Function of the SINR

In this section, we analyze the coverage probability (CCDF of the SINR) of the active MTs. The results are illustrated in Figs. 3.5 and 3.6 for $\epsilon = 1$ and $\epsilon = 0.75$, respectively, and by assuming $p_{\max} \rightarrow \infty$.

In both figures, we observe a good agreement between mathematical frameworks and

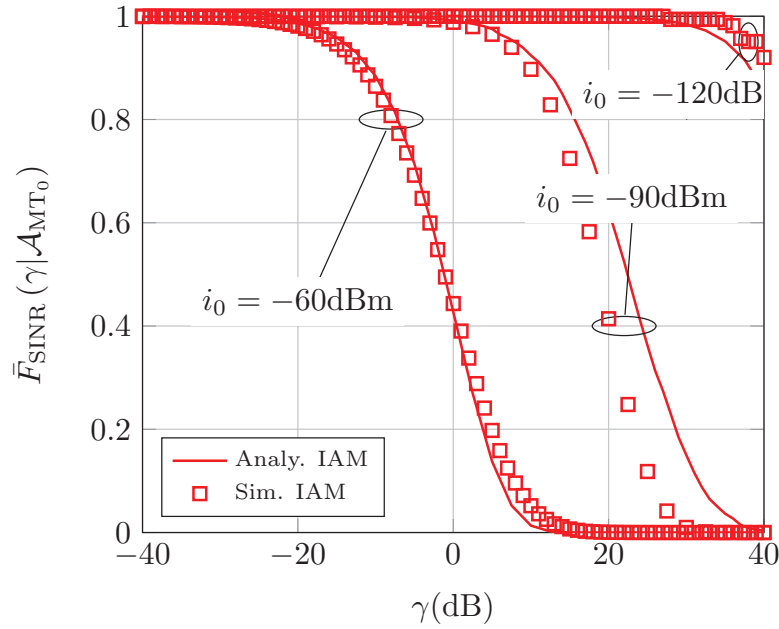


Figure 3.5: CCDF of the SINR for the typical MT conditioned on being active for IAM with $\epsilon = 1$, $t^{(1)}/t^{(2)} = 9$ dB, $p_{\max} \rightarrow \infty$ and $i_0 = \{-120, -90, -60\}$ dBm.

Monte Carlo simulations. In particular, the figures confirm, once again, that the coverage probability of IAM increases as i_0 decreases. In Fig. 3.5, for example, almost all the active MTs have a SINR greater than 20 dB if $i_0 = -120$ dBm. This good SINR is obtained because IAM keeps under control the interference by muting the MTs that create more interference. Based on Fig. 3.2, in fact, we note that only a small fraction of the MTs are allowed to be active for $i_0 = -120$ dBm. The active MTs, however, better exploit the available bandwidth. Similar conclusions can be drawn for $\epsilon = 0.75$ shown in Fig. 3.6. The main difference is that, in this latter figure, IAM provides almost the same coverage probability for $i_0 = -60$ dBm and $i_0 = -90$ dBm. The reason is that the MTs transmit with less power if $\epsilon = 0.75$ and, thus, there is almost no difference between the two interference constraints. This brings to our attention that the design of the UL of HCNs requires to jointly optimize i_0 , p_0 , p_{\max} and ϵ , in order to identify the desired operating regime that fulfills the requirements in terms of system fairness and interference mitigation. The proposed mathematical frameworks can be used to this end.

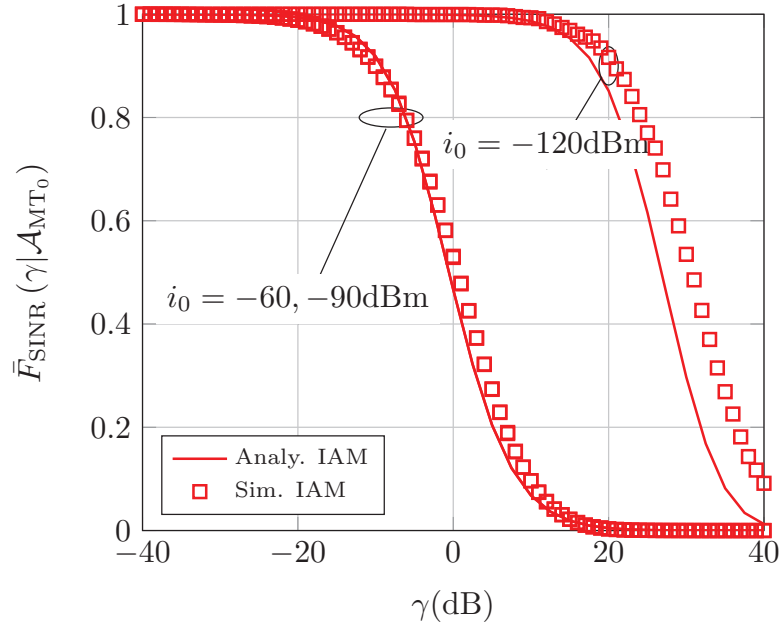


Figure 3.6: CCDF of the SINR for the typical MT conditioned on being active for IAM with $\epsilon = 0.75$, $t^{(1)}/t^{(2)} = 9$ dB, $p_{\max} \rightarrow \infty$ and $i_0 = \{-120, -90, -60\}$ dBm.

3.6.3 Spectral Efficiency and Binary Rate

In this section, the average SE and average BR are analyzed, as well as the IAFPC⁶ and IAM schemes are compared against each other for several system setups.

In Fig. 3.7, the average SE of IAFPC and IAM schemes is analyzed and three conclusions can be drawn. By comparing the average SE of the IAFPC scheme based on the definition given in Section VI (i.e., for AMC schemes) and on the Shannon formula, we note, as expected, that the latter formula provides optimistic estimates of the average SE. By comparing the average SE of the IAM scheme for typical (active and muted) MTs and active (only) MTs, we note a different performance trend as a function of i_0 . As for the active MTs, the average SE increases as i_0 decreases. As for the typical MTs, on the other hand, the average SE decreases as i_0 decreases. This is because the lower i_0 is the more MTs are turned off, which on average, contributes to reduce the SE of the typical MT. By comparing the average SE of IAFPC and IAM schemes, we evince that IAFPC outper-

⁶It is worth noting that the average SE of the IAFPC scheme based on the Shannon formula was analyzed in [47]. In the present chapter, we focus our attention of the more practical definition provided in Section VI.

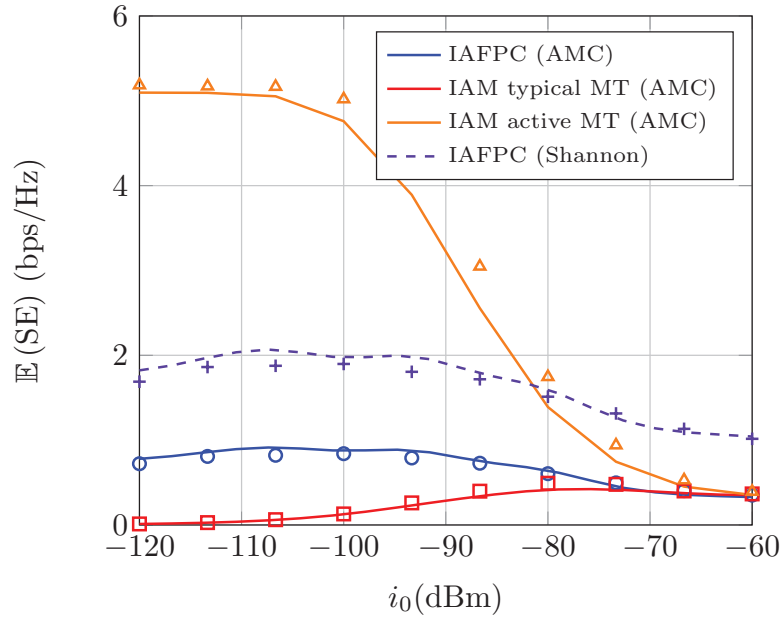


Figure 3.7: Comparison of average SE of IAFPC and IAM for $\epsilon = 1$, $t^{(1)}/t^{(2)} = 9$ dB and $p_{\max} \rightarrow \infty$. As for IAFPC, the average SE based on the Shannon formula is shown as well.

forms IAM for all relevant values of the maximum interference constraint i_0 , since all the MTs are active under the IAFPC scheme. The average SE of the active MTs under the IAM scheme is, however, much better than that of the IAFPC scheme, since the other-cell interference is reduced.

As discussed in Section I, however, the SE does not provide information on the amount of bandwidth that the scheduler allocates to each active MT.

This trade-off is captured by the average BR, which is shown Fig. 3.8. As far as the average BR is concerned, in particular, we note that IAFPC and IAM schemes provide opposite trends compared to those evinced from the analysis of the average SE of the typical MT. More precisely, IAM provides a better average BR than IAFPC and there exists an optimal value of i_0 that maximizes it. This optimal value of i_0 emerges if the typical MT is considered, i.e., the MT may be either active or inactive. The figure, however, shows the average BR achieved only by the active MTs as well. In this case, we note that the MTs that satisfy both power and interference constraints achieve a very high throughput due to the reduce level of interference that is generated in this case. In a

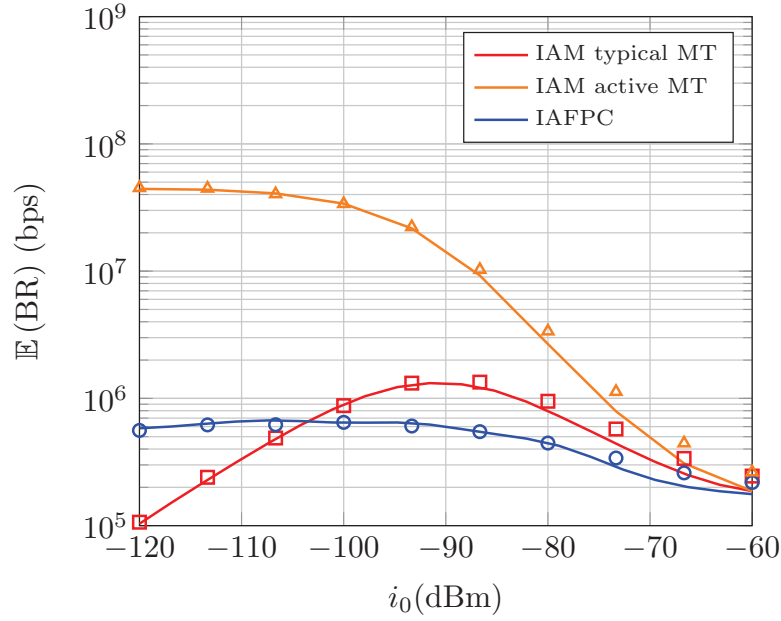


Figure 3.8: Comparison of average BR of IAFPC and IAM for $\epsilon = 1$, $t^{(1)}/t^{(2)} = 9$ dB and $p_{\max} \rightarrow \infty$. As for IAM, two cases are considered: the typical MT and the typical active MT.

nutshell, IAM outperforms IAFPC in terms of average BR because the available bandwidth is shared among fewer MTs (only those active), which results in a higher throughput for each of them. Even though some MTs may be turned off in IAM, this may not necessarily be considered as a downside from the user's perspective: in high-mobility scenarios, for example, some MTs may prefer to be muted for some periods of time if their reward is achieving a higher throughput once they are allowed to transmit. In Fig. 3.9, we study the impact of p_{\max} for a given maximum interference constraint i_0 . We observe that p_{\max} plays a critical role as well and highly affects the average BR. This figure confirms, once again, that both p_{\max} and i_0 constraints need to be appropriately optimized in order for IAM to outperform IAFPC. In Fig. 3.10, we illustrate the potential of IAM of reducing the variance of the interference compared with IUM, while still guaranteeing the same average BR. As discussed in the previous sections, this is beneficial for implementing AMC schemes. The figure shows a four-order magnitude reduction of the variance of the interference for the considered setup of parameters.

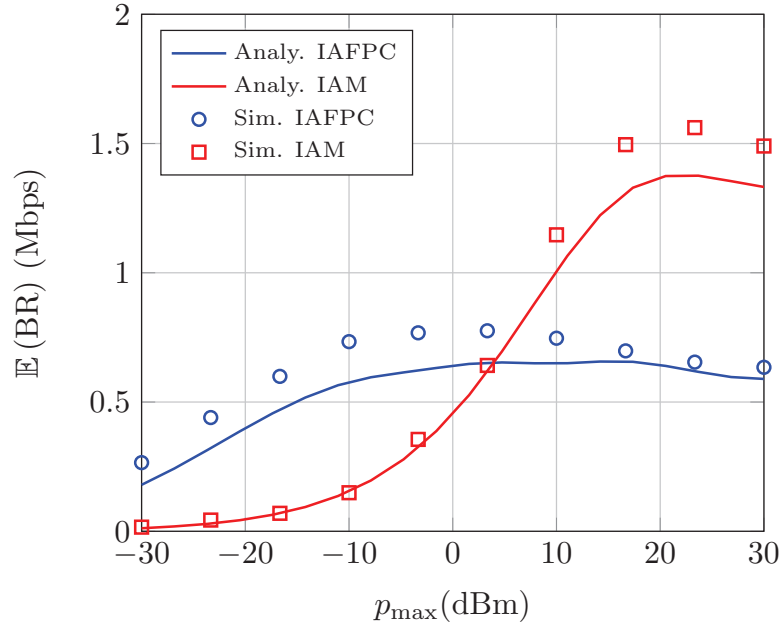


Figure 3.9: Comparison of average BR of IAFPC and IAM for $\epsilon = 1$, $t^{(1)}/t^{(2)} = 9$ dB and $i_0 = -90$ dBm.

3.6.4 Impact of the Association Weights: On UL-DL Decoupling

As shown in [26] and [32], optimizing the performance of HCNs for DL transmission does not necessarily result in optimizing their performance in the UL. Based on the GCA criterion studied in Section IV, this implies that different cell association weights (i.e., a different ratio $t^{(1)}/t^{(2)}$ for two-tier HCNs) may be needed in the DL and in the UL. However, this approach, which is referred to as UL-DL decoupling, introduces additional implementation challenges, which require the modification of the existing network architecture and control plane.

In this section, motivated by these considerations, we analyze and compare IAM, IAFPC and IUFPC schemes as a function of $t^{(1)}/t^{(2)}$. The setup $t^{(1)}/t^{(2)} = 0$ dB corresponds to the SPLA criterion. Some numerical illustrations are provided in Figs. 3.11 and 3.12, where the probability that the typical MT is active and the average BR are shown, respectively.

In Fig. 3.12, in particular, we compare the average BR of IUFPC and IAM schemes. The figure highlights important differences between these two interference management

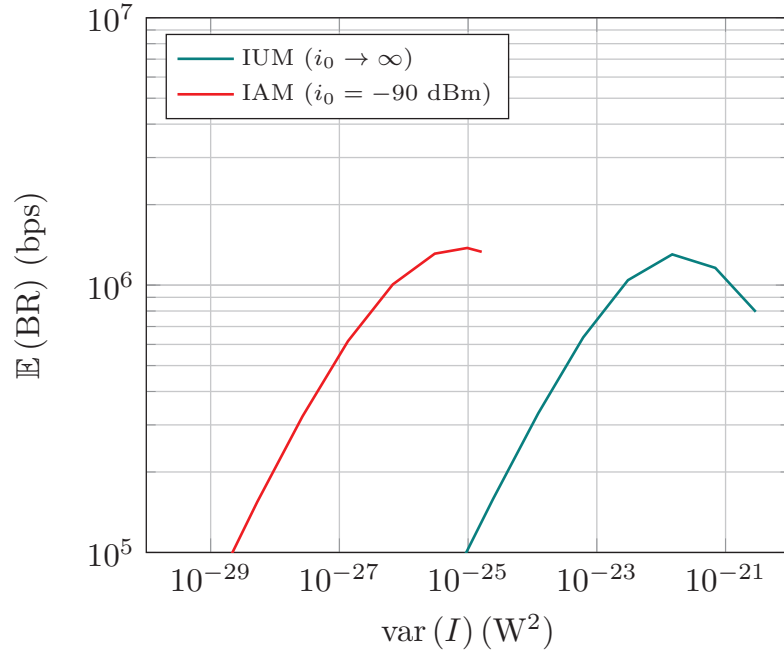


Figure 3.10: Average BR as a function of the variance of the interference for IAM ($i_0 = -90$ dBm) and IUM ($i_0 \rightarrow \infty$) schemes with $p_{\max} = 5$ dBm and $t^{(1)}/t^{(2)} = 9$ dB.

schemes for improving the performance of the UL of HCNs. First of all, we note that the average BR of the IUFPC scheme decreases as the ratio $t^{(1)}/t^{(2)}$ increases. More specifically, the best average BR is obtained if the SPLA criterion is used, which is in agreement with previously published papers [27]. This originates from the fact that the larger $t^{(1)}/t^{(2)}$ is, the more MTs are associated with more distance BSs, which, due to the use of power control, results in increasing the interference in the UL. The performance trend is, on the other hand, different if the IAM scheme is used. In this case, there are several values of i_0 that provide a better average BR compared with IUFPC. In addition, the average BR increases as $t^{(1)}/t^{(2)}$ increases, since the excess interference that is generated under the IUFPC scheme is now kept under control by imposing the maximum interference constraint i_0 . As observed in previous figures, Fig. 3.11 confirms that this gain is obtained since more MTs are turned off.

Figures 3.11 and 3.12 confirm the findings in **Remark 5** and, in particular, the existence of an operating regime where the performance of IAM is independent of the association weights. Let us consider, for example, the setup for $i_0 = -60$ dBm. In this

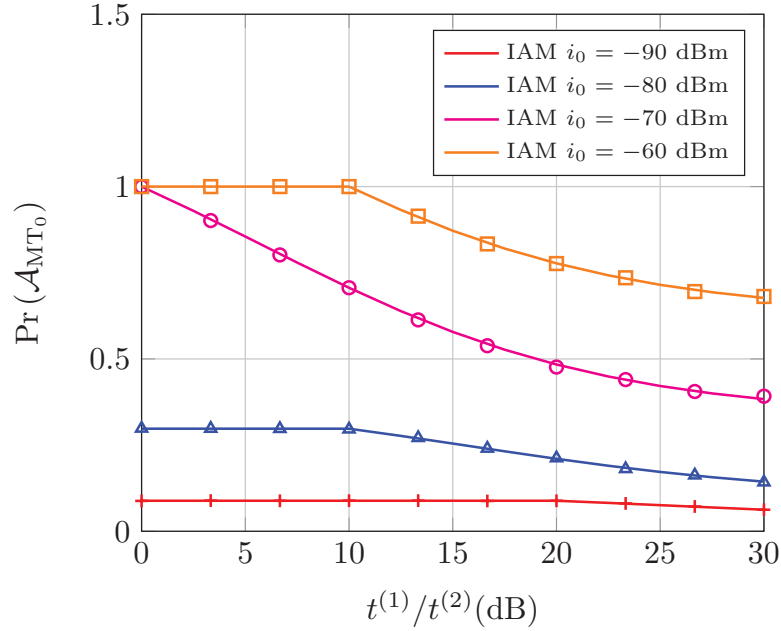


Figure 3.11: Probability the typical MT is active as a function of $t^{(1)}/t^{(2)}$ for IUFPFC ($i_0 \rightarrow \infty$) and IAM with $i_0 = \{-90, -80, -70, -60\}$ dBm. $p_{\max} \rightarrow \infty$ for both schemes.

case, $i_0 > p_0$ and hence, according to **Remark 5**, the system is interference-unaware if $t^{(1)}/t^{(2)} \in [-10, +10]$ dB. Figure 3.12, more specifically, confirms that IAM is interference-unaware since it provides the same average BR as IUFPFC for $t^{(1)}/t^{(2)} \in [-10, +10]$ dB⁷. Similar conclusions can be drawn for other values of i_0 , where different operating regimes can be identified as predicted in **Remark 5**. If $i_0 = -90$ dBm, in particular, then $i_0 < p_0$ and the system is independent of the cell association criterion for $t^{(1)}/t^{(2)} \in [-20, +20]$, which is confirmed in Figs. 3.11 and 3.12. It is worth mentioning that the values of $t^{(1)}/t^{(2)}$ for which the considered system model is cell association independent are usually adopted in practical engineering applications. In particular, the authors of [26, 88] have shown that the optimal cell association ratio that optimizes the DL is usually less than 20 dB. This is in agreement and compatible with the findings in Figs. 3.11 and 3.12. In view of the numerical results and theoretical insights derived in this work, it is possible to state the following arguments in favor of such Interference-Aware Muting procedure:

1. Taking into account the periods where the typical MT is active and those where it

⁷Only positive values (in dB) of the association weights $t^{(1)}/t^{(2)}$ are shown in Figs. 3.11 and 3.12.

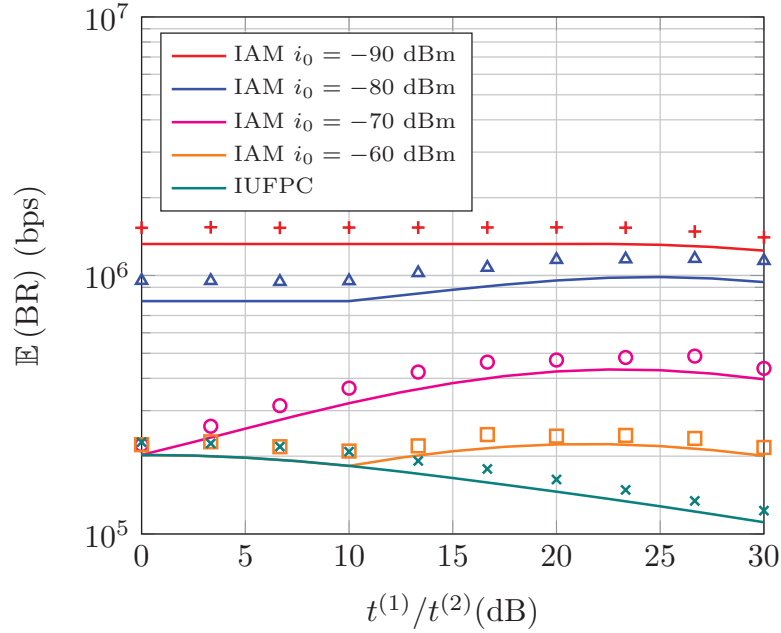


Figure 3.12: Average BR as a function of $t^{(1)}/t^{(2)}$ for IUFPC ($i_0 \rightarrow \infty$) and IAM with $i_0 = \{-90, -80, -70, -60\}$ dBm. $p_{\max} \rightarrow \infty$ for both schemes.

is muted, the average BR is increased with IAM compared to IAFPC and IUFPC.

2. Thanks to mobility and shadowing, MTs are only muted for a given period of time.
3. Since muted MTs do not transmit, its average transmitted power is reduced compared to IAFPC and IUFPC. This has been studied with Fig. 3.1.
4. With IAM, there is a regime where the UL performance is independent of cell association, which eases joint design of UL and DL transmissions as it have been discussed above.
5. It is straightforward to extend the developed model to consider other approaches where IAM take place only in a portion of the resources (e.g., bandwidth), leading to a higher system fairness. Let us consider, for instance, that the system bandwidth is split in two orthogonal sub-bands, e.g., \mathcal{B}_A and \mathcal{B}_M . \mathcal{B}_A is restricted to active MTs, i.e., those whose interference is smaller than i_0 , whereas the other sub-band is used to the rest of MTs⁸.

⁸Although it is possible to study more general frameworks for IAM, we have focused on the case

3.7 Discussion

In this chapter, we have studied the performance of IAM: an interference management scheme for enhancing the throughput of HCNs. With the aid of stochastic geometry, we have developed a general mathematical approach for analyzing and optimizing its performance as a function of several system parameters. Simplified and insightful expressions of the throughput and other relevant performance indicators have been proposed for simplified but relevant case studies, such as in the presence of channel inversion power control and equal cell association weights. Among the many performance trends that have been identified, we have proved that, while optimizing the DL and the UL of HCNs necessitates, in general, to use different cell association weights, there exist some operating regimes where IAM is cell association independent. This is shown to simplify the design of HCNs, since no changes in their control plane is needed compared with conventional cellular networks. The mathematical frameworks and findings have been substantiated against Monte Carlo simulations, as well as the achievable performance of IAM has been compared against other IAFPC and IUFPC schemes, by highlighting several important trade-offs in terms of system fairness and system throughput. Our analysis has unveiled that the design of HCNs based on IAM necessitates the optimization of several parameters, among which the maximum transmit power constraint of the MTs, the maximum interference constraint at the BSs, and the fractional power control compensation factor.

These aforementioned contributions appear in [50], which has been accepted for publication, and [51], which is a work under review.

3.8 Appendix: Proof of Proposition 2

The probability that a MT is active is by definition as follows:

$$\Pr(\mathcal{A}_{\text{MT}_0}) = \sum_{j \in \mathcal{K}} \sum_{m \in \mathcal{K}} \Pr\left(\mathcal{X}_{\text{MT}_0}^{(j,m)}, \mathcal{A}_{\text{MT}_0}\right) \quad (3.39)$$

considered in this chapter due to space limitations and to study deeper the effect of MTs muting.

where $\Pr\left(\mathcal{X}_{\text{MT}_0}^{(j,m)}, \mathcal{A}_{\text{MT}_0}\right)$ is the probability that the MT is active, is associated to tier j and that the most interfered BS belongs to tier m . If $j \neq m$, it can be written as follows:

$$\Pr\left(\mathcal{X}_{\text{MT}_0}^{(j,m)}, \mathcal{A}_{\text{MT}_0}\right) \stackrel{(a)}{=} \mathbb{E}_{R_{\text{MT}_0,(1)}^{(m)}} \mathbb{E}_{R_{\text{MT}_0,(1)}^{(j)}, R_{\text{MT}_0,(2)}^{(j)}} \left[\begin{aligned} & \mathbf{1}\left(R_{\text{MT}_0,(1)}^{(m)} > \left(\frac{t^{(m)}}{t^{(j)}}\right)^{\frac{1}{\alpha}} R_{\text{MT}_0,(1)}^{(j)}\right) \times \mathbf{1}\left(R_{\text{MT}_0,(1)}^{(m)} < R_{\text{MT}_0,(2)}^{(j)}\right) \times \\ & \mathbf{1}\left(R_{\text{MT}_0,(1)}^{(j)} < \frac{1}{\tau} \left(\frac{p_{\max}}{p_0}\right)^{\frac{1}{\alpha\epsilon}}\right) \times \mathbf{1}\left(R_{\text{MT}_0,(1)}^{(m)} > \left(\frac{p_0}{i_0}\right)^{\frac{1}{\alpha}} \frac{(\tau R_{\text{MT}_0,(1)}^{(j)})^\epsilon}{\tau}\right) \end{aligned} \right] \quad (3.40)$$

where (a) is obtained by definition of expectation formulated with the aid of indicator functions.

To compute this expectation, the PDF of the distance of the nearest BS and of the joint PDF of the distances of the nearest and second nearest BSs are needed. By definition of PPP, they are equal to $f_{R_{\text{MT}_0,(1)}^{(j)}}(r) = 2\pi\lambda^{(j)}re^{-\pi\lambda^{(j)}r^2}$ and $f_{R_{\text{MT}_0,(1)}^{(j)}, R_{\text{MT}_0,(2)}^{(j)}}(r_1, r_2) = 4(\pi\lambda^{(j)})^2 r_1 r_2 e^{-\pi\lambda^{(j)}r_2^2}$ for $r_1 < r_2$, respectively, [52]. With the aid of these PDFs, we obtain:

$$\Pr\left(\mathcal{X}_{\text{MT}_0}^{(j,m)}, \mathcal{A}_{\text{MT}_0}\right) = \int_{r_1^{(j)}=0}^{\frac{1}{\tau} \left(\frac{p_{\max}}{p_0}\right)^{\frac{1}{\alpha\epsilon}}} \int_{r_1^{(m)}=\max\left(\left(\frac{p_0}{i_0}\right)^{\frac{1}{\alpha}} \frac{(\tau r_1^{(j)})^\epsilon}{\tau}, \left(\frac{t^{(m)}}{t^{(j)}}\right)^{\frac{1}{\alpha}} r_1^{(j)}\right)}^{\infty} f_{R_{\text{MT}_0,(1)}^{(m)}}\left(r_1^{(m)}\right) \int_{r_2^{(j)}=\max\left(r_1^{(j)}, r_1^{(m)}\right)}^{\infty} f_{R_{\text{MT}_0,(1)}^{(j)}, R_{\text{MT}_0,(2)}^{(j)}}\left(r_1^{(j)}, r_2^{(j)}\right) dr_2^{(j)} dr_1^{(m)} dr_1^{(j)} \quad (3.41)$$

The computation of the two-fold integral leads to the function $\nu^{(j)}(v)$ that is provided in (3.9).

The case $j = m$ can be solved by using an approach similar to the previous case. The final result corresponds to the function $\eta^{(j)}(v)$ available in (3.10).

By combining both cases $j = m$ and $j \neq m$, $\Pr\left(\mathcal{X}_{\text{MT}_0}^{(j,m)}, \mathcal{A}_{\text{MT}_0}\right)$ can be written as

follows:

$$\Pr \left(\mathcal{X}_{\text{MT}_0}^{(j,m)}, \mathcal{A}_{\text{MT}_0} \right) = \int_0^{\frac{1}{\tau} \left(\frac{p_{\max}}{p_0} \right)^{\frac{1}{\alpha \epsilon}}} \left(\mathbf{1}(j \neq m) \nu^{(j,m)}(v) + \mathbf{1}(j = m) \eta^{(j)}(v) \right) dv \quad (3.42)$$

The proof follows by computing the summation over $m \in \mathcal{K}$ in (3.39).

3.9 Appendix: Proof of Lemma 5

The Laplace transform of the interference can be expressed as follows:

$$\begin{aligned} \mathcal{L}_I \left(s | \mathcal{X}_{\text{MT}_0}^{(j)} \right) &= \mathbb{E}_I \left[e^{-sI} | \mathcal{X}_{\text{MT}_0}^{(j)} \right] = \prod_{k \in \mathcal{K}} \mathbb{E}_{\Psi^{(k)}} \\ &\prod_{\text{MT}_i \in \Psi^{(k)}} \mathbb{E}_{R_{\text{MT}_i}} \left[\mathbb{E}_{H_{\text{MT}_i}} \exp \left(-s H_{\text{MT}_i} (\tau D_{\text{MT}_i})^{-\alpha} (\tau R_{\text{MT}_i})^{\alpha \epsilon} p_0 \mathbf{1} \left(\mathcal{O}_{\text{MT}_i}^{(j,k)} \right) \mathbf{1} \left(\mathcal{Z}_{\text{MT}_i} \right) \right) | \mathcal{X}_{\text{MT}_i}^{(k)}, \mathcal{A}_{\text{MT}_i} \right] \end{aligned} \quad (3.43)$$

By applying the Probability Generating Functional (PGF) theorem in [61] and computing the expectation with respect to the channel fading, $\mathcal{L}_I \left(s | \mathcal{X}_{\text{MT}_0}^{(j)} \right)$ is as follows:

$$\exp \left(- \sum_{k \in \mathcal{K}} 2\pi \lambda^{(k)} \int_{\rho=0}^{\infty} \mathbb{E}_{R_{\text{MT}_i}} \left[\mathbf{1} \left(\mathcal{O}_{\text{MT}_i}^{(j,k)} \right) \mathbf{1} \left(\mathcal{Z}_{\text{MT}_i} \right) \frac{s (\tau \rho)^{-\alpha} (\tau R_{\text{MT}_i})^{\alpha \epsilon} p_0}{1 + s (\tau \rho)^{-\alpha} (\tau R_{\text{MT}_i})^{\alpha \epsilon} p_0} \rho | \mathcal{X}_{\text{MT}_i}^{(k)}, \mathcal{A}_{\text{MT}_i} \right] d\rho \right) \quad (3.44)$$

By conditioning on the event $\mathcal{Q}_{\text{MT}_i}^{(n)}$ defined in (3.2) and by using the total probability theorem, $\mathcal{L}_I \left(s | \mathcal{X}_{\text{MT}_0}^{(j)} \right)$ can be written as follows:

$$\begin{aligned} &\exp \left(- \sum_{k \in \mathcal{K}} 2\pi \lambda^{(k)} \sum_{n \in \mathcal{K}} \Pr \left(\mathcal{Q}_{\text{MT}_i}^{(n)} | \mathcal{X}_{\text{MT}_i}^{(k)}, \mathcal{A}_{\text{MT}_i} \right) \right. \\ &\left. \int_{\rho=0}^{\infty} \mathbb{E}_{R_{\text{MT}_i}} \left[\mathbf{1} \left(\mathcal{O}_{\text{MT}_i}^{(j,k)} \right) \mathbf{1} \left(\mathcal{Z}_{\text{MT}_i} \right) \frac{s (\tau \rho)^{-\alpha} (\tau R_{\text{MT}_i})^{\alpha \epsilon} p_0}{1 + s (\tau \rho)^{-\alpha} (\tau R_{\text{MT}_i})^{\alpha \epsilon} p_0} \rho | \mathcal{X}_{\text{MT}_i}^{(k,n)}, \mathcal{A}_{\text{MT}_i} \right] d\rho \right) \end{aligned} \quad (3.45)$$

The next step is the computation of the expectation with respect to R_{MT_i} by condi-

tioning on $\mathcal{X}_{\text{MT}_i}^{(k,n)} \cap \mathcal{A}_{\text{MT}_i}$ and by applying the definition of the event $\mathcal{O}_{\text{MT}_i}^{(j,k)}$ in (3.5) and of $\mathcal{Z}_{\text{MT}_i}$ in (3.6). In particular, by conditioning on $\mathcal{X}_{\text{MT}_i}^{(k,n)} \cap \mathcal{A}_{\text{MT}_i}$ for $\text{MT}_i \in \Psi^{(k)}$, the distances R_{MT_i} are independent and identically distributed random variables whose PDF is in (3.11). With some algebra, $\mathcal{L}_I \left(s | \mathcal{X}_{\text{MT}_0}^{(j)} \right)$ can be written as follows:

$$\exp \left(- \sum_{k \in \mathcal{K}} 2\pi\lambda^{(k)} \sum_{n \in \mathcal{K}} \Pr \left(\mathcal{Q}_{\text{MT}_i}^{(n)} | \mathcal{X}_{\text{MT}_i}^{(k)}, \mathcal{A}_{\text{MT}_i} \right) \int_{r=0}^{\infty} f_{R_{\text{MT}_i}} \left(r | \mathcal{X}_{\text{MT}_i}^{(k,n)}, \mathcal{A}_{\text{MT}_i} \right) \int_{\rho=\max \left(\left(\frac{t^{(j)}}{t^{(k)}} \right)^{\frac{1}{\alpha}} r, \left(\frac{p_0}{i_0} \right)^{\frac{1}{\alpha}} \frac{(\tau r)^\epsilon}{\tau} \right)}^{\infty} \frac{s (\tau \rho)^{-\alpha} (\tau r)^{\alpha \epsilon} p_0}{1 + s (\tau \rho)^{-\alpha} (\tau r)^{\alpha \epsilon} p_0} \rho d\rho dr \right) \quad (3.46)$$

The proof follows by computing the inner integral.

Chapter 4

Multi-User Coverage Probability in the Uplink of Cellular Systems

We analyze the coverage probability of multi-user uplink cellular networks with fractional power control. We use a stochastic geometry approach where the mobile users are distributed as a Poisson Point Process (PPP), whereas the serving base station (BS) is placed at the origin. Using conditional thinning, we are able to calculate the coverage probability of k users which are allocated a set of orthogonal resources in the cell of interest, obtaining analytical expressions for this probability considering their respective distances to the serving BS. These expressions give useful insights on the interplay between the power control policy, the interference level and the degree of fairness among different users in the system.

4.1 Introduction

Aiming to satisfy the ever-increasing demand for higher data rates, modern cellular technologies like Long Term Evolution (LTE) use aggressive frequency reuse policies, which have accentuated the problem of inter-cell interference compared to previous standards [89]. This interference is highly dependent on the transmitted power of the different users, whose random positions and mobility affects the ability of the base stations (BS) to mitigate this problem. This causes huge differences on the received Signal to Interference plus Noise Ratio (SINR) due to path loss, being specially critical for cell-edge users, that tend

to have a poorer performance compared to users located closer to the BS.

Each BS must also ensure a certain Quality of Service (QoS) for every user; hence, power control becomes a fundamental mechanism in the uplink (UL), as it impacts on the fairness among the users in the serving cell as well as on the level of interference caused to neighbor cells. Compared to the downlink (DL), the UL poses additional challenges since: (1) users positions are coupled with its serving BS, and (2) when power control is used, the interference level coming from a certain user depends not only on the distance of the BS to this user, but also on the distance between this interfering user and its serving BS. Additionally, even without power control, the interference behavior in the UL and DL is rather dissimilar. In the DL, those transmissions intended for cell-edge users tend to have stronger interference than for cell-interior ones, whereas in the UL all transmissions from the users inside the cell experience an interference with the same statistics.

Stochastic geometry has emerged as a promising tool to analyze the performance of cellular systems, being an alternative to traditional approaches based on Wyner-type interference and hexagonal grid models, whose accuracy is known to be limited in different circumstances [25]. This approach typically considers the positions of transmitting nodes as a Poisson Point Process (PPP) where the receiver is placed at the origin [19] of a 2-D spatial grid. Despite being originally considered for ad-hoc and sensor networks due to the arbitrary positions of the nodes in such networks, the irregular cell patterns in modern cellular networks makes it the perfect technique to analyze their performance [21].

While most works based on random spatial models have focused on DL scenarios, their adequacy for modeling UL cellular networks has recently been addressed in [29]. In this work, the authors provided the first known analytical results for the coverage probability of a typical user in a UL set-up, where fractional power control was implemented. As main assumptions, validated with realistic simulation models, they considered that the distances between interfering users and its serving BS are independent and identically distributed (i.i.d.), and that the BS falls in the Voronoi tessellation of each user. Based on this new approach, new analyses have been conducted in other UL scenarios involving fractional frequency reuse [90] or multi-tier cellular networks [31].

Previous works in the literature are usually focused on only one active link between the transmitter and receiver nodes. Specifically, in [29] their analysis considers the link between the serving BS of interest (placed at the origin) and a typical user. Since this

randomly selected user can be located anywhere in the cell (cell interior, cell-edge, etc.), results are averaged over all spatial positions inside the cell. Although these results yield interesting insights on the performance of a typical user, they do not provide a clear understanding about the fairness among the users, or the performance of cell-edge users. Results concerning the coverage probability of UL cellular networks with multiple users are not available in the literature to the best of our knowledge.

In this chapter, we present an analytical framework for the analysis of multi-user UL cellular systems with fractional power control, based on conditional thinning [91, 92]. This technique has been used to model non-uniform user location distributions in DL transmissions [91] and different traffic load of each tier in heterogeneous networks [92]. In our work, conditional thinning is used to obtain the set of interfering users for an arbitrary UL transmission allocated over one out of k orthogonal resource blocks (RBs).

Using this new approach, the coverage probability of the l^{th} user is obtained and ordered according to the distance from the user to the serving BS, which allocates k RBs to k scheduled users ($1 \leq l \leq k$). The joint distribution of the distances between the l^{th} and k^{th} users to the serving BS is also derived. Results give useful insights on the relation between power control and fairness among users.

The rest of the chapter is structured as follows. In Section 4.2, we describe the system model and introduce our analytical framework based on conditional thinning. The main mathematical results are presented in Section 4.3, namely the joint distribution of the distances between the l^{th} and k^{th} users to the serving BS, and the multi-user coverage probability. Numerical results are given in Section 4.4, whereas main conclusions are drawn in section 4.5.

Notation: Throughout this chapter, $|\cdot|$ stands for the Lebesgue measure, $\mathbb{E}[\cdot]$ for the expectation operator and $\mathbb{P}[\cdot]$ for a probability measure. Random Variables (RVs) are represented with capital letters X whereas deterministic variables are associated with lower case letters x . The conditional expectation of X conditioned on $Y = y$ is denoted as $\mathbb{E}_{X|y}[X|y]$. $B(o, r)$ represents the closed ball centered at the origin o being $r = \|x\|$ the distance from $x \in \mathbb{R}^2$ to o .

4.2 System Model

4.2.1 System Model Description

In this chapter we propose a system model that allows for a tractable analysis of multi-user UL scenarios with fractional power control, assuming one antenna at both transmitter and receiver sides. This model is illustrated in Fig. 4.1.

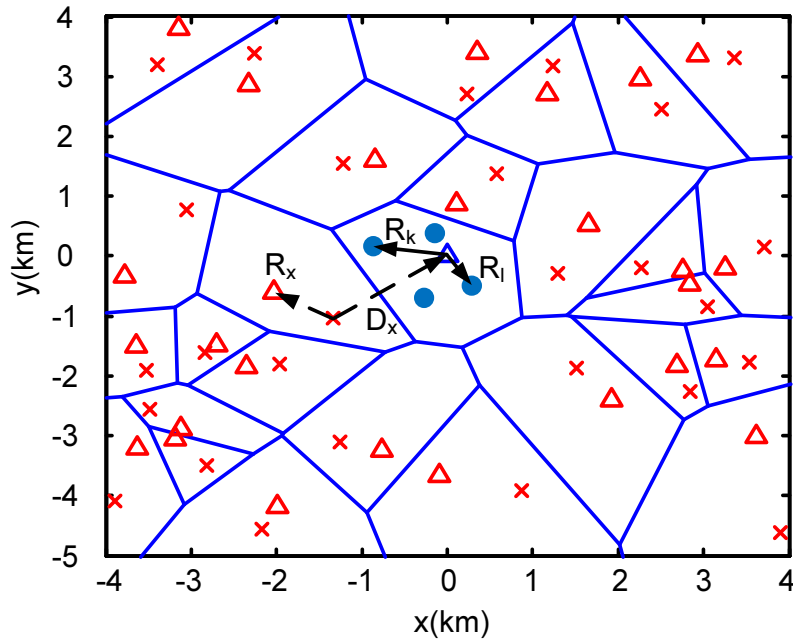


Figure 4.1: System model of multi-user UL cellular system. BSs are represented by triangles (blue: serving BS), scheduled users inside the serving cell are represented by blue dots, interfering users for the l^{th} user transmission are depicted with a red cross. The distance from one interfering user to its serving BS (R_x) and to the target BS (D_x) are represented as an example. Only scheduled users are represented.

The target BS is considered to be placed at the origin allocating k RBs among users. Each BS perform round robin scheduling for each RB, i.e. a user is selected randomly without repetition for each RB. Each user is allocated at most a single RB at each time and all users have the same probability of being selected. We consider that the density of users is much greater than the density of BSs so all RBs are allocated (fully loaded cells), i.e. all cells have more than k users and k of them are scheduled. The scheduled users, which are represented with blue dots, are ordered according to their distance to its serving

BS, i.e. the origin. We focus on the l^{th} scheduled user placed at distance R_l from the origin with $0 \leq R_1 \leq \dots \leq R_l \leq \dots \leq R_k$. The BS positions of the interfering cells are indicated by red triangles, whereas the interfering users for the l^{th} user data transmission are represented by red crosses.

Since fractional power control is considered, the transmitted power depends on the distance between the user and its serving BS. This distance is represented as R_x for an interfering user placed at $x \in \Phi_{i,l}$, where $\Phi_{i,l}$ denotes the random set of interfering user locations for l^{th} user data transmission. Similarly, the distance between the interfering user located at x and the target BS (i.e. the origin) is represented as D_x .

Power loss due to propagation is modeled using a standard path loss model with $\alpha > 2$, whereas a Rayleigh model is assumed for small-scale fading. Fractional power control with parameter ϵ is assumed, hence the received signal power at distance D_x from a user placed at distance R_x from its BS is given by $G_x R_x^{\alpha\epsilon} D_x^{-\alpha}$, where G_x is the fading coefficient that follows an exponential distribution with mean $1/\mu$. Thus, the SINR for the l^{th} user data transmission follows the next expression

$$\text{SINR}_l = \frac{G_l R_l^{\alpha(\epsilon-1)}}{I_l + \sigma^2} \quad (4.1)$$

where σ^2 is the AWGN noise power and I_l accounts for the interference experienced by the l^{th} user transmission, given by

$$I_l = \sum_{x \in \Phi_{i,l}} G_x R_x^{\alpha\epsilon} D_x^{-\alpha} \quad (4.2)$$

It is important to note that in the UL, the interference suffered by all k users transmission has the same statistics since interfering users positions scheduled at each RB are expected to have the same distribution. Hence, from now on we will omit the sub-index l in Φ_i for notation simplicity.

4.2.2 Proposed Analytical Model

The proposed model for multi-user uplink analysis is illustrated in Fig. 4.2. This model uses *conditional thinning* in order to deal with multiple active links within the cell of interest. Let us consider the target BS to be placed at the origin and an uniform PPP

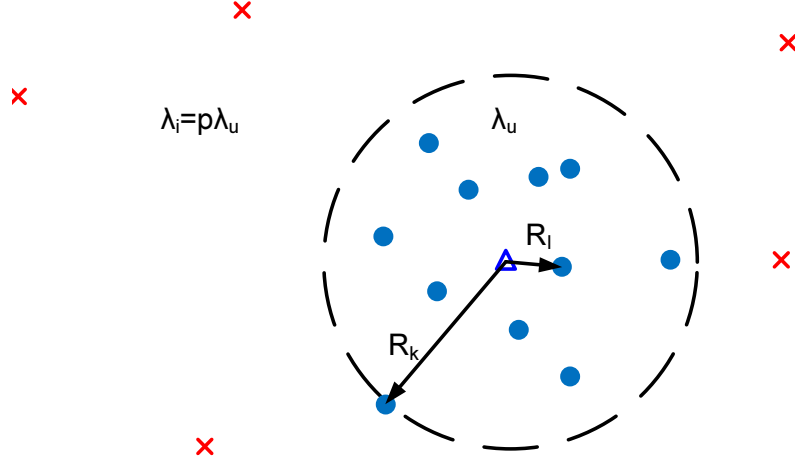


Figure 4.2: Multi-User UL set-up based on conditional thinning for $k = 11$. Interfering users for the l^{th} user transmission are represented with red crosses.

Φ of intensity λ over \mathbb{R}^2 that represents the set of scheduled users. We use conditional thinning as follows:

First, the k nearest points of Φ to the origin are selected. These points represent the locations of k users scheduled in k RBs. Then, thinning with probability p is performed to all points except those k inside the closed ball $B(o, r_k)$, being r_k the distance to the k^{th} point.

The resulting set of points outside the ball $B(o, r_k)$ is a non-uniform PPP Φ_i of intensity measure $\Lambda_i(A) = p\lambda|A \setminus B(o, r_k)|$ [93]. Such random set of points represents the interfering user locations for the l^{th} user data transmission. Since these interfering users are using one of k available RBs, we choose the thinning probability to be $p = 1/k$. As the model considers that there is only one user scheduled per RB per cell, the intensity of BSs is exactly the same as the intensity of interfering users. The random set of k nearest points around the origin Φ_d represents the scheduled users and it has an intensity measure $\Lambda_d(A) = \lambda|A \cap B(o, r_k)|$.

As in [29] distances $\{R_x\}$ from each interfering user to its serving BS are assumed to be i.i.d. RVs following Rayleigh distributions with

$$f_{R_x}(r_x) = 2\pi p\lambda r_x e^{-p\lambda\pi r_x^2}, r_x \geq 0 \quad (4.3)$$

Hence, notice that the proposed model is equivalent to the model presented in [29] for

$p = 1$, and $k = l = 1$.

4.2.3 Simulation Model

In order to assess the validity of the proposed analysis model, we also introduce a more realistic model for simulation. A uniform PPP Φ_b of intensity λ_b representing the BS locations is first considered. Since in the analysis model the intensity of BSs is the same as that of interfering users, we use $\lambda_b = \lambda/k$ aiming to compare the results of both models.

The association between user and BS is based on distance, hence the Voronoi tessellation is performed over Φ_b where one randomly chosen point is the target BS. Then, k points representing the k scheduled users are placed randomly inside the target cell, whereas only one user is placed in each interfering cell. Notice that both sets of points, scheduled users inside the target cell and interfering users, are not a PPP. To explain that, recall that the number of points falling in a Voronoi cell tends to be higher as the cell is bigger; in our case, one interfering user falls in any cell independently of its size. Since there is an interfering user in each interfering cell we model the case of a fully loaded network where the density of users is much greater than the density of BSs and there are not empty cells.

4.3 Mathematical Results

After presenting the analytical framework for the analysis of multi-user UL cellular networks, we now present the main mathematical contributions of this chapter. First, we derive the joint distribution of the distances between the l^{th} and k^{th} users and the serving BS. Then, we use this result to calculate the coverage probability of the l^{th} user in the investigated scenario.

4.3.1 Joint Distribution of Distances

In the analytical model, the k users of interest are ordered according to their distances to the serving BS (i.e., the origin), and the interfering users are located at a distance greater than R_k . This interdependence affects the distribution of the SINR for the l^{th} user

transmission, due to the inherent correlation between R_l and R_k . In the next lemma, we calculate their joint pdf.

Lemma 8. *The joint pdf of R_l and R_k with $0 < l < k$ is*

$$f_{R_l, R_k}(r_l, r_k) = \frac{4e^{-\pi r_k^2 \lambda} (\lambda \pi)^k r_k r_l^{2l-1} (r_k^2 - r_l^2)^{k-l-1}}{(k-l-1)!(l-1)!} \quad (4.4)$$

where $0 \leq r_l \leq r_k$.

Proof. The calculation of the joint pdf follows a similar procedure as in [91]. Hence, we define disjoint sets in order to use the independence property of the PPP. Let us consider the next disjoint sets

$$\begin{aligned} \Psi_1 &= \{x \in \mathbb{R}^2 : \|x\| \leq r_l\} \\ \Psi_2 &= \{x \in \mathbb{R}^2 : r_l < \|x\| \leq r_l + dr_l\} \\ \Psi_3 &= \{x \in \mathbb{R}^2 : r_l + dr_l < \|x\| \leq r_k\} \\ \Psi_4 &= \{x \in \mathbb{R}^2 : r_k < \|x\| \leq r_k + dr_k\} \end{aligned} \quad (4.5)$$

The joint pdf of R_l and R_k with $0 < l < k$ is by definition

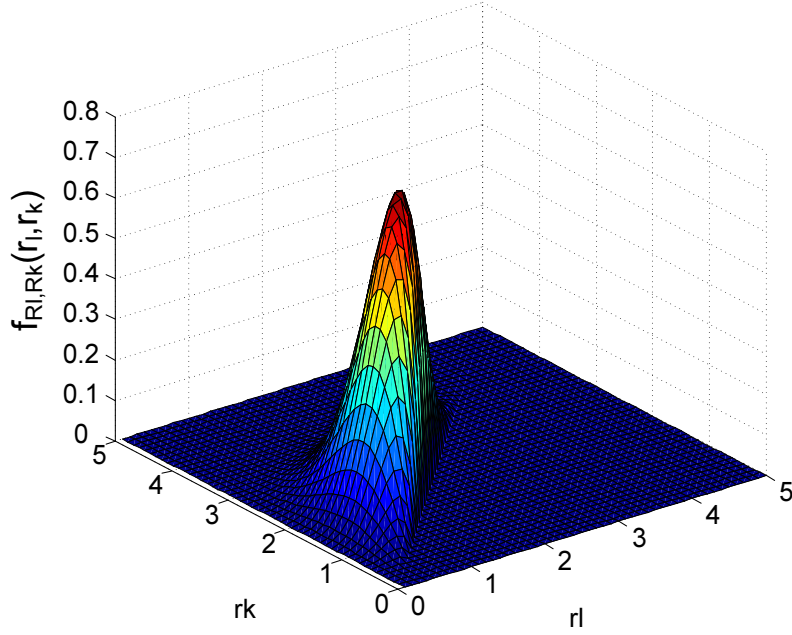
$$f_{R_l, R_k}(r_l, r_k) = \lim_{\substack{dr_l \rightarrow 0 \\ dr_k \rightarrow 0}} \frac{\mathbb{P}\{R_l \in \Psi_2, R_k \in \Psi_4\}}{dr_l dr_k} \quad (4.6)$$

Notice that the numerator can be expressed as follows:

$$\begin{aligned} \mathbb{P}\{R_l \in \Psi_2, R_k \in \Psi_4\} &= \\ \mathbb{P}\{\Phi(\Psi_1) = l-1\} \cdot \mathbb{P}\{\Phi(\Psi_2) = 1\} \cdot \mathbb{P}\{\Phi(\Psi_3) = k-l-1\} \cdot \mathbb{P}\{\Phi(\Psi_4) = 1\} \end{aligned} \quad (4.7)$$

being $\Phi(\Psi)$ a random counting measure of a Borel set Ψ . Since Φ is a uniform PPP, $\Phi(\Psi)$ follows Poisson distribution with mean $\lambda|\Psi|$ [93]. Substituting the probability of each event in (4.7) and calculating the limits in (4.6) yields the desired pdf. \square

Figs. 4.3 and 4.4 illustrate the joint pdf of the distances for the second and the k^{th} user, when $k = 4$ and $k = 50$, respectively. The correlation is more noticeable when l and k have similar values.

Figure 4.3: Joint pdf for $l = 2$ and $k = 4$ with $\lambda = 0.24$

4.3.2 Multi-User Coverage Probability

The coverage probability represents the probability for a user to have a SINR higher than certain threshold t . The main result is stated in Theorem 3, which corresponds to the coverage probability of the l^{th} user.

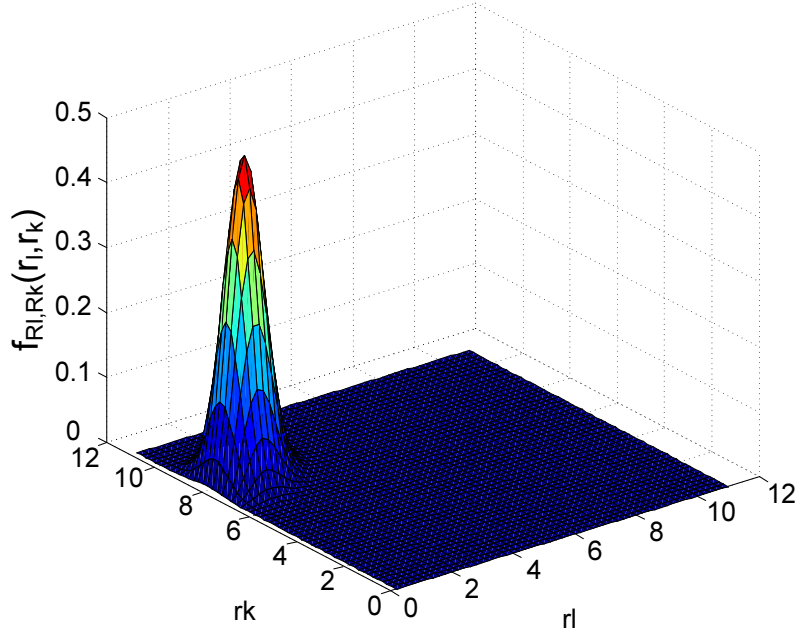
Theorem 3 (Multi-user coverage probability). *The coverage probability of the l^{th} user considering a system with k RBs that are distributed among k active users with $l < k$ is given by:*

$$p_c(l, k, t, \lambda, p, \alpha, \epsilon, \mu, \sigma^2) = \mathbb{E}_{R_l, R_k} [\xi(r_l, r_k)] = \int_0^\infty \int_{r_l}^\infty \xi(r_l, r_k) f_{R_l, R_k}(r_l, r_k) dr_k dr_l \quad (4.8)$$

where $f_{R_l, R_k}(r_l, r_k)$ is the joint pdf of distances and

$$\xi(r_l, r_k) = e^{-\mu t \sigma^2 r_l^{\alpha(1-\epsilon)}} \mathcal{L}_{I_l | r_l, r_k}(\mu t r_l^{\alpha(1-\epsilon)}) \quad (4.9)$$

being $\mathcal{L}_{I_l | r_l, r_k}(s)$ the Laplace transform of the interference conditioned on r_l and r_k . This

Figure 4.4: Joint pdf for $l = 2$ and $k = 50$ with $\lambda = 0.24$

term evaluated at $s = \mu t r_l^{\alpha(1-\epsilon)}$ has the following expression

$$\mathcal{L}_{I_l|r_l, r_k}(\mu t r_l^{\alpha(1-\epsilon)}) = \exp\left(-2\pi p \lambda \int_{r_k}^{\infty} \left(1 - \int_0^{\infty} \frac{\pi p \lambda e^{-p\lambda\pi q}}{1 + t r_l^{\alpha(1-\epsilon)} q^{\alpha\epsilon/2} v^{-\alpha}} dq\right) v dv\right) \quad (4.10)$$

Proof. The coverage probability for the l^{th} user can be expressed as

$$\begin{aligned} p_c(l, k, t, \lambda, p, \alpha, \epsilon, \mu, \sigma^2) &= \mathbb{P}[\text{SINR}_l > t] \stackrel{(a)}{=} \int_0^{\infty} \mathbb{P}[\text{SINR}_l > t | r_l] f_{R_l}(r_l) dr_l \\ &= \int_0^{\infty} \mathbb{P}[G_l > t(I_l + \sigma^2)r_l^{\alpha(1-\epsilon)} | r_l] f_{R_l}(r_l) dr_l \\ &\stackrel{(b)}{=} \int_0^{\infty} \mathbb{E}_{I_l} \left[\mathbb{P}[G_l > t(i_l + \sigma^2)r_l^{\alpha(1-\epsilon)} | r_l, i_l] \right] f_{R_l}(r_l) dr_l \\ &\stackrel{(c)}{=} \int_0^{\infty} e^{-\mu t \sigma^2 r_l^{\alpha(1-\epsilon)}} \mathbb{E}_{I_l|r_l} \left[e^{-\mu t I_l r_l^{\alpha(1-\epsilon)}} | r_l \right] f_{R_l}(r_l) dr_l \end{aligned} \quad (4.11)$$

where (a) and (b) follow from the total probability theorem, while (c) follows from the fact that G_l has an exponential distribution with mean $1/\mu$.

The term $\mathcal{L}_{I_l|r_l}(s) = \mathbb{E}_{I_l|r_l} [e^{-sI_l} | r_l]$ represents the Laplace transform of the interference

conditioned on r_l . The RV R_l and R_k are correlated as $R_l \leq R_k$. Since I_l depends on R_k due to the fact that the interfering users are placed farther than R_k , the RV I_l also depends on R_l . Hence we have to deal with such dependence as follows

$$\begin{aligned}\mathcal{L}_{I_l|r_l}(s) &= \mathbb{E}_{I_l|r_l} \left[\mathbb{E}_{R_k} \left[e^{-sI_l} | r_l, r_k \right] \right] \\ &= \mathbb{E}_{I_l|r_l} \left[\int_{r_l}^{\infty} e^{-sI_l} f_{R_k|r_l}(r_k) dr_k | r_l \right] \\ &= \int_{r_l}^{\infty} \mathbb{E}_{I_l|r_l, r_k} \left[e^{-sI_l} | r_l, r_k \right] f_{R_k|r_l}(r_k) dr_k\end{aligned}\quad (4.12)$$

where the total probability theorem and linearity of expectation operator have been used.

The term $\mathcal{L}_{I_l|r_l, r_k}(s) = \mathbb{E}_{I_l|r_l, r_k} \left[e^{-sI_l} | r_l, r_k \right]$ stands for the Laplace transform of the interference conditioned on r_l and r_k and can be expressed as

$$\begin{aligned}\mathcal{L}_{I_l|r_l, r_k}(s) &= \mathbb{E}_{\Phi_i, \{G_x\}} \left[e^{-s \sum_{x \in \Phi_i} G_x R_x^{\alpha \epsilon} D_x^{-\alpha}} \right] \\ &\stackrel{(a)}{=} \mathbb{E}_{R_x, D_x} \left[\prod_{x \in \Phi_i} \mathbb{E}_{G_x} \left[e^{-s G_x R_x^{\alpha \epsilon} D_x^{-\alpha}} \right] \right] \\ &\stackrel{(b)}{=} \mathbb{E}_{D_x} \left[\prod_{x \in \Phi_i} \mathbb{E}_{R_x} \left[\frac{\mu}{\mu + s R_x^{\alpha \epsilon} D_x^{-\alpha}} \right] \right] \\ &\stackrel{(c)}{=} \exp \left(-2\pi \lambda p \int_{r_k}^{\infty} \left(1 - \int_0^{\infty} \frac{\mu \pi \lambda p e^{-p \lambda \pi q} dq}{\mu + s q^{\frac{\alpha \epsilon}{2}} v^{-\alpha}} \right) v dv \right)\end{aligned}\quad (4.13)$$

where the dependence with R_l and R_k resides in the non-uniform PPP Φ_i since its intensity is $\Lambda_i(A) = p\lambda|A \setminus B(o, r_k)|$. Step (a) comes from the fact that the fading is independent of the PPP, (b) comes from the independence assumption between R_x and D_x and (c) from the Probability Generating Functional (PGFL) [93] and the assumption of R_x following a Rayleigh distribution as in [29].

Substituting (4.13) and (4.12) with $s = \mu t r_l^{\alpha(1-\epsilon)}$ in (4.11) and taking into account that the conditional pdf $f_{R_k|r_l}(r_k)$ can be obtained from the joint pdf and the marginal pdf of R_l as $f_{R_k|r_l}(r_k) = f_{R_l, R_k}(r_l, r_k) / f_{R_l}(r_l)$, the proof is completed. \square

Theorem 3 provides the coverage probability of the l^{th} user with $l < k$. The following lemma gives the coverage probability for the cell-edge user.

Lemma 9. *The coverage probability of the k^{th} user follows the next expression*

$$p_c(k, t, \lambda, p, \alpha, \epsilon, \mu, \sigma^2) = \int_0^\infty \xi(r_k) f_{R_k}(r_k) dr_k \quad (4.14)$$

where $f_{R_k}(r_k)$ is the marginal pdf distribution of the k^{th} nearest point [94] given by

$$f_{R_k}(r_k) = 2 \frac{(\lambda\pi)^k}{(k-1)!} r_k^{2k-1} e^{-\lambda\pi r_k^2} \quad (4.15)$$

and

$$\xi(r_k) = e^{-\mu t \sigma^2 r_k^{\alpha(1-\epsilon)}} \mathcal{L}_{I_k|r_k}(\mu t r_k^{\alpha(1-\epsilon)}) \quad (4.16)$$

where $\mathcal{L}_{I_k|r_k}(\mu t r_k^{\alpha(1-\epsilon)})$ the Laplace transform of the interference affecting the k^{th} user transmission conditioned on r_k , given by

$$\begin{aligned} \mathcal{L}_{I_k|r_k}(\mu t r_k^{\alpha(1-\epsilon)}) = \\ \exp\left(-2\pi p \lambda \int_{r_k}^\infty \left(1 - \int_0^\infty \frac{\pi p \lambda e^{-p\lambda q}}{1 + t r_k^{\alpha(1-\epsilon)} q^{\alpha\epsilon/2} v^{-\alpha}} dq\right) v dv\right) \end{aligned} \quad (4.17)$$

Proof. The proof is analogous to Theorem 3 except from the fact that the SINR of the k^{th} user transmission only depends on the distance to the origin of one particular user; note that when $l < k$ the SINR depends both on R_l and R_k . Hence, the Laplace transform of the interference only depends on R_k and only the marginal pdf of R_k is necessary. \square

4.4 Numerical Results

4.4.1 Coverage probability

We now evaluate the expressions for the coverage probability previously derived, and compare these results with our simulation model. Different values of the power control factor ϵ are used so as to provide a clear understanding of the relation between power control and fairness among users.

Fig. 4.5 shows the coverage probability considering different numbers of RBs per cell, i.e. $k = \{10, 25, 50\}$, assuming a full power control policy ($\epsilon = 1$). We see how the coverage

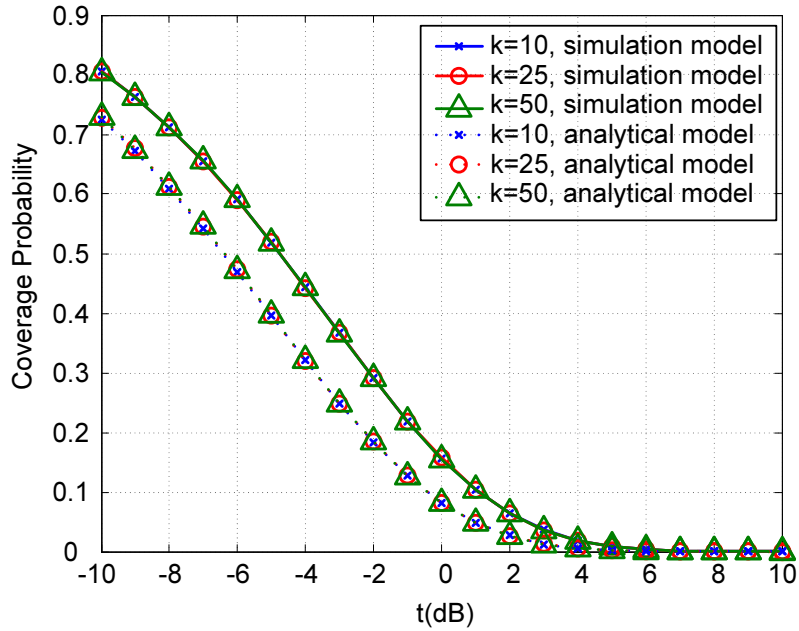


Figure 4.5: Coverage probability for $k = \{10, 25, 50\}$ with full power control ($\epsilon = 1$), without noise, $\alpha = 2.5$, $\lambda_b = 0.24$

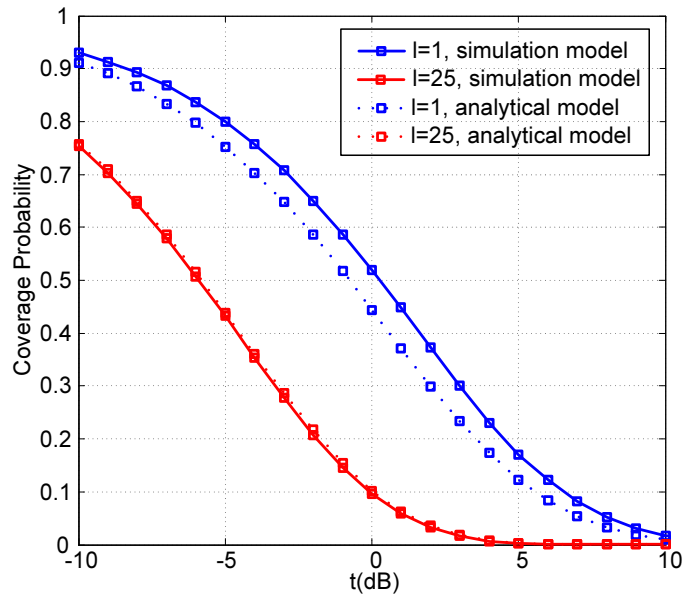


Figure 4.6: Coverage probability for cell-interior $l = 1$ and cell-edge $l = k$ with $k = 25$, $\epsilon = 0.75$, without noise, $\alpha = 2.5$, $\lambda_b = 0.24$

probability is the same for all k scheduled users, i.e. it does not depend on l for both analytical and simulation models. This is coherent with the fact that full compensation of path loss makes all user transmissions to have the same average received power. Since the interference experienced by all user transmissions is the same, the coverage is also the same. Hence, in this case the fairness between users is maximal. We also observe how the analytical model provides slightly more pessimistic results than the simulation model.

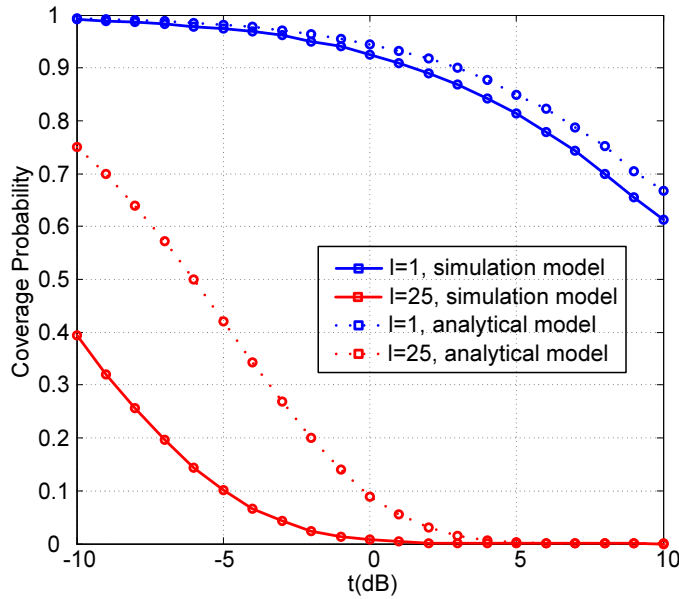


Figure 4.7: Coverage probability for cell-interior $l = 1$ and cell-edge $l = k$ with $k = 25$, without power control $\epsilon = 0$, without noise, $\alpha = 2.5$, $\lambda_b = 0.24$

Fig. 4.6 illustrates the coverage probability for cell-interior ($l = 1$) and cell-edge ($l = k$) users with $k = 25$ and a power control factor $\epsilon = 0.75$. We observe how both analytical and simulation models still behave quite close to each other. In both models, since the compensation of path loss is not total, transmissions from users closer to the BS are associated to higher SINR values than those in the cell-edge, so there exists a difference in coverage between users.

Fig. 4.7 shows the coverage probability in the absence of power control, which corresponds to the worse case in terms of fairness. Hence, we observe that the difference in coverage between cell-interior $l = 1$ and cell-edge $l = k$ users is maximal. We also see how for the cell-edge user the analytical model yields a coverage significantly greater than the simulation model. The reason behind that is related to the different distribution of points

used to model scheduled user locations in both models. As mentioned in section 4.2, in the analytical model user locations form a PPP, whereas in the simulation model this does not hold. This issue has a significant impact on the pdf of the distances R_l specially for cell-edge users, and is addressed in detail in the next subsection.

4.4.2 Marginal distributions of distances

One of the assumptions of the proposed model follows from [29] and states that R_x with $x \in \Phi_i$ are i.i.d. Rayleigh distributed RVs. Fig. 4.8 shows the theoretical (Rayleigh) distribution used in the analytical model and the empirical distribution obtained from the simulation model. We observed that both pdfs are quite similar, so it is expected that the statistics of the transmitted power of the interfering users are also close to each other.

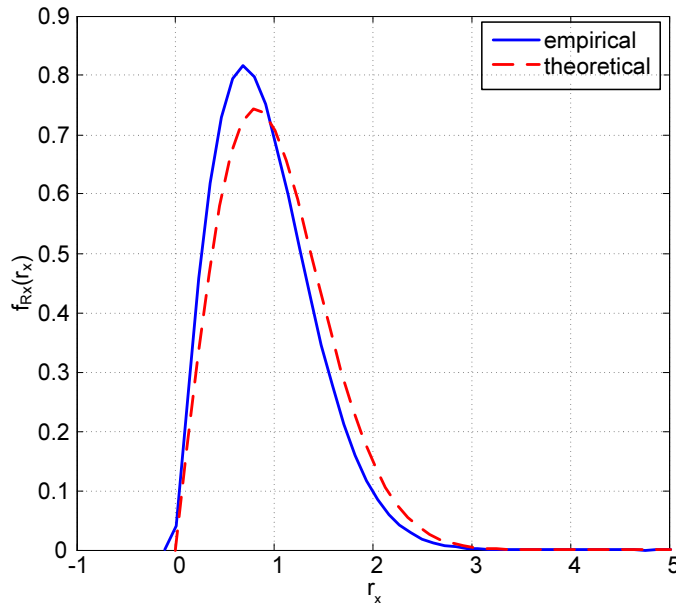


Figure 4.8: Empirical and theoretical pdf of R_x .

Fig. 4.9 shows the marginal pdfs of R_l for the closest and the farthest user to the target BS. For the cell-interior user ($l = 1$) we see that both the empirical and theoretical pdfs are rather similar; hence, we may expect that coverage results from both models are also similar (as illustrated in the previous figures). However, for cell-edge users both pdfs have different shapes. Specifically, we notice that the distances of cell-edge users in the analytical model tend to be lower than the distances in the simulation model. This

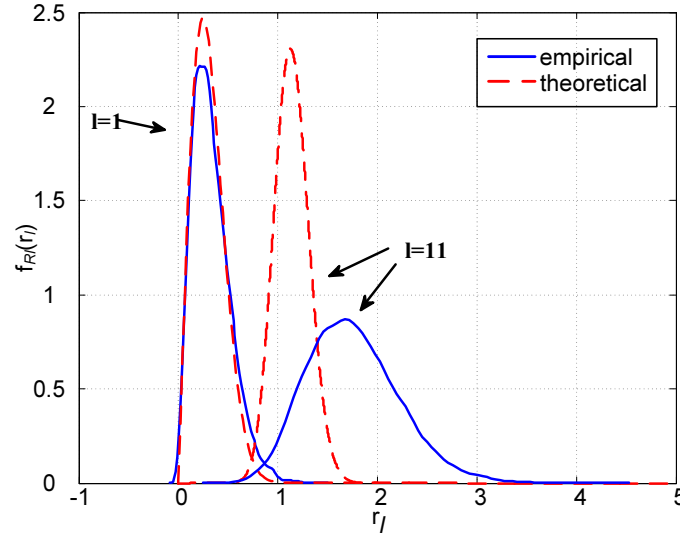


Figure 4.9: Empirical and theoretical pdfs of R_l , ($l = 1, k = 11$) and ($l = k = 11$)

explains the difference in coverage probability, specially in the absence of power control as exhibited in Fig. 4.7. Since the distance for the cell-edge user tends to be lower in the analytical model when power control is not used, the desired signal tends to be higher and so the coverage probability grows. This is mitigated by using power control, since this technique aims to obtain equal received power from all users independently of their positions.

4.5 Discussion

We proposed a tractable analysis model for multi-user uplink cellular networks based on conditional thinning. Assuming that there are k active users scheduled on k orthogonal resources, the joint distribution of the distances from the target BS to the l^{th} user and to the farthest k^{th} user have been obtained. Thinning outside the target cell with probability $1/k$ is used to obtain the actual set of interfering users. A more realistic model with BSs distributed as PPP and one interfering user within its Voronoi cell has been simulated as well. Results show that fractional power control permits to increase fairness among users, at the expense of reducing the coverage probability of cell-interior users as ϵ grows. The coverage results provided by the analysis model are close to the simulation models when power control is used; the difference of behavior in the absence of power control is

also discussed by studying the marginal distributions of the distances of the users to the serving BS.

These aforementioned contributions have been published in [52].

Chapter 5

Coverage of Cellular Systems Under Hoyt fading

In this section, we provide a closed-form approximation for the coverage probability of cellular systems under Hoyt (Nakagami- q) fading. The proposed framework expresses the fading as conditional functions with exponential distribution. Then, the expectation over the distance towards the serving Base Stations (BS) is split in two finite range integrals that can be accurately approximated by means of Gauss-Chebyshev rule. The accuracy of the proposed framework is validated through extensive Monte Carlo simulations.

5.1 Introduction

Due to the irregular nature of 4G deployments, stochastic geometry has appeared recently as a promising and accurate tool for performance analysis of cellular networks [20]. In the pioneering work from [21] it is derived the coverage probability of a cellular network under Rayleigh fading (for the desired link) as a single improper integral. Closed-form expressions are only obtained for some special cases, e.g., for a path loss exponent, $\alpha = 4$. Afterwards, such an approach has been successfully used to study the performance of different scenarios and techniques like enhanced Inter-Cell Interference Coordination (eICIC) [88], advanced interference-aware power control [47], fractional frequency Reuse [90] or uplink/downlink decoupling [26].

For tractability, in those papers it is assumed Rayleigh distribution for the desired link.

Nevertheless, Rayleigh fading is not an appropriate distribution to small scale fading in many scenarios. In this context, Hoyt (Nakagami- q) distribution appears has an interesting tool, since it models fading conditions more severe than Rayleigh, and it includes both Rayleigh fading and one-sided Gaussian fading as special cases [39]. There are some approaches to deal with general fading distributions. In [20] it is proposed to use the Plancherel-Parseval theorem. Gil-Pealez inversion theorem is used in [40] to derive the coverage probability and rate of a cellular network. However, these approaches generally add a single improper integral compared to the case of Rayleigh fading.

In this chapter, we derive a closed-form expression for the coverage probability under Hoyt fading. Such a results also simplifies the coverage probability as given in [21], which is expressed as a single improper integral.

5.2 System Model

We consider the downlink of a cellular network where BSs are distributed according to a uniform Poisson Point Process (PPP), $\Phi_{\text{BS}} = \{\text{BS}_1, \text{BS}_2, \dots\}$, whose density is λ_{BS} . Mobile Terminals (MTs), are also located according to a uniform PPP and they are associated to the nearest BS. Transmitted signals undergoes independent fading for different locations according to a Hoyt distribution with scale parameter $q \in [0, 1]$ and unitary mean. The Probability Density Function (PDF) of the square envelope of the fading can be expressed as a conditional exponential distribution as follows [95]

$$f_H(h) = \mathbb{E}_{\Theta} [f_{H|\theta}(h) | \Theta = \theta] = \mathbb{E}_{\theta} \left[\frac{1}{\gamma(\theta, q)} e^{-h/\gamma(\theta, q)} | \Theta = \theta \right], \quad (5.1)$$

where $\gamma(\theta, q) = \left(1 - \frac{1-q^2}{1+q^2} \cos(\theta)\right)$ and Θ is uniformly distributed between 0 and π . It is considered a path loss law with a path loss slope, τ , and a path loss exponent, $\alpha > 2$. The Signal to Interference plus Noise Ration (SINR) of the typical MT, which can be assumed to be placed at the origin without loss of generality, is expressed as

$$\text{SINR}_{\text{MT}_0} = \frac{H_{\text{BS}_0} (\tau R_{\text{BS}_0})^{-\alpha} \rho_{\text{BS}}}{I + \sigma_n^2}, \quad (5.2)$$

being H_{BS_0} and R_{BS_0} the fading and distance with the serving BS, ρ_{BS} is the transmit power per Hertz, I is the interference term and σ_n^2 is the noise spectral efficiency. The

interference term can be expressed as

$$I = \sum_{\text{BS}_i \in \Phi_{\text{BS}}} H_{\text{BS}_i} (\tau R_{\text{BS}_i})^{-\alpha} \rho_{\text{BS}} \mathbf{1}(R_{\text{BS}_i} > R_{\text{BS}_0}), \quad (5.3)$$

being $\mathbf{1}(\mathcal{A})$, the indicator function, which is 1 when the condition \mathcal{A} is true and 0 otherwise.

Finally, the coverage probability, or equivalently, the Complementary Cumulative Distribution (CCDF) of the SINR, is written as $\mathcal{P}_c = \Pr(\text{SINR}_{\text{MT}_0} > \gamma)$.

5.3 Performance Analysis

The first result that is derived is the Laplace transform of the interference, which is given with the following lemma.

Lemma 10. *The Laplace transform of the interference of the typical MT under Hoyt fading can be expressed as*

$$\begin{aligned} \mathcal{L}_I(s) \approx \exp \left(- \frac{\lambda_{\text{BS}} r^2 \pi^2 \rho_{\text{BS}} s}{n_\theta (\alpha - 2) (\tau r)^\alpha} \sum_{j_2=1}^{n_\theta} \gamma(\theta_{j_2}, q) \left| \sin \left(\frac{2j_2 - 1}{2n_\theta} \pi \right) \right| \right. \\ \left. {}_2F_1 \left(1, \frac{\alpha - 2}{\alpha}, 2 - \frac{2}{\alpha}, - \frac{s \rho_{\text{BS}}}{(\tau r)^\alpha} \gamma(\theta_{j_2}, q) \right) \right), \end{aligned} \quad (5.4)$$

where n_θ represent the number of terms in the Gauss-Chebyshev approximation and

$$\theta_j = \frac{\pi}{2} \left[\cos \left(\frac{2j - 1}{2n_\theta} \pi \right) + 1 \right]. \quad (5.5)$$

Proof. The Laplace transform of the interference can be written as

$$\begin{aligned} \mathcal{L}_I(s) &\stackrel{(a)}{=} \exp \left(-2\pi \lambda_{\text{BS}} \int_{v=r}^{\infty} \left(1 - \mathbb{E}_\Theta \mathbb{E}_{H|\Theta} \left[\exp \left(\frac{-sH \rho_{\text{BS}}}{(\tau v)^\alpha} \right) \right] \right) v dv \right) \\ &\stackrel{(b)}{=} \exp \left(-2\lambda_{\text{BS}} \int_{\theta_2=0}^{\pi} \int_{v=r}^{\infty} \frac{s (\tau v)^{-\alpha} \rho_{\text{BS}} \gamma(\theta_2, q)}{1 + s (\tau v)^{-\alpha} \rho_{\text{BS}} \gamma(\theta_2, q)} v dv d\theta_2 \right), \end{aligned} \quad (5.6)$$

where (a) comes after applying the Probability Generating Functional (PGFL) of the PPP over the BS locations [20], applying the indicator function in (A.28) over the integration limits and expressing the expectation over the Hoyt fading as an conditional exponential distribution according to (A.26); and (b) comes after performing expectation over the fading and reordering the resulting terms. Finally, applying Gauss-Chebyshev integration rule completes the proof. \square

The Laplace transform of the interference can be used as a moment generating functional for the moments of the interference, [47]. Additionally, it is necessary to obtain the coverage probability, which is given with the next theorem.

Theorem 4. *The coverage probability of the typical MT can be expressed in closed-form as follows*

$$\mathcal{P}_c = \frac{\pi}{2n_r} \sum_{i=1}^{n_r} \left(\mu(r_i) + \frac{\mu(r_i^{-1})}{t^2} \right) \left| \sin \left(\frac{2i-1}{2n_r} \pi \right) \right|, \quad (5.7)$$

where

$$\begin{aligned} \mu(r) = & \sum_{j_1=1}^{n_\theta} \left| \sin \left(\frac{2j_1-1}{2n_\theta} \pi \right) \right| \frac{\lambda_{BS} r \pi^2}{n_\theta} \exp \left(-\pi \lambda_{BS} r^2 \right. \\ & - \frac{t \sigma_n^2 (\tau r)^\alpha}{\rho_{BS} \gamma(\theta_1, q)} - \frac{\lambda t r^2 \pi^2}{(\alpha-2) n_\theta} \sum_{j_2=1}^{n_\theta} \frac{\gamma(\theta_{j_2}, q)}{\gamma(\theta_{j_1}, q)} \\ & \left. {}_2F_1 \left(1, \frac{\alpha-2}{\alpha}, 2 - \frac{2}{\alpha}, \frac{-t \gamma(\theta_{j_2}, q)}{\gamma(\theta_{j_1}, q)} \right) \right| \left| \sin \left(\frac{2j_2-1}{2n_\theta} \pi \right) \right| \end{aligned} \quad (5.8)$$

and $r_i = \frac{1}{2} \left[\cos \left(\frac{2i-1}{2n_r} \pi \right) + 1 \right]$.

Proof. The coverage probability can be written as

$$\begin{aligned} \mathcal{P}_c & \stackrel{(a)}{=} \mathbb{E}_{R_{BS_0}} \mathbb{E}_I \mathbb{E}_\Theta \left[\bar{F}_{H|\theta_1} \left(t (I + \sigma_n^2) (\tau R_{BS_0})^\alpha \rho_{BS}^{-1} \right) | \Theta = \theta_1 \right] \\ & \stackrel{(b)}{=} \mathbb{E}_{R_{BS_0}} \mathbb{E}_\Theta \left[e^{-\frac{t \sigma_n^2 (\tau R_{BS_0})^\alpha}{\gamma(\theta_1, q) \rho_{BS}}} \mathcal{L}_I \left(t \frac{\gamma(\tau R_{BS_0})^\alpha}{\gamma(\theta_1, q) \rho_{BS}} \right) | \Theta = \theta_1 \right], \end{aligned} \quad (5.9)$$

where (a) comes after reordering the expression of the SINR, applying the total probability theorem over R_{BS_0} and I and expressing the Hoyt fading as a conditional exponential distribution; and (b) comes after performing expectation over the conditioned fading, which as exponential distribution, and performed expectation over the interference term. Then, performing expectation over R_{BS_0} and Θ and substituting the Laplace transform of Lemma 10 on the above expression, yields

$$\mathcal{P}_c = \int_{r=0}^1 \mu(r) dr + \int_{r=1}^{\infty} \mu(r) dr \quad (5.10)$$

□

The left hand side finite range integral can be approximated with n_r terms by Gauss-Chebyshev. For the right hand side improper integral, it is performed the change of variables $r \rightarrow 1/v$, which transform the integral into a finite range integral that can be approximated by means of Gauss-Chebyshev rule.

5.4 Numerical Results

In this section the proposed framework is validated with simulation. It is considered a path loss slope and a path loss exponent as $\tau = 2.6$ and $\alpha = 3.8$ respectively. The BS density is $\lambda_{BS} = 2 \times 10^{-6}$. It is considered a transmit power of $\rho_{BS} = 0$ dBm/Hz and a noise spectral density of $\sigma_n^2 = -174$ dBm/Hz.

The next figure represents the coverage probability, or equivalently the cdf of the SINR, for the case of Rayleigh fading, i.e., $q = 1$ and for severe fading $q = 0.05$. Nevertheless, the coverage probability for high values of the SINR threshold is roughly the same as for the Rayleigh fading case. The obtained expressions are evaluated with $n_r = 100$ and $n_\theta = 5$ terms.

It is observed a good match between simulation and analytical results. It is observed that severe fading degrades the coverage probability especially, for small SINR threshold values.

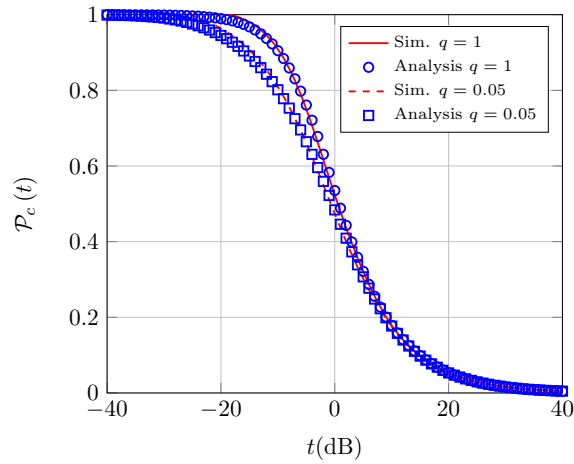


Figure 5.1: Coverage probability versus the SINR threshold, t , for $q = 1$ and $q = 0.05$.

5.5 Discussion

We have derived a closed-form expression for the coverage probability of Hoyt (Nakagami- q) fading. The proposed framework, relies on expressing the fading as a conditional exponential distribution and on splitting the integral over the distance towards the serving BS as a two finite range integrals that can be approximated with Gauss-Chebyshev rule. It is observed that, with severe fading, the coverage probability for small SINR threshold values degrades dramatically, whereas the coverage for high SINR values remains the same as for the Rayleigh case.

These contributions appear in [53], which is under review.

Chapter 6

Performance Analysis of Cloud-Radio Access Networks

In this section, a novel non-orthogonal multiple access (NOMA)-enabled framework for cloud-radio access networks (CRANs) is proposed. In this framework, two users are scheduled in the same resources according to NOMA; however the performance of cell-edge users is enhanced by means of coordinating beamforming. Stochastic geometry is invoked for modeling the proposed framework, where the positions of BSs follow a cluster point process. In an effort to characterize the performance of the proposed framework, simple expressions in terms of outage probability are derived for both nearby users and the cell-edge users. It is analytically demonstrated that the average beamforming gain is a liner function with respect to the number of cooperating base stations. Numerical results verify the accuracy of analysis and reveal that the proposed framework is capable of greatly enhancing the performance of cell-edge users.

6.1 Introduction

Cloud radio access networks (CRANs) are envisioned as one of the key ingredients of future 5G networks [12]. This approach consists on centralizing functionalities by means of a pool of computational resources, which is known as central unit (CU). The CU is connected through high speed links with several radio remote heads (RRH) that acts as BSs from the user's perspective [12]. In [33] and [34] it is considered CRANs where the

analysis focuses on a single cluster of cooperating BSs. In [33] it is obtained an exact expression for the outage probability under dynamic cell selection and an approximated expression in the high SNR regime for coordinated beamforming. [34] focus on the case of coordinated beamforming and provides an accurate expression for the outage probability, which is valid for any value of SNR.

Non-orthogonal multiple access (NOMA) has recently attracted much attention, due to its potential to increase spectrum efficiency in 5G networks [16] [96]. In [35] it is proposed a scheme where b BSs transmits jointly to k users according to NOMA based access. To improve the performance it is proposed an opportunistic algorithm to select the set of cooperating BSs. A NOMA-based scheme with coordinated multi-point (CoMP) transmission is proposed in [36]. Nevertheless, since the scheme is based on Alamuti codes, the number of cooperating BSs is smaller than 3. A comon factor of the aforementioned works in [33–36] is that the interference from other clusters, which is the main limiting factor, is not considered.

In this work a novel NOMA-based scheme for CRANs with coordinated beamforming is proposed and analyzed. On the one hand, this scheme benefits from NOMA in order to increase the spectral efficiency, since two mobile terminals (MTs) are scheduled per BS. On the other hand, it benefits from cooperation, since each cluster of BSs performs coordinated beamforming to improve the performance of cell-edge MTs. To model the locations of BSs in CRANs, it has been considered a cluster point process (CPP), where a minimum distance over the cluster centers is imposed to avoid spatial overlapping between different clusters. This model involves two sources of spatial correlation: one from the cluster process and another from the minimum distance, that complicate the problem at hand. Besides this, to assess the performance of the system in realistic conditions, both the intra-cluster interference due to NOMA and the inter-cluster interference from other clusters are considered.

Our main contributions can be summarized as follows: 1) we demonstrate that the beamforming gain can be expressed as a mixture Erlang distribution; 2) we prove that the moments of the beamforming gain are linear functions with respect to the number of BS per cluster; 3) we derive simple expressions for the outage probability of cell-edge MTs with the aid of the k -th derivative of the Lapalce transform of the inter-cluster interference; and 4) we show that the proposed scheme greatly improves the performance

of the cell-edge MT.

6.2 System Model

6.2.1 Spatial and Propagation Modeling

We focus on the downlink (DL) of CRANs where BSs are organized in different clusters that can share information. BSs' locations are modeled according to a homogeneous independent CPP [61]. The parent point process, which models cluster centers, is represented as $\Phi_C \subset \mathbb{R}^2$ and follows a Matérn hard core point process (HCPP) of type II whose density is λ_C and minimum distance between points is d_{\min} . For a cluster centered at $x \in \Phi_C$, the daughter point process is represented as $\Phi_{\text{BS}}^{(x)} = \Phi_{\text{BS}}^{(o)} + x$, where $o = (0, 0)$ represents the origin and $\Phi_{\text{BS}}^{(o)}$ follows a binomial point process (BPP) of n_{BS} points inside a ring whose inner radius is r_e and outer radius is r_c . The outer radius represent the cluster size, whereas the inner radius represents a guard zone where BSs are not allowed. This is because the center of each cluster is the region which suffers from more intra-cluster interference. It is considered that the worst MT in terms of SINR of each cluster is placed at the cluster center whereas a single MT (i.e., near MT) is associated with each BS. Cells are modeled as disks whose radius are r_{BS} .

The fading between locations x and y is expressed as $H_{x,y} \sim \mathcal{CN}(0, 1)$, which follows a complex normal distribution. Independent fading is considered for different locations. A bounden path loss model is assumed and thus the path loss between x and y is expressed as $(1 + R_{x,y}^\alpha)$. We represent the instantaneous link gain as $G_{x,y} = H_{x,y} / \sqrt{1 + R_{x,y}^\alpha}$.

6.2.2 Proposed CRAN-NOMA Scheme

BSs of the same cluster transmit jointly to cell-edge MTs to boost their performance. To increase the spectrum efficiency, BSs schedule in the same resource block (RB) the data intended for its near MT and cell-edge MT. Hence, near MTs performs successive interference cancellation (SIC) to cancel-out the intra-cluster interference from data intended for the cell-edge MT. Fig. 6.1, illustrates the proposed scheme.

More formally, the transmitted signal for the i -th BS that belongs to the q -th cluster expressed as follows

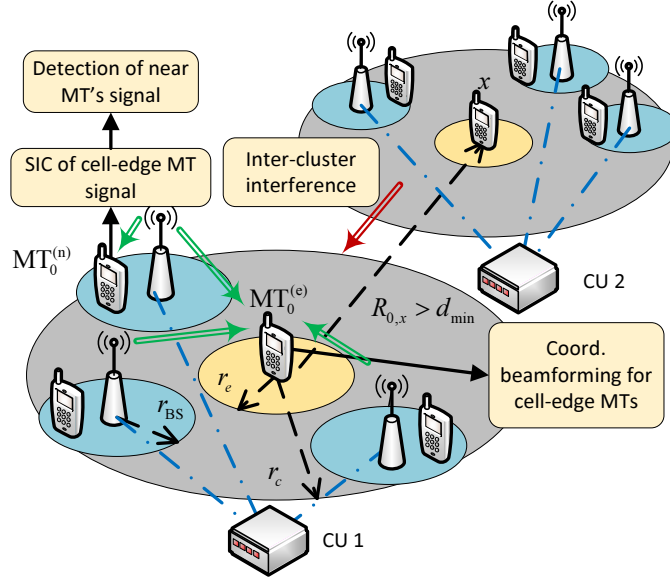


Figure 6.1: Illustration of the proposed NOMA-based scheme with coordinated beamforming for CRANs. The probe near MT and probe cell-edge MT are represented as $MT_0^{(n)}$ and $MT_0^{(e)}$, respectively. It is drawn a single interfering cluster, which is centered at x .

$$X_{BS_{i,q}} = \sqrt{p_{BS}a_n} \cdot S_{MT_{i,q}^{(n)}} + \sqrt{p_{BS}a_e} \cdot W_{BS_{i,q},MT_q^{(e)}} \cdot S_{MT_q^{(e)}}, \quad (6.1)$$

where $S_{MT_q^{(e)}} \in \mathbb{C}$ and $S_{MT_{i,q}^{(n)}} \in \mathbb{C}$ are the symbols intended for the cell-edge and near MTs respectively, p_{BS} is the nominal transmit power per BS, $a_n \in \mathbb{R}$ and $a_e \in \mathbb{R}$ with $a_n + a_e = 1$ are the power allocations coefficients for near and cell-edge MTs respectively. The q -th cluster is centered at $C_q \in \Phi_C$, hence, the location of the i -th BS is written as $BS_{i,q} \in \Phi_{BS}^{(C_q)}$. The beamforming weight for the transmission intended towards the cell-edge MT, which is placed at $MT_q^{(e)} = C_q$, is represented as $W_{BS_{i,q},MT_q^{(e)}}$.

Following the same approach as in [34] the beamforming weight are expressed as

$$W_{BS_{k,0},MT_0^{(e)}} = G_{BS_{k,0},MT_0^{(e)}}^* \Xi_{MT_0^{(e)}}^{-\frac{1}{2}}, \quad (6.2)$$

being $\Xi_{MT_0^{(e)}}$ the beamforming gain for the cell-edge MT, $MT_0^{(e)}$, which can be formulated as appears below

$$\Xi_{\text{MT}_0^{(e)}} = \sum_{\text{BS}_{k,0} \in \Phi_{\text{BS}}^{(C_0)}} \left| G_{\text{BS}_{k,0}, \text{MT}_0^{(e)}} \right|^2 \quad (6.3)$$

6.2.3 Signal Model

The intra-cluster interference for cell-edge MTs can be expressed as $\Xi_{\text{MT}_0^{(e)}} a_n p_{\text{BS}}$. Therefore, the SINR for the cell-edge MTs is written as

$$\text{SINR}_{\text{MT}_0^{(e)}} = \frac{\Xi_{\text{MT}_0^{(e)}} a_e \rho_{\text{BS}}}{\Xi_{\text{MT}_0^{(e)}} a_n \rho_{\text{BS}} + I_{\text{inter}} \rho_{\text{BS}} + 1}, \quad (6.4)$$

where $\rho_{\text{BS}} = p_{\text{BS}}/\sigma_n^2$ is the transmit SNR and I_{inter} appears below

$$I_{\text{inter}} = \sum_{C_q \in \Phi_C \setminus \{C_0\}} \sum_{\text{BS}_{k,q} \in \Phi_{\text{BS}}^{(C_q)}} \left| G_{\text{BS}_{k,q}, \text{MT}_0^{(e)}} \right|^2 \left(a_n + a_e \left| W_{\text{BS}_{k,q}, \text{MT}_q^{(e)}} \right|^2 \right). \quad (6.5)$$

The message intended for cell-edge MTs is transmitted with an Spectral Efficiency (SE) of SE_e bps/Hz. Hence, it is assumed that the user is not capable of correctly receiving a message if its SINR is smaller than $2^{\text{SE}_e} - 1$, which means that the MT is in outage.

As for the near MTs, they first try to decode the message intended for the cell-edge MT, which is normally transmitted with a higher power since $a_e > a_n$. Then, if such a message is correctly received, they cancel-out the intra-cell interference and try to decode their own message.

The SINR to decode the symbol intended for the cell-edge MT is given below

$$\text{SINR}_{\text{MT}_{0,0}^{(n)}}^{(e)} = \frac{\left| G_{\text{BS}_{0,0}, \text{MT}_{0,0}^{(n)}} \right|^2 \left| W_{\text{BS}_{0,0}, \text{MT}_0^{(e)}} \right|^2 a_e \rho_{\text{BS}}}{\left| G_{\text{BS}_{0,0}, \text{MT}_{0,0}^{(n)}} \right|^2 a_n \rho_{\text{BS}} + I_{\text{intra}} \rho_{\text{BS}} + I_{\text{inter}} \rho_{\text{BS}} + 1}, \quad (6.6)$$

where the term I_{inter} is given in (6.5), and I_{intra} , which represents the intra-cluster interference, appears next

$$I_{\text{intra}} = \sum_{\text{BS}_{k,0} \in \Phi_{\text{BS}}^{(C_0)} \setminus \{\text{BS}_{0,0}\}} \left| G_{\text{BS}_{k,0}, \text{MT}_{0,0}^{(n)}} \right|^2 \left(a_n + a_e \left| W_{\text{BS}_{k,0}, \text{MT}_k^{(e)}} \right|^2 \right). \quad (6.7)$$

Once the interference from the transmission towards the cell-edge MT has been canceled, the near MT decode its own symbol. The SINR to decode such a symbol can be written as

$$\text{SINR}_{\text{MT}_{0,0}^{(n)}}^{(n)} = \frac{\left| G_{\text{BS}_{k,0}, \text{MT}_{0,0}^{(n)}} \right|^2 a_n \rho_{\text{BS}}}{I_{\text{intra}} \rho_{\text{BS}} + I_{\text{inter}} \rho_{\text{BS}} + 1}. \quad (6.8)$$

In (6.5), Φ_C follows a Matérn HCPP of type II. Such a point process complicates the analysis because its probability generating functionals do not exist, [55]. For the sake of tractability, it is proposed the following assumption over the interference.

Assumption 3. *Let us consider a probe MT, which can be either a near or cell-edge MT, it is placed at the origin and belongs to the probe cluster, C_0 . In such setting, the inter-cluster interference can be approximated as appears below*

$$I_{\text{inter}} = \sum_{C_q \in \Phi_C \setminus \{C_0\}} \sum_{\text{BS}_{k,q} \in \Phi_{\text{BS}}^{(C_q)}} \frac{\left| H_{\text{BS}_{k,q}, x} \right|^2}{1 + R_{\text{BS}_{k,q}, x}^\alpha} \left(a_n + a_e \left| W_{\text{BS}_{k,q}, \text{MT}_q^{(e)}} \right|^2 \right) \mathbf{1}(\|C_q\| > d_{\min}), \quad (6.9)$$

where now Φ_C is a homogeneous Poisson Point Process (PPP) whose density is λ_C .

Finally, the normalized transmit power of a given BS, $\text{BS}_{i,q}$, is defined as $P_{\text{BS}_{i,q}} = \left(a_n + a_e \left| G_{\text{BS}_{i,q}, \text{MT}_q^{(e)}} \right|^2 / \Xi_{\text{MT}_q^{(e)}} \right)$.

6.3 Performance Analysis

The analysis of the proposed scheme is presented through this section. To this end, the first result that is provided, is the Probability Density Function (PDF) of the distance towards a given BS, that belongs to the q -th cluster. Such a result is given with the following lemma.

Lemma 11. *The PDF of the distance, U , between a point placed at the origin and a randomly chosen BS from the q -th cluster, which is centered around C_q , only depends on the distance towards it, $r = \|C_q\|$, and it can be expressed as appears below*

$$f_U(u|r) = \frac{g(u, r_c, r) - g(u, r_e, r)}{\pi(r_c^2 - r_e^2)}, \quad (6.10)$$

being

$$g(u, r_d, d) = \begin{cases} 2\pi u, & \text{if } u \leq r_d - d \\ \frac{(d^2 - r_d^2 - u^2) \cdot d \cdot u + r \cdot (d^2 - u^2 + r_d^2)}{\sqrt{(d+u-r_d)(d-u+r_d)(-d+u+r_d)(d+r_d+u)}} \\ + \frac{r_d u}{d \sqrt{1 - \frac{(d^2 - u^2 + r_d^2)^2}{4d^2 r_d^2}}} + 2r \cdot \operatorname{arcsec}\left(\frac{2du}{d^2 + u^2 - r_d^2}\right), & \text{if } |r_d - d| < u < d + r_d \\ 0, & \text{otherwise} \end{cases} \quad (6.11)$$

Proof. The proof consist on deriving the Cumulative Density Function (CDF) of U as the quotient of the area of the intersection between the disk centered at the origin and a ring centered at C_q and the area of such a ring. The radius of the disk is r whereas the inner and outer radius of the ring are r_e and r_c respectively. □

Lemma 12. *The PDF of the beamforming gain for the cell-edge MT can be expressed as a finite mixture of Erlang distributions as follows*

$$f_{\Xi}(\xi) \approx \sum_{q=1}^{n_M} \sum_{i=1}^{n_{GC}} \sum_{k=1}^{t_{q,i}} \omega_{q,i,k} f_{\text{Er}}(\xi; k, 1 + r_i^\alpha), \quad (6.12)$$

being $f_{\text{Er}}(x; k, \lambda)$ the Erlang distribution with shape parameter, k , and rate parameter, λ ; n_{GC} is a parameter related to the accuracy of the approximation; n_M the number of permutations of n_{GC} elements whose sum is n_{BS} and

$$r_i = \frac{1}{2} \left(\cos\left(\frac{2i-1}{n_{GC}}\pi\right) + 1 \right) (r_c - r_e) + r_e, \quad (6.13)$$

$$\omega_{q,i,k} = \frac{\frac{\beta_k}{\lambda^k (t_{q,1}! \cdots t_{q,n_{GC}}!)}}{\sum_{p=1}^{n_M} \sum_{j=1}^{n_{GC}} \sum_{\ell=1}^{t_{p,j}} \frac{\beta_\ell}{\lambda^\ell (t_{p,1}! \cdots t_{p,n_{GC}}!)}}}, \quad (6.14)$$

$$\beta_k = \frac{1}{(t_i - k)!} \frac{d^{(t_i - k)}}{ds^{(t_i - k)}} (1 + r_i^\alpha + s)^{t_i} \prod_{i=1}^{n_{GC}} \left(\frac{r_i (1 + r_i^\alpha)}{1 + r_i^\alpha + s} \left| \sin \left(\frac{2i - 1}{2n_{GC}} \pi \right) \right| \right)^{t_i} \Big|_{s=-1-r_i^\alpha}. \quad (6.15)$$

Proof. The proof follows the same procedure as in [34] which consist on the next steps: i) it is derived the Laplace transform of $\Xi_{\text{MT}_0^{(e)}}$, which is expressed as a finite integral to the n_{BS} ; ii) it is applied Gauss-Chebyshev integration rule to write the integral as a finite sum of n_{GC} terms; iii) it is applied the multinomial theorem to write the sum to the n_{BS} as a sum of polynomials ; iv) it is applied partial fraction expansion to have the sum of terms of the form $\beta_k (1 + r_i^\alpha + s)^{-k}$ whose inverse Laplace transform exist. Then, obtaining the inverse Laplace transform yields a finite sum for the PDF of $\Xi_{\text{MT}_0^{(e)}}$ as in [34]. Finally, identifying in the inner terms as the Erlang distribution and applying $\sum_{q=1}^{n_M} \sum_{i=1}^{n_{GC}} \sum_{k=1}^{t_{q,i}} \omega_{q,i,k} = 1$ to have a finite mixture distribution completes the proof. \square

Since it has been used Gauss-Chebyshev integration rule to derive Lemma 12, such a result is an approximation. Nevertheless, an exact expression for the moments of the beamforming gain are given below

Lemma 13. *The exact expression of the mean and variance of the beamforming gain are give below*

$$\begin{aligned} \mathbb{E} [\Xi_x] &= -n_{\text{BS}} \mu_{\Xi}^{(1)}(0) \\ \text{var} (\Xi_x) &= n_{\text{BS}} \left(\mu_{\Xi}^{(2)}(0) - \left(\mu_{\Xi}^{(1)}(0) \right)^2 \right), \end{aligned} \quad (6.16)$$

where

$$\begin{aligned}
\mu_{\Xi}^{(1)}(0) &= \frac{2(r_c r_e)^{-\alpha}}{(\alpha - 2)(r_c^2 - r_e^2)} (r_e^\alpha r_c^2 \chi(\alpha, r_c^\alpha) - r_c^\alpha r_e^2 \chi(\alpha, r_e^\alpha)) \\
\mu_{\Xi}^{(2)}(0) &= \frac{4r_c^\alpha r_e^\alpha (r_c r_e)^{-2\alpha}}{\alpha^2 (r_c - r_e)(r_c + r_e)} \left[\frac{r_c^\alpha r_e^2 \alpha}{1 + r_e^\alpha} - \frac{r_e^\alpha r_c^2 \alpha}{1 + r_c^\alpha} + \right. \\
&\quad \left. \frac{\alpha - 2}{(r_c r_e)^{-\alpha}} \left(B\left(-r_e^\alpha, 2 - \frac{2}{\alpha}, 0\right) - B\left(-r_c^\alpha, 2 - \frac{2}{\alpha}, 0\right) \right) \right], \tag{6.17}
\end{aligned}$$

being $\chi(\alpha, x)$ the Gauss Hypergeometric function as $\chi(\alpha, x) = {}_1F_2\left(1, \frac{\alpha+2}{\alpha}; 2 + \frac{2}{\alpha}; -x\right)$ and $B(z, a, b)$ the incomplete Beta function.

Proof. The Laplace transform of $\Xi_{\text{MT}_0^{(e)}}$ can be written as

$$\mathcal{L}_{\Xi}(s) = \left(\int_{r_e \leq r \leq r_c} \frac{2r}{r_c^2 - r_e^2} \frac{1 + r^\alpha}{1 + s + r^\alpha} dr \right)^{n_{\text{BS}}}, \tag{6.18}$$

where it has applied the independence of the distribution of the fading and distance towards the cell-edge MT for different BSs within the same cluster, C_0 . Then, it has been performed expectation over the distribution of $\{R_{k,0}\}$. Finally, Using the Laplace transform as a moment generating function completes the proof. \square

Remark 12. In view of **Lemma 13**, it can be stated that both, the mean and the variance, of the beamforming gain are linear functions with respect to n_{BS} . Additionally, its slope is always positive and only depends on r_c , r_e and α . Hence, both metrics are monotonically increasing functions with respect to n_{BS} .

Proposition 8. The beamforming gain for a cell-edge MT, can be accurately approximated by an Inverse Gamma distribution whose parameters can be obtained by Moment Matching (MM) as follows:

$$k_{\Xi} = \frac{(\mathbb{E}[\Xi])^2}{\text{var}(\Xi)} + 2; \quad \lambda_{\Xi} = \left(\frac{(\mathbb{E}[\Xi])^2}{\text{var}(\Xi)} + 1 \right) \mathbb{E}[\Xi], \tag{6.19}$$

hence, the Laplace transform can be written as

$$\mathcal{L}_{\Xi}(s; k_{\Xi}, \lambda_{\Xi}) \approx \frac{2(\lambda_{\Xi}s)^{\frac{k_{\Xi}}{2}}}{\Gamma(k_{\Xi})} K_{k_{\Xi}}\left(2\sqrt{\lambda_{\Xi}s}\right), \quad (6.20)$$

where $\Gamma(x)$ is the Gamma function and $K_z(x)$ is the modified Bessel function of the 2nd kind.

Proof. The proof comes after implying the equivalence between the mean and variance of $\Xi_{\text{MT}_0^{(e)}}$ with those of an Inverse Gamma distribution. Then, solving the system of equations to obtain the shape, k_{Ξ} , and rate, λ_{Ξ} , parameters completes the proof. \square

Lemma 14. *The Laplace transform of the normalized transmit power, $P_{\text{BS}_{i,q}}$, for a randomly chosen BS can be written as follows*

$$\mathcal{L}_{P_{\text{BS}}}(s) \approx e^{-sa_n} \int_{v=r_e}^{r_c} \frac{2v}{r_c^2 - r_e^2} \left(1 + \frac{a_e s}{(1+v^\alpha)\lambda_{\Xi}}\right)^{-k_{\Xi}} dv. \quad (6.21)$$

Proof. Approximating the fading as $\left|H_{\text{BS}_{i,0},\text{MT}_0^{(e)}}\right|^2 \approx 1$ and performing expectation over $R_{\text{BS}_{i,0},\text{MT}_0^{(e)}}$ yields to an expression where it appears the Laplace transform of $\Xi_{\text{MT}_0^{(e)}}^{-1}$. In

Proposition 8 the Laplace transform of $\Xi_{\text{MT}_0^{(e)}}$ is approximated as an Inverse Gamma distribution, and thus $\mathcal{L}_{\Xi^{-1}}(s)$ can be expressed as $\mathcal{L}_{\Xi^{-1}}(s) = (1 + s\lambda_{\Xi}^{-1})^{-k_{\Xi}}$, which completes the proof. \square

The next Lemma provides the Laplace transform of the inter-cluster interference.

Lemma 15. *Let us assume a given MT, which can be either a near MT or a cell-edge MT. The Laplace transform of the inter-cluster interference can be written as*

$$\mathcal{L}_{I_{\text{inter}}}(s) \approx \exp\left(-2\pi\lambda_c \int_{r>d_{\min}} \left(1 - \mathcal{L}_{P_{\text{BS}}}\left(\frac{s}{(1+r^\alpha)}\right)^{n_{\text{BS}}}\right) r dr\right). \quad (6.22)$$

Proof. Thanks to **Assumption 3**, it can be applied the Probability Generating Functional (PGFL) of the PPP [61] to obtain the Laplace transform of the interference. Then,

it is applied the indicator $\mathbf{1}(\|C_q\| > d_{\min})$ to the integration limits of the resulting expression. Finally, approximating the fading by its mean value, i.e., $\left|H_{\text{BS},k,q,\text{MT}_0^{(e)}}\right|^2 \approx 1$ and the distance towards the i -th BS of the q -th cluster as the distance towards its cluster center, $r = \|C_q\|$ completes the proof. \square

Theorem 5. *If the condition $a_e - \gamma_e a_n < 0$ holds, then, the outage probability for a given cell-edge MT can be expressed as follows*

$$P_{\text{out}}^{\text{MT}_0^{(e)}} \approx 1 - \sum_{q=1}^{n_M} \sum_{i=1}^{n_{\text{GC}}} \sum_{k=1}^{t_i} \sum_{n=0}^{k-1} \omega_{q,i,k} \frac{(1+r_i^\alpha)^n}{n!} \times \nu_1^n (-1)^n \frac{d^n}{ds^n} \left[e^{-s\rho_{\text{BS}}^{-1}} \mathcal{L}_{I_{\text{inter}}}(s) \right] \Big|_{s=\nu_1(1+r_i^\alpha)}, \quad (6.23)$$

where $\mathcal{L}_{I_{\text{inter}}}(s)$ is given with **Lemma 15**, $\nu_1 = \frac{\gamma_e}{a_e - \gamma_e a_n}$ and being $\gamma_e = 2^{\text{SE}_e} - 1$ the SINR threshold to achieve a SE of SE_e bps/Hz. If $a_e - \gamma_e a_n < 0$, then, the outage probability is 1.

Proof. If $a_e < \gamma_e a_n$ the outage probability is 1. In the case $a_e - \gamma_e a_n > 0$, the outage probability can be written as

$$P_{\text{out}}^{\text{MT}_0^{(e)}} = \mathbb{E}_I \left[F_{\Xi_{\text{MT}_0^{(e)}}} \left(\nu_1 \left(I + \frac{1}{\rho_{\text{BS}}} \right) \right) \right] \approx 1 - \sum_{q=1}^{n_M} \sum_{i=1}^{n_{\text{GC}}} \sum_{k=1}^{t_i} \sum_{n=0}^{k-1} \omega_{q,i,k} \frac{(1+r_i^\alpha)^n}{n!} \nu_1^n \mathbb{E}_I \left[\left(I + \rho_{\text{BS}}^{-1} \right)^n e^{-(1+r_i^\alpha)\nu_1(I+\rho_{\text{BS}}^{-1})} \right], \quad (6.24)$$

where it has been used the fact that $\Xi_{\text{MT}_0^{(e)}}$ can be expressed as a finite mixture of Erlang distributions. Finally, applying the derivative property in the s domain of the Laplace transform completes the proof. \square

Lemma 16. *The Laplace transform of the intra-cluster interference, conditioned on being placed at a distance, v , towards its cluster center is given below*

$$\begin{aligned} \mathcal{L}_{I_{\text{intra}}|r}(s) &= \left(\frac{\pi (r + r_c - |r - r_c|)}{2n_{\text{GC}}} \right)^{n_{\text{BS}}-1} \\ &\times \left(\sum_{i=1}^{n_{\text{GC}}} f_{U|r}(u_i|r) \mathcal{L}_{P_{\text{BS}}} \left(\frac{s}{1 + u_i^\alpha} \right) \left| \sin \left(\frac{2i-1}{2n_{\text{GC}}} \pi \right) \right| \right)^{n_{\text{BS}}-1}, \end{aligned} \quad (6.25)$$

where $\mathcal{L}_{P_{\text{BS}}}(s)$ is given with **Lemma 14**, $f_{U|r}(u|r)$ is given with **Lemma 11** and

$$u_i = \frac{1}{2} \left[\cos \left(\frac{2i-1}{n_{\text{GC}}} \pi \right) + 1 \right] (r + r_c - |r - r_c|) + |r - r_c|. \quad (6.26)$$

Proof. It has been approximated the fading by its average value, i.e., $\left| H_{\text{BS}_{k,0}, \text{MT}_{0,0}^{(n)}} \right|^2 \approx 1$ and it has been assumed statistical independence between $R_{\text{BS}_{k,0}, \text{MT}_{0,0}^{(n)}} = U_k$ and $P_{\text{BS}_{k,0}}$. Finally, expressing the expectation over U_k as a finite integral, and applying Gauss-Chebyshev completes the proof. \square

The following lemma, provides the CDF of $Q_{\text{MT}_{0,0}^{(n)}}$, which is defined as $Q_{\text{MT}_{0,0}^{(n)}} = \left| G_{\text{BS}_{0,0}, \text{MT}_{0,0}^{(n)}} \right|^2 / (I\rho_{\text{BS}} + 1)$.

Lemma 17. *The CDF of $Q_{\text{MT}_{0,0}^{(n)}}$, conditioned on being the distance between the near MT and its cluster center, r , can be written as*

$$\begin{aligned} F_Q(q|r) &= 1 - \frac{\pi r_{\text{BS}}}{2n_{\text{GC}}} \sum_{i=1}^{n_{\text{GC}}} \frac{2v_i}{r_{\text{BS}}^2} e^{-q(1+v_i^\alpha)} \left| \sin \left(\frac{2i-1}{n_{\text{GC}}} \pi \right) \right| \\ &\times \mathcal{L}_{I_{\text{intra}}|r}(q(1+v_i^\alpha)\rho_{\text{BS}}) \mathcal{L}_{I_{\text{inter}}}(q(1+v_i^\alpha)\rho_{\text{BS}}), \end{aligned} \quad (6.27)$$

where $\mathcal{L}_{I_{\text{intra}}|r}(s)$ and $\mathcal{L}_{I_{\text{inter}}}(s)$ are given in **Lemma 16** and **Lemma 15** respectively, and

$$v_i = \frac{1}{2} \left[\cos \left(\frac{2i-1}{n_{\text{GC}}} \pi \right) + 1 \right] r_{\text{BS}}. \quad (6.28)$$

Proof. The proof comes after conditioning over the aggregate interference and $R_{\text{BS}_0^{(0)}, \text{MT}_0^{(n)}}$ and then applying Gauss-Chebyshev rule over the resulting expression. \square

Lemma 18. The CDF of $|W_{\text{BS}_{k,0}, \text{MT}_0^{(e)}}|^2$ is given below

$$F_{|W|^2}(x) \approx 1 - \frac{\pi(r_c - r_e)}{2n_{\text{GC}}} \sum_{i=1}^{n_{\text{GC}}} \frac{2r_i}{r_c^2 - r_e^2} \times \mathcal{L}_{\Xi}(x(1+r_i^\alpha)) \left| \sin\left(\frac{2i-1}{n_{\text{GC}}}\pi\right) \right|, \quad (6.29)$$

where r_i is given in (6.13)

Proof. The proof comes after performing expectation over the fading, identifying the Laplace transform of Ξ in the resulting expression and finally applying Gauss-Chebyshev rule. \square

Theorem 6. The outage probability of a randomly chosen near MT can be expressed as

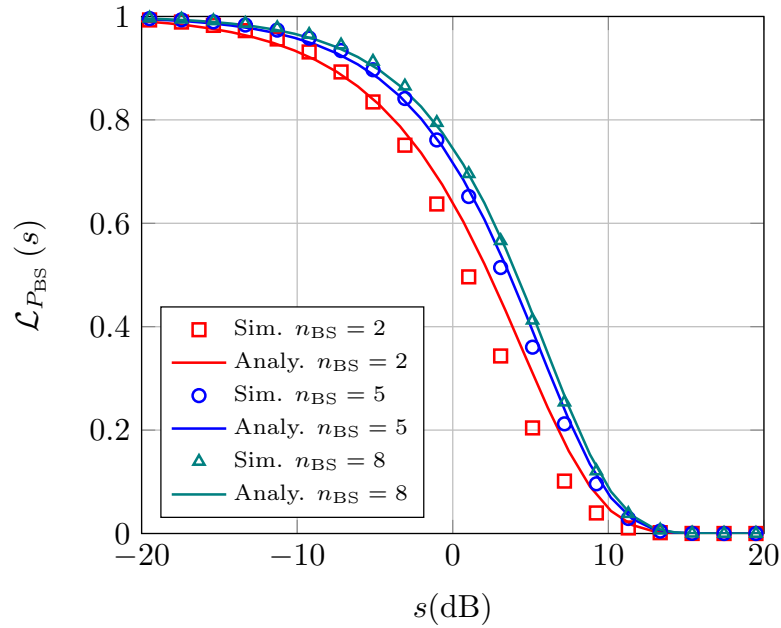
$$P_{\text{out}}^{\text{MT}_0^{(n)}} \approx F_{|W|^2}\left(\frac{\gamma_1 a_n}{a_e}\right) + \frac{\pi(r_c - r_e)}{2n_{\text{GC}}} \sum_{i=1}^{n_{\text{GC}}} \frac{2r_i}{r_c^2 - r_e^2} \times \mathcal{L}_{\Xi}\left(\frac{\gamma_1 a_n}{a_e}(1+r_i^\alpha)\right) \left| \sin\left(\frac{2i-1}{n_{\text{GC}}}\pi\right) \right| \times F_Q\left(\max\left(\frac{\gamma_e}{\left(\frac{a_e}{1+r_i^\alpha} - \gamma_e a_n\right)\rho_{\text{BS}}}, \frac{\gamma_n}{a_e \rho_{\text{BS}}}\right) \middle| r_i\right), \quad (6.30)$$

where $\mathcal{L}_{\Xi}(s)$ is given with **Proposition 8** and $F_Q(q|r)$ with **Lemma 17**.

Proof. An outage occurs if the near MT is not capable to decode the symbol intended for him or for the cell-edge MT. We have an outage related to the symbol intended for the cell-edge MT if $\text{SINR}_{\text{MT}_0^{(n)}}^{(e)} < \gamma_e$. Reordering the above expression, yields to the conclusion that there is an outage if $|W_{\text{BS}_0^{(0)}, \text{MT}_0^{(e)}}|^2 < \frac{\gamma_e a_n}{a_e}$. If $|W_{\text{BS}_0^{(0)}, \text{MT}_0^{(e)}}|^2 > \frac{\gamma_e a_n}{a_e}$, an outage occurs when $Q_{\text{MT}_0^{(n)}} < \mathcal{E}_e$, with $\mathcal{E}_e = \gamma_e / \left[\rho_{\text{BS}} \left(|W_{\text{BS}_0^{(0)}, \text{MT}_0^{(e)}}|^2 a_e - \gamma_e a_n \right) \right]$. Analogously, an outage when decoding the symbol intended for the near MT occurs if $Q_{\text{MT}_0^{(n)}} < \mathcal{E}_n$, with $\mathcal{E}_n = \gamma_n / a_n \rho_{\text{BS}}$. Obtaining the probability of the events $Q_{\text{MT}_0^{(n)}} < \mathcal{E}_e$ and $Q_{\text{MT}_0^{(n)}} < \mathcal{E}_n$ completes the proof. \square

Table 6.1: Simulation setup.

Parameter	Value	Parameter	Value
ρ_{BS} (dB)	65	n_{BS}	5
r_c (m)	500	r_e (m)	50
r_{BS} (m)	10	α	3
$\text{SE}^{(e)} = \text{SE}^{(n)}$ (bps/Hz)	0.1	a_e	0.9
n_{GC}	10	Realizations	10^4
λ_C (points/m ²)	3×10^{-7}	d_{min} (m)	10^3

Figure 6.2: Comparison of the Laplace transform the normalized transmit power for $n_{\text{BS}} = \{2, 5, 8\}$.

6.4 Numerical Results

In this section, the mathematical frameworks and findings derived in the previous sections are validated with the aid of Monte Carlo simulations. Simulations do not consider any approximation, e.g., the underlying point process for cluster centers is a Martérn HCPCP of type II, and the exact beamforming gain and transmit power is computed. The simulation parameters are summarized in Table 6.1

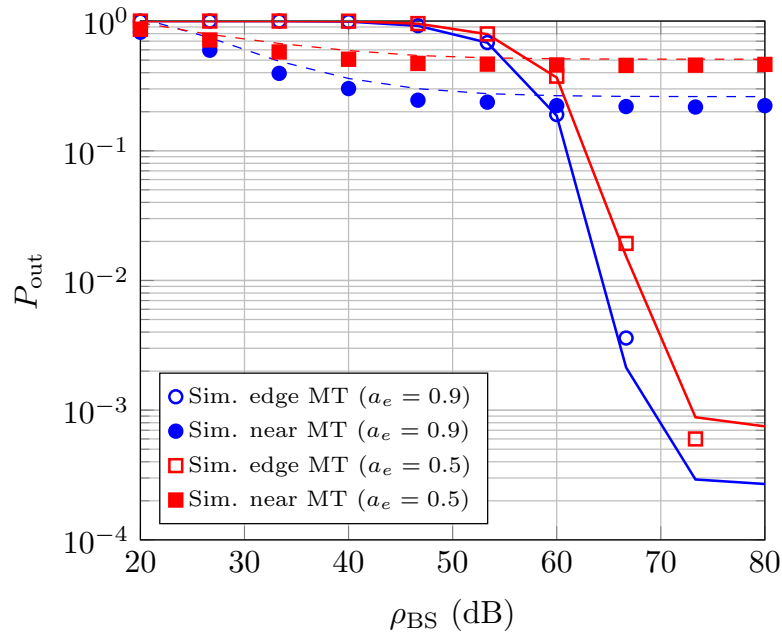


Figure 6.3: Comparison of the outage probability for near and cell-edge MTs versus the transmit SNR, ρ_{BS} . The case $a_e = 0.9$ is represented with blue color and circles and the case $a_n = 0.5$ with red color and squares.

With Fig. 6.2, it is illustrated the accuracy of the analytical expression given with **Lemma 14** for $n_{BS} = \{2, 5, 8\}$. It is observed a tight match between simulation and analytical results. The outage probability for cell-edge and near MTs is illustrated with Fig. 6.3 and Fig. A.11. Fig. 6.3 shows the outage probability as a function of the transmit SNR, ρ_{BS} for $a_n = \{0.5, 0.9\}$. Results reveals the following trends: 1) the performance of near MTs becomes interference-limited for a smaller transmit power than the cell-edge MTs and 2) a power allocation factor of $a_e = 0.9$ leads to a better performance than $a_e = 0.5$ for both cell-edge and near MT. The reason behind 1) is related to the fact that intra-cluster interference is the dominant factor for near MTs, when they try to decode their own symbol. Cell-edge MTs also suffer from intra-cluster interference because of NOMA, nevertheless, thanks to the beamforming strategy, the desired signal is greater than the intra-cluster interference. 2) is due to the fact that near MTs needs to decode successfully the symbol intended for cell-edge MTs in order to perform SIC. Fig. A.11 illustrates the outage probability versus the number of cooperating BSs per cluster. As it can be observed, cell-edge MTs greatly increases their performance with n_{BS} , whereas

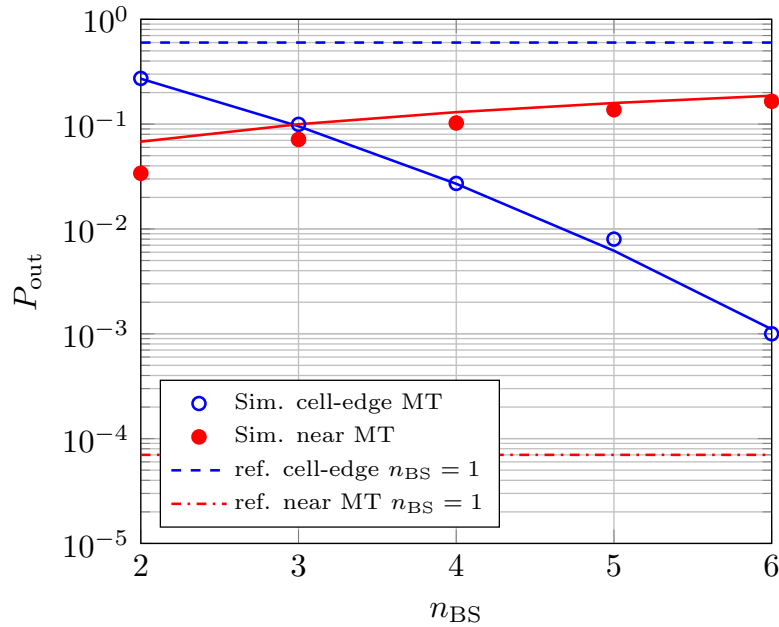


Figure 6.4: Comparison of the outage probability for near and cell-edge MTs versus the number of BSs per cluster, n_{BS} for $a_e = 0.9$. The special case $n_{BS} = 1$ is added as a reference value for comparison.

the performance of near MTs is slightly worsen. In particular, for near MTs, the outage probability is roughly 0.1 and 0.2 for $n_{BS} = 2$ and $n_{BS} = 6$ respectively. However, the outage probability for cell-edge MTs decreases 3 orders of magnitude for the same number of BSs. The special case $n_{BS} = 1$ is also considered. In this case, there is not intra-cluster interference for near MTs. Hence, near MTs exhibit a small outage probability; however the price to pay is that the outage probability of cell-edge is very high.

6.5 Discussion

In this chapter a novel scheme for Cloud-Radio Access Networks has been proposed. Such an scheme considers that two users are scheduled for transmission at the same BS according to NOMA. Nevertheless, worst users, in terms of SINR, benefits from cooperation between a cluster of BSs that are connected through high speed links. The mathematical analysis has demonstrated that the beamforming gain can be modeled as a mixture of Erlang distributions, and the average beamforming gain is a linear function with respect to the

number of cooperating BSs. Simple expressions for the outage probability of the near and cell-edge users has been obtained. Results has revealed that BS cooperation greatly improves the performance of cell-edge users, which increases with the number of BSs.

These contributions appear in [54], which is under review.

Chapter 7

Performance Analysis of Geo-Location Based Access for Vehicular Communications

LTE V2X is the response of the 3GPP standardization body to the high market expectations related to vehicular communications for safety and infotainment services. To fulfill the stringent requirements in terms of reliability associated with safety applications, geo-location based access (GLOC) has been proposed for direct Vehicle-to-Vehicle (V2V) communication. Such a scheme aims at maximizing the distance of co-channel transmitters (i.e. transmitter that use the same resources) while preserving a low latency when accessing the resources and a low overhead. In this chapter we analyze, with the aid of stochastic geometry, the delivery of periodic and non-periodic broadcast messages with GLOC, taking into account path loss and fading as well as the random locations of transmitting vehicles. Analytical results include the average interference, average Binary Rate (BR), capture probability, i.e., the probability of successful message transmission, and Energy Efficiency (EE). Mathematical analysis reveals interesting insights about the system performance, which are validated through extensive Monte Carlo simulations. In particular, it is shown that the capture probability is an increasing function with exponential dependence with respect to the transmit power and it is demonstrated that an arbitrary high capture probability can be achieved, as long as the number of access resources is high enough. Finally, to facilitate the system-level design of GLOC, it is obtained the



optimum transmit power, which fulfill a given minimum capture probability constraint while maximizing the EE of the system.

7.1 Introduction

Intelligent Transportation Systems (ITS) require direct Vehicle-to-Vehicle (V2V) communication to provide safety and infotainment services. Within the safety applications two types of broadcast messages can be identified: periodic and non-periodic messages [97]. Periodic messages aim at achieving vehicle awareness and consist on the periodic transmission of broadcast status messages, informing nearby vehicles of their position, velocity and direction. On the other hand, non-periodic, e.g. event-driven messages, are transmitted to respond to specific hazardous situations. There have been several standardization activities aiming at offering a reliable communications with low latency and cost. On the one hand, Dedicated Short-Range Communications (DSRC) has been developed using IEEE 802.11p, which is based on Carrier Sense Multiple Access (CSMA). Nevertheless, 802.11p suffers from the main limitations related to 802.xx standards, such as poor scalability to high traffic density and poor support of high mobility [17]. Hence, solutions based on 4G and 5G cellular networks come to the fore [98]. LTE V2X is the response of the 3GPP standardization body to the high market expectations and will use the same principles as those that are envisioned for Device-to-Device (D2D) communications. The 3GPP specifies two phases for both D2D and V2V communications: 1) neighbours discovery, where vehicles announce their presence and status periodically to the surrounding nodes; and 2) direct communication, where asynchronous events are reported [99]. Additionally, there are two mechanisms to access the resources in V2V communications: scheduled and autonomous mode. The scheduled mode involves the exchange of transmission requests and grants with the Base Stations (BSs), and it may suffer from long delays. Hence, the autonomous mode is normally preferred where it is possible for the devices to select the transmission resources without network involvement. Yet, the network has a key role in providing synchronization.

For autonomous mode the 3GPP propose the use of Geo-Location based access (GLOC) [98, Sect. 23.14.1.1. (support for V2X sidelink)], [100]. With this technique, vehicles access the channel based on its position. The road is divided into segments, where each segment

is associated with a single orthogonal Access Resource (AR).

The mapping between ARs and segments is made to maximize the co-channel distance, which is the minimum distance between two segments that use the same set of ARs. In [100], it is proposed GLOC for the discovery and communication phase in V2V communications. It is shown through simulation that the benefits of this technique are: (i) high reliability, since the distance to interfering vehicles can be increased with the number of ARs and (ii) MAC layer does not add any delay on accessing the channel, i.e., vehicles start their transmission once they have data to transmit.

7.1.1 Stochastic Geometry Analysis of Vehicular Networks

Besides simulation based studies like [100], analytical models can provide further insights about the inter-plays among reliability and binary rate as well as the number of ARs for medium access, or the transmit power. Additionally, mathematical analysis leads to expressions that can be evaluated quickly and allows to perform optimization of the most relevant performance metrics. Here is where stochastic geometry [61] appears as a promising tool, since it allows tractable and realistic analysis due to the random nature of the location of transmitting nodes in Vehicular Ad Hoc Networks (VANETs). For instance, [42] analyzes, with the aid of stochastic geometry, the capture probability, average throughput and mean density progress of transmitted packets for the case of unicast transmissions with ALOHA. In [43], CSMA for unicast multi-hop communications is considered with several routing strategies. It also considers multi-lane abstraction model which is more accurate than single-lane models for wide roads. The case of a head vehicle that broadcasts info and control messages to a sectorized cluster of client vehicles is considered in [44]. This work models the positions of vehicles as a Cox process whose density follows a Fox distribution; however, the interference caused by other transmitting vehicles is not taken into account. The performance of IEEE 802.11p is assessed with the aid of stochastic geometry and queuing theories in [46]. Here it is modelled the temporal characteristics CSMA, which adds a delay on the transmission because of the back-off counter. To account for the spatial dependence, which is derived from the carrier sensing, and also for the temporal behavior, which is derived from the back-off counter, a discrete Matérn Hard Core Point Process (HCPP) is proposed to model the locations of concurrent transmitters.

7.1.2 Main Contributions

In this work, GLOC access technique is analyzed taking into account the velocity-dependent safe distance, d_{safe} , between vehicles of the same lane. Such a safe distance imposes some correlation between locations of the vehicles, since there are no neighboring vehicles closer than d_{safe} . Due to this minimum distance, we have chosen the Matérn HCPP of type II to model the locations of vehicles within the same lane. This point process considers initially that points are drawn according to a PPP whose density is λ_b . Then, a random mark, which is uniformly distributed between 0 and 1, is given to each point. Those points that have a neighbor closer than the minimum distance with a smaller mark are removed [61]. After the thinning process the resulting density is $\lambda_L = (1 - e^{-2\lambda_b d_{\text{safe}}}) / (2d_{\text{safe}})$. However, such a point process is generally intractable, and only some moments of the interference can be obtained without resorting to approximations [55]. To overcome such an intractability, we will use conditional thinning as in [47]. In simple terms, the locations of vehicles are first assumed to be placed according to a PPP whose density is λ_L . Then, spatial constraints (correlation) in the form of a minimum distance between points, d_{safe} , are imposed by means of an indicator function, but only in the proximity of the transmitter and the receiver. Hence, the main difference between Matérn HCPP of type II and the proposed approximation based on conditional thinning is that with the latter approach, it is not imposed the minimum distance between each point. Instead, it is only applied to those points that are near to the receiver and the transmitter; however the spatial densities are the same in both point process, i.e. λ_L . Additionally, it is considered that the length of the road is much higher than its width, and hence it is assumed that locations of the vehicles in each lane can be modeled as points in the real line. Based on these modeling assumptions we provide the following contributions:

1) *Mathematical framework for analysis of geo-location based access:* We propose a mathematical framework for the analysis of GLOC considering a minimum distance between vehicles of the same lane. Two kinds of resource allocation schemes are considered: Single-Lane Partition (SLP) and Multi-Lane Partition (MLP), which have different trade-offs and mainly differ on whether lane-finding is required or not. With SLP, the road is divided in different segments, whereas with MLP, each lane is divided in segments. Both broadcast messages, i.e., periodic and non-periodic, are modeled to obtain a complete understanding about the capabilities of GLOC as a MAC for ITS. Additionally, system-

level parameters like message size, reporting rate, broadcast distance, etc. are taken from recommendations of the 3GPP Work Items [56] and [57] to study the support of LTE for V2V services. The path loss slope and path loss exponent is taken from [58]. Interestingly, the path loss exponent in V2V channels, α , is normally smaller than 2 [58–60]. This fact has implications on the spatial modeling, because the Probability Generating Functional (PGFL) of the PPP in \mathbb{R}^d , with $d \in \mathbb{N}^+$, only exists for a path loss exponent, $\alpha > d$ [61]. If $\alpha < 2$, this means that only PPPs in the real line ($d = 1$) can be considered to conduct the analysis. Finally, mathematical expressions for a wide variety of performance indicators have been obtained, leading to a deep understanding of the studied techniques. In particular, the capture probability, the average interference, the average Binary Rate (BR) and the average Energy Efficiency (EE) are derived.

2) *Theoretical insights*: Many useful insights have been obtained from the derived expressions. Interestingly, it has been shown that: (i) the capture probability is an increasing function with respect to the transmit power with exponential dependence; (ii) the system is noise-limited for MLP when the number of ARs is high enough whereas it is interference-limited in case of SLP; (iii) the average interference diverges when it is evaluated in co-channel segments (i.e. segments related to the same AR) with SLP, whereas it always converges for the case of MLP. The fact that with MLP the system is noise-limited for a given number of ARs means that it is possible to achieve an arbitrary high capture probability by increasing the transmit power.

3) *Optimization*: The optimum transmit power that achieves a capture probability greater or equal than a given threshold while maximizing the EE is obtained. Such minimum capture probability is expressed as a percentage, δ , of the maximum capture probability that can be achieved. Interestingly, the same optimal transmit power is obtained under SLP and MLP allocation schemes.

7.2 Related Work

7.2.1 MAC schemes for Vehicular Communications

Depending on the location of resource allocation process, MAC schemes can be classified on centralized or distributed. In centralized schemes, a central unit, e.g. a Road Side Unit (RSU) or a BS, allocates transmission resources to the vehicles. An advantage of

centralized approaches is that they can avoid collisions; however, they have three main drawbacks: (i) they are complex as they require an association procedure and infrastructure; (ii) they add an overhead due to control channels; and (iii) they add a delay. For these reasons distributed solutions are normally preferred. These solutions can be classified as: 1) contention-based; 2) resource reservation; 3) hybrid schemes; and 4) Geo-location based access.

1) *Contention-based*: These schemes rely on carrier sensing and back-off windows to reduce collisions [101, 102]. Optionally, 802.11p includes the Request to Send (RTS)/Clear to Send (CTS) exchange to mitigate the hidden node problem. Most of the studies about contention-based schemes that can be easily adapted to 802.11p, focus on controlling the rate or obtaining an adequate contention window for a given setting. In particular, an adaptive mobility-based algorithm is proposed in [101]. This algorithm selects an appropriate pair of contention window size and communication range based on the average vehicle density and speed. In [102] it is proposed a congestion control method that estimates the number of collisions to adjust the reporting rate of status broadcast messages. Nevertheless, those schemes do not solve 802.11p drawbacks as high number of collisions with high traffic densities and poor support of high mobility [17].

2) *Resource reservation*: These methods aim at ensuring that each resource is used at most by a given vehicle among the one-hop neighbors [103, 104]. Here, it is assumed that only one-hop neighbors can either establish a direct communications and/or produce a collision. In [104] it is proposed a Time Division Multiple Access (TDMA) scheme with resource reservation. With the proposed scheme, each vehicle periodically sends the list of active one-hop neighbours, and their associated reserved slots. Nevertheless, such an approach do not resolve completely collisions when trying to reserve an idle slot, or when two vehicles with the same reserved slot enters in the same one-hop set. Additionally, those methods are associated with a high overhead, since every vehicle has to broadcast the list of neighbours and reserved slots.

3) *Hybrid access*: These methods combines different technologies with CSMA [105, 106]. In [105] it is selected a head vehicle per cluster, which deliver and collect safety messages, using contention-free TDMA whereas inter-cluster communication between head vehicles is performed with CSMA. In [106] it is considered a multi-channel structure, where CSMA is used for delivery of safety messages on a common channel and token ring is used

in different channels for different clusters of vehicles. Nevertheless, these approaches are generally complex since they consider different technologies and still have reliability issues that are inherited from CSMA.

4) *Geo-location based access*: These schemes, which are also known as Spatial Division Multiple Access (SDMA), consists on a discretization procedure where the road is divided in segments, and a mapping function that allocates orthogonal ARs or slots¹ to different segments [107, 108]. Then, vehicles determine the segment where they belong, based on their geo-location information and use the associated AR. In [109] it is proposed a GLOC based access to improve reliability and security. To avoid bandwidth inefficiency, vehicles use slots associated with empty segments.

Compared with existing approaches, GLOC offer potentially the following benefits: 1) high reliability, 2) low overhead, 3) low latency and 4) it represents a simple protocol which facilitates its implementation. 1) is because increasing the number of ARs increases the co-channel distance, and hence reduce collisions. 2) and 3) are due to the fact that it is not needed any reservation nor information exchange to access the resources, i.e., the vehicles estimate their position and transmit in the corresponding AR as soon as they have data to transmit. These aforementioned potential benefits and the fact that such a scheme has not been analysed mathematically ([100, 107–109] focus on simulation results) motivated us to study in deep such an scheme. The main weakness of GLOC might be bandwidth inefficiency, specially at low vehicle densities, which is due to the fact that any time instant it could be many empty segments and hence unused ARs. Nevertheless, this issue can be mitigated by using techniques like [109]. Additionally, an appropriate choice of segment size and number of ARs according to the vehicle density mitigate such problem.

7.2.2 Energy Efficiency in Vehicular Communications

Although reliability, latency and throughput are normally the main performance indicators in vehicular communications, EE, has also recently received important attention for the financial and environmental considerations [110]. Energy efficiency is even more relevant

¹Some works ([107–109]) use TDMA to define ARs as slots for Geo-location based access. In our work, which is focused on 3GPP LTE V2X technology, it is considered Single-Carrier Frequency Division Multiple Access (SC-FDMA), and hence ARs are defined in the frequency domain.

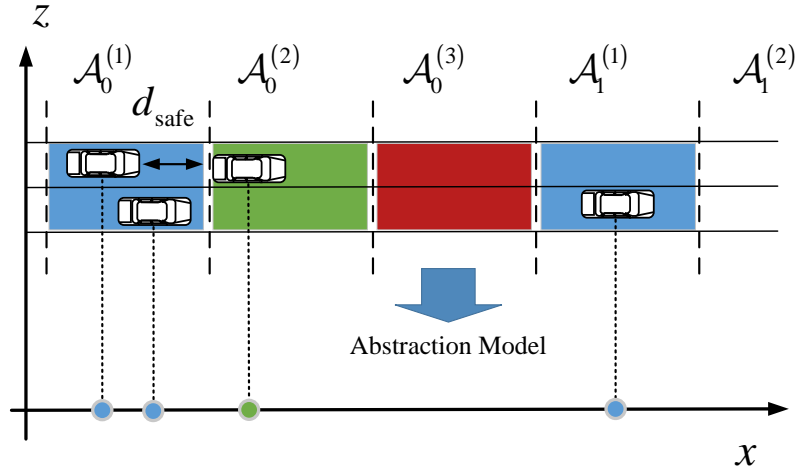


Figure 7.1: Sketch of GLOC based access with SLP for a two-lane road and 3 ARs. Different colors are associated to different ARs. On the bottom it is shown the abstraction model for the study of the road where positions of vehicles are treated as points in the real line.

if electric cars are considered as a widely used means of transportation in the future [111]. Additionally, minimizing the energy consumption in VANETs is beneficial to reduce the greenhouse gas emission (CO_2) [112, 113]. In this context, a game theoretic model is proposed in [114] to decide whether to disseminate the information or not, based on the current energy situation of the vehicular network. The proposed algorithm minimizes the energy consumption, overhead and time. In [112], it is considered three routing strategies that determine the set of relying vehicles and communication range that maximizes the EE. In [113], an hybrid spectrum access scheme in V2I uplink scenario in cognitive VANETs is proposed to increase the EE. In [115], it is proposed a method for cluster head selection that maximizes the EE in heterogeneous vehicular networks.

7.3 System Model

A straight road with n_L lanes is considered as appears in figures 7.1 and 7.2 ($n_L = 2$), where the length of the road is much greater than its width and thus the z coordinate can be neglected. As pointed out in [56], there is a velocity-dependent safe distance between vehicles of the same lane, referred to d_{safe} . Hence, positions of vehicles within the same lane are assumed to follow a Matérn HCPP of type II, $\Phi_L = \{V_0, V_1, \dots\} \subset \mathbb{R}$, whose

density is λ_L and its minimum distance between points is d_{safe} . The assumption of a minimum distance between vehicles leads to a maximum vehicle density per lane, which is $\lambda_{L,\text{max}} = 1/(2d_{\text{safe}})$. It is assumed that at a given time instant a vehicle has data to transmit with probability p_a ; hence the set of active vehicles $\Phi_L^{(a)} = \{\text{VT}_0, \text{VT}_1, \dots\}$ is obtained through independent thinning from Φ_L with density $\lambda_L p_a$. A summary of main symbols and functions is provided in Table 7.1.

7.3.1 Resource Partition Schemes

With GLOC, the road is divided into segments of length d_A meters, and each segment is associated with a given orthogonal AR. The useful system bandwidth, b_w , is divided between the ARs. At a given time instant, each vehicle with data to transmit determines its current segment based on its position and then, it transmits with the mapped AR. The mapping between segments and ARs is made to maximize the co-channel distance. Modeling the location of the vehicles randomly in terms of point processes allow us to treat the VANET as a snapshot of a stationary random field of communicating vehicles, where realizations of such point process are associated with different vehicle locations. Hence, it is assumed that the segment does not change during the transmission of a single message. Besides, it is considered that the vehicles are aware of the mapping between segments and ARs, and the position and size of the segments. This can be achieved following the same process as specified in [98, Sect. 23.14.1.1. (support for V2X sidelink)]. We propose two resource partition schemes, identified as SLP and MLP, that mainly differ on whether lane-finding is required or not. With SLP, the road is divided in different segments, whereas with MLP, each lane is divided in segments.

The frequency allocation process of SLP is depicted as appears next:

1. The road is divided into segments of d_A meters. Each segment consists of n_L lanes.
2. A bandwidth of b_w/n_{AR} is allocated to each AR, where n_{AR} is the number of ARs.
3. The segments are grouped into consecutive clusters of n_{AR} segments. A single orthogonal AR is allocated to every segment within a given cluster. The mapping between segments and ARs is made with maximum co-channel distance criterion, aiming at minimizing the interference.

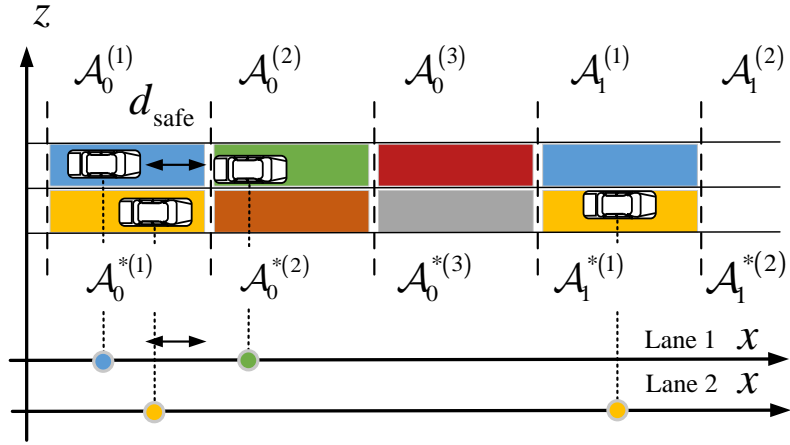


Figure 7.2: Sketch of GLOC based access with MLP for a two-lane road and 6 ARs. Different colors are associated to different ARs. On the bottom it is shown the abstraction model for the study of each lane where positions of vehicles are treated as points in the real line.

A sample of SLP scheme for $n_{AR} = 3$ and $n_L = 2$ is shown in the top of Fig. 7.1, whereas the mathematical abstraction model as a one-dimensional point process is illustrated at the bottom of the figure. In this case, each color (blue, green and red) represents a different AR whereas segments are represented as $\mathcal{A}_c^{(j)}$, where j identifies the AR, and c identifies the cluster.

On the other hand, MLP considers that each segment only contains a single lane. The process to allocate frequencies with MLP is described as follows:

1. The system bandwidth is equally divided among lanes. Therefore, there is b_w/n_L Hz available for each lane and there is no interference among different lanes.
2. Each lane is divided into segments of d_A meters.
3. A bandwidth of $b_w/(n_{AR} \cdot n_L)$ is allocated to each AR, where n_{AR} is the number of ARs per lane. Thus, the overall number of ARs is $n_L \cdot n_{AR}$.
4. The segments of each lane are grouped in consecutive clusters of n_{AR} segments. A single orthogonal AR is allocated to every segment within a given cluster. The mapping among segments of the same lane and ARs is made with maximum co-channel distance criterion, aiming at minimizing the interference.

Fig. 7.2 illustrates a sample of MLP for $n_{AR} = 3$ and $n_L = 2$. In this case $\mathcal{A}_c^{(j)}$ represents segments that belong to lane 1 whereas $\mathcal{A}_c^{*(j)}$ represents segments related to lane 2. The abstraction model for each lane is represented at the bottom of the figure.

Each scheme has different pros and cons. With SLP it is not required to identify the lane in which the vehicle is traveling, which relaxes the requirement imposed to position estimation. On the other hand, MLP considers that vehicles are capable of estimating their position and also their current lane; however, this can be achieved using similar techniques as proposed in [116]. Additionally, the requisites imposed over position estimation for 5G are around 30 cm, which assures lane-awareness [99]. On the negative side, it can be noticed that SLP leads to a higher density of co-channel interfering vehicles, since each segment has several lanes. Additionally, the minimum distance towards the nearest interfering vehicle is reduced, since in this case an interfering vehicle could be located in the same location as the receiver in a different lane. This does not happen in case of MLP thanks to the minimum (inter-vehicle) safe distance. Nevertheless the bandwidth for each AR is lower in MLP, since the bandwidth is also divided among lanes.

These differences have also implications on the mathematical modeling of SLP and MLP. In particular, with SLP there is not a minimum distance between vehicles, and hence the position of interfering vehicles can be modeled as a PPP. The bandwidth per AR and vehicle densities are also different, as summarized in Table 7.2.

The analysis is performed for a typical transmitter, i.e., a randomly selected Vehicle Transmitter (VT). This transmitter is named the probe VT, and it is represented with symbol VT_0 . In this chapter we made an abuse of notation since VT_0 is used to represent the probe VT as well as its position in the real line. Analogously, its associated AR is the probe AR, which is denoted by AR_0 . Symbol $\mathcal{A}_c^{(j)}$ identifies the segment associated with j -th AR within cluster c . The set that represents all the segments associated with AR j is represented as $\mathcal{A}^{(j)} = \bigcup_{c=-\infty}^{\infty} \mathcal{A}_c^{(j)}$. Fig. 7.3 shows a sketch of the abstraction model, either for SLP or MLP. In case of SLP, this abstraction model is related to a given road, whereas in case of MLP it is related to a given lane. Without loss of generality, it is considered that the probe segment, $\mathcal{A}_0^{(AR_0)}$, is centered at the origin. Being the probe segment centered at the origin, the c -th co-channel segment, $\mathcal{A}_c^{(AR_0)}$, can be expressed as

Table 7.1: Summary of main symbols and functions used throughout the chapter.

Symbol	Definition
$\lfloor \cdot \rfloor, \lceil \cdot \rceil$	Floor and ceil functions
${}_2F_1(\cdot, \cdot, \cdot, \cdot)$	Gauss hypergeometric function defined in [77] (Ch. 15).
$\mathbb{E}[\cdot]$	Expectation operator
$\Pr(\cdot)$	Probability measure
$\mathbf{1}(\cdot)$	Indicator function
$\mathfrak{b}_x(r)$	Ball centered at x with radius r
n_L	Number of lanes
d_{safe}	Safe distance between vehicles
d_{max}	Maximum communication distance
Φ_L, λ_L	HCPP that models locations of vehicles within the same lane and its density
$\Phi_L^{(a)}, \lambda_L^{(a)}$	Thinned HCPP that models locations of active vehicles within the same lane and its density
d_A	Segment's length
b_w	Useful system's bandwidth
n_{AR}	With SLP it is the number of orthogonal resources. With MLP it is the number of orthogonal resources per lane
$\mathcal{A}_c^{(j)}$	Segment associated with the j -th AR within cluster c
$\mathcal{A}^{(j)}$	Union of all the segments associated with the j -th AR
τ, α	Slope and exponent of the path loss function
ρ_{VT}	Transmit power per Hz
b_{AR}	Bandwidth of a single AR
Φ, λ	Point process that models the location of vehicles in the abstraction model for SLP and MLP
$\Phi^{(a)}, \lambda^{(a)}$	Thinned point process that model the location of active vehicles in the abstraction model for SLP and MLP
VT_0, AR_0	Probe vehicle transmitter and its related AR
$\text{VT}_i, H_{\text{VT}_i}$	Generic active vehicle and its fading towards the probe receiver
σ_n^2, I	Noise power and aggregate interference

Table 7.2: Modeling Differences between SLP and MLP

Scheme	λ	b_{AR}	Minimum dist.	Type of Φ
SLP	$\lambda_L \cdot n_L$	b_w/n_{AR}	0	PPP
MLP	λ_L	$b_w/(n_{AR}n_L)$	d_{safe}	HCPP ²

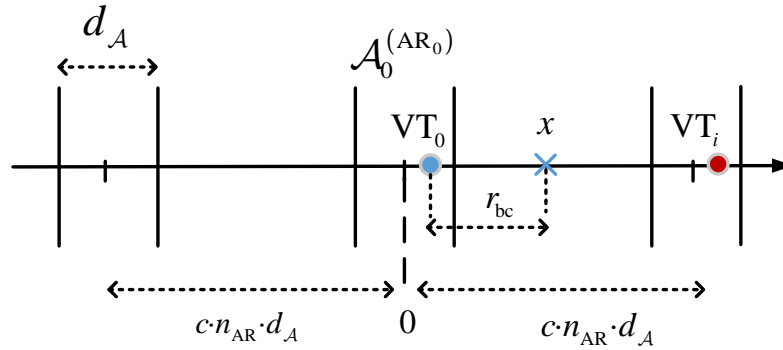


Figure 7.3: Illustration of co-channel segments in the abstraction model. The probe transmitter is represented as VT_0 , the probe AR and segment as AR_0 and $\mathcal{A}_0^{(AR_0)}$ respectively, the probe receiver as a blue x and a single interfering vehicle as VT_i . The length of each segment is represented as d_A and thus $n_{AR} \cdot d_A$ is the minimum co-channel distance.

$$\mathcal{A}_c^{(AR_0)} = \left\{ y \in \mathbb{R} : cn_{AR}d_A - \frac{d_A}{2} \leq y < cn_{AR}d_A + \frac{d_A}{2} \right\} \quad (7.1)$$

The c -th co-channel segment is centered around $c \cdot n_{AR} \cdot d_A$, with $c \in \mathbb{Z}$.

7.3.2 Signal Modeling

Transmitted signals suffer from Rayleigh fading, hence the channel power gain is exponentially distributed with unitary mean. Path loss is modeled through a path loss slope τ and a path loss exponent α . Having a receiver placed at location x , the SINR can be expressed as follows

$$\text{SINR}(x) = \frac{H_{VT_0} (\tau |VT_0 - x|)^{-\alpha} \rho_{VT}}{I(x) + \sigma_n^2} \quad (7.2)$$

where $|\cdot|$ the Euclidean distance, H_{VT_0} is the fading power gain between VT_0 and the test receiver, ρ_{VT} is the transmit power per Hz, σ_n^2 is the noise power and $I(x)$ the received interference at x . It is assumed that there is a maximum communication range given by d_{\max} , hence a receiver cannot detect signals from transmitters farther than d_{\max} . Thus the interference term can be expressed as follows

$$I(x) = \sum_{VT_i \in \Phi^{(a)} \setminus \{VT_0\}} H_{VT_i} (\tau |VT_i - x|)^{-\alpha} \times \rho_{VT} \mathbf{1}(VT_i \in \mathcal{A}^{(AR_0)}) \mathbf{1}(VT_i \in \mathbf{b}_x(d_{\max})) \quad (7.3)$$

being $\Phi^{(a)}$ the set of active vehicles in the abstraction model; $\mathbf{1}(\cdot)$ the indicator function and $\mathbf{b}_x(d_{\max})$ the ball centered at x with radius d_{\max} . H_{VT_i} is the fading between VT_i and x . As it has been justified before, in case of SLP, $\Phi^{(a)}$ is a PPP obtained through independent thinning, with probability p_a , from Φ . However, in case of MLP, $\Phi^{(a)}$ is obtained through independent thinning over Φ , which is now a Matérn HCPP of type II. Such point process is difficult to analyze because its probability generating functionals do not exist, [55]. Hence, the following assumption over the interference is proposed for the sake of tractability.

Assumption 4. *The interference term in case of MLP can be approximated as appears below*

$$I(x) = \sum_{VT_i \in \Phi^{(a)}} H_{VT_i} (\tau |VT_i - x|)^{-\alpha} \rho_{VT} \mathbf{1}(VT_i \in \mathcal{A}^{(RB_0)}) \times \mathbf{1}(|VT_i - x| > d_{\text{safe}}) \mathbf{1}(|VT_i - VT_0| > d_{\text{safe}}) \quad (7.4)$$

where $\Phi^{(a)}$ is a PPP with density $\lambda_L p_a$.

The reasoning behind **Assumption 4** is explained below. For tractability, it is assumed that $\Phi^{(a)}$ follows a PPP, instead of a thinned version of a HCPP that represents the locations of active vehicles within the same lane. The correlations in the actual point process are captured in the form of spatial constraints by means of a dependent thinning with two indicator functions. These constraints guarantee that there are no vehicles nearer than d_{safe} to the probe transmitter nor to the test receiver, which is placed at x . It

should be noticed that this dependent thinning leads to a point process which is not a homogeneous PPP.

Remark 13 (Exact analysis). *In the forthcoming analysis: (i) the results for the SLP case are exact, since there is PPP as the generative process of the locations of active vehicles; and (ii) the results for the MLP case are approximations due to **Assumption 4**.*

7.3.3 Key Performance Indicators

The capture probability represents the probability that a message is correctly received. Having a receiver placed at location x , it is expressed as the probability of the SINR being higher than a given threshold, γ , which is the CCDF of the SINR.

We consider that each transmitter uses a fixed Modulation and Coding Scheme (MCS). Here, we use the same abstraction as in [83, 117] to represent the goodput, or equivalently the BR of correctly received bits as

$$\text{BR}(x) = \mathbf{1}(\text{SINR}(x) > \gamma) \cdot b_{\text{AR}} \cdot \log_2(1 + \gamma) \quad (7.5)$$

where b_{AR} represents the bandwidth associated with a given AR and it is given in Table 7.2 for SLP and MLP. On the other hand, γ , which is a system-level parameter, represents the SINR threshold associated with the considered MCS, where $\log_2(1 + \gamma)$ is its spectral efficiency in terms of bps/Hz.

The EE is defined as the quotient between the BR and the transmit power in a given AR, which can be written in terms of b/J as follows

$$\text{EE}(x) = \frac{\log_2(1 + \gamma)}{\rho_{\text{VT}}} \mathbf{1}(\text{SINR}(x) > \gamma) \quad (7.6)$$

where the bandwidth term, b_w , is canceled out since it appears in the definition of BR and also in the expression of the transmit power in a given AR.

7.3.4 Broadcast Message Types

As it is mentioned in the introduction, there are two types of broadcast messages: non-periodic and periodic. For non-periodic messages, it is assumed that the probability of being active, i.e., with data to transmit, depends on traffic conditions and other related

human issues and thus it is a fixed parameter. The case of periodic messages is different, since in this case, the probability of being active depends on the periodic rate and the time needed to transmit the message. This latter metric depends on the spectral efficiency of the MCS and also of the AR bandwidth, b_{AR} . Hence, for the case of periodic messages, the probability of being active is expressed as follows

$$p_a = \frac{m_{bc}}{b_{AR} t_{rep} \log_2(1 + \gamma)} \quad (7.7)$$

where t_{rep} is the reporting latency, i.e., the time between two consecutive messages and m_{bc} is the message size in bits. It should be noticed that the time required to transmit the message, which is $m_{bc}/(b_{AR} \log_2(1 + \gamma))$, cannot be higher than t_{rep} . This imposes the following inequality over the above parameters that must be fulfilled $m_{bc}/(b_{AR} \log_2(1 + \gamma)) < t_{rep}$.

Remark 14 (Density of active vehicles). *In view of (7.7) and Table 7.2 it should be noticed that the density of active vehicles transmitting periodic messages, $\lambda \cdot p_a$, is the same for SLP and MLP schemes for the same n_{AR} .*

7.4 Analysis of the Interference and Capture Probability

In this section, main performance metrics related to Single-Lane Partition and Multi-Lane Partition are derived. Given the broadcast nature of the considered transmissions, a probe receiver placed at a distance r_{bc} from the probe transmitter, VT_0 , is considered. Hence, the metrics of interest - capture probability, average BR and average EE - are evaluated at $x = VT_0 + r_{bc}$.

7.4.1 Single-Lane Partition (SLP)

To obtain the capture probability, we first compute the Laplace transform the interference, which is given with the following lemma.

Lemma 19. *With SLP, the Laplace transform of the interference evaluated at $x \in \mathbb{R}$ can be written as*

$$\mathcal{L}_{I(x)}(s) = \exp \left(-\lambda \cdot p_a \sum_{c=-\lfloor d_{\max}/(n_{\text{AR}}d_{\mathcal{A}}) \rfloor}^{\lceil d_{\max}/(n_{\text{AR}}d_{\mathcal{A}}) \rceil} \kappa(c, s, x) \right) \quad (7.8)$$

where the function $\kappa(c, s, x)$ ³ appears in (7.9)

$$\begin{aligned} \kappa(c, s, x) = & \sum_{j \in \{1,2\}} \mathbf{1} \left(\mu_L^{(j)} < \mu_U^{(j)} \right) \left(\mu_U^{(j)} {}_2F_1 \left(1, \frac{1}{\alpha}, 1 + \frac{1}{\alpha}, \frac{(\tau \mu_U^{(j)})^\alpha}{-s \cdot \rho_{\text{VT}}} \right) \right. \\ & \left. - \mu_L^{(j)} {}_2F_1 \left(1, \frac{1}{\alpha}, 1 + \frac{1}{\alpha}, \frac{(\tau \mu_L^{(j)})^\alpha}{-s \cdot \rho_{\text{VT}}} \right) \right) \end{aligned} \quad (7.9)$$

and

$$\begin{aligned} \mu_U^{(1)} &= \min \left(c \cdot n_{\text{AR}} \cdot d_{\mathcal{A}} + \frac{d_{\mathcal{A}}}{2} - x, d_{\max} \right) \\ \mu_L^{(2)} &= -\max \left(c \cdot n_{\text{AR}} \cdot d_{\mathcal{A}} - \frac{d_{\mathcal{A}}}{2} - x, -d_{\max} \right) \\ \mu_L^{(1)} &= \max \left(\mu_L^{(2)}, 0 \right); \quad \mu_U^{(2)} = -\min \left(\mu_U^{(1)}, 0 \right) \end{aligned} \quad (7.10)$$

Proof. The proof is given in Appendix 7.8. □

Theorem 7. *With SLP, the CCDF of the SINR, or equivalently the capture probability, at a distance r_{bc} from the typical vehicle transmitter, VT_0 , appears below*

$$\bar{F}_{\text{SINR}(\text{VT}_0+r_{\text{bc}})}(\gamma) = \frac{e^{-\frac{\gamma \sigma_n^2}{\rho_{\text{VT}}} (\tau r_{\text{bc}})^\alpha}}{d_{\mathcal{A}}} \int_{v=-\frac{d_{\mathcal{A}}}{2}}^{\frac{d_{\mathcal{A}}}{2}} \mathcal{L}_{I(v+r_{\text{bc}})} \left(\frac{\gamma (\tau r_{\text{bc}})^\alpha}{\rho_{\text{VT}}} \right) dv \quad (7.11)$$

³The dependence of functions $\mu_L^{(j)}(c, x)$ and $\mu_U^{(j)}(c, x)$ with c and x has not been written in (7.9), (7.10) and (7.29) for convenience.

where $\mathcal{L}_{I(x)}(s)$ is the Laplace transform of the interference, which is given in **Lemma 19**, with $s = \frac{\gamma}{\rho_{\text{VT}}} (\tau r_{\text{bc}})^\alpha$ and $x = \text{VT}_0 + r_{\text{bc}}$.

Proof. Since the probe transmitter is chosen at random from the set of active vehicles, its position inside the probe cluster, which is represented as VT_0 , is uniformly distributed within the interval $[-d_{\mathcal{A}}/2, d_{\mathcal{A}}/2)$. Hence, the CCDF of the SINR at $x = \text{VT}_0 + r_{\text{bc}}$ can be written as

$$\begin{aligned}
 \bar{F}_{\text{SINR}(\text{VT}_0+r_{\text{bc}})}(\gamma) &= \Pr(\text{SINR}(\text{VT}_0 + r_{\text{bc}}) > \gamma) \\
 &\stackrel{\text{(a)}}{=} \mathbb{E}_{\text{VT}_0} \left[\Pr \left(H_{\text{VT}_0} > \frac{\gamma (\tau r_{\text{bc}})^\alpha}{\rho_{\text{VT}}} (I(\text{VT}_0 + r_{\text{bc}}) + \sigma_n^2) \right) \right] \\
 &\stackrel{\text{(b)}}{=} \mathbb{E}_{\text{VT}_0} \mathbb{E}_I \left[e^{-\frac{\gamma}{\rho_{\text{VT}}} (I(\text{VT}_0+r_{\text{bc}})+\sigma_n^2)(\tau r_{\text{bc}})^\alpha} \right] \\
 &\stackrel{\text{(c)}}{=} \frac{e^{-\frac{\gamma}{\rho_{\text{VT}}} \sigma_n^2 (\tau r_{\text{bc}})^\alpha}}{d_{\mathcal{A}}} \int_{v=-d_{\mathcal{A}}/2}^{d_{\mathcal{A}}/2} \mathcal{L}_{I(v+r_{\text{bc}})} \left(\frac{\gamma}{\rho_{\text{VT}}} (\tau r_{\text{bc}})^\alpha \right) \cdot dv
 \end{aligned} \tag{7.12}$$

where (a) comes after reordering the expression of the SINR and applying the total probability theorem over position VT_0 ; (b) after performing expectation over the fading and conditioning over the interference term and (c) after expressing the expectation over VT_0 in integral form and identifying the Laplace transform of the interference. \square

Corollary 5. *The capture probability with SLP in the limiting case where $n_{\text{AR}} \rightarrow \infty$ is given as follows*

$$\lim_{n_{\text{AR}} \rightarrow \infty} \bar{F}_{\text{SINR}(\text{VT}_0+r_{\text{bc}})}(\gamma) = \frac{e^{-\frac{\gamma \sigma_n^2}{\rho_{\text{VT}}} (\tau r_{\text{bc}})^\alpha}}{d_{\mathcal{A}}} \int_{v=-\frac{d_{\mathcal{A}}}{2}}^{\frac{d_{\mathcal{A}}}{2}} \exp \left(-\lambda p_a \kappa \left(0, \frac{\gamma \sigma_n^2}{\rho_{\text{VT}}} (\tau r_{\text{bc}})^\alpha, v + r_{\text{bc}} \right) \right) dv
 \tag{7.13}$$

Proof. The proof follows the fact that when $n_{\text{AR}} \rightarrow \infty$ the indicator function given in (7.29), $\mathbf{1}(y \in \mathbf{b}_x(d_{\text{max}}))$, is non zero only for $c = 0$. \square

Remark 15 (Intra-segment interference limited regime). *In view of Corollary 5 it can be observed that the capture probability when n_{AR} tends to infinity is limited by the interference*

of the probe segment ($c = 0$), which is related to those cases where an interfering vehicle is transmitting in the same segment as the probe vehicle transmitter.

It has been necessary to obtain the Laplace transform of the interference to compute the CCDF of the SINR. Besides, the Laplace transform of the interference is useful to obtain the average interference, which provides further insights. The following Lemma gives such result.

Lemma 20. *The average received interference at x , being the probe segment centered at the origin can be expressed as*

$$\begin{aligned} \mathbb{E}[I(x)] &= \frac{\lambda p_a \rho_{VT}}{\alpha - 1} \sum_{c=-\lfloor d_{\max}/(n_{AR}d_A) \rfloor}^{\lceil d_{\max}/(n_{AR}d_A) \rceil} \sum_{j \in \{1,2\}} \left(\mu_L^{(j)}(c, x) \left(\mu_U^{(j)}(c, x) \right)^\alpha - \tau^{-\alpha} \left(\mu_U^{(j)}(c, x) \right)^{1-\alpha} \right) \\ &\quad \times \mathbf{1} \left(\mu_L^{(j)}(c, x) < \mu_U^{(j)}(c, x) \right) \end{aligned} \quad (7.14)$$

Proof. Using the fact that the Laplace transform can be used as a moment generating function, the average interference can be written as $\mathbb{E}[I(x)] = - \left| \frac{d}{ds} \mathcal{L}_{I(x)}(s) \right|_{s=0}$. Hence the proof consists on obtaining the derivative of (7.8) and then particularizing for $s = 0$. \square

Remark 16 (Convergence of the interference). *In view of (7.14) it can be stated that the average interference is only finite for $x \notin \mathbf{b}_{c \cdot n_{AR} \cdot d_A}(d_A/2)$, since for $x \in \mathbf{b}_{c \cdot n_{AR} \cdot d_A}(d_A/2)$ we have $\mu_U^{(2)}(c, x) = 0$ which makes the average interference tends to infinity.*

7.4.2 Multi-Lane Partition (MLP)

The Laplace transform of the interference for the case of MLP is given by the following lemma.

Lemma 21. *In case of MLP, the Laplace transform of the interference evaluated at the probe receiver, placed at x is given by*

$$\mathcal{L}_{I(x)}(s) = \exp \left(-\lambda \cdot p_a \sum_{c=-\lfloor d_{\max}/(n_{RB}d_A) \rfloor}^{\lceil d_{\max}/(n_{RB}d_A) \rceil} \zeta(c, s, x) \right) \quad (7.15)$$

where $\zeta(c, s, x)$ is written in (7.16)

$$\begin{aligned} \zeta(c, s, x) = & \sum_{i \in \{1,2\}} \sum_{j \in \{1,2\}} \mathbf{1} \left(\mu_L^{(i,j)} < \mu_U^{(i,j)} \right) \left(\mu_U^{(i,j)} {}_2F_1 \left(1, \frac{1}{\alpha}, 1 + \frac{1}{\alpha}, \frac{(\tau \mu_U^{(i,j)})^\alpha}{-s \cdot \rho_{VT}} \right) \right. \\ & \left. - \mu_L^{(i,j)} {}_2F_1 \left(1, \frac{1}{\alpha}, 1 + \frac{1}{\alpha}, \frac{(\tau \mu_L^{(i,j)})^\alpha}{-s \cdot \rho_{VT}} \right) \right) \end{aligned} \quad (7.16)$$

and

$$\begin{aligned} \mu_U^{(1,1)} &= \min \left(c \cdot n_{RB} \cdot d_A + \frac{d_A}{2} - x, d_{\max} \right) \\ \mu_L^{(2,2)} &= -\max \left(c \cdot n_{RB} \cdot d_A - \frac{d_A}{2} - x, -d_{\max} \right) \\ \mu_L^{(1,1)} &= \max \left(\mu_L^{(2,2)}, d_{\text{safe}}, d_{\text{safe}} - x + v \right) \\ \mu_U^{(2,1)} &= \min \left(\mu_U^{(1,1)}, v - x - d_{\text{safe}} \right) \\ \mu_L^{(2,1)} &= \max \left(\mu_L^{(2,2)}, d_{\text{safe}} \right) \\ \mu_L^{(2,1)} &= \max \left(\mu_L^{(2,2)}, d_{\text{safe}} \right) \\ \mu_U^{(1,2)} &= -\min \left(\mu_U^{(1,1)}, -d_{\text{safe}} \right) \\ \mu_L^{(1,2)} &= -\max \left(\mu_L^{(2,2)}, d_{\text{safe}} - x + v \right) \\ \mu_U^{(2,2)} &= -\min \left(\mu_U^{(1,1)}, -d_{\text{safe}}, v - x - d_{\text{safe}} \right) \end{aligned} \quad (7.17)$$

Proof. The proof is given in Appendix 7.9. □

Corollary 6. *In the special case, $d_A < d_{\text{safe}} < (n_{AR} - 1)d_A$ and $|x| < n_{AR}d_A/2$, the Laplace transform of the interference can be simplified into the following expression*

$$\mathcal{L}_{I(x)}(s) = \exp \left(-\lambda \cdot p_a \sum_{c = -\lfloor \frac{d_{\max}}{n_{AR}d_A} \rfloor}^{\lfloor \frac{d_{\max}}{n_{RB}d_A} \rfloor} \kappa(c, s, x) \mathbf{1}(c \neq 0) \right) \quad (7.18)$$

where $\lambda = \lambda_L$ for the MLP case (Table 7.2).

Proof. The proof consists on noticing that in the case where $d_A < d_{\text{safe}} < (n_{\text{AR}} - 1)d_A$ holds, then, the indicator function $\mathbf{1}(|\text{VT}_i - \text{VT}_0| > d_{\text{safe}})$ is equal to 0 if $\text{VT}_i \in [-d_A/2, d_A/2)$ and 1 otherwise. This means that there is no interfering vehicles inside the probe segment. Additionally, if $|x| < n_{\text{AR}}d_A/2$, then $\mathbf{1}(|\text{VT}_i - x| > d_{\text{safe}}) = 1$. Hence, in view of **Assumption 4**, the analysis is analogous to the case of SLP, but taking into account that there is no intra-segment interference, which is captured in the indicator function $\mathbf{1}(c \neq 0)$. \square

The next theorem gives the capture probability with MLP.

Theorem 8. *The capture probability of a probe receiver placed at a distance r_{bc} from the transmitter with MLP is*

$$\bar{F}_{\text{SINR}(\text{VT}_0+r_{\text{bc}})}(\gamma) = e^{-\frac{\gamma}{\rho_{\text{VT}}}\sigma_n^2(\tau r_{\text{bc}})^\alpha} \int_{v=-d_A/2}^{d_A/2} \frac{\mathbf{1}(v \notin \mathfrak{b}_{v+r_{\text{bc}}}(d_{\text{safe}}))}{|\mathcal{D}(v+r_{\text{bc}})|} \mathcal{L}_{I(v+r_{\text{bc}})} \left(\frac{\gamma}{\rho_{\text{VT}}} (\tau r_{\text{bc}})^\alpha \right) \cdot dv \quad (7.19)$$

where $\mathcal{L}_{I(x)}(s)$ is given in **Lemma 21** and $|\mathcal{D}(x)|$, which represents the Lebesgue measure of the relative complement of the interval $[-d_A/2, d_A/2)$ with respect to the set $\mathfrak{b}_x(d_{\text{safe}})$, and it is written as

$$|\mathcal{D}(x)| = \int_{w=-d_A/2}^{d_A/2} \mathbf{1}(w \notin \mathfrak{b}_x(d_{\text{safe}})) \cdot dw \quad (7.20)$$

Proof. The proof follows from having the probe vehicle uniformly distributed inside the region $\mathcal{D}(x) = [-d_A/2, d_A/2) \setminus \mathfrak{b}_x(d_{\text{safe}})$, and hence the pdf of its position is given as $f_{\text{VT}_0}(v) = \mathbf{1}(v \in \mathcal{D}(x)) / |\mathcal{D}(x)|$. Then, conditioning over the position of the probe vehicle and over interference, and reordering completes the proof. \square

Remark 17 (Exponential dependence). *In view of **Theorems 7** and **8**, it can be observed that the capture probability for both, SLP and MLP, only depends on ρ_{VT} as $c_1^{(k)} \exp(-c_2/\rho_{\text{VT}})$, with the label k being either equal to SLP or MLP, i.e., $k = \{\text{SLP}, \text{MLP}\}$. Such an expression is an increasing function with respect to ρ_{VT} , where $c_1^{(k)}$ and c_2 depend*

on other system parameters, and thus, they are constants with respect to ρ_{VT} . Analogously, the capture probability depends on the noise power, σ_n^2 , as $c_1^{(k)} \exp(-c_2 \frac{\Delta}{\sigma_n^2})$, which is a decreasing function with respect to σ_n^2 . Therefore, the maximum capture probability, for a given set of system parameters, is equal to $c_1^{(k)}$, and it is achieved either in the limit, $\rho_{\text{VT}} \rightarrow \infty$, or in the no-noise case ($\sigma_n^2 = 0$).

Remark 18 (Noise-limited regime). *The system is noise limited, and thus, there is no interference if $d_{\text{safe}} > d_{\mathcal{A}}$ and $n_{\text{AR}} > (2d_{\text{max}} + d_{\mathcal{A}}) / d_{\mathcal{A}}$.*

Proof. With MLP, if $d_{\text{safe}} > d_{\mathcal{A}}$ there is no intra-segment interference. Hence, in this case it is possible to determine the number of ARs, n_{AR} , that leads to a system without interference. This is guaranteed if the distance between the probe receiver, which is placed at $x = \text{VT}_0 + r_{\text{bc}}$, and the nearest interfering vehicle in the nearest co-channel segment is higher than d_{max} (worst case scenario). Such an scenario involves that the probe vehicle is placed at $\text{VT}_0 = d_{\mathcal{A}}/2$ and the probe receiver is placed at the maximum communication range, with $r_{\text{bc}} = d_{\text{max}}$. Therefore, in this case, the nearest interfering vehicle must be placed at a distance towards the probe receiver greater than d_{max} . This requires that $n_{\text{AR}}d_{\mathcal{A}} - d_{\mathcal{A}} > 2d_{\text{max}}$. Reordering the above inequality completes the proof. \square

As it can be noticed from **Remark 18**, by augmenting n_{AR} it is possible to assure no interference, which allows to greatly increase the capture probability by increasing the transmit power.

Corollary 7. *In the special case of $r_{\text{bc}} > d_{\mathcal{A}}$, the capture probability is given as*

$$\bar{F}_{\text{SINR}(\text{VT}_0+r_{\text{bc}})}(\gamma) = \frac{e^{-\frac{\gamma}{p_{\text{VT}}}\sigma_n^2(\tau r_{\text{bc}})^\alpha}}{d_{\mathcal{A}}} \int_{v=-d_{\mathcal{A}}/2}^{d_{\mathcal{A}}/2} \mathcal{L}_{I(v+r_{\text{bc}})}\left(\frac{\gamma}{p_{\text{VT}}}(\tau r_{\text{bc}})^\alpha\right) \cdot dv \quad (7.21)$$

where the Laplace transform of the interference is now given in **Lemma 21**.

Proof. The proof comes after realizing that, in case of $r_{\text{bc}} > d_{\mathcal{A}}$, then $|\mathcal{D}(v + r_{\text{bc}})|$ is $d_{\mathcal{A}}$ and $\mathbf{1}(v \notin \mathbf{b}_{v+r_{\text{bc}}}(d_{\text{safe}}))=1$. \square

The average interference is given in the following lemma.

Table 7.3: Summary of mathematical results as functions of ρ_{VT}

Metric	$\bar{F}_{\text{SINR}}(\gamma)$	$\mathbb{E}[\text{BR}]$	$\mathbb{E}[\text{EE}]$
SLP	$c_1^{(\text{SLP})} e^{-\frac{c_2}{\rho_{VT}}}$	$\frac{b_w}{n_{\text{RB}}} \cdot \log_2(1 + \gamma) \cdot c_1^{(\text{SLP})} e^{-\frac{c_2}{\rho_{VT}}}$	$\frac{\log_2(1 + \gamma)}{\rho_{VT}} \cdot c_1^{(\text{SLP})} e^{-\frac{c_2}{\rho_{VT}}}$
MLP	$c_1^{(\text{MLP})} e^{-\frac{c_2}{\rho_{VT}}}$	$\frac{b_w}{n_{\text{RB}} \cdot n_L} \cdot \log_2(1 + \gamma) \cdot c_1^{(\text{MLP})} e^{-\frac{c_2}{\rho_{VT}}}$	$\frac{\log_2(1 + \gamma)}{\rho_{VT}} \cdot c_1^{(\text{MLP})} e^{-\frac{c_2}{\rho_{VT}}}$
	$c_2 = \gamma \sigma_n^2 (\tau r_{bc})^\alpha$	$c_1^{(\text{SLP})} = \frac{1}{d_A} \int_{v=-\frac{d_A}{2}}^{\frac{d_A}{2}} \mathcal{L}_{I(v+r_{bc})} \left(\frac{\gamma (\tau r_{bc})^\alpha}{\rho_{VT}} \right) dv$	
	$c_1^{(\text{MLP})} = \int_{v=-d_A/2}^{d_A/2} \frac{\mathbf{1}(v \notin \mathbf{b}_{v+r_{bc}}(d_{\text{safe}}))}{ \mathcal{D}(v+r_{bc}) } \mathcal{L}_{I(v+r_{bc})} \left(\frac{\gamma}{\rho_{VT}} (\tau r_{bc})^\alpha \right) \cdot dv$		

Lemma 22. *With MLP, the average received interference at x , being the probe segment centered at the origin, can be expressed as*

$$\begin{aligned}
 \mathbb{E}[I(x)] &= \frac{\lambda p_a \rho_{VT}}{\alpha - 1} \sum_{c=-\lfloor \frac{d_{\text{max}}}{n_{\text{AR}} d_A} \rfloor}^{\lfloor \frac{d_{\text{max}}}{n_{\text{AR}} d_A} \rfloor} \sum_{i \in \{1,2\}} \sum_{j \in \{1,2\}} \\
 &\quad \left(\mu_L^{(i,j)}(c, x) \left(\mu_U^{(i,j)}(c, x) \right)^\alpha - \tau^{-\alpha} \left(\mu_U^{(i,j)}(c, x) \right)^{1-\alpha} \right) \\
 &\quad \times \mathbf{1} \left(\mu_L^{(i,j)}(c, x) < \mu_U^{(i,j)}(c, x) \right)
 \end{aligned} \tag{7.22}$$

Proof. The proof is analogous to **Lemma 20**. Hence, it has been obtained the derivative of the Laplace transform of the interference, which is given in **Lemma 21**, and the resulting expression has then been particularized for $s = 0$. \square

7.5 Binary Rate, Energy Efficiency and Optimal Transmit Power

7.5.1 Binary Rate and Energy Efficiency

Besides the capture probability, another key performance indicator for system design is the average BR. This result is given in the following Lemma.

Lemma 23. *The average BR at a distance r_{bc} from the typical vehicle transmitter, VT_0 , appears below*

$$\mathbb{E}[\text{BR}(VT_0 + r_{bc})] = b_{AR} \cdot \log_2(1 + \gamma) \cdot \bar{F}_{\text{SINR}}(\gamma) \quad (7.23)$$

where b_{AR} is given in Table 7.2 and $\bar{F}_{\text{SINR}}(\gamma)$ is either given in **Theorem 7** or **8** depending on the considered scheme, i.e., SLP or MLP respectively.

Proof. The proof consists on performing expectation over (7.5) and realizing that the term $\mathbb{E}[\mathbf{1}(\text{SINR}(VT_0 + r_{bc}) > \gamma)]$ is the CCDF of the SINR. □

Remark 19 (Average rate when n_{AR} tends to infinity). *In view of **Lemma 23** and **Corollary 5** it can be stated that for a finite SINR threshold, γ , the average BR tends to 0 as n_{AR} tends to infinity.*

Proof. The proof consists on noting that the CCDF of the SINR is equal or smaller than 1, hence for a finite γ the term n_{AR} in the denominator of (7.23) makes the average BR tend to 0. □

Lemma 24. *The average EE at a distance r_{bc} from the typical vehicle transmitter, VT_0 , appears below*

$$\mathbb{E}[\text{EE}(VT_0 + r_{bc})] = \frac{\log_2(1 + \gamma)}{\rho_{VT}} \cdot \bar{F}_{\text{SINR}(VT_0 + r_{bc})}(\gamma) \quad (7.24)$$

where $x = VT_0 + r_{bc}$ and $\bar{F}_{\text{SINR}}(\gamma)$ is either given in **Theorem 7** or **8** depending on the considered scheme, i.e., SLP or MLP respectively.

Proof. The proof is analogous to the case of **Lemma 23**. □

In view of **Remark 17**, the capture probability, average BR and EE can be written as it appears in Table 7.3.

7.5.2 Optimal Transmit Power

In this section, the optimal transmit power that maximizes the EE, subject to a minimum capture probability, is derived. Such a constrain is expressed as a percentage, δ , of the

maximum capture probability that can be achieved according to **Remark 17**. More formally, the optimization problem is formulated as follows

$$\begin{aligned} & \underset{\rho_{VT}}{\text{maximize}} \mathbb{E}[\text{EE}] \\ & \text{subject to } \bar{F}_{\text{SINR}}(\gamma) \geq c_1^{(k)} \delta \\ & \quad 0 < \delta < 1 \end{aligned} \quad (7.25)$$

where k is a label that can be either equal to SLP or MLP, i.e., $k = \{\text{SLP}, \text{MLP}\}$ and the metrics $\mathbb{E}[\text{EE}]$ and $\bar{F}_{\text{SINR}}(\gamma)$ are given in Table 7.3 for SLP and MLP⁴. Solving (A.44) leads to the following theorem.

Theorem 9. *The optimal transmit power, for SLP and MLP, can be written as appears below*

$$\rho_{VT}^* = \begin{cases} c_2 & \text{if } 0 < \delta \leq e^{-1} \\ c_2 \ln^{-1}(1/\delta) & \text{if } 1 > \delta > e^{-1} \end{cases} \quad (7.26)$$

leading to the following EE and capture probability

$$\mathbb{E}[\text{EE}]^* = \begin{cases} \frac{c_1^{(k)}}{c_2} \log_2(1 + \gamma) e^{-1} & \text{if } 0 < \delta \leq e^{-1} \\ \frac{c_1^{(k)}}{c_2} \ln\left(\frac{1}{\delta}\right) \log_2(1 + \gamma) \delta & \text{if } 1 > \delta > e^{-1} \end{cases} \quad (7.27)$$

$$\bar{F}_{\text{SINR}}^*(\gamma) = \begin{cases} c_1^{(k)} e^{-1} & \text{if } 0 < \delta \leq e^{-1} \\ c_1^{(k)} \delta & \text{if } 1 > \delta > e^{-1} \end{cases} \quad (7.28)$$

where, again, $k = \{\text{SLP}, \text{MLP}\}$.

Proof. The average EE is a concave function in the open interval $\rho_{VT} \in (0, \infty)$. Hence, it has a single critical point, which is placed at $\rho_{VT} = c_2$, that leads to the global maximum. Nevertheless, the constrain over the capture probability imposes that the solution must lie between the following interval $\rho_{VT} \in [c_2 \ln^{-1}(1/\delta), \infty)$. It should be noticed that the average EE is an increasing function for $\rho_{VT} < c_2$ and a decreasing function for $\rho_{VT} > c_2$.

⁴Throughout this section as well as in Table 7.3, it is neglected the dependence with $x = VT_0 + r_{bc}$ in $\mathbb{E}[\text{BR}(VT_0 + r_{bc})]$, $\mathbb{E}[\text{EE}(VT_0 + r_{bc})]$ and $\bar{F}_{\text{SINR}}(VT_0 + r_{bc})$ for the sake of simplicity.

Table 7.4: Simulation Parameters

Parameter	Value	Parameter	Value
(τ, α)	(490, 1.68)	λ_L (vehicles/m)	$0.8 \cdot 84^{-1}$
d_{safe} (m)	42	n_L	2
d_A (m)	42	n_{AR}	10
p_a (non-periodic)	0.25	$(m_{\text{bc}}, t_{\text{rep}})$ (bits,ms)	2400, 100
ρ_{VT} (dBm/Hz)	-40	γ (dB)	5
σ_n^2 (dBm/Hz)	-165	d_{max} (km)	56
b_w (MHz)	9	r_{bc} (m)	150

Hence, if $\delta < e^{-1}$, the critical point fulfills the constrain over the capture probability, which leads to the solution $\rho_{\text{VT}}^* = c_2$. On the other hand, if $\delta > e^{-1}$, the constrain governs the optimal transmit power which is now $\rho_{\text{VT}}^* = c_2 \ln^{-1}(1/\delta)$. \square

Remark 20 (Independence of the optimal transmit power). *In view of **Theorem 9** it can be stated that the optimal transmit power is independent of the considered scheme, i.e., SLP or MLP. This is due to the fact that the optimal transmit power only depends on c_2 and δ .*

7.6 Numerical Results

In this section, analytical results are illustrated and validated with extensive Monte Carlo simulations in order to assess GLOC performance. The simulation setup is chosen from the guidelines given in [56, 58, 97]. In particular, it is considered a velocity-dependent safe distance between vehicles, according to 3GPP simulation assumptions for LTE V2X [56]: $d_{\text{safe}}(\text{m}) = 2.5 \cdot v(\text{m/s})$. Assuming a vehicle velocity of 60 km/h, this leads to a safe distance of 42 m. Such a minimum distance yields to a maximum vehicle density per lane of $\lambda_{L,\text{max}} = 1/(2d_{\text{safe}}) = 84^{-1}$ [61]. A high density of vehicles is considered, and hence the density per lane is set to 80% of the maximum density. The system bandwidth is 10 MHz, as given in [56]; however, excluding guard-bands in LTE this leads to 9 MHz of useful bandwidth. With non-periodic messages, it is considered a probability of being active, i.e.,

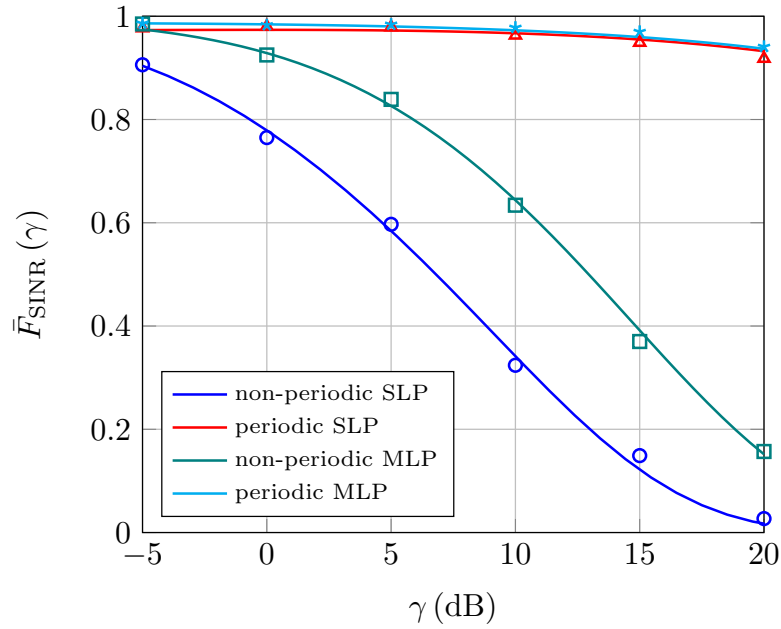


Figure 7.4: Capture probability versus the SINR threshold, γ , for SLP ($d_{\text{safe}} = 0$ m) and for MLP ($d_{\text{safe}} = 42$) with periodic and non-periodic broadcast messages. Analytical results are represented with solid lines whereas simulation results are represented with marks.

with data to transmit, of 0.25. On the other hand, with periodic messages it is considered a message size of 2400 bits and reporting time of 100 ms as given in [56]. The path loss is taken from [58], where a vast measurement campaign over 5.2 GHz is performed. It is considered that VTs transmit with -40 dBm/Hz, a thermal noise power of -174 dBm/Hz and a noise figure of 9 dB as pointed out in [56], which leads to $\sigma_n^2 = -165$ dBm/Hz.

Simulation parameters are summarized in Table 7.4. Simulations are carried out averaging over 10^4 spatial realizations. Through this section, analytical results are drawn with solid lines whereas markers are used for simulation results. As stated in **Remark 13**, results related with SLP are exact whereas results related to MLP are approximations. Nevertheless a good match between simulation and analysis is observed in both cases.

7.6.1 Impact of the SINR threshold and the traffic activity

In this sub-section, it is evaluated the effect of the density of concurrent transmitters and also, the impact of rate, or equivalently, the SINR threshold, γ , that leads to the correct

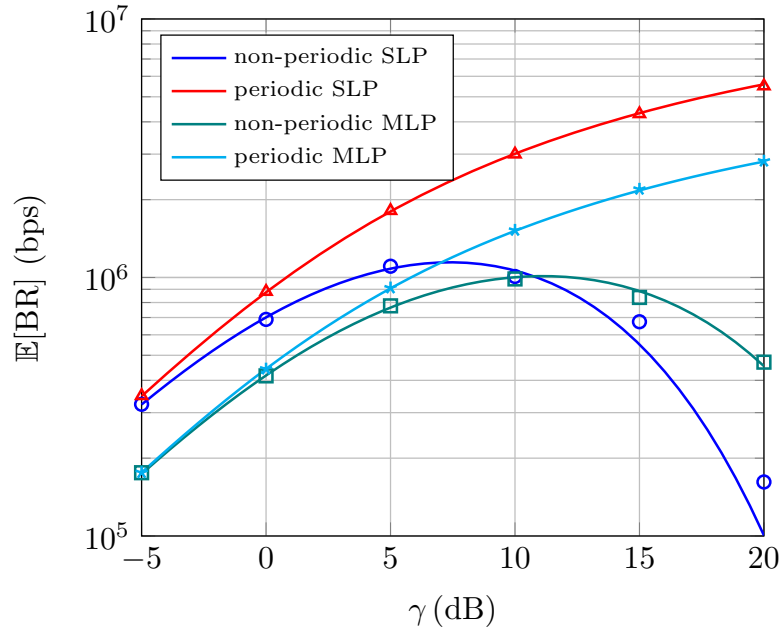


Figure 7.5: Average BR versus the SINR threshold, γ , for SLP ($d_{\text{safe}} = 0$ m) and for MLP ($d_{\text{safe}} = 42$ m) with periodic and non-periodic broadcast messages.

reception of a message transmitted with $\log_2(1+\gamma)$ bps/Hz. Fig. 7.4 illustrates the capture probability for SLP and MLP with both periodic and non-periodic messages versus γ . In the case of non-periodic messages, MLP scheme achieves a higher capture probability than SLP. This is due to the fact that with MLP there is no intra-segment interference, as well as to the fact that the density of interfering vehicles is smaller. If we focus on the case of periodic messages, it is observed a higher capture probability than in the case of non-periodic messages. This is because in this latter case, the probability of being active, which depends on (7.7), is greatly smaller than in the case of non-periodic messages. According to **Remark 14**, the density of active vehicles in case of periodic reporting is the same in SLP and MLP schemes. However, SLP, contrary to MLP, has intra-segment interference, which explains why SLP has a slightly smaller capture probability, as it can be observed from Fig. 7.4.

The average BR of correctly received messages versus the SINR threshold is shown in Fig. 7.5. Three trends can be observed from the figure. Firstly, it can be noticed that the average BR of periodic messages is higher than non-periodic messages. This is related to the smaller capture probability that exhibits non-periodic messages as it has

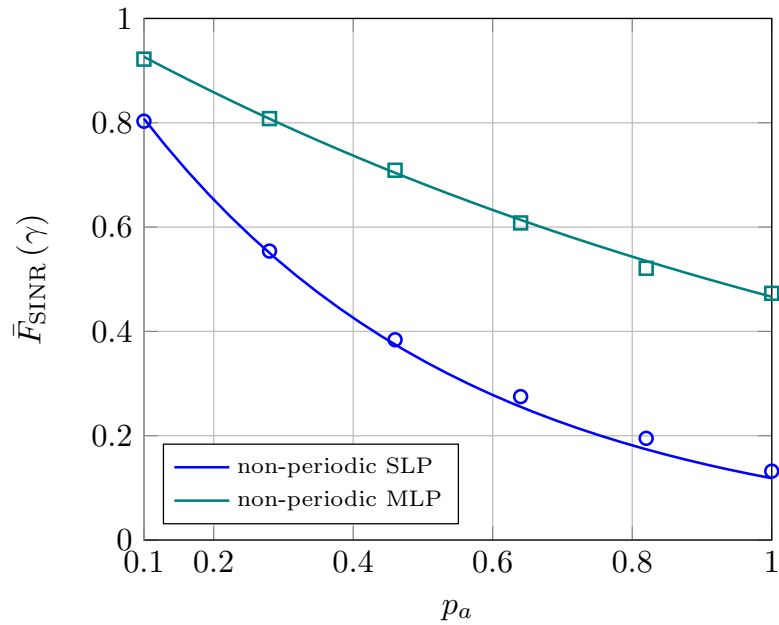


Figure 7.6: Capture probability versus the probability of being active related to non-periodic broadcast messages with SLP and MLP schemes.

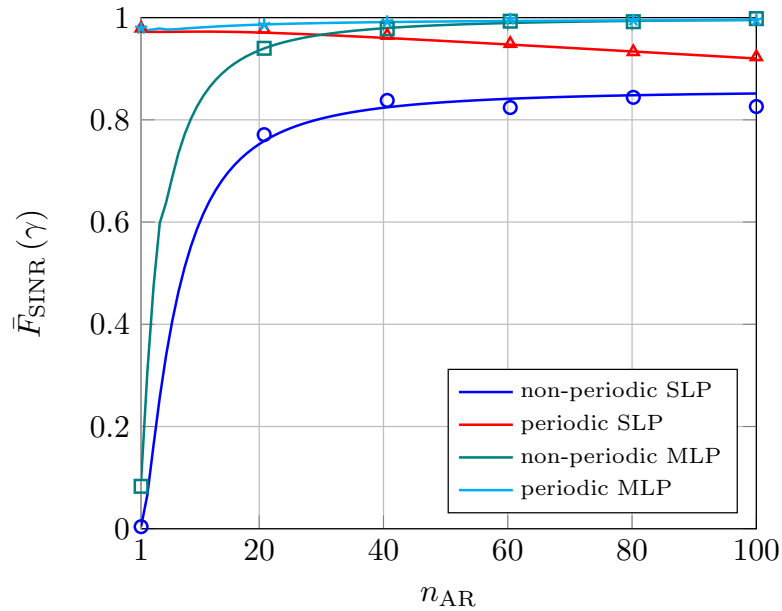


Figure 7.7: Capture probability versus the number of ARs, n_{AR} , for SLP ($d_{\text{safe}} = 0$ m) and for MLP ($d_{\text{safe}} = 42$ m) with periodic and non-periodic broadcast messages.

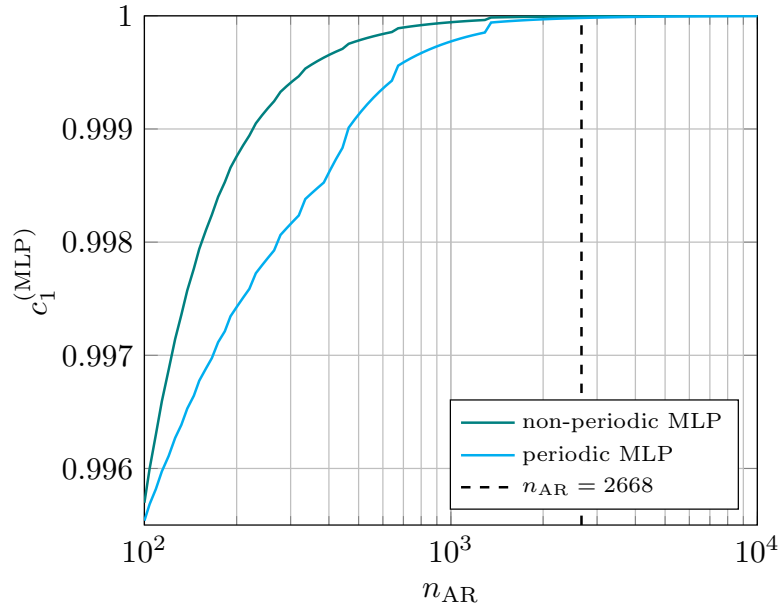


Figure 7.8: Maximal capture probability, $c_1^{(\text{MLP})}$, for n_{AR} ranging from 10^2 to 10^4 , under MLP ($d_{\text{safe}} = 42$ m) with periodic and non-periodic broadcast messages with $r_{\text{bc}} = 150$ m, $d_{\text{max}} = 56$ km and $\gamma = 5$ dB.

been discussed above. Secondly, it can be observed that SLP leads to a higher average BR, which is due to the fact that with this scheme the bandwidth per AR is higher. Finally, it is observed that there exist a value of γ that maximizes the average BR.

Fig. 7.6 illustrates that the capture probability is a decreasing function with respect to p_a as expected, which is related to the higher interference as the density of transmitting vehicles increases.

7.6.2 Impact of the number of Access Resources

Throughout this sub-section, the impact of the number of ARs is studied. In particular, Fig. 7.7 illustrates the capture probability when n_{AR} is ranging from 1 to 100. It is observed that in the case of non-periodic messages, with a high active probability ($p_a = 0.25$), increasing n_{AR} greatly increases the capture probability for both SLP and MLP. This scenario highlights the great potential of GLOC for non-periodic messages where reliability plays a crucial role. Such a trend is also observed with periodic messages under MLP; however, with SLP the capture probability of periodic messages is a decreasing

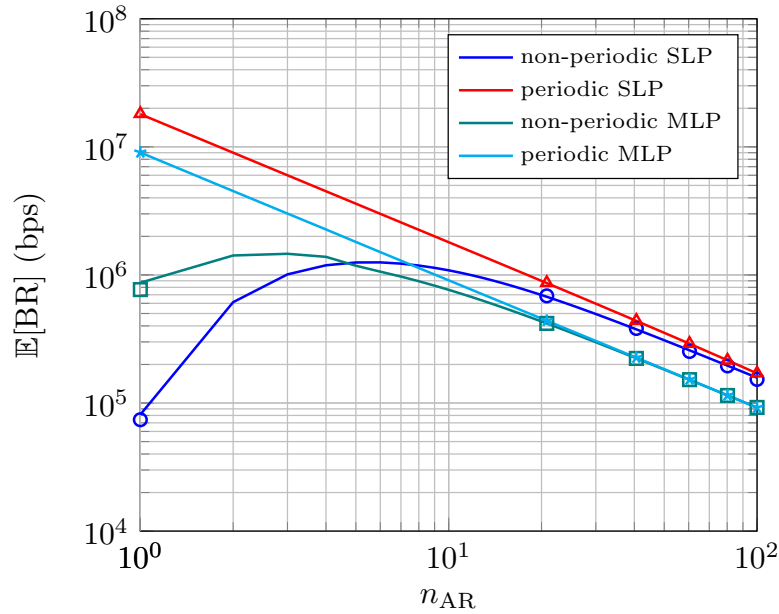


Figure 7.9: Average BR versus the number of ARs, n_{AR} , for SLP ($d_{safe} = 0$ m) and for MLP ($d_{safe} = 42$ m) with periodic and non-periodic broadcast messages.

function with n_{AR} . To understand this, let us remark that increasing n_{AR} tend to reduce the interference, since it rises the co-channel distance. On the other hand, increasing n_{AR} , leads to an increment of the probability of being active, p_a , which also increases the intra-segment interference. The growth of the probability of being active is due to the fact that the time to transmit a periodic message rises with n_{AR} . Hence, in case of SLP, intra-segment interference dominates over the capture probability, which diminishes with n_{AR} . In case of MLP the capture probability grows with respect to n_{AR} , since there is no intra-segment interference, and also because rising n_{AR} increases the distance to interfering vehicles. In particular, with MLP it is obtained reliabilities of 99.55% and 99.76% with non-periodic and periodic messages respectively, at a distance of 150 m with $n_{AR} = 100$.

V2X communications have to be highly reliable. The exact reliability target changes from standard to standard and depending on the application, e.g., 95% (ITS), 99% (LTE V2X) and 99.999% (5G V2X) [56, 97, 118].

Hence, providing a very high capture probability is a paramount issue. One of the great benefits of MLP is that, according to **Remark 18**, it is possible to move the system from an interference-limited into a noise-limited regime by increasing n_{AR} ; once the system is

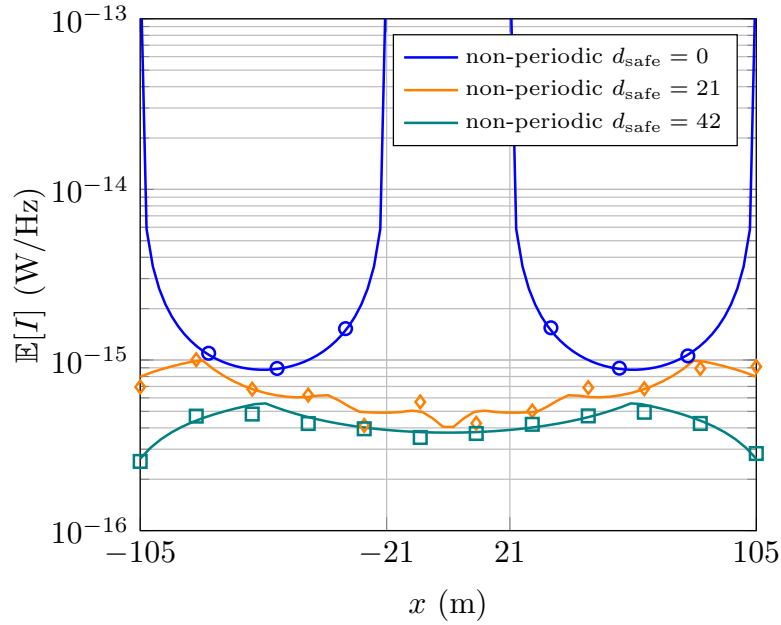


Figure 7.10: Average interference for different locations, $x \in [-105, +105]$ m, for SLP and MLP with $d_{\text{safe}} = \{21, 42\}$ with non-periodic messages, $\lambda = 0.8/84$ vehicles/m and $n_{\text{AR}} = 3$.

noise-limited, the capture probability can be increased by increasing the transmit power as stated in **Remark 17**. This is illustrated in Fig. 7.8 where it is shown the maximum capture probability, $c_1^{(\text{MLP})}$, which it is achieved for $\rho_{\text{VT}} \rightarrow \infty$. As stated in **Remark 18**, for our simulation assumptions the system is noise-limited for $n_{\text{AR}} > 2668$.

Finally, Fig. 7.9 illustrates the average BR versus n_{AR} . It is shown that, when $10 < n_{\text{AR}} < 100$, SLP achieves a higher average BR than MLP since ARs have more bandwidth in the former case. Regarding non-periodic messages, it is shown that there exist an optimal value of n_{AR} , which maximizes the average BR. Finally, it is shown that the average BR is a decreasing function with n_{AR} , and it tends to 0 as $n_{\text{AR}} \rightarrow \infty$, as stated in **Remark 19**.

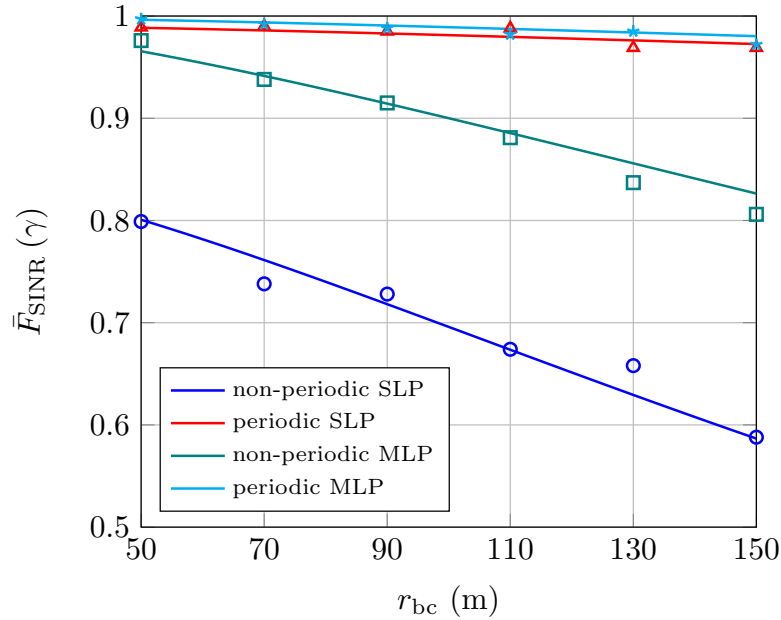


Figure 7.11: Capture probability versus the broadcast distance, r_{bc} , for SLP ($d_{safe} = 0$ m) and for MLP ($d_{safe} = 42$ m) with periodic and non-periodic broadcast messages.

7.6.3 Impact of the broadcast distance and the segment size: r_{bc} and d_A

The average interference is evaluated in Fig. 7.10 for locations, $x \in \mathbb{R}$, ranging from -105 to $+105$ m, where the probe segment is centered at $x = 0$. As it is stated in **Remark 16**, it can be observed that without a minimum distance between points, the interference does not converge within co-channel segments, which are centered at multiples of n_{AR} . It is used the same density λ with both SLP and MLP to assess the effect of the minimum distance between vehicles in the interference. As it is expected, the average interference is reduced as the minimum distance between points, d_{safe} , is increased.

Fig. 7.11 shows the capture probability versus the broadcast distance, where it is observed the reduction in capture probability as r_{bc} increases. However, it can be observed that the dependence with r_{bc} is higher in case of non-periodic than in case of periodic messages.

The capture probability versus the segment size is represented in Fig. 7.12. To understand this result, two aspects should be taken into account. On the one hand, increasing

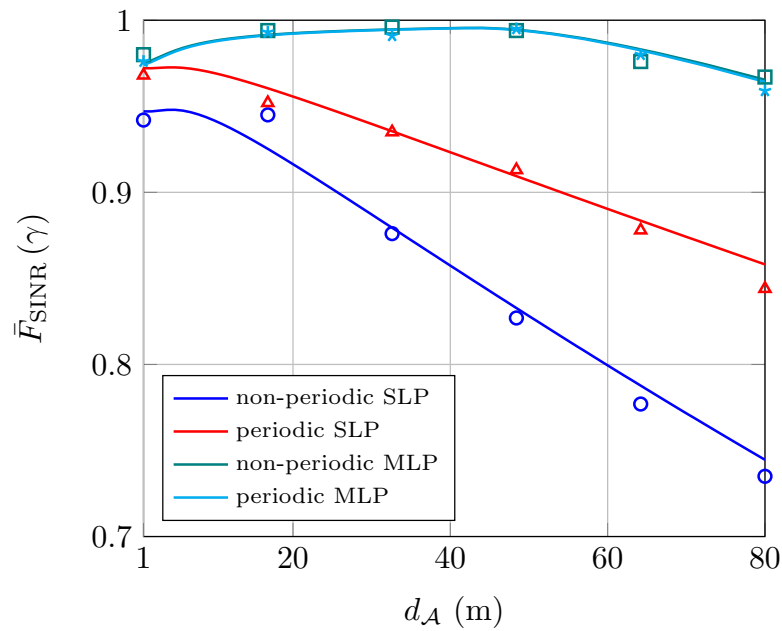


Figure 7.12: Capture probability versus the segment size, d_A , for SLP ($d_{\text{safe}} = 0$ m) and for MLP ($d_{\text{safe}} = 42$ m) with periodic and non-periodic broadcast messages.

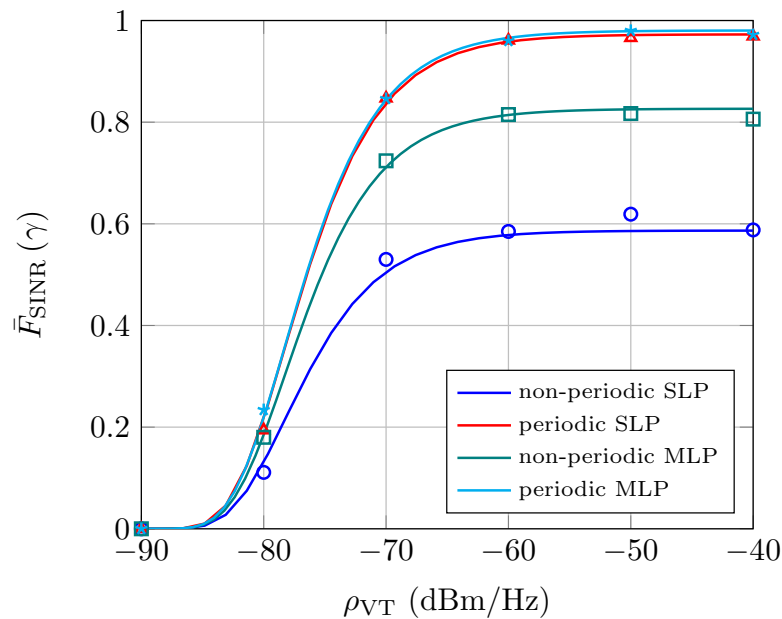


Figure 7.13: Capture probability versus the transmit power per Hz, ρ_{VT} , for SLP ($d_{\text{safe}} = 0$ m) and for MLP ($d_{\text{safe}} = 42$ m) with periodic and non-periodic broadcast messages.

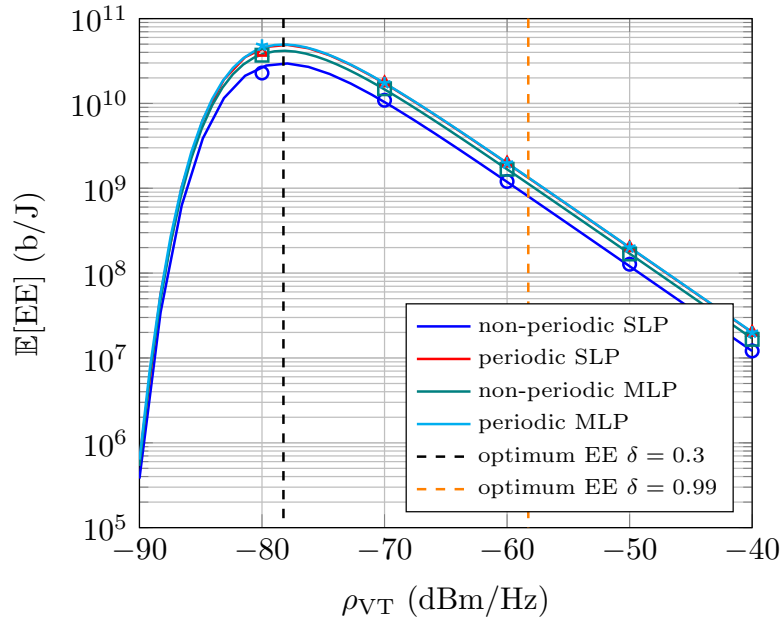


Figure 7.14: Average EE versus the transmit power per Hz, ρ_{VT} , for SLP ($d_{\text{safe}} = 0$ m) and for MLP ($d_{\text{safe}} = 42$ m) with periodic and non-periodic broadcast messages.

d_A rises the distance to co-channel segments, since this distance depends on $n_{AR}d_A$. However, if d_A grows the segment-size also rises, which may lead to intra-segment interference. With SLP, it is shown that the capture probability decreases as d_A increases roughly below 10 m. This is because, since there exist intra-segment interference, the interference rises as d_A increases. With MLP, the capture probability grows as n_{AR} rises for $n_{AR} < 42$ m. This is due to the fact that increasing d_A rises the distance to co-channel segments. Then, for $n_{AR} > 42$ m, if n_{AR} grows the capture probability decreases since there is now intra-segment interference, which is due to the fact that $d_A > d_{\text{safe}}$.

7.6.4 Transmit Power and Optimum Energy Efficiency

In this sub-section it is shown the effect of the transmit power. Then, its optimal value in terms of EE is studied. **Remark 17** is illustrated in Fig. 7.13. It is shown that the capture probability is an increasing function with ρ_{VT} , and its maximum value, $c_1^{(k)}$, is roughly achieved when ρ_{VT} is high enough.

The average EE versus ρ_{VT} is shown in Fig. 7.14, where it is observed that the global

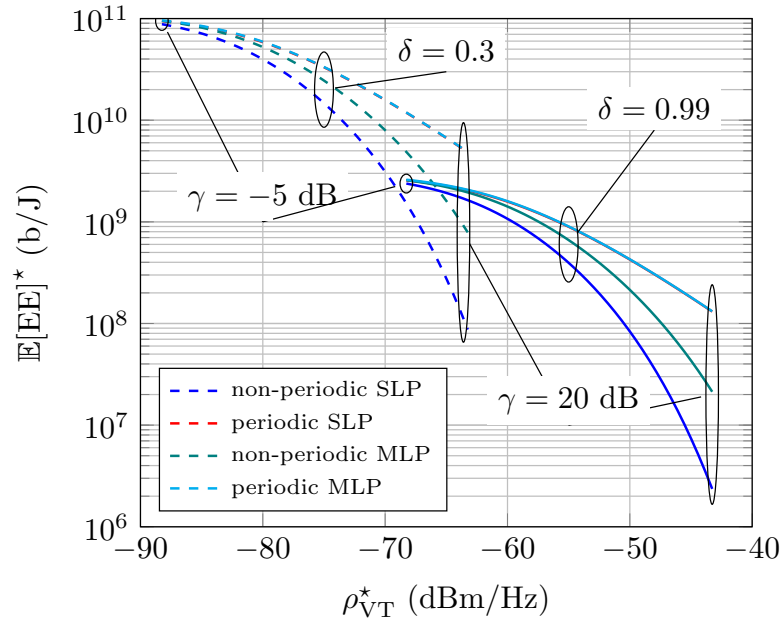


Figure 7.15: Optimum EE versus the optimum transmit power per Hz, ρ_{VT}^* , for SLP ($d_{\text{safe}} = 0$ m) and for MLP ($d_{\text{safe}} = 42$ m) with periodic and non-periodic broadcast messages. Each pair of values $(\mathbb{E}[\text{EE}]^*, \rho_{VT}^*)$ is obtained for a different SINR threshold, γ , ranging from -5 dB to 20 dB.

(unconstrained optimum) of the EE is achieved with $\delta = 0.3$, as stated in **Theorem 9**. If a higher capture probability, i.e., higher δ , must be satisfied, the optimal transmit power leads to a smaller capture probability, as it is observed for $\delta = 0.99$ in the figure. Specifically, for MLP with $\delta = 0.99$, it is observed that the optimal EE, which is around $1.4 \cdot 10^9$ b/J, is achieved at $\rho_{VT} = -58.27$ dBm/Hz. In that case, the capture probability of periodic and non-periodic messages is 97.41% and 96.27% respectively, but the transmit power is around 20 dB smaller than in the baseline case ($\rho_{VT} = -40$ dBm/Hz).

Fig. 7.15 illustrates the optimum EE versus the optimal transmit power for different γ values ranging from -5 to 20 dBs. Hence, in this figure, every pair of the form $(\mathbb{E}[\text{EE}]^*, \rho_{VT}^*)$ is obtained for a different SINR threshold. As it is expected, a smaller γ yields to a higher optimal EE, and a smaller optimal transmit power. Additionally, increasing the capture probability reduces the optimal EE and increases the optimal transmit power. The capture probability associated with Fig. 7.15 is illustrated in Fig. 7.16.

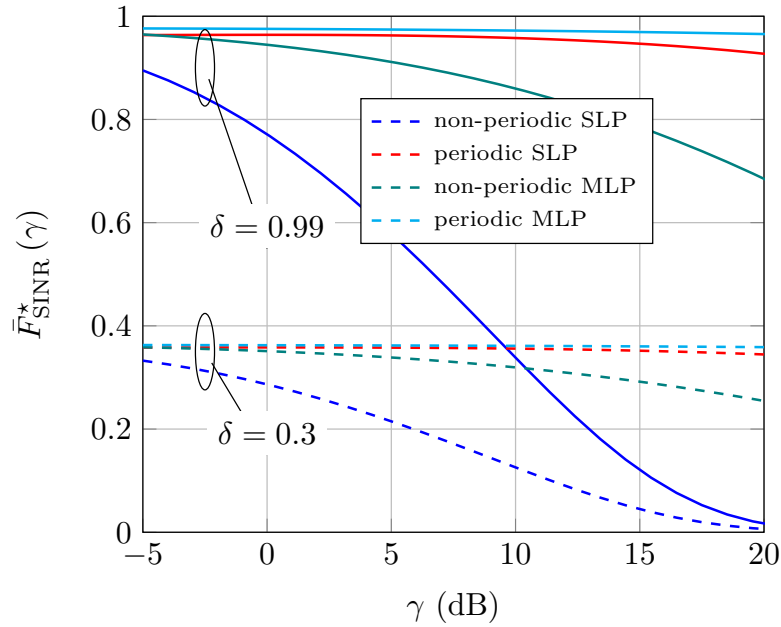


Figure 7.16: Capture probability versus the SINR threshold, γ , associated with the optimum transmit power, ρ_{VT}^* as appear in Fig 7.15.

7.7 Discussion

This chapter proposes an abstraction model that allows a tractable analysis and optimization of Geo-Location based access in vehicular networks. With such a technique, the road is divided in segments and a single orthogonal Access Resource (AR) is associated with a given segment. The mapping between segments and ARs is made aiming to maximize the co-channel distance. Vehicles determines its corresponding segment based on its geographical position, therefore reducing the interference when accessing the channel. Two frequency allocation schemes are considered: Single-Lane Partition (SLP) and Multi-Lane Partition (MLP). MLP distinguish between different lanes and hence it can avoid intra-segment interference, however it uses the bandwidth less efficiently than SLP since it requires orthogonal bandwidth allocations to each lane. A wide set of analytical results are obtained aiming at providing a deep understanding about the proposed schemes. From these analytical results, theoretical insights are derived. In particular, it has been shown that: (i) the capture probability is an increasing function with respect to the transmit power with exponential dependence; (ii) the system is noise-limited for MLP when the

number of ARs is high enough, whereas it is interference-limited in case of SLP; (iii) the average interference diverges when it is evaluated in co-channel segments with SLP, whereas it always converges for the case of MLP. Interestingly, (iii) means that with MLP it is possible to obtain a capture probability as high as necessary, by increasing the number of ARs and transmit power. This facilitates the implementation of safety applications that requires very high reliability. In particular, with MLP it has been obtained reliabilities of 99.55% and 99.76% with non-periodic and periodic messages respectively, at a distance of 150 m. Finally, the optimum transmit power that achieves maximal EE subject to a minimum capture probability is also obtained. Specifically, for MLP it is observed that the optimal EE is achieved with a transmit power of -58.27 dBm/Hz which is 20 dB smaller than baseline case while keeping a 99% of the maximum capture probability.

These aforementioned contributions appear in [62], which has been accepted for publication, and [63], which is a work under second round of reviews.

7.8 Appendix: Proof of Lemma 19

In case of SLP, the Laplace of the interference can be written as follows

$$\begin{aligned}
 \mathcal{L}_{I(x)}(s) &= \mathbb{E}_{I(x)} \left[e^{-sI(x)} \right] \\
 &\stackrel{(a)}{=} \mathbb{E}_{\Phi^{(a)}} \left[\prod_{\text{VT}_i \in \Phi^{(a)} \setminus \{\text{VT}_0\} \cap \mathfrak{b}(x, d_{\max})} \mathbb{E}_{H_{\text{VT}_i}} \exp \left(-s H_{\text{VT}_i} (\tau |\text{VT}_i - x|)^{-\alpha} \rho_{\text{VT}} \mathbf{1}(\text{VT}_i \in \mathcal{A}^{(\text{AR}_0)}) \right) \right] \\
 &\stackrel{(b)}{=} \exp \left(-\lambda \cdot p_a \int_{\mathbb{R}} \frac{s (\tau |y - x|)^{-\alpha} \rho_{\text{VT}}}{1 + s (\tau |y - x|)^{-\alpha} \rho_{\text{VT}}} \mathbf{1}(y \in \mathcal{A}^{(\text{AR}_0)}) \cdot \mathbf{1}(y \in \mathfrak{b}_x(d_{\max})) dy \right) \\
 &\stackrel{(c)}{=} \exp \left(-\lambda \cdot p_a \sum_{c=-\infty}^{\infty} \int_{y=c \cdot n_{\text{AR}} \cdot d_A - \frac{d_A}{2}}^{c \cdot n_{\text{AR}} \cdot d_A + \frac{d_A}{2}} \frac{s (\tau |y - x|)^{-\alpha} \rho_{\text{VT}}}{1 + s (\tau |y - x|)^{-\alpha} \rho_{\text{VT}}} \mathbf{1}(y \in \mathfrak{b}_x(d_{\max})) dy \right) \quad (7.29)
 \end{aligned}$$

where (a) comes after expressing exponential of the summation that defines the interference as a product over the PPP $\Phi^{(a)}$; (b) after applying the PGFL [61] of the PPP and performing expectation over the fading and (c) after expressing the region $\mathcal{A}^{(\text{AR}_0)}$ as a summation of co-channel segments. Then, we can proceed as appears below

$$\begin{aligned}
 \mathcal{L}_{I(x)}(s) &\stackrel{(a)}{=} \exp \left(-\lambda \cdot p_a \sum_{c=-\lfloor d_{\max}/(n_{\text{RB}}d_{\mathcal{A}}) \rfloor}^{\lceil d_{\max}/(n_{\text{RB}}d_{\mathcal{A}}) \rceil} \int_{t=\max(c \cdot n_{\text{RB}} \cdot d_{\mathcal{A}} - \frac{d_{\mathcal{A}}}{2} - x, -d_{\max})}^{\min(c \cdot n_{\text{RB}} \cdot d_{\mathcal{A}} + \frac{d_{\mathcal{A}}}{2} - x, d_{\max})} \frac{s(\tau|t|)^{-\alpha} \rho_{\text{VT}}}{1 + s(\tau|t|)^{-\alpha} \rho_{\text{VT}}} \cdot dt \right) \\
 &\stackrel{(b)}{=} \exp \left(-\lambda \cdot p_a \sum_{c=-\lfloor d_{\max}/(n_{\text{RB}}d_{\mathcal{A}}) \rfloor}^{\lceil d_{\max}/(n_{\text{RB}}d_{\mathcal{A}}) \rceil} \left[\mathbf{1} \left(\mu_L^{(1)} < \mu_U^{(1)} \right) \int_{t=\mu_L^{(1)}}^{\mu_U^{(1)}} \frac{sH_{\text{VT}_i}(\tau t)^{-\alpha} \rho_{\text{VT}}}{1 + sH_{\text{VT}_i}(\tau t)^{-\alpha} \rho_{\text{VT}}} \cdot dt \right. \right. \\
 &\quad \left. \left. + \mathbf{1} \left(\mu_L^{(2)} < \mu_U^{(2)} \right) \int_{t=\mu_L^{(2)}}^{\mu_U^{(2)}} \frac{sH_{\text{VT}_i}(-\tau t)^{-\alpha} \rho_{\text{VT}}}{1 + sH_{\text{VT}_i}(-\tau t)^{-\alpha} \rho_{\text{VT}}} \cdot dt \right] \right) \quad (7.30)
 \end{aligned}$$

where (a) comes after applying the maximum distance to the integration limits and performing the change of variables $t = y - x$ and (b) comes after expressing the absolute value function as $|t| = t \cdot \mathbf{1}(t \geq 0) - t \cdot \mathbf{1}(t < 0)$ and applying the indicator functions to the integration limits. Finally, performing both integrals and reordering completes the proof.

7.9 Appendix: Proof of Lemma 21

The Laplace transform of the interference can be written as

$$\begin{aligned}
 \mathcal{L}_{I(x)}(s) &\stackrel{(a)}{=} \mathbb{E} \left[\exp \left(-s \sum_{\text{VT}_i \in \Phi^{(a)} \setminus \{\text{VT}_0\}} H_{\text{VT}_i}(\tau|\text{VT}_i - x|)^{-\alpha} \rho_{\text{VT}} \right. \right. \\
 &\quad \left. \left. \times \mathbf{1}(\text{VT}_i \in \mathbf{b}_x(d_{\max})) \mathbf{1}(\text{VT}_i \in \mathcal{A}^{(\text{RB}_0)}) \mathbf{1}(|\text{VT}_i - x| > d_{\text{safe}}) \mathbf{1}(|\text{VT}_i - v| > d_{\text{safe}}) \right) \right] \\
 &\stackrel{(b)}{=} \exp \left(-\lambda \cdot p_a \sum_{c=-\lfloor d_{\max}/(n_{\text{RB}}d_{\mathcal{A}}) \rfloor}^{\lceil d_{\max}/(n_{\text{RB}}d_{\mathcal{A}}) \rceil} \int_{t=\max(c \cdot n_{\text{RB}} \cdot d_{\mathcal{A}} - \frac{d_{\mathcal{A}}}{2} - x, -d_{\max})}^{\min(c \cdot n_{\text{RB}} \cdot d_{\mathcal{A}} + \frac{d_{\mathcal{A}}}{2} - x, d_{\max})} \frac{s(\tau|t|)^{-\alpha} \rho_{\text{VT}}}{1 + s(\tau|t|)^{-\alpha} \rho_{\text{VT}}} \right. \\
 &\quad \left. \times \mathbf{1}(|t| > d_{\text{safe}}) \cdot \mathbf{1}(|t + x - v| > d_{\text{safe}}) \cdot dt \right) \quad (7.31)
 \end{aligned}$$

where (a) comes after applying **Assumption 4** and reordering the resulting expression and (b) after applying the PGFL of the PPP, performing expectation over the fading, expressing the region $\mathcal{A}^{(\text{AR}_0)}$ as a summation of co-channel segments and performing the change of variables $t = y - x$. Then, we proceed as follows

$$\begin{aligned}
 & \exp \left(-\lambda \cdot p_a \sum_{c=-\lceil d_{\max}/(n_{\text{RB}}d_{\mathcal{A}}) \rceil}^{\lceil d_{\max}/(n_{\text{RB}}d_{\mathcal{A}}) \rceil} \int_{t=\max(c \cdot n_{\text{RB}} \cdot d_{\mathcal{A}} - \frac{d_{\mathcal{A}}}{2} - x, -d_{\max})}^{\min(c \cdot n_{\text{RB}} \cdot d_{\mathcal{A}} + \frac{d_{\mathcal{A}}}{2} - x, d_{\max})} \frac{s(\tau t)^{-\alpha} \rho_{\text{VT}}}{1 + s(\tau t)^{-\alpha} \rho_{\text{VT}}} \right. \\
 & \quad \times \mathbf{1}(t > d_{\text{safe}}) \cdot \mathbf{1}(|t + x - v| > d_{\text{safe}}) \cdot dt \\
 & \quad \left. + \int_{t=\max(c \cdot n_{\text{RB}} \cdot d_{\mathcal{A}} - \frac{d_{\mathcal{A}}}{2} - x, -d_{\max})}^{\min(c \cdot n_{\text{RB}} \cdot d_{\mathcal{A}} + \frac{d_{\mathcal{A}}}{2} - x, d_{\max})} \frac{s(-\tau t)^{-\alpha} \rho_{\text{VT}}}{1 + s(-\tau t)^{-\alpha} \rho_{\text{VT}}} \times \mathbf{1}(t < -d_{\text{safe}}) \cdot \mathbf{1}(|t + x - v| > d_{\text{safe}}) \cdot dt \right)
 \end{aligned} \tag{7.32}$$

where it has expressed the absolute value function as $|t| = t \cdot \mathbf{1}(t \geq 0) - t \cdot \mathbf{1}(t < 0)$ and it has applied the resulting indicator functions to the integration limits. It should be noticed that the following equations holds

$$\begin{aligned}
 \mathbf{1}(|t + x - v| > d_{\text{safe}}) &= \mathbf{1}(t > d_{\text{safe}} - x + v) + \mathbf{1}(t < v - x - d_{\text{safe}}) \\
 \mathbf{1}(|t + x - v| > d_{\text{safe}}) &= \mathbf{1}(t > d_{\text{safe}} - x + v) + \mathbf{1}(t < v - x - d_{\text{safe}})
 \end{aligned} \tag{7.33}$$

Finally, substituting the above expressions into (7.32), performing the resulting integrals and reordering completes the proof.

Chapter 8

Conclusions

This dissertation have addressed the modelling, analysis and optimization of interference mitigation techniques for HCNs and vehicular communications, which are expected to be two key elements in next generation cellular networks.

This chapter aims at summarizing the main contributions and future work after this thesis. In particular, section 8.1 lists the main conclusions of each chapter. Finally, section 8.2 depicts the future lines that can be followed.

8.1 Synthesis of the Dissertation

The interference is the main limiting factor in wireless systems. Hence in this thesis it has been proposed and analyzed two mechanisms for interference mitigation. In particular it is analyzed an Interference-Aware Fractional Power Control (IAFPC) for the UL of HCNs that keeps the generated interference under a given threshold, i_0 . To account for novel concepts in HCNs like UL/DL decoupling a generalized cell association has been considered, which includes the coupled and decoupled settings as special cases. The proposed mathematical framework avoids the mathematical intractability of the problem by means of conditional thinning, which adds the necessary correlation that exist between the probe Mobile Terminal (MT), the probe Base Station (BS) and the most interfered BS. Besides this, two accurate approximations for the Laplace transform of the interference have been proposed: i) Sigmoidal approximation and ii) Moment Matching (MM). The former relies on approximating the Laplace transform by a Sigmoidal function whose



parameters are obtained by means of logistic regression. The latter considers a given distribution to model the interference and then it performs MM to obtain the distribution's parameters. Finally, to simplify further the expressions and obtain interesting insights, it has been carried out asymptotic analysis. The analysis reveals that IAFPC outperforms the classical Interference-Unaware Fractional Power control (IUFPC) in terms of Spectral Efficiency (SE), average transmitted power, and mean and variance of the interference.

Then, we investigate the performance of a scheduling algorithm where the Mobile Terminals (MTs) may be turned off if they cause a level of interference greater than a given threshold. This approach, which is referred to as Interference Aware Muting (IAM), may be regarded as an interference-aware scheme that, contrary to IAFPC, is aimed to reduce the level of interference at the Medium Access Control (MAC) layer, instead than in the physical layer. IAM is studied in terms of average transmit power, mean and variance of the interference, coverage probability, Spectral Efficiency (SE), and Binary Rate (BR), which accounts for the amount of resources allocated to the typical MT. In order to account for the BR it is used the probability mass function (PMF) of the number of active, i.e., non-muted MTs per cell, and it is considered a scheduling algorithm that divides the available bandwidth between the active MTs. Additionally it is proposed a novel framework to obtain the BR and SE by using Adaptive Modulation and Coding (AMC), which provides results closer to real implementations. Our system-level analysis unveils that IAM increases the BR and reduces the average transmit power and the mean and variance of the interference even further than IAFPC. Besides, it is proved that an operating regime exists, where the performance of IAM is independent of the cell association criterion, which simplifies the joint design of UL and DL transmissions. The cost to pay is that MTs are muted at some time instants, and hence the fairness among the different MTs to access the resources is reduced.

Afterwards, a multi-user UL model to assess the coverage probability of different MTs in each cell is proposed. This framework allows us to assess the fairness as the difference between the coverage probability of the best and worst MTs. It is proven that with a full channel inversion power control, the fairness of the system is maximal, since all the MTs exhibit the same coverage probability. Then, the coverage probability of cellular systems under Nakagami-q (Hoyt) distribution is obtained in closed-form. This fading distribution allows us to consider more severe fading conditions than those obtained with Rayleigh

fading.

A novel Non orthogonal Multiple Access (NOMA) based access scheme for Cloud Radio Access Networks (CRANs) is proposed. It is shown that the proposed scheme greatly improves the performance of cell-edge MTs thanks to the use of beamforming while the spectral efficiency is high thanks to the use of NOMA.

Finally, the performance of a MAC algorithm for vehicular communications is investigated. With this strategy the vehicles access the resources for direct Vehicle to Vehicle (V2V) communication based on its geographical information. Here, the road is divided in segments and orthogonal Access Resources (ARs) are allocated to consecutive segments. The mapping is made aiming to maximize the co-channel distance. The analysis demonstrates that there exists an operation regime, for a given number of ARs, where the performance is noise-limited. This means that the capture probability, i.e., the probability of successful message reception, can be arbitrary increased by increasing the transmit power. Then, the optimal transmit power that maximizes the Energy Efficiency (EE) of the system subject to a minimum capture probability constraint is derived.

8.2 Future Work

In this section some future directions are pointed out:

- One of the key ingredients in 5G cellular networks is the shift to higher frequency bands, i.e., millimeter wave (mmW), which poses additional challenges, since the blockages need to be appropriately modelled. A major area of future research is to extend the concepts introduced in this thesis like IA for interference mitigation with mmW based networks.
- Building on the proposed multi-user model from Chapter 4 and IA scheduling algorithm from Chapter 3, it would be possible to derive a mathematical framework for the case of both, channel-aware and IA scheduling algorithms to boost the performance. Additionally, it would be interesting to solve the issues related to the fairness that exist with IAM.
- The mathematical framework to study the proposed NOMA based scheme for CRANs might be extended to account for more metrics, like, the binary rate. It would be

also appealing to compare the performance of the proposed framework with an Orthogonal Multiple Access (OMA) alternative to better understand its benefits and weakness.

- Besides the V2V communications, the 5G cellular networks are expected to provide connectivity in other vehicular environments like, drone communications and railway communications. Since each application has its own features and challenges, one future line is to develop stochastic geometry frameworks, based on the work presented in Chapter 7 for these scenarios.

Appendix A

Resumen en castellano

Este capítulo sirve de resumen a la tesis doctoral que se presenta. En primer lugar se hace una breve introducción al tema tratado en la tesis. Después se presentan los principales resultados obtenidos en la tesis, agrupados como distintos trabajos en los que se estudian técnicas concretas para mitigar la interferencia en redes heterogéneas y vehiculares. Dichos estudios tienen en común la existencia de ciertas correlaciones espaciales en los procesos punto subyacentes que complican el análisis matemático. Por último, este capítulo finaliza la tesis esbozando las conclusiones obtenidas.

A.1 Motivación

Con la llegada de los teléfonos y tabletas inteligentes, que exigen mayores tasas de datos cada año, la red celular ha sufrido una profunda revisión. La respuesta de los organismos de normalización como el 3GPP (3rd Generation Partnership Project) a esta demanda ha conducido a la cuarta generación (4G), que introduce conceptos como redes heterogéneas (HCNs, Heterogeneous Cellular Networks), desacoplamiento de los enlaces ascendente y descendente (UL/DL) y técnicas cooperativas conscientes de la interferencia (IA, Interference-Aware) para la mitigación de interferencias.

Por otro lado, la evolución de 4G, bajo estándares comerciales como LTE-A (Long Term Evolution-Advanced) y LTE-A Pro, facilita el camino hacia 5G, que traerá nuevos servicios y aplicaciones y mejorará el rendimiento general del sistema. Entre los nuevos servicios que ofrecerá la evolución de 4G (LTE-A Pro) y 5G, encontramos la comunicación

directa entre vehículos, que será asistida por la red celular. Este tipo de comunicación tiene como objetivo aumentar la seguridad en la carretera y, por lo tanto, impone severas restricciones de fiabilidad sobre los mensajes que se intercambian.

Todas estas técnicas y conceptos que se proponen para las futuras redes celulares requieren un modelo matemático preciso y manejable para el análisis de prestaciones. Este análisis nos permite sacar conclusiones teóricas sobre los principales indicadores de las prestaciones del sistema que conducen a una comprensión profunda de las técnicas consideradas. Además, nos permite realizar su optimización, determinando el conjunto óptimo de parámetros que maximizan una determinada métrica.

Debido a la naturaleza aleatoria e irregular que exhiben las HCNs, así como las redes vehiculares, la geometría estocástica ha aparecido recientemente como una herramienta matemática muy prometedora para el modelado y análisis a nivel de sistema. Sin embargo, algunas características de las HCNs y las redes vehiculares, como el control de potencia, la planificación dinámica de recursos o la planificación de frecuencias, imponen correlaciones espaciales sobre el proceso puntual subyacente que complica significativamente el análisis matemático.

Por lo tanto, el objetivo principal de esta tesis es obtener expresiones analíticas cerradas para los indicadores clave de las prestaciones del sistema en redes HCNs, así como en redes vehiculares. El foco está aquí en proporcionar una expresión simple a problemas complejos, donde algunas correlaciones espaciales complican la tratabilidad del problema. Con las expresiones derivadas, se han obtenido ideas interesantes sobre el rendimiento del sistema.

La interferencia es el principal factor limitante en los sistemas inalámbricos. Por lo tanto, en esta tesis se han propuesto y analizado dos mecanismos para mitigar las interferencias en el enlace ascendente de redes heterogéneas y un mecanismo de acceso al medio de forma distributida en redes vehiculares.

En concreto, se analiza un control de potencia fraccionado consciente de la interferencia (IAFPC, Interference-Aware Fractional Power Control) para la UL de HCNs que mantiene la interferencia generada bajo un umbral dado, i_0 . A continuación, investigamos el rendimiento de un algoritmo de planificación en el que los MTs pueden ser silenciados si causan un nivel de interferencia superior a un determinado umbral. Este enfoque, que se ha denominado IAM (Interference-Aware Muting), puede considerarse como un esquema de mitigación de interferencias que, contrariamente a IAFPC, tiene como objetivo reducir

el nivel de interferencia en la capa de Control de Acceso al Medio (MAC), en lugar de hacerlo en la capa física. Gracias al desvanecimiento a largo plazo, también conocido como *shadowing*, y a la movilidad que caracteriza a los MTs, los usuarios silenciados sólo permanecen inactivos durante un periodo de tiempo. No obstante, el hecho de silenciar algunos MTs reduce la justicia en cuanto al acceso a los recursos en el sistema.

Así pues, para completar la discusión sobre la justicia en redes celulares se propone un marco matemático para el análisis de sistemas multi-usuario. El resultado principal es la probabilidad de cobertura de los distintos MTs que pertenecen a la misma celda en el caso del UL con control de potencia fraccionado. De este modo, se puede dar una definición de justicia, teniendo en cuenta la diferencia de probabilidad de cobertura entre el mejor y peor MT en lugar de hacerlo como la probabilidad de acceder a los recursos.

Finalmente, se investiga el rendimiento de un algoritmo MAC para comunicaciones vehiculares. Con esta estrategia los vehículos acceden a los recursos para la comunicación directa Vehículo a Vehículo (V2V, Vehicle-to-Vehicle) basada en su información geográfica y así se disminuye la interferencia en el sistema.

El resto del capítulo queda estructurado como sigue. La sección A.2 hace un resumen del estudio del mecanismo propuesto de control de potencia IAFPC. El análisis del mecanismo de planificación de recursos IAM se resume en la sección A.3. El modelo para obtener la probabilidad de cobertura multi-usuario se discute en la sección A.4. La sección A.7 se dedica al mecanismo de acceso al medio distribuida en redes vehiculares. Por último, las conclusiones obtenidas con esta tesis doctoral se detallan en la sección A.8.

A.2 Control de Potencia Fraccionado Consciente de la Interferencia

En este trabajo, se presenta un nuevo marco para el modelado y análisis del enlace ascendente de redes heterogéneas con control de potencia consciente de la interferencia, IAFPC. El modelo matemático propuesto para el análisis es un modelo general que considera como casos particulares los métodos de control de potencia estudiados hasta la fecha [26, 29, 31]. El marco propuesto para el análisis se basa una técnica conocida como *conditional thinning*, con el fin de modelar adecuadamente las posiciones de los MTs interferentes y de tener en cuenta la correlación espacial con la ubicación de la BS que da servicio al MT de prueba.

El caso que nos ocupa es más complicado que el caso considerado hasta la fecha, que analiza el control de potencia fraccionado clásico (FPC, Fractional Power Control), ya que en nuestro caso hay que considerar también la correlación espacial que hay entre los MTs y la BS más interferida por la transmisión de cada MT. Además, es necesario tratar con funciones no lineales que dependen de las distancias hacia la BS de servicio y hacia la BS más interferida. Todas estas cuestiones hacen que el cálculo de la distribución de la SINR no sea una tarea sencilla. Para superar la complejidad matemática del problema que nos ocupa, proponemos dos aproximaciones para la transformada de Laplace de la interferencia agregada: i) aproximación usando una función sigmoide y ii) ajuste de momentos (MM, Moment Matching). Además, se realiza un análisis asintótico para simplificar aún más las expresiones y obtener conclusiones teóricas acerca del rendimiento del sistema. Con el análisis asintótico se evita la necesidad de aproximar la interferencia para reducir la complejidad de las expresiones obtenidas.

A.2.1 Modelo de Sistema

Consideramos una red heterogénea o HCN compuesta por dos niveles, es decir, macro BSs (MBSs) y BS pequeñas (SBS, Small-cell BSs). Las BSs del nivel $j \in \mathcal{K} = \{1, 2\}$ se distribuyen espacialmente en \mathbb{R}^2 de acuerdo con un PPP uniforme, $\Phi^{(j)} = \{BS_0^{(j)}, BS_1^{(j)}, \dots\}$, de densidad $\lambda^{(j)}$ donde $BS_i^{(j)}$ es la ubicación de la i -ésima BS del nivel j -ésimo. Los MTs se distribuyen espacialmente de acuerdo con otro PPP independiente y uniforme, $\Phi_{MT} = \{MT_0, MT_1, \dots\}$, de densidad λ_{MT} . La señal transmitida sufre desvanecimiento multi-camino y desvanecimiento a largo plazo (*shadowing*). Las pérdidas de propagación entre dos puntos separados por una distancia r se modelan como $(\tau \cdot r)^\alpha$, donde α y τ son el exponente y la pendiente de las pérdidas de propagación. El criterio de asociación entre MTs y BSs se basa en un criterio de máxima potencia pesada media recibida tal y como se describe en [26]. Los pesos de las asociaciones se representan con el símbolo $t^{(j)}$ para cada nivel $j \in \mathcal{K}$. Para introducir las correlaciones necesarias entre las posiciones de cada MT y la BS que le da servicio definimos el evento $\mathcal{X}_{MT_i}^{(j)}$ como: MT_i se asocia con nivel j . La definición matemática de este evento aparece en el capítulo 2.

El control de potencia dado por IAFPC [49], implica que cada MT causa menos interferencia que un umbral, i_0 , a la BS a la que más interfiera. Además, el MT tiene una restricción a la potencia que nunca podrá exceder p_{\max} . Se supone que el control de poten-

cia puede adaptarse a las variaciones lentas del enlace, por lo tanto sólo puede compensar la pérdida de propagación y el *shadowing*. La potencia de transmisión se puede expresar como sigue:

$$p_{\text{MT}}(R_{\text{MT}_0}, U_{\text{MT}_0}) = \min(p_0 (\tau R_{\text{MT}_0})^{\alpha\epsilon}, i_0 (\tau U_{\text{MT}_0})^\alpha, p_{\text{max}}) \quad (\text{A.1})$$

donde R_{MT_0} es la distancia entre el MT de prueba y la BS que le da servicio, U_{MT_0} la distancia entre el MT de prueba y la BS a la que interfiere más, p_0 es la potencia recibida objetivo y ϵ es el factor de compensación parcial del enlace, donde $\epsilon = 1$ implica compensación total de las pérdidas de propagación y del *shadowing*.

El evento $\mathcal{Q}_{\text{MT}_i}^{(m)}$ se define como: *la BS más interferida para el i -ésimo MT, MT_i , pertenece al nivel m* . Por tanto, podemos definir el evento $\mathcal{X}_{\text{MT}_i}^{(j,m)} = \mathcal{X}_{\text{MT}_i}^{(j)} \cap \mathcal{Q}_{\text{MT}_i}^{(m)}$ como sigue: *MT_i está asociado con el nivel j y su BS más interferida pertenece al nivel m* .

La SINR del MT de prueba, MT_0 , puede expresarse como sigue

$$\text{SINR}_{\text{MT}_0} = \frac{H_{\text{MT}_0} (\tau R_{\text{MT}_0})^{-\alpha} p_{\text{MT}}(R_{\text{MT}_0}, U_{\text{MT}_0})}{I_{\text{exact}} + \sigma_n^2} \quad (\text{A.2})$$

donde H_{MT_0} es el desvanecimiento multi-camino del enlace deseado, R_{MT_0} y U_{MT_0} son las distancias hacia la BS que da servicio y la BS más interferida respectivamente, I_{exact} es la interferencia agregada y σ_n^2 es la potencia de ruido. El *shadowing* no aparece explícitamente porque se incluye en el análisis dentro del proceso punto subyacente gracias al teorema del desplazamiento aleatorio (*displacement theorem*, [93]).

El criterio de asociación establece una correlación entre las posiciones de los MT interferentes y la BS de prueba. Dicha correlación se recoge con el siguiente evento $\mathcal{O}_{\text{MT}_i}^{(j,k)}$ definido como: *el MT i -ésimo, MT_i , recibe mayor potencia pesada de la BS que le da servicio que de la BS de prueba*.

Finalmente, es necesario definir un evento para tener en cuenta la correlación que i_0 introduce en los MTs interferentes ya que no pueden estar en una posición en la que interfieran más que i_0 a la BS de prueba. Esto obliga a definir el evento $\mathcal{Z}_{\text{MT}_i}$ como sigue: *el MT_i causa menos interferencia a la BS de prueba, BS_0 que i_0* .

Gracias a estos eventos, cuya expresión matemática aparece en el capítulo 2, se puede dar una expresión analítica de la interferencia, que incluye las correlaciones necesarias,

como sigue:

$$I = \sum_{k \in \mathcal{K}} \sum_{\text{MT}_i \in \Psi^{(k)}} H_{\text{MT}_i} (\tau D_{\text{MT}_i})^{-\alpha} p_{\text{MT}} (R_{\text{MT}_i}, U_{\text{MT}_i}) \mathbf{1} \left(\mathcal{O}_{\text{MT}_i}^{(j,k)} \right) \mathbf{1} (Z_{\text{MT}_i}) \quad (\text{A.3})$$

donde $\Psi^{(k)}$ es el PPP de los MT interferentes que están planificados en el recurso físico (PRB, Physical Resource Block) de interés. La densidad de dicho PPP es $\lambda^{(k)}$.

A.2.2 Resultados Teóricos

En esta sub-sección se van a resumir algunos de los resultados teóricos obtenidos tras hacer el análisis de la técnica IAFPC. Uno de los resultados principales, es la transformada de Laplace de la interferencia, ya que puede usarse como función generadora de momentos para obtener la media y la varianza de la interferencia. Por comodidad, dicha expresión aparece a continuación

$$\mathcal{L}_I \left(s | \mathcal{X}_{\text{MT}_0}^{(j)} \right) = \exp \left(\beta^{(j)} (s) \right) \quad (\text{A.4})$$

donde

$$\beta^{(j)} (s) = - \sum_{k \in \mathcal{K}} 2\pi \lambda^{(k)} \sum_{n \in \mathcal{K}} \Pr \left(\mathcal{Q}_{\text{MT}_i}^{(n)} | \mathcal{X}_{\text{MT}_i}^{(k)} \right) \int_{r=0}^{\infty} \int_{u=\left(\frac{t^{(n)}}{t^{(k)}}\right)^{\frac{1}{\alpha}} r}^{\infty} f_{R_{\text{MT}_i}, U_{\text{MT}_i}} \left(r, u | \mathcal{X}_{\text{MT}_i}^{(k,n)} \right) \chi (s, r, u) dr du \quad (\text{A.5})$$

mientras que $p_{\text{MT}} (r, u)$ está dado en (A.1). El término $f_{R_{\text{MT}_i}, U_{\text{MT}_i}} \left(r, u | \mathcal{X}_{\text{MT}_i}^{(k,n)} \right)$ es la función densidad de probabilidad (pdf, probability density function), de las distancias hacia la BS que da servicio y la BS más interferida por el MT interferente, MT_i . Dicha pdf se ha obtenido de forma cerrada tal y como aparece en el **Lema 2**. Por último, la función $\chi (s, r, u)$ aparece en forma cerrada en el capítulo 2.

Por otro lado, distribución de la SINR se ha obtenido en términos de su ccdf (complementary cumulative density function), expresada como aparece a continuación

$$\begin{aligned} \bar{F}_{\text{SINR}}(\gamma) &= \sum_{j \in \mathcal{K}} \sum_{m \in \mathcal{K}} \Pr(\mathcal{X}_{\text{MT}_0}^{(j,m)}) \int_{v=0}^{\infty} \int_{w=\left(\frac{t^{(m)}}{t^{(j)}}\right)^{\frac{1}{\alpha}} v}^{\infty} f_{R_{\text{MT}_0}, U_{\text{MT}_0}}(v, w | \mathcal{X}_{\text{MT}_0}^{(j,m)}) e^{-\frac{\gamma \sigma_n^2 (\tau v)^\alpha}{p_{\text{MT}}(v,w)}} \\ &\times \mathcal{L}_I\left(\frac{\gamma (\tau v)^\alpha}{p_{\text{MT}}(v, w)} | \mathcal{X}_{\text{MT}_0}^{(j)}\right) dv dw \end{aligned} \quad (\text{A.6})$$

Tal y como puede observarse de (A.6), la ccdf de la SINR es una expresión que depende de la transformada de Laplace de la interferencia y tiene dos integrales anidadas. Por tanto, para reducir la complejidad de $\bar{F}_{\text{SINR}}(\gamma)$, es necesario proporcionar una expresión cerrada para la transformada de Laplace de la interferencia. Para conseguir este último objetivo, se proponen dos aproximaciones: i) aproximación Sigmoideal, y ii) ajuste de momentos (MM, Moment Matching).

La primera aproximación propone aproximar la transformada de Laplace de la interferencia, por una función sigmoide, teniendo el eje s en decibelios. De este modo se hace la siguiente aproximación

$$\mathcal{L}_{\bar{I}}\left(s | \mathcal{X}_{\text{MT}_0}^{(j)}\right) = \frac{1}{1 + e^{b_0(10 \log_{10}(s) - s_0^{\text{(dB)})}}} \quad (\text{A.7})$$

donde $s_0^{\text{(dB)}}$ y b_0 son los dos únicos parámetros de la aproximación. El primero de los parámetros está relacionado con el cruce de la función con 0.5, mientras que el segundo está relacionado con la pendiente de la función en dicho punto. Dichos parámetros se pueden obtener por regresión logística a partir de un conjunto reducido de valores de $\mathcal{L}_I\left(s | \mathcal{X}_{\text{MT}_0}^{(j)}\right)$.

La otra alternativa consiste en proponer una distribución de probabilidad para modelar la interferencia y hacer ajuste de momentos (MM, Moment Matching) para obtener los parámetros que definen la distribución. En realidad, ni siquiera es necesario proponer una distribución de probabilidad que pueda ser definida con una pdf. Basta con proponer directamente una función que dependa de n parámetros como la transformada de Laplace de una distribución, dicha función debe ser derivable n veces y al particularizar su derivada n -ésima en $s = 0$ debe dar un valor finito. Es por ello que es este enfoque se le ha denominado TDA (Transformed Distribution Approach).

Usando la expresión de la ccdf de la SINR dada en (A.6) y alguna de las expresiones cerradas de la transformada de Laplace que se ha comentado, es posible representar la ccdf de la eficiencia espectral, (SE, Spectral Efficiency) como sigue

$$\bar{F}_{\text{SE}}(\xi) = \sum_{j \in \mathcal{K}} \sum_{m \in \mathcal{K}} \Pr\left(\mathcal{X}_{\text{MT}_0}^{(j,m)}\right) \bar{F}_{\text{SINR}}\left(2^\xi - 1 | \mathcal{X}_{\text{MT}_0}^{(j,m)}\right) \quad (\text{A.8})$$

La eficiencia espectral media la podemos obtener a partir de su ccdf ya que, al ser la SE una variable aleatoria positiva, se puede representar como: $\mathbb{E}[\text{SE}] = \int_{\xi > 0} \bar{F}_{\text{SE}}(\xi) d\xi$.

El marco matemático definido para IAFPC, tiene especial interés, ya que permite modelar el mecanismo de control de potencia fraccionado clásico (FPC), que es inconsciente de la interferencia, como un caso particular cuando $i_0 \rightarrow \infty$.

Además, para simplificar más las expresiones obtenidas, sin necesidad de usar las aproximaciones Sigmoidal o TDA, se ha realizado análisis asintótico. Se dice que dos funciones $f(x)$ y $f^{(x \sim a)}(x)$ son asintóticamente similares cuando x es cercano a a si se cumple la siguiente igualdad: $\lim_{x \rightarrow a} \frac{f(x)}{f^{(x \sim a)}(x)} = 1$. Ésto nos permite hacer el análisis cuando i_0 toma una valor pequeño, pero sin llegar a ser 0. Del análisis asintótico en el régimen de i_0 bajo se obtiene la siguiente expresión cerrada para la potencia media cuando se tiene una asociación basada en pérdidas de propagación mínimas

$$\mathbb{E}\left[P_{\text{MT}_0}^{(i_0 \sim 0)}\right] = i_0 \left(\frac{\tau}{\sqrt{\pi\lambda}}\right)^\alpha \Gamma\left(2 + \frac{\alpha}{2}\right) \quad (\text{A.9})$$

donde $\Gamma(x)$ es la función Gamma.

Conclusiones teóricas: de la expresión dada en (A.9) se derivan las siguientes afirmaciones:

1. La potencia media transmitida se reduce si la interferencia máxima permitida, i_0 , se reduce. Además, ambas métricas lo hacen de forma proporcional.
2. Aumentar la densidad de BS disminuye la potencia media transmitida. Esto ocurre porque al haber más BSs, la BS más interferida recibe mayor potencia interferente, y por tanto hay que reducir la potencia de transmisión.
3. Aumentar el exponente de las pérdidas de propagación aumenta la potencia trans-

mitida, ya que llega menos interferencia a la BS más interferida y se requiere mayor potencia para compensar las pérdidas de propagación con la BS que da servicio.

4. Es interesante remarcar que, en este régimen, la potencia media no depende de la pendiente de las pérdidas de propagación, τ , aunque sí de su exponente, α .

El caso de asociación mediante un criterio de minimización de las pérdidas de propagación tiene especial relevancia, ya que se ha demostrado en [26, 32] que dicha asociación maximiza las prestaciones en el UL de HCNs. Para este mismo caso especial de asociación se ha obtenido la siguiente expresión para la transformada de Laplace de la interferencia, sin usar las aproximaciones mencionadas (Sigmoidal y TDA):

$$\mathcal{L}_I^{(i_0 \sim 0)}(s) = \exp\left(-\frac{4si_0}{\alpha-2} \cdot {}_2F_1\left(1, \frac{\alpha-2}{\alpha}; 2 - \frac{2}{\alpha}; -si_0\right)\right) \quad (\text{A.10})$$

Conclusión teórica: tal y como puede apreciarse de (A.10), dicha expresión no depende de λ . Como la media, varianza y el resto de momentos de la interferencia se obtienen como derivadas de su transformada de Laplace, esto quiere decir que ningún estadístico de la interferencia depende de la densidad de BSs.

A.2.3 Resultados Numéricos

En esta sub-sección se presentan algunos resultados numéricos para evaluar las prestaciones del mecanismo de control de potencia evaluado. A menos que se indique lo contrario, los resultados obtenidos mediante simulación aparecen con marcadores mientras que los resultados teóricos aparecen con líneas continuas.

La Fig. A.1 representa en azul la potencia media transmitida de un MT elegido al azar (MT típico o de prueba) en función del umbral de interferencia máxima en el sistema, i_0 . Se aprecia que la potencia media se reduce si i_0 decrece, como era de esperar. Un valor más estricto de i_0 disminuye la potencia de transmisión. Además, se observa que ese truncamiento de la potencia de transmisión puede deberse a la potencia máxima de transmisión (curva para $p_{\max} = 5$ dBm). En color verde aparece el caso límite cuando i_0 tiende a ∞ . Este caso se corresponde con un mecanismo FPC clásico y por tanto insensible a la interferencia. Se observa que para un valor de i_0 suficientemente alto ($i_0 = -60$ dBm), IAFPC se comporta como FPC. Por último el análisis asintótico aparece

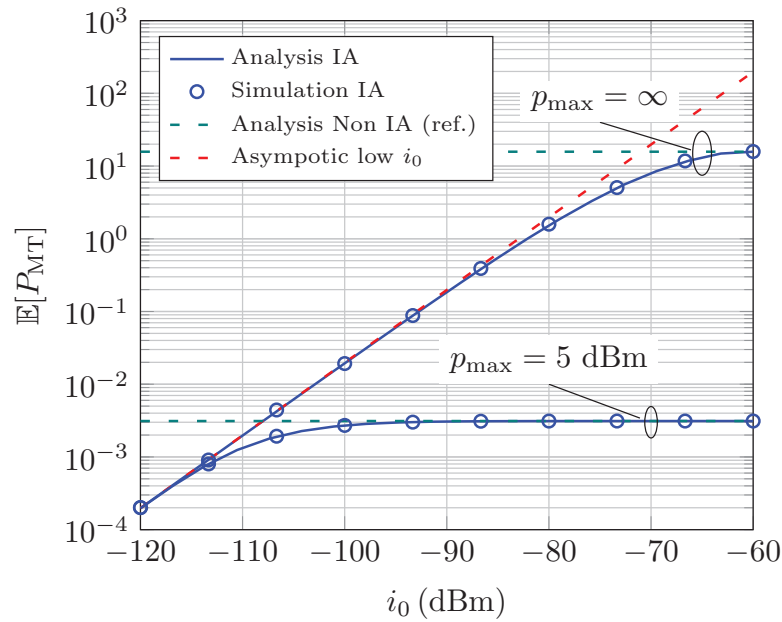


Figure A.1: Potencia media transmitida en función de i_0 para IAFPC y FPC clásico (incosciente de la interferencia) con $\epsilon = 1$, $p_{\max} \rightarrow \infty$ y $p_{\max} = 5$ dBm.

como una curva roja. Tal y como era de esperar, se aprecia que dicho resultado es preciso cuando el valor de i_0 es bajo.

La Fig. A.2 ilustra la transformada de Laplace de la interferencia para IAFPC condicionada en el evento $\mathcal{X}_{\text{MT}_0}^{(1)}$ para distintas aproximaciones y para dos valores distintos de i_0 , que son -60 y -120 dBm. La aproximaciones consideradas son la aproximación sigmoideal (curva azul) y TDA usando funciones exponencial (curva negra) y algebraica (curva verde). La transformada de Laplace sin hacer aproximaciones aparece representada con círculos rojos. Por otro lado la aproximación sigmoideal usa 8 puntos igualmente espaciados entre $s^{(\text{dB})} = 80$ and $s^{(\text{dB})} = 200$ para obtener los parámetros b_0 and $s_0^{(\text{dB})}$ mediante regresión logística. Se aprecia que tales aproximaciones dan lugar a resultados precisos en cuanto a la transformada de Lapalce y además conducen a expresiones cerradas.

La siguiente figura ilustra la eficiencia espectral media para IAFPC en función de i_0 (curva azul). Se observa que existe un valor de i_0 óptimo que maximiza dicha métrica. Esto se debe a que disminuir i_0 tiene dos efectos opuestos. Por un lado, disminuir i_0 cuando el sistema está limitado por interferencia (valores altos de i_0) implica reducir de forma inteligente aquellas transmisiones que generan demasiada interferencia y se mejoran

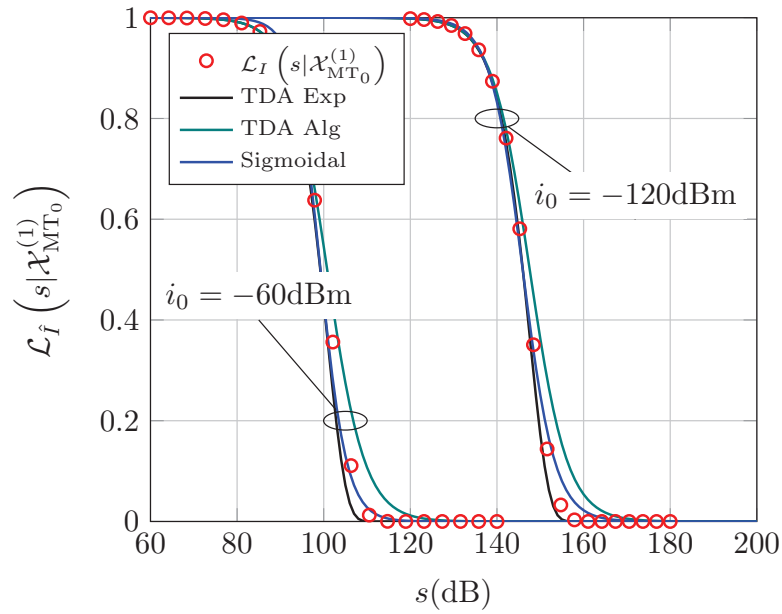


Figure A.2: Transformada de Laplace de la interferencia para IAFPC condicionada en el evento $\mathcal{X}_{MT_0}^{(1)}$ usando diferencias aproximaciones.

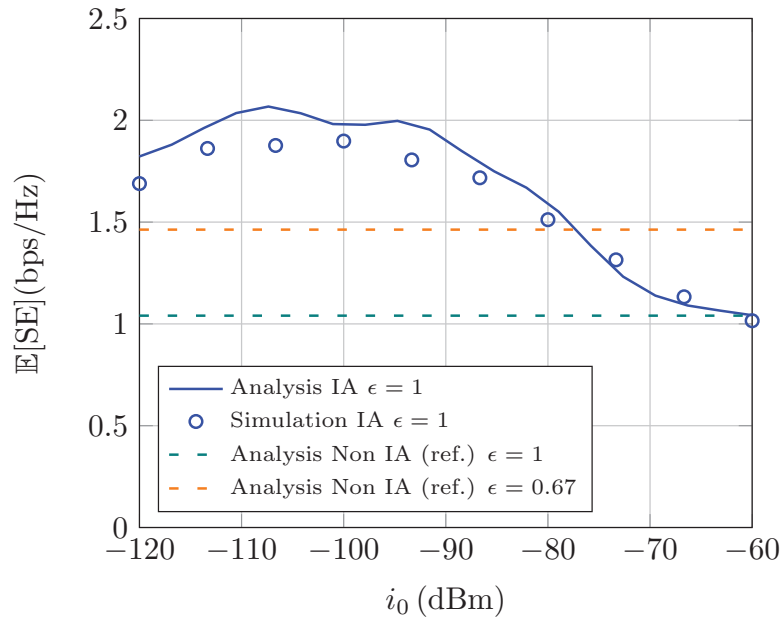


Figure A.3: Eficiencia espectral media en función de i_0 para IAFPC con $p_{\max} \rightarrow \infty$.

por tanto las prestaciones del sistema. Por otro lado, cuando el sistema está limitado por ruido (i_0 tiene valores pequeños) reducir i_0 implica disminuir la potencia de señal deseada comparado con la potencia de ruido, que ya domina sobre la interferencia.

Como valores de referencia, en verde y naranja aparece la eficiencia espectral media para un control de potencia inconsciente de la interferencia, FPC, con dos valores distintos de ϵ . El valor $\epsilon = 1$ se corresponde con una compensación total de las pérdidas de propagación. El valor $\epsilon = 0.67$ es, en cambio, el valor óptimo que maximiza la SE media con FPC. Esta figura ilustra por tanto que IAFPC mejora considerablemente el SE medio con respecto al mecanismo FPC clásico. Además de la Fig. A.1 se desprende que IAFPC también reduce la potencia media, lo cual aumenta la vida útil de la batería de los móviles. Por último, en el capítulo 2 aparecen numerosos resultados que demuestran que IAFPC también mejora la interferencia media y la varianza de la interferencia en el sistema, lo cual aporta numerosas ventajas prácticas en sistemas reales.

A.3 Planificación de Terminales Móviles Consciente de la Interferencia

En esta sección se resumen los resultados del estudio de la técnica de planificación de recursos IAM. Dicha técnica se analiza en términos de potencia media de transmisión, media y varianza de la interferencia, probabilidad de cobertura, SE y Régimen Binario (BR). Esta última métrica representa, a diferencia de la SE, la cantidad de recursos asignados al MT típico. Para contabilizar el BR se utiliza la función de masa de probabilidad (PMF, Probability Mass Function) del número de MTs activos (no silenciados) por celda, y se considera un algoritmo de planificación de recursos que divide el ancho de banda disponible entre los MT activos. Además, se propone un nuevo marco matemático para obtener el BR y SE mediante el uso de modulación y codificación adaptativas (AMC, Adaptive Modulation and Coding), que proporciona resultados más cercanos a las implementaciones reales. El análisis revela que IAM aumenta la BR y reduce la potencia de transmisión promedio y la media y la varianza de la interferencia incluso más que IAFPC. Además, se demuestra que existe un régimen de funcionamiento, en el que el rendimiento de IAM es independiente del criterio de asociación, lo que simplifica el diseño conjunto de transmisiones de los enlaces UL y DL. El precio a pagar es que los MTs se silencien en

algunos instantes y, por tanto, se reduce la justicia entre usuarios a la hora de acceder a los recursos.

A.3.1 Modelo de Sistema

El modelo de sistema es similar al expuesto en la sección anterior tanto para las posiciones de las estaciones BS y los MTs como para la propagación de las señales o la asociación entre MTs y BSs. La diferencia está, en que en este caso se considera el mecanismo de control fraccionado de potencia, que es inconsciente de la interferencia y cuya potencia transmitida viene dada por la siguiente función: $p_{\text{MT}}(r) = p_0(\tau r)^{\alpha\epsilon}$; siendo r la distancia hacia la BS que da servicio, p_0 la potencia recibida objetivo y ϵ el factor de compensación parcial.

La planificación dinámica de recursos IAM consta de dos pasos que realiza cada BS y se detallan a continuación:

1. Determinar el conjunto de MTs activos. Los MTs activos son aquellos cuya transmisión no causa mayor nivel de interferencia que i_0 a ninguna BS, y no requiere transmitir con más potencia que p_{max} .
2. Una vez que se ha determinado el conjunto de MTs activos, se divide el ancho de banda del sistema, b_w , entre ellos. Por ello, si $N_{\text{BS}_n}^{\mathcal{A}(j)}$ es el número de MTs activos de la BS n -ésima del tier j , el ancho de banda para la transmisión de cada MT es $b_w/N_{\text{BS}_n}^{\mathcal{A}(j)}$.

Por último, para poder hacer el análisis hay que tener en cuenta un nuevo tipo de correlación en la posición de los MTs, que viene derivado del proceso de silenciado de los MTs. Esta correlación se introduce en el análisis mediante el evento $\mathcal{A}_{\text{MT}_i}$, que se define como: *el MT i -ésimo pertenece al conjunto de MTs activos de la BS que le da servicio*. El resto de eventos necesarios para modelar la interferencia también se tienen en cuenta en este modelo matemático y tienen el mismo significado tal como se detalla en el capítulo 3.

En la inmensa mayoría de artículos centrados en el análisis de prestaciones usando geometría estocástica, para obtener la SE o el BR se usa la fórmula de Shannon mediante la cual la SE se puede expresar como sigue: $\text{SE} = \log_2(1+\text{SINR})$ bps/Hz. Este resultado se corresponde con la SE a la que se puede transmitir manteniendo una probabilidad de error

arbitrariamente pequeña. Se considera aquí un sistema ideal en el que el transmisor tiene perfecto conocimiento del estado del canal, y el receptor tiene una complejidad infinita. No obstante, en sistemas reales, el transmisor no tiene un conocimiento perfecto del estado del canal, y el receptor tiene una complejidad limitada. La modulación y codificación adaptativa (AMC, Adaptive Modulation and Coding) es la solución práctica en sistemas reales como LTE. En esta solución la BS estima la SINR a partir de los pilotos que mandan los MTs. Dichos valores de SINR, una vez que están cuantificados, se concen como CQIs, (Channel Quality Indicators). Se usan 4 bits para su representación, lo cual conduce a $n_{\text{CQI}} = 16$ valores posibles. Una vez que se ha estimado dicha SINR, la BS elige el esquema de modulación y codificación (MCS, Modulation and Coding Scheme) para conseguir una BLER (Block Error Rate) menor o igual a una BLER objetivo, que en LTE es de 0.1. Para elegir ese MCS la BS usa unas tablas que contienen los umbrales de SINR, $\gamma_{i_{\text{CQI}}}$, $i_{\text{CQI}} \in [1, n_{\text{CQI}}]$. Así pues, dado un conjunto de umbrales de SINR, $\gamma_{i_{\text{CQI}}}$, la SE para un MT, MT_0 , con un valor de SINR, $\text{SINR}_{\text{MT}_0}$, se expresa como sigue:

$$\text{SE}_{\text{MT}_0} = \sum_{i_{\text{CQI}}=1}^{n_{\text{CQI}}} \text{SE}_{i_{\text{CQI}}} \mathbf{1}(\text{SINR}_{\text{MT}_0} \in [\gamma_{i_{\text{CQI}}}, \gamma_{i_{\text{CQI}+1}})) \quad (\text{A.11})$$

donde $\gamma_1 < \dots < \gamma_{n_{\text{CQI}}}$. El valor $i_{\text{CQI}} = 0$ está asociado con la no transmisión. Por otro lado $\bigcap_{i_{\text{CQI}}=1}^{n_{\text{CQI}}} [\gamma_{i_{\text{CQI}}}, \gamma_{i_{\text{CQI}+1}}) = \emptyset$, $\gamma_{n_{\text{CQI}+1}} \rightarrow \infty$.

El BR se determina a partir del SE y de la asignación de ancho de banda para la transmisión de cada MT que haga el planificador. En nuestro caso se representa como sigue: $\text{BR}_{\text{MT}_0} = b_w / N_{\mathcal{B}_{\text{MT}_0}}^{\mathcal{A}} \cdot \text{SE}_{\text{MT}_0}$ (bps) ; donde $N_{\mathcal{B}_{\text{MT}_0}}^{\mathcal{A}}$ es el número de MTs asociados a la misma BS que MT_0 . Es importante remarcar que este marco matemático para la AMC considera los umbrales como un parámetro del modelo. Dichos umbrales no se pueden obtener de forma analítica si se usan códigos correctores prácticos como son los turbo códigos, y otros efectos no ideales como el error en la estimación de la SINR, o la limitación de complejidad en el cálculo de las medidas LLR (Log Likelihood Ratio). Por tanto, en este trabajo se han usado unos umbrales de SINR, obtenidos por medio de un simulador de enlace realista que considera un turbo decodificador de baja complejidad basado en el algoritmo SOVA (Soft Output Viterbi Algorithm) [119], además de las citadas no idealidades que ocurren en sistemas reales para el cálculo de dichos umbrales [1]. En el capítulo 3 aparecen los umbrales considerados.

A.3.2 Resultados Teóricos

Uno de los resultados teóricos principales para el caso de asociación generalizada es la probabilidad de estar activo, que aparece a continuación

$$\Pr(\mathcal{A}_{\text{MT}_0}) = \sum_{j \in \mathcal{K}} \int_{v > 0} \mathbf{1} \left(v < \frac{1}{\tau} \left(\frac{p_{\max}}{p_0} \right)^{\frac{1}{\alpha}} \right) (\nu^{(j)}(v) + \eta^{(j)}(v)) dv \quad (\text{A.12})$$

donde $\nu^{(j)}(v)$ y $\eta^{(j)}(v)$ aparecen definidos como una expresión cerrada en (A.13) y (A.14)

$$\begin{aligned} \nu^{(j)}(v) = & 2\pi v \lambda^{(j)} \left(e^{-\pi \lambda^{(j)} v^2} \times \left(e^{-\pi \lambda^{(\tilde{j})} \max^2 \left(\left(\frac{p_0}{i_0} \right)^{\frac{1}{\alpha}} \frac{(\tau v)^\epsilon}{\tau}, \left(\frac{t^{(\tilde{j})}}{t^{(j)}} \right)^{\frac{1}{\alpha}} v \right)} - e^{-\pi \lambda^{(\tilde{j})} v^2} \right) \times \right. \\ & \mathbf{1} \left(v > \max \left(\left(\frac{p_0}{i_0} \right)^{\frac{1}{\alpha}} \frac{(\tau v)^\epsilon}{\tau}, \left(\frac{t^{(\tilde{j})}}{t^{(j)}} \right)^{\frac{1}{\alpha}} v \right) \right) \\ & \left. + \frac{\lambda^{(\tilde{j})}}{\lambda^{(j)} + \lambda^{(\tilde{j})}} e^{-\pi(\lambda^{(j)} + \lambda^{(\tilde{j})}) \max^2 \left(\left(\frac{p_0}{i_0} \right)^{\frac{1}{\alpha}} \frac{(\tau v)^\epsilon}{\tau}, \left(\frac{t^{(\tilde{j})}}{t^{(j)}} \right)^{\frac{1}{\alpha}} v, v \right)} \right) \end{aligned} \quad (\text{A.13})$$

$$\begin{aligned} \eta^{(j)}(v) = & 2\pi v \lambda^{(j)} \left(e^{-\pi \lambda^{(\tilde{j})} \left(\frac{t^{(\tilde{j})}}{t^{(j)}} \right)^{\frac{2}{\alpha}} v^2} \times \left(e^{-\pi \lambda^{(j)} \max^2 \left(\left(\frac{p_0}{i_0} \right)^{\frac{1}{\alpha}} \frac{(\tau v)^\epsilon}{\tau}, v \right)} - e^{-\pi \lambda^{(j)} \left(\frac{t^{(\tilde{j})}}{t^{(j)}} \right)^{\frac{2}{\alpha}} v^2} \right) \times \right. \\ & \mathbf{1} \left(v > \left(\frac{t^{(j)}}{t^{(\tilde{j})}} \right)^{\frac{1}{\alpha}} \max \left(\left(\frac{p_0}{i_0} \right)^{\frac{1}{\alpha}} \frac{(\tau v)^\epsilon}{\tau}, v \right) \right) \\ & \left. + \frac{\lambda^{(j)}}{\lambda^{(j)} + \lambda^{(\tilde{j})}} e^{-\pi(\lambda^{(j)} + \lambda^{(\tilde{j})}) \max^2 \left(\left(\frac{p_0}{i_0} \right)^{\frac{1}{\alpha}} \frac{(\tau v)^\epsilon}{\tau}, v, \left(\frac{t^{(\tilde{j})}}{t^{(j)}} \right)^{\frac{1}{\alpha}} v \right)} \right) \end{aligned} \quad (\text{A.14})$$

La probabilidad de estar activo dada en (A.12) es además un indicador de la justicia entre los MTs a la hora de acceder a los recursos. Si esta probabilidad es 1 quiere decir que todos los MTs tienen la misma probabilidad de acceder a los recursos.

La transformada de Laplace de la interferencia se obtiene como sigue:

$$\mathcal{L}_I \left(s | \mathcal{X}_{\text{MT}_0}^{(j)} \right) = \exp \left(\beta^{(j)}(s) \right) \quad (\text{A.15})$$

$$\beta^{(j)}(s) = - \sum_{k \in \mathcal{K}} 2\pi \lambda^{(k)} \sum_{n \in \mathcal{K}} \Pr \left(\mathcal{Q}_{\text{MT}_i}^{(n)} | \mathcal{X}_{\text{MT}_i}^{(k)}, \mathcal{A}_{\text{MT}_i} \right) \int_0^\infty f_{R_{\text{MT}_i}} \left(r | \mathcal{X}_{\text{MT}_i}^{(k,n)}, \mathcal{A}_{\text{MT}_i} \right) \chi(s, r) dr, \quad (\text{A.16})$$

la cual es una expresión que consta de una sola integral ya que, tal y como se detalla en el capítulo 3, $f_{R_{\text{MT}_i}} \left(r | \mathcal{X}_{\text{MT}_i}^{(k,n)}, \mathcal{A}_{\text{MT}_i} \right)$, $\chi(s, r)$ y $\Pr \left(\mathcal{Q}_{\text{MT}_i}^{(n)} | \mathcal{X}_{\text{MT}_i}^{(k)}, \mathcal{A}_{\text{MT}_i} \right)$ se obtienen en forma cerrada.

Finalmente, la ccdf de la SINR queda como sigue:

$$\begin{aligned} \bar{F}_{\text{SINR}}(\gamma) &= \sum_{j \in \mathcal{K}} \sum_{m \in \mathcal{K}} \Pr \left(\mathcal{X}_{\text{MT}_0}^{(j,m)}, \mathcal{A}_{\text{MT}_0} \right) \\ &\times \int_0^\infty f_{R_{\text{MT}_0}} \left(v | \mathcal{X}_{\text{MT}_0}^{(j,m)}, \mathcal{A}_{\text{MT}_0} \right) e^{-\gamma \sigma_n^2 (\tau v)^{\alpha(1-\epsilon)} p_0^{-1}} \mathcal{L}_I \left(\gamma (\tau v)^{\alpha(1-\epsilon)} p_0^{-1} | \mathcal{X}_{\text{MT}_0}^{(j)} \right) dv \end{aligned} \quad (\text{A.17})$$

que es una expresión que consta de dos integrales anidadas.

Conclusión teórica: A raíz de las expresiones obtenidas es posible determinar que existen tres regiones de funcionamiento en función de los pesos de asociación que se describen a continuación:

1. Régimen inconsciente de la interferencia. En este régimen de funcionamiento la ccdf de la SINR, y por tanto el resto de métricas que dependen de ella como el BR y el SE no dependen del parámetro i_0 . Este régimen ocurre si $i_0 > p_0$ y $t^{(1)}/t^{(2)}(\text{dB}) \in [-i_0/p_0, i_0/p_0]$, donde $t^{(1)}/t^{(2)}(\text{dB})$ es el cociente entre los pesos de asociación de las MBS y SBS respectivamente expresado en dB.
2. Régimen consciente de la interferencia e independiente de la asociación. En este régimen, las prestaciones dependen de i_0 , pero no dependen del cociente $t^{(1)}/t^{(2)}$. Este régimen se da cuando $i_0 < p_0$ y $t^{(1)}/t^{(2)}(\text{dB}) \in [-p_0/i_0, p_0/i_0]$.

3. Régimen consciente de la interferencia y dependiente de la asociación. Si no se dan ninguna de las condiciones anteriores se está en este régimen. En este régimen las prestaciones dependen tanto de i_0 como del cociente de $t^{(1)}/t^{(2)}$.

El segundo régimen de funcionamiento es de especial interés ya que facilita la optimización conjunta de la asociación para los enlaces UL y DL. Para entender esto basta recordar que en el caso desacoplado se tiene un conjunto de pesos de asociación $t^{(1)}/t^{(2)}$ para el UL, y otro par de pesos $\hat{t}^{(1)}/\hat{t}^{(2)}$ para el DL. En este caso la optimización conjunta del UL y DL resulta sencilla porque ambos enlaces se pueden optimizar por separado [26]. Tal y como se demuestra en [6] el cociente óptimo de pesos del DL en un escenario típico ronda los 20 dB. En el caso del UL, se demuestra en [26, 32] que la asociación basada en mínimas pérdidas de propagación es la que maximiza las prestaciones. Esta asociación se corresponde con un cociente de los pesos de asociación igual a 0 dBs, ($t^{(1)}/t^{(2)} = 0$ dB). Por desgracia el desacoplo de la asociación para el UL y DL no resulta atractivo desde el punto de vista de la implementación, ya que plantea numerosos desafíos prácticos [8].

Afortunadamente, IAM facilita la optimización conjunta del UL y DL en el caso acoplado (en el que existe un único par de pesos de asociación). Como existe una región de funcionamiento en la que las prestaciones del UL son independientes de los pesos de asociación, basta con elegir el cociente $t^{(1)}/t^{(2)}$ de forma que se maximizen las prestaciones del DL.

El BR medio se puede expresar matemáticamente como sigue:

$$\mathbb{E}[\text{BR}_{\text{MT}_0}] = \sum_{j \in \mathcal{K}} \sum_{m \in \mathcal{K}} \sum_{i_{\text{CQI}}=1}^{n_{\text{CQI}}} \Pr\left(\mathcal{X}_{\text{MT}_0}^{(j,m)}, \mathcal{A}_{\text{MT}_0}\right) \frac{\text{SE}_{i_{\text{CQI}}} 3.5^{3.5} b_w (3.5\lambda^{(j)} + \lambda_{\text{MTP}} p)}{\left(1 - \left(1 - \frac{\lambda_{\text{MTP}} p}{\lambda^{(j)}}\right)^{3.5}\right)^{-1} \lambda_{\text{MTP}} p \left(1 - \frac{\lambda_{\text{MTP}} p}{\lambda^{(j)}}\right)^{3.5}} \times \left(\bar{F}_{\text{SINR}}\left(\gamma_{i_{\text{CQI}}}\middle|\mathcal{X}_{\text{MT}_0}^{(j,m)}, \mathcal{A}_{\text{MT}_0}\right) - \bar{F}_{\text{SINR}}\left(\gamma_{i_{\text{CQI}}+1}\middle|\mathcal{X}_{\text{MT}_0}^{(j,m)}, \mathcal{A}_{\text{MT}_0}\right)\right) \quad (\text{A.18})$$

donde se ha usado el atajo $p = \Pr(\mathcal{X}_{\text{MT}_0}^{(j)}, \mathcal{A}_{\text{MT}_0})$ para simplificar la expresión. Se puede expresar que dicha ecuación es una función cerrada de la cdf de la SINR.

A continuación se presentan algunos resultados para el caso especial de asociación a la BS con menores pérdidas de propagación ($t^{(1)}/t^{(2)} = 0$ dB), $\epsilon = 1$ y con una potencia máxima de transmisión muy alta ($p_{\text{max}} \rightarrow \infty$). Este caso tiene especial interés ya que en [26, 32] se demuestra que este criterio de asociación maximiza las prestaciones del UL con

control de potencia fraccionado, FPC.

En el citado escenario de especial relevancia, la potencia media transmitida en el régimen consciente de la interferencia ($i_0 < p_0$) se puede escribir como sigue:

$$\mathbb{E} [p_{\text{MT}} (R_{\text{MT}_0})] = \frac{\tau^\alpha \Gamma \left(1 + \frac{\alpha}{2}\right)}{(\pi \lambda)^{\frac{\alpha}{2}} p_0^{\frac{\alpha}{2}}} i_0^{\frac{2}{\alpha} + 1} \quad (\text{A.19})$$

Conclusión teórica: en vista de la expresión anterior se puede determinar que la potencia media transmitida se escala de forma polinómica con el exponente, $2/\alpha + 1$, como una función de i_0 . Nuevamente, un incremento de la densidad de BSs implica un decremento de la potencia media transmitida ya que crece la interferencia generada.

En el mismo caso especial la cdf de la SINR se puede expresar de la siguiente manera:

$$\bar{F}_{\text{SINR}} (\gamma | \mathcal{A}_{\text{MT}_0}) = \exp \left(-\frac{\gamma \sigma_n^2}{p_0} - 2 \frac{\gamma}{\alpha - 2} \left(\frac{i_0}{p_0} \right)^{\frac{\alpha+2}{\alpha}} {}_2F_1 \left(1, \frac{\alpha - 2}{\alpha}, 2 - \frac{2}{\alpha}, -\gamma \left(\frac{i_0}{p_0} \right) \right) \right) \quad (\text{A.20})$$

Conclusión teórica: A raíz de (A.20) se puede afirmar que la cdf de la SINR en dicho caso particular es independiente de la densidad de BS. Esto ocurre porque al considerar control de potencia total ($\epsilon = 1$) la potencia de la señal deseada no varía al subir o bajar la densidad de BSs mientras que la interferencia tampoco varía con la densidad de BS gracias a IAM.

A.3.3 Resultados Numéricos

En esta sección se presentan algunos resultados numéricos obtenidos para IAM. Las prestaciones de IAM se comparan con las de IAFPC para determinar la bondad y la debilidad de cada método. En la Fig. A.4 aparece una comparación de ambas técnicas en términos de la potencia media transmitida. De dicha comparativa se desprenden las siguientes conclusiones: i) IAM da lugar a menor potencia media transmitida que IAFPC y ii) IAFPC da lugar a menor potencia que el mecanismo clásico de FPC (insconiente de la interferencia).

La Fig. A.5 ilustra el BR medio de IAM con AMC tanto para el MT típico como para los MTs activos. También aparecen el BR medio de IAFPC. Se pueden extraer las siguientes conclusiones de la figura:

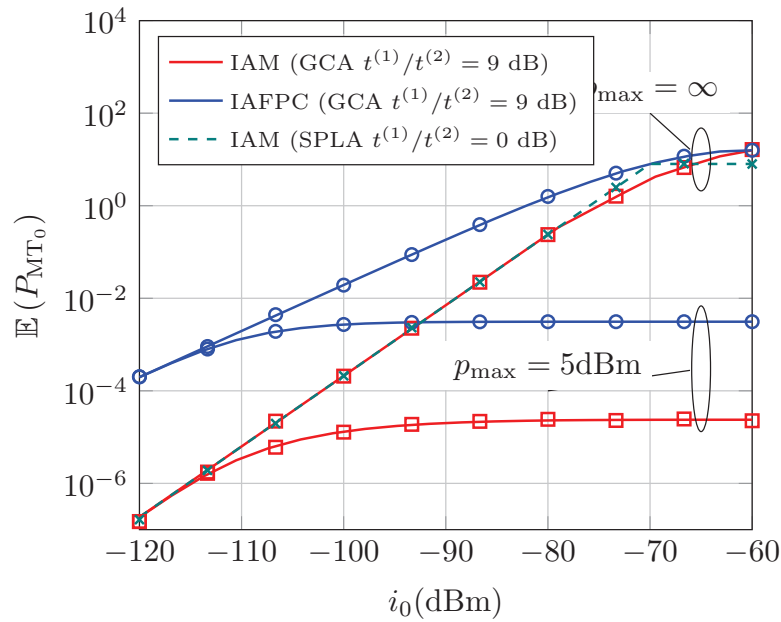


Figure A.4: Potencia media transmitida en función de i_0 para IAM y IAFPC con $\epsilon = 1$ y dos valores de la potencia máxima de transmisión: $p_{\max} \rightarrow \infty$ y $p_{\max} = 5$ dBm.

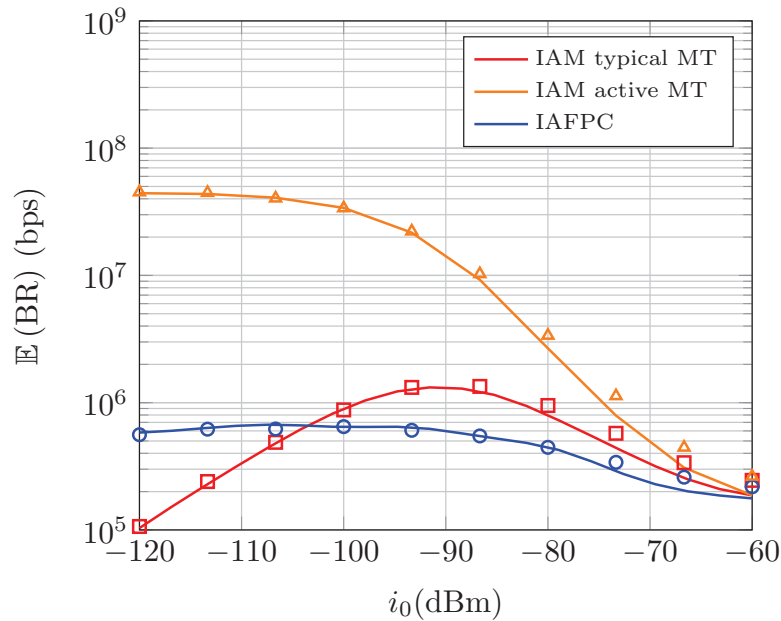


Figure A.5: BR medio para IAM y IAFPC para $\epsilon = 1$, $t^{(1)}/t^{(2)} = 9$ dB y $p_{\max} \rightarrow \infty$. Para IAM se consideran tanto las prestaciones del MT típico como de los MTs activos.

1. Valores pequeños de i_0 dan lugar a un BR medio máximo para los MTs activos con IAM (curva naranja) que viene determinado por el MCS de más alta SE. El BR medio de los MTs activos es el BR promediado sobre los MTs que están activos en un instante de tiempo determinado. También puede entenderse como el BR medio de un MT promediado sólo en los instantes en los que está activo (sin tener en cuenta los silencios).
2. Existe un valor de i_0 que maximiza el BR medio para el MT típico. La existencia de un máximo se debe a dos efectos opuestos. Por un lado disminuir i_0 implica que los MTs activos aumentan mucho el BR porque la interferencia se reduce mucho. Por otro lado, disminuir i_0 implica que los MTs están silenciados más tiempo y por tanto al promediar se reduce el BR medio.
3. El máximo valor de BR medio con IAM supera al conseguido con IAFPC. Esto quiere decir que desde el punto de vista de cada MT, conviene usar IAM, ya que aunque en algunos instantes el MT esté silenciado, su BR medio teniendo en cuenta tanto los periodos de silencio como los de actividad es mayor que si se usa IAFPC.

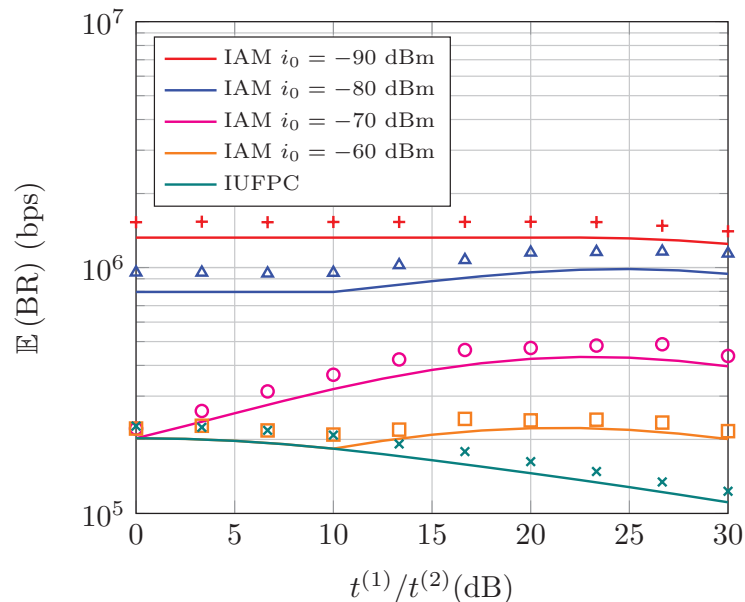


Figure A.6: BR medio como función de $t^{(1)}/t^{(2)}$ para FPC ($i_0 \rightarrow \infty$) y IAM con $i_0 = \{-90, -80, -70, -60\}$ dBm y $p_{\max} \rightarrow \infty$.

Las figuras Fig. A.6 y Fig. A.7 ilustran el BR medio y la probabilidad de estar activo respectivamente, en función de la asociación. Las regiones de funcionamiento pueden observarse en dichas figuras. En concreto, sabemos de los resultados teóricos que con $i_0 = -60$ dBm ($p_0 = -70$ dBm), tenemos que $i_0 > p_0$, y por tanto el sistema es inconsciente de la interferencia para $t^{(1)}/t^{(2)} \in [-10, 10]$ dB. Esto se puede corroborar tras observar ambas figuras.

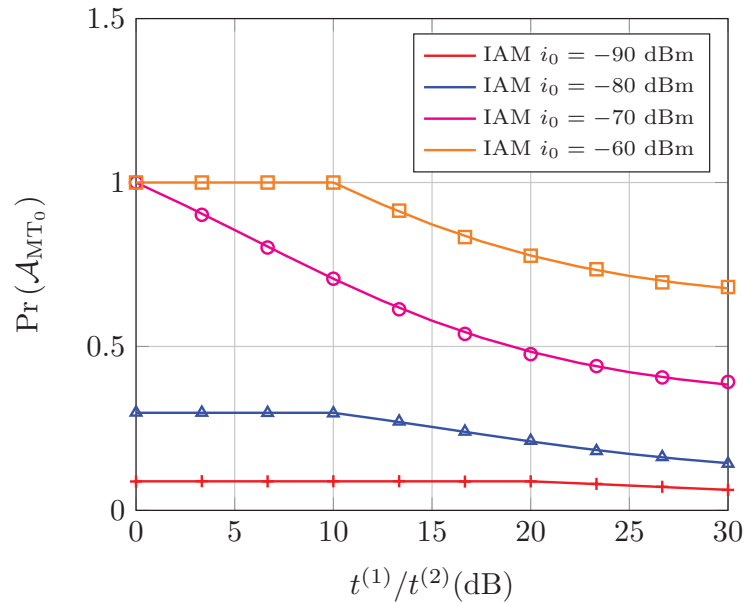


Figure A.7: Probabilidad de estar activo para el MT típico en función de $t^{(1)}/t^{(2)}$ para IAM con $i_0 = \{-90, -80, -70, -60\}$ dBm y $p_{\max} \rightarrow \infty$.

En concreto se observa que el BR medio para $i_0 = -60$ dBm (curva naranja) en $t^{(1)}/t^{(2)} \in [-10, 10]$ dB es exactamente el mismo que el que se obtiene con un mecanismo FPC clásico (curva verde) y por tanto inconsciente de la interferencia (IUFPC, Interference-Unaware Fractional Power Control). De especial relevancia es el caso $i_0 = -90$ dBm (curva roja). Tal y como se aprecia en la Fig. A.5 es el valor que maximiza el BR medio con IAM. En este caso, sabemos que el sistema es independiente de la asociación para $t^{(1)}/t^{(2)} \in [-20, 20]$ dB. Esto se observa en ambas figuras ya que tanto el BR medio como la probabilidad de estar activo no dependen de la asociación. Esto facilita la optimización conjunta de las transmisiones en los enlaces UL y DL en el caso acoplado; ya que bastaría con elegir el valor de i_0 que maximice las prestaciones en el UL. Luego bastaría

elegir el valor de la asociación que maximice las prestaciones en el DL. Si ese valor cae dentro del intervalo $t^{(1)}/t^{(2)} \in [-20, 20]$ las prestaciones del UL no se ven afectadas.

El precio a pagar es que la justicia entre MTs, en cuanto al acceso a los recursos, se reduce. Eso se observa en la Fig. A.7, donde se aprecia que la probabilidad de acceder a los recursos para el MT típico es menor que 1.

A.4 Probabilidad de Cobertura en Sistemas Multi-Usuario

En esta sección se resume el análisis y resultados de un modelo que permite evaluar la probabilidad de cobertura, o equivalentemente, la cdf de la SINR, para cada uno de los MTs asociados con una celda. El modelo, que se centra en el UL de una red homogénea con control de potencia fraccionado (FPC), considera que cada celda tiene k MTs planificados en recursos ortogonales. La comparación de la probabilidad de cobertura del mejor y del peor MT permite evaluar la justicia entre los MTs en cuanto a la probabilidad de cobertura.

A.4.1 Modelo de Sistema

Se considera que las posiciones de las BSs se pueden modelar como un PPP uniforme en el plano de densidad $\lambda_b = \lambda/k$. Cada BS da servicio a k MTs que son planificados en cada intervalo de transmisión en recursos ortogonales, y por tanto la densidad de MTs es λ . Los MTs se asocian a la BS más cercana. De cara a evaluar la probabilidad de cobertura los MTs, éstos son ordenados en función de la distancia a la BS que da servicio. De este modo el MT, MT_l , es el l -ésimo MT más cercanos a la BS que le da servicio. La SINR de dicho MT se expresa como

$$\text{SINR}_l = \frac{G_l R_l^{\alpha(\epsilon-1)}}{I_l + \sigma^2} \quad (\text{A.21})$$

donde $I_l = \sum_{x \in \Phi_{i,l}} G_x R_x^{\alpha\epsilon} D_x^{-\alpha}$. $\Phi_{i,l}$ es el proceso punto de los MTs interferentes para el MT l -ésimo mientras que G_x y G_l son los desvanecimientos multi-camino entre el MT interferente y el MT l -ésimo con la BS de prueba. Por otro lado, D_x y R_x son las distancias

entre el MT interferente con la BS de prueba y con la BS que le da servicio, respectivamente. La potencia transmitida por un MT a distancia r de la BS que le da servicio es $r^{\alpha\epsilon}$, (se asume una potencia objetivo y una pendiente de las pérdidas de propagación unitarias).

Como el criterio de asociación se basa en distancia mínima con la BS que da servicio y las posiciones de las BS siguen un PPP, las celdas están formadas por polígonos aleatorios que resultan de hacer la tesselación de Voronoi. Por tanto, es matemáticamente inviable obtener la transformada de Laplace de la interferencia de forma exacta. Así, para hacer el análisis se asume que los interferentes están más lejos de la BS de prueba que el MT k -ésimo, que es el más lejano.

Los resultados de simulación consideran el modelo exacto, en el que las BSs siguen un PPP uniforme de densidad λ_b , y se distribuyen de forma aleatoria k MTs dentro de cada celda, que se obtiene mediante la teselación de Voronoi. Sin embargo el análisis considera la suposición antes mencionada en la que se considera que los MTs interferentes se sitúan más lejos que el MT k -ésimo.

A.4.2 Resultados Teóricos

Uno de los resultados principales es la pdf conjunta de la distancia a la BS de prueba de los MTs l -ésimo y k -ésimo. Dicha pdf se representa a continuación.

$$f_{R_l, R_k}(r_l, r_k) = \frac{4e^{-\pi r_k^2 \lambda} (\lambda \pi)^k r_k r_l^{2l-1} (r_k^2 - r_l^2)^{k-l-1}}{(k-l-1)!(l-1)!} \quad (\text{A.22})$$

donde $0 \leq r_l \leq r_k$.

El resultado principal es la probabilidad de cobertura del MT l -ésimo, que se expresa a continuación.

$$p_c(l, k, t, \lambda, p, \alpha, \epsilon, \mu, \sigma^2) = \int_0^\infty \int_{r_l}^\infty \xi(r_l, r_k) f_{R_l, R_k}(r_l, r_k) dr_k dr_l \quad (\text{A.23})$$

donde

$$\xi(r_l, r_k) = e^{-\mu t \sigma^2 r_l^{\alpha(1-\epsilon)}} \mathcal{L}_{I_l | r_l, r_k}(\mu t r_l^{\alpha(1-\epsilon)}) \quad (\text{A.24})$$

siendo $\mathcal{L}_{I_l|r_l, r_k}(s)$ la transformada de Laplace de la interferencia condicionada en r_l y r_k . Este término, evaluado en $s = \mu tr_l^{\alpha(1-\epsilon)}$ tiene la siguiente forma

$$\mathcal{L}_{I_l|r_l, r_k}(\mu tr_l^{\alpha(1-\epsilon)}) = \exp\left(-2\pi p\lambda \int_{r_k}^{\infty} \left(1 - \int_0^{\infty} \frac{\pi p\lambda e^{-p\lambda\pi q}}{1 + tr_l^{\alpha(1-\epsilon)} q^{\alpha\epsilon/2} v^{-\alpha}} dq\right) v dv\right) \quad (\text{A.25})$$

A.4.3 Resultados Numéricos

Es importante recalcar que en el sistema considerado los k MTs que hay en cada celda acceden a los recursos en cada intervalo de transmisión. Por tanto, en este sistema, la justicia en cuanto al acceso a los recursos es máxima. El objeto de estudio se centra en la justicia entre usuarios en cuanto a las prestaciones, y en concreto, en cuanto a la probabilidad de cobertura.

La Fig. A.8 ilustra la probabilidad de cobertura para el más cercano MT ($l = 1$) y el más lejano ($l = k$) MT cuando se usa un factor de compensación parcial de 0.75. En este caso se aprecia que, a pesar de que todos los MTs acceden por igual a los recursos, la justicia entre los MTs de una celda no es total, ya que la probabilidad de cobertura del MT más cercano a la BS de prueba, MT_1 , es mejor que la del MT más lejano, MT_k .

La Fig. A.9 ilustra en cambio la probabilidad de cobertura de los MTs más cercanos y el más lejano para una compensación total de las pérdidas de propagación. En este caso la justicia en términos de cobertura es máxima porque todos los MTs tienen las mismas prestaciones. Es interesante remarcar que el factor de compensación parcial, ϵ , que maximiza las prestaciones del MT típico (uno elegido al azar), suele ser menor que uno ($\epsilon < 1$) tal y como puede verse en la Fig. 2.10 y en multitud de trabajos en la literatura [26, 29, 32]. Esto se debe a que $\epsilon = 1$ genera mucha interferencia a las celdas vecinas si no se usa alguna técnica de mitigación de interferencias como IAFPC o IAM. Por tanto, las figuras A.8 y A.9 ponen de manifiesto una vez más el compromiso que existe entre maximizar las prestaciones, como cobertura o BR, y la justicia entre los usuarios.

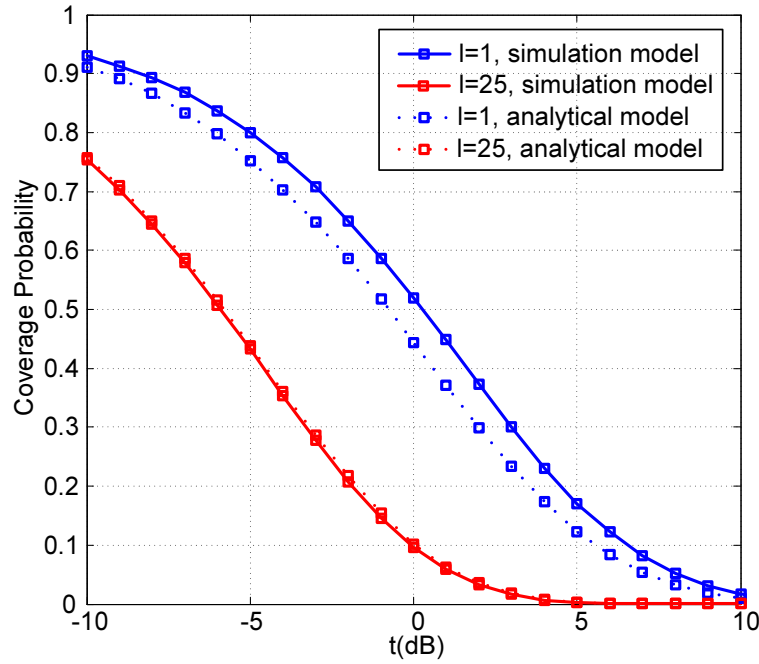


Figure A.8: Probabilidad de cobertura para $k = \{10, 25, 50\}$ con compensación parcial de las pérdidas de propagación ($\epsilon = 0.75$), para el caso sin ruido con $\alpha = 2.5$, $\lambda_b = 0.24$

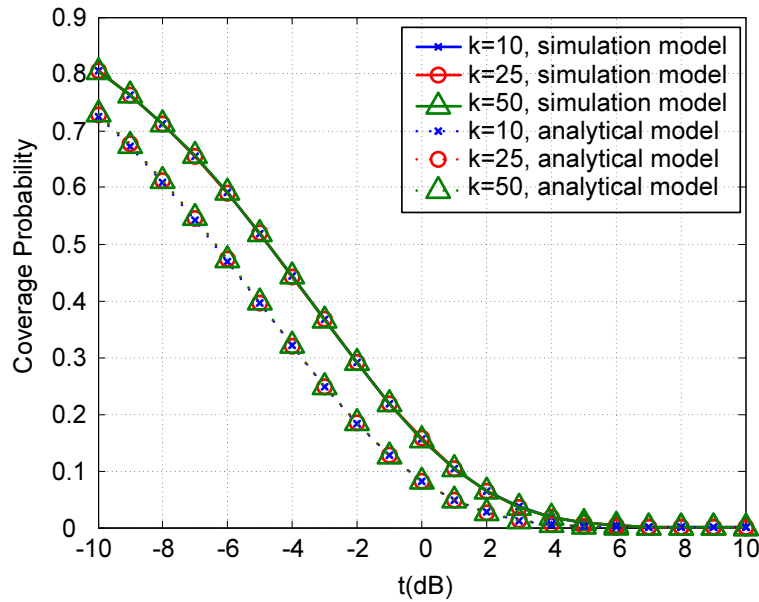


Figure A.9: Probabilidad de cobertura para $k = \{10, 25, 50\}$ con compensación total de las pérdidas de propagación ($\epsilon = 1$), para el caso sin ruido con $\alpha = 2.5$, $\lambda_b = 0.24$.

A.5 Probabilidad de Cobertura con Desvanecimiento Hoyt

En esta trabajo, se deriva una aproximación cerrada de la probabilidad de cobertura de los sistemas celulares bajo un desvanecimiento tipo Hoyt (Nakagami-q). El análisis realizado expresa el desvanecimiento como funciones condicionadas con distribución exponencial. Después, la esperanza sobre la distancia hacia la estación base que da servicio se divide en dos integrales finitas que pueden aproximarse mediante la regla de Gauss-Chebyshev. La exactitud de las expresiones obtenidas se valida con simulación Monte Carlo.

A.5.1 Modelo de Sistema

Consideramos el DL de una red celular homogénea, donde las BSs están distribuidas acorde a un PPP, $\Phi_{BS} = \{BS_1, BS_2, \dots\}$, cuya densidad es λ_{BS} . Los MTs están distribuidos acorde a un PPP, y cada MT se asocia a la BS más cercana. Las señales transmitidas sufren desvanecimiento con distribución Hoyt (Nakagami-q), con un factor de escala, $q \in [0, 1]$ y media unitaria. La PDF de la envolvente al cuadrado del desvanecimiento se puede expresar como una exponencial condicionada como sigue [95]:

$$f_H(h) = \mathbb{E}_\Theta [f_{H|\theta}(h) | \Theta = \theta] = \mathbb{E}_\theta \left[\frac{1}{\gamma(\theta, q)} e^{-h/\gamma(\theta, q)} | \Theta = \theta \right], \quad (\text{A.26})$$

donde $\gamma(\theta, q) = \left(1 - \frac{1-q^2}{1+q^2} \cos(\theta)\right)$ y Θ se distribuye de manera uniforme entre 0 y π . Se considera una ley de pérdidas de propagación con una pendiente de pérdidas, τ , y un exponente de las pérdidas, $\alpha > 2$. La relación SINR del MT típico, que puede considerarse que está situado en el origen sin pérdida de generalidad, sigue la siguiente ecuación

$$\text{SINR}_{\text{MT}_0} = \frac{H_{BS_0} (\tau R_{BS_0})^{-\alpha} \rho_{BS}}{I + \sigma_n^2}, \quad (\text{A.27})$$

siendo H_{BS_0} y R_{BS_0} el desvanecimiento y la distancia con la BS servidora respectivamente, ρ_{BS} es la potencia de transmisión por Hz, I es el término interferente y σ_n^2 es la potencia de ruido. La interferencia se expresa como sigue

$$I = \sum_{BS_i \in \Phi_{BS}} H_{BS_i} (\tau R_{BS_i})^{-\alpha} \rho_{BS} \mathbf{1}(R_{BS_i} > R_{BS_0}), \quad (\text{A.28})$$

siendo $\mathbf{1}(\mathcal{A})$, la función indicadora.

A.5.2 Resultados Teóricos

La probabilidad de cobertura del MT típico se puede expresar de forma cerrada como sigue:

$$\mathcal{P}_c = \frac{\pi}{2n_r} \sum_{i=1}^{n_r} \left(\mu(r_i) + \frac{\mu(r_i^{-1})}{t^2} \right) \left| \sin \left(\frac{2i-1}{2n_r} \pi \right) \right|, \quad (\text{A.29})$$

donde

$$\begin{aligned} \mu(r) = & \sum_{j_1=1}^{n_\theta} \left| \sin \left(\frac{2j_1-1}{2n_\theta} \pi \right) \right| \frac{\lambda_{\text{BS}} r \pi^2}{n_\theta} \exp \left(-\pi \lambda_{\text{BS}} r^2 \right. \\ & - \frac{t \sigma_n^2 (\tau r)^\alpha}{\rho_{\text{BS}} \gamma(\theta_1, q)} - \frac{\lambda t r^2 \pi^2}{(\alpha-2) n_\theta} \sum_{j_2=1}^{n_\theta} \frac{\gamma(\theta_{j_2}, q)}{\gamma(\theta_{j_1}, q)} \\ & \left. {}_2F_1 \left(1, \frac{\alpha-2}{\alpha}, 2 - \frac{2}{\alpha}, \frac{-t \gamma(\theta_{j_2}, q)}{\gamma(\theta_{j_1}, q)} \right) \right| \left| \sin \left(\frac{2j_2-1}{2n_\theta} \pi \right) \right| \end{aligned} \quad (\text{A.30})$$

$$\text{y } r_i = \frac{1}{2} \left[\cos \left(\frac{2i-1}{2n_r} \pi \right) + 1 \right].$$

A.5.3 Resultados Numéricos

La siguiente figura representa la probabilidad de cobertura para el caso Rayleigh ($q = 1$) y para un caso de desvanecimiento severo ($q = 0.05$). Se aprecia un buen ajuste entre los resultados teóricos y los obtenidos por simulación. De la figura se observa que la probabilidad de cobertura para valores de SINR altos es aproximadamente la misma para los casos $q = 1$ y $q = 0.05$. No obstante, la probabilidad para valores de SINR umbral por debajo 0 dB depende mucho de la severidad del desvanecimiento.

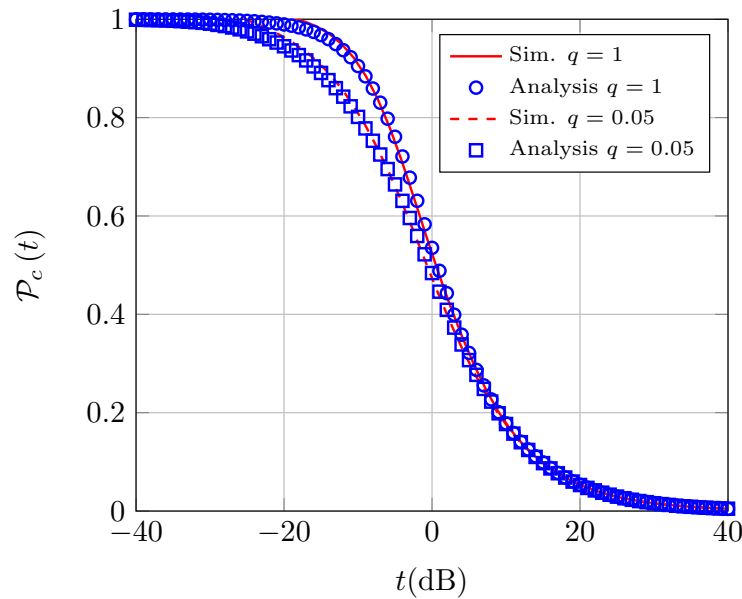


Figure A.10: Probabilidad de cobertura en función de la SINR umbral, t , para $q = 1$ y $q = 0.05$.

A.6 Acceso Múltiple No Ortogonal para CRANs

En esta sección, se propone un nuevo esquema de acceso múltiple no ortogonal (NOMA, Non-Orthogonal Multiple Access) para redes de acceso de radio en la nube (CRAN, Cloud Radio Access Networks). En este esquema, dos usuarios están planificados en los mismos recursos según NOMA. Sin embargo, se realiza conformación coordinada de haces para mejorar las prestaciones de los peores usuarios en términos calidad del enlace (usuarios de borde). De cara al modelado matemático, se asume que las posiciones de las BSs siguen un proceso de punto de tipo cluster. En un esfuerzo por caracterizar el rendimiento del esquema, se derivan expresiones simples en términos de probabilidad de interrupción (*outage*) tanto para los usuarios cercanos como para los usuarios de borde de celda. Se demuestra analíticamente que la ganancia media de conformado del haz es una función de lineal con respecto al número de BSs cooperantes. Los resultados numéricos verifican la exactitud del análisis y revelan que el marco propuesto es capaz de mejorar en gran medida el rendimiento de los usuarios de borde.

A.6.1 Modelo de Sistema

Nos centramos en el DL de una red CRAN donde las BSs se organizan en distintos grupos (*clusters*) que pueden compartir información. Las posiciones de las BSs se modelan acorde a un proceso tipo cluster [61]. El proceso punto padre, que modela los centros de los clusters, se representa como $\Phi_C \subset \mathbb{R}^2$ y sigue un proceso Matérn (HCPP, Hard Core Point Process) de tipo II cuya densidad es λ_C y su mínima distancia entre puntos es d_{\min} [61]. Para un cluster centrado en $x \in \Phi_C$, el proceso punto hijo se representa como $\Phi_{\text{BS}}^{(x)} = \Phi_{\text{BS}}^{(o)} + x$, donde $o = (0, 0)$ representa el origen y $\Phi_{\text{BS}}^{(o)}$ sigue un proceso punto binomial (BPP, Binomial Point Process) de n_{BS} puntos dentro de un anillo cuyo radio interior es r_e y el exterior es r_c . El radio exterior representa el tamaño del cluster mientras que el radio interior representa una región de guarda donde no se posicionan BSs para reducir la interferencia. Esto se hace porque la interferencia crece al acercarse al centro del cluster. Se considera que el peor MT en términos de calidad del enlace está situado en el centro del cluster, mientras que cada BS da servicio a un MT cercano en el recurso de interés. Se considera en este trabajo que las celdas son discos de radio r_{BS} . El desvanecimiento entre las posiciones x e y se expresa como $H_{x,y} \sim \mathcal{CN}(0, 1)$, y sigue una distribución compleja normal. Se asume desvanecimiento independiente para distintas localizaciones. Se considera un modelo de pérdidas de propagación acotado, por tanto, las pérdidas de propagación entre las posiciones x e y se expresan como $(1 + R_{x,y}^\alpha)$. La ganancia instantánea de un enlace entre x e y se representa como $G_{x,y} = H_{x,y} / \sqrt{1 + R_{x,y}^\alpha}$.

Las BSs del mismo cluster transmiten de forma simultánea al mismo MT de borde para mejorar sus prestaciones. Para mejorar la eficiencia espectral, las BSs planifican en el mismo recurso (RB, Resource Block) las señales deseadas tanto para su MT cercano como para el MT de borde. Por tanto, los MTs cercanos realizan cancelación sucesiva de interferencias (SIC, Successive Interference Cancellation) para eliminar la interferencia de los datos dirigidos al MT de borde. El MT de borde no realiza SIC porque, se asigna más potencia a su transmisión gracias a los coeficientes de asignación de potencia.

De manera más formal, la señal transmitida por la BS i -ésima que pertenece al q -ésimo cluster se expresa como sigue

$$X_{\text{BS}_{i,q}} = \sqrt{p_{\text{BS}} a_n} \cdot S_{\text{MT}_{i,q}^{(n)}} + \sqrt{p_{\text{BS}} a_e} \cdot W_{\text{BS}_{i,q}, \text{MT}_q^{(e)}} \cdot S_{\text{MT}_q^{(e)}}, \quad (\text{A.31})$$

donde $S_{\text{MT}_q^{(e)}} \in \mathbb{C}$ y $S_{\text{MT}_{i,q}^{(n)}} \in \mathbb{C}$ son los símbolos dirigidos a los MTs cercano y de borde respectivamente, p_{BS} es la potencia nominal por BS, $a_n \in \mathbb{R}$ y $a_e \in \mathbb{R}$ con $a_n + a_e = 1$ y $a_e \geq a_n$ son los coeficientes de asignación de potencia para los MTs cercanos y de borde respectivamente. El q -ésimo cluster está centrado en la posición C_q .

La SINR para los MTs de borde se expresa como sigue

$$\text{SINR}_{\text{MT}_0^{(e)}} = \frac{\Xi_{\text{MT}_0^{(e)}} a_e \rho_{\text{BS}}}{\Xi_{\text{MT}_0^{(e)}} a_n \rho_{\text{BS}} + I_{\text{inter}} \rho_{\text{BS}} + 1}, \quad (\text{A.32})$$

donde $\Xi_{\text{MT}_0^{(e)}}$ es la ganancia de conformación de haz coordinada, $\rho_{\text{BS}} = p_{\text{BS}}/\sigma_n^2$ es la SNR de transmisión y I_{inter} es la interferencia.

El mensaje dirigido para el MT de borde se transmite con una SE de SE_e bps/Hz. Por tanto se asume que el MT no es capaz de decodificar el mensaje con éxito si su SINR es menor que $2^{\text{SE}_e} - 1$, lo cual significa que el MT está en *outage*.

Para los MTs cercanos, primero intentan decodificar el mensaje dirigido al MT de borde. Después, si este mensaje se decodifica correctamente, cancelan la interferencia intra-celda e intentan decodificar su propio mensaje.

La SINR para decodificar el símbolo dirigido al MT de borde aparece a continuación

$$\text{SINR}_{\text{MT}_{0,0}^{(n)}}^{(e)} = \frac{\left| G_{\text{BS}_{0,0}, \text{MT}_{0,0}^{(n)}} \right|^2 \left| W_{\text{BS}_{0,0}, \text{MT}_0^{(e)}} \right|^2 a_e \rho_{\text{BS}}}{\left| G_{\text{BS}_{0,0}, \text{MT}_{0,0}^{(n)}} \right|^2 a_n \rho_{\text{BS}} + I_{\text{intra}} \rho_{\text{BS}} + I_{\text{inter}} \rho_{\text{BS}} + 1}, \quad (\text{A.33})$$

donde I_{inter} representa la interferencia entre clusters, y I_{intra} , representa la interferencia intra-cluster.

Una vez que la interferencia intra-celda, que viene de la transmisión al MT de borde, ha sido cancelada, los MTs cercanos decodifican su propio mensaje. La SINR en este caso se representa como sigue:

$$\text{SINR}_{\text{MT}_{0,0}^{(n)}}^{(n)} = \frac{\left| G_{\text{BS}_{k,0}, \text{MT}_{0,0}^{(n)}} \right|^2 a_n \rho_{\text{BS}}}{I_{\text{intra}} \rho_{\text{BS}} + I_{\text{inter}} \rho_{\text{BS}} + 1}. \quad (\text{A.34})$$

A.6.2 Resultados Teóricos

La media y varianza de la ganancia de conformación de haz coordinada se expresa como sigue:

$$\begin{aligned}\mathbb{E}[\Xi_x] &= -n_{\text{BS}}\mu_{\Xi}^{(1)}(0) \\ \text{var}(\Xi_x) &= n_{\text{BS}} \left(\mu_{\Xi}^{(2)}(0) - \left(\mu_{\Xi}^{(1)}(0) \right)^2 \right),\end{aligned}\quad (\text{A.35})$$

donde $\mu_{\Xi}^{(1)}(0)$ y $\mu_{\Xi}^{(2)}(0)$ están definidas en el capítulo 6.

Conclusión teórica: La ganancia media de la conformación de haz es una función lineal creciente con respecto al número de BSs por cluster.

La probabilidad de *outage* para los MTs de borde viene dada por la siguiente expresión

$$\begin{aligned}P_{\text{out}}^{\text{MT}_0^{(e)}} &\approx 1 - \sum_{q=1}^{n_{\text{M}}} \sum_{i=1}^{n_{\text{GC}}} \sum_{k=1}^{t_i} \sum_{n=0}^{k-1} \omega_{q,i,k} \frac{(1+r_i^\alpha)^n}{n!} \\ &\times \nu_1^n (-1)^n \frac{d^n}{ds^n} \left[e^{-s\rho_{\text{BS}}^{-1}} \mathcal{L}_{I_{\text{inter}}}(s) \right] \Big|_{s=\nu_1(1+r_i^\alpha)},\end{aligned}\quad (\text{A.36})$$

donde $w_{q,i,k}$ y $\mathcal{L}_{I_{\text{inter}}}(s)$ aparecen en el capítulo 6, $\nu_1 = \frac{\gamma_e}{a_e - \gamma_e a_n}$ y $\gamma_e = 2^{\text{SE}_e} - 1$ es el umbral de SINR para tener una SE de SE_e bps/Hz. Si $a_e - \gamma_e a_n < 0$, entonces la probabilidad de *outage* es 1.

Por otro lado, la probabilidad de *outage* para los MTs cercanos se expresa como

$$\begin{aligned}P_{\text{out}}^{\text{MT}_o^{(n)}} &\approx F_{|W|^2} \left(\frac{\gamma_1 a_n}{a_e} \right) + \frac{\pi (r_c - r_e)}{2n_{\text{GC}}} \sum_{i=1}^{n_{\text{GC}}} \frac{2r_i}{r_c^2 - r_e^2} \\ &\times \mathcal{L}_{\Xi} \left(\frac{\gamma_1 a_n}{a_e} (1+r_i^\alpha) \right) \left| \sin \left(\frac{2i-1}{n_{\text{GC}}} \pi \right) \right| \\ &\times F_Q \left(\max \left(\frac{\gamma_e}{\left(\frac{a_e}{1+r_i^\alpha} - \gamma_e a_n \right) \rho_{\text{BS}}}, \frac{\gamma_n}{a_e \rho_{\text{BS}}} \right) \Big| r_i \right),\end{aligned}\quad (\text{A.37})$$

$F_Q(q)$, $F_{|W|^2}(x)$ y $\mathcal{L}_{\Xi}(s)$ vienen dados en el capítulo 6.

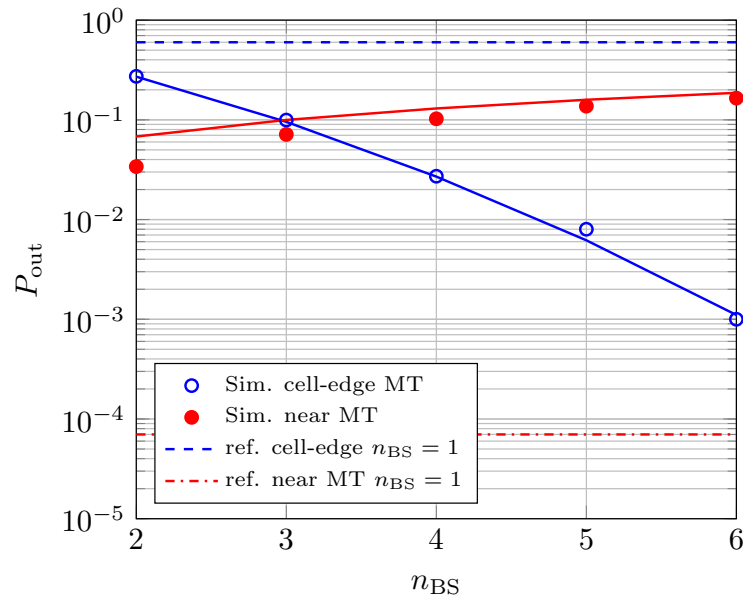


Figure A.11: Comparación de la probabilidad de *outage* para los MTs cercano y lejano en función del número de BSs por cluster, n_{BS} . El caso $n_{BS} = 1$ se añade como referencia.

Como puede apreciarse tanto la probabilidad de outage para el MT cercano como para el de borde son funciones sencillas.

A.6.3 Resultados Numéricos

La siguiente figura ilustra la probabilidad de outage para los MTs cercanos y de borde en función del número de BSs cooperantes por cluster. Se observa que conforme aumenta el número de BSs cooperantes las prestaciones de los MTs de borde aumentan significativamente. El precio a pagar es una pequeña reducción de las prestaciones de los MTs cercanos.

A.7 Mecanismo de Acceso al Medio Distribuido Basado en la Posición para Redes Vehiculares

En este trabajo se modela, analiza y optimiza un mecanismo de acceso al medio distribuido para redes vehiculares. El modelo considera la distancia de seguridad dependiente de

la velocidad que existe entre vehículos del mismo carril. Esto impone una correlación espacial entre los vehículos que complica el análisis. Para tener en cuenta esta correlación se ha propuesto nuevamente un marco matemático basado en el *conditional thinning*. Se han analizado dos mecanismos de planificación de frecuencias espacialmente a lo largo de la carretera que se diferencian en el hecho de si el sistema tiene que distinguir entre el carril en el que circulan los vehículos o no. Además, se considera la transmisión de tipos de mensajes de difusión, periódicos y no periódicos. Entre las métricas analizadas se encuentra la probabilidad transmitir un mensaje correctamente (probabilidad de captura), el BR medio y la eficiencia energética (EE, Energy Efficiency) media. Entre los resultados teóricos más relevantes destaca el hecho de demostrar que existe una región en la que el sistema está limitado por ruido (en lugar de por interferencia) y la optimización del sistema. Dicha optimización consiste en obtener la potencia de transmisión que maximiza la EE sujeta a una probabilidad de captura mínima.

A.7.1 Modelo de Sistema

Se considera una carretera recta de n_L carriles en la que la longitud de la misma es mucho mayor que su anchura, lo cual permite desprestigiar la coordenada z , tal y como se ilustra en la Fig. A.12. Se asume que existe una distancia mínima entre vehículos del mismo carril, que viene dado por la distancia de seguridad, d_{safe} . Por tanto las posiciones de los vehículos se pueden modelar como un proceso punto del tipo HCPP (Hard Core Point Process). de tipo II, $\Phi_L = \{V_0, V_1, \dots\}$, cuya densidad es λ_L . Se asumen que en cada instante de tiempo un vehículo tiene datos para transmitir con probabilidad p_a . Por tanto el proceso punto de vehículos activos, $\Phi^{(a)}$, se determina a partir de un *independent thinning* sobre Φ_L .

El mecanismo propuesto de acceso al medio, denominado GLOC (Geo-LOCation based access), considera que la carretera se divide en segmentos de longitud d_A , donde cada segmento está asociado con un recurso ortogonal (AR, Access Resource). El ancho de banda del sistema, b_w , se divide a partes iguales entre en número total de ARs. En un instante de tiempo, cada vehículo con datos para transmitir determina el segmento en el que se encuentra a partir de su posición GPS (Global Positioning System), y después, transite usando el AR asociado a dicho segmento. El mapeo entre ARs y segmentos se hace siguiendo un criterio de maximizar la distancia co-canal. Se proponen dos particiones de

la carretera en segmentos, denominadas SLP (Single-Lane Partition) y MLP (Multi-Lane Partition), que se diferencia en los requisitos de precisión impuestos a la estimación de la posición. Ambos esquemas están ilustrados en las figuras A.12 y A.13 respectivamente.

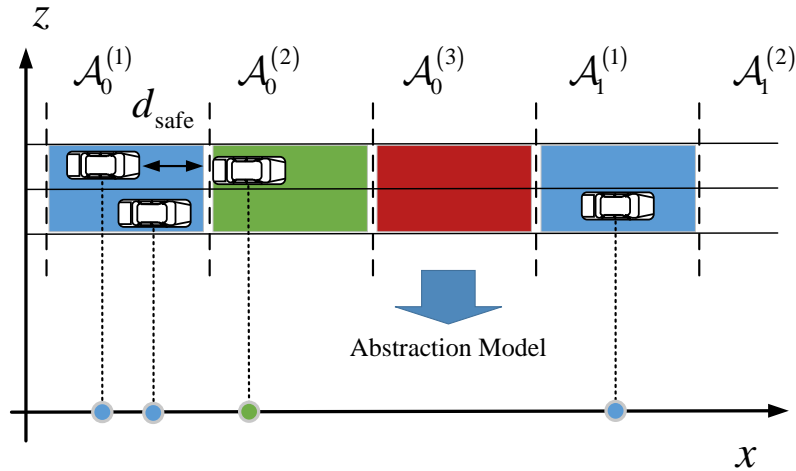


Figure A.12: Diagrama de GLOC con SLP para una carretera de dos carriles y 3 ARs. Los distintos colores están asociados a distintos ARs. En la parte inferior de la figura se muestra el modelo de abstracción usado para el análisis donde las posiciones de los vehículos son puntos en la recta real.

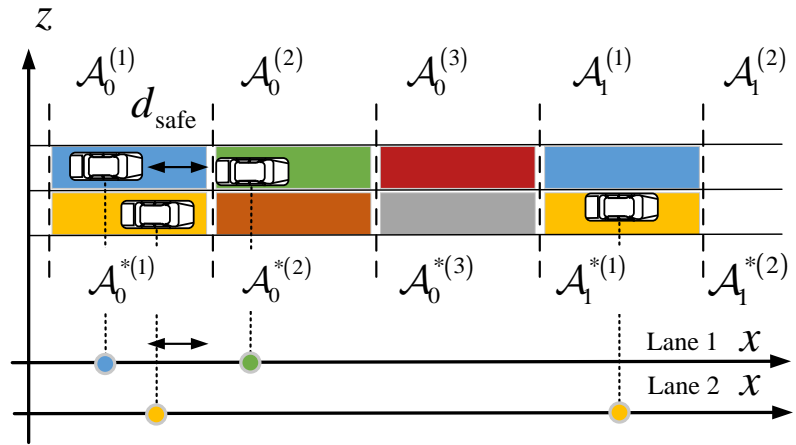


Figure A.13: Diagrama de GLOC con SLP para una carretera de dos carriles y 6 ARs. Los distintos colores están asociados a distintos ARs. En la parte inferior de la figura se muestra el modelo de abstracción usado para el análisis donde las posiciones de los vehículos son puntos en la recta real.

La ventaja de MLP sobre SLP radica en que gracias a que existe una distancia mínima

entre vehículos del mismo carril, y los distintos carriles usan recursos ortogonales, existe una distancia mínima al interferente más cercano, lo cual aumenta la SINR. Si la distancia mínima, d_{safe} , es mayor que la longitud del segmento, $d_{\mathcal{A}}$, entonces no existe interferencia dentro del segmento de prueba. En cambio con SLP no hay una distancia mínima hacia el interferente más cercano ya que los distintos carriles tienen los mismos ARs.

Por otro lado, la ventaja de SLP sobre MLP es que para el mismo ancho de banda de sistema, b_w , cada AR tiene un ancho de banda mayor. Una discusión más profunda de estos y otros aspectos aparece en el capítulo 7.

La SINR evaluada en la posición x sigue esta expresión

$$\text{SINR}(x) = \frac{H_{\text{VT}_0} (\tau |\text{VT}_0 - x|)^{-\alpha} \rho_{\text{VT}}}{I(x) + \sigma_n^2} \quad (\text{A.38})$$

donde H_{VT_0} es el desvanecimiento multi-camino con el vehículo receptor, que está situado en x , ρ_{VT} es la potencia de transmisión por Hz, $I(x)$ la potencia interferente y σ_n^2 la potencia de ruido. La interferencia se puede expresar como sigue:

$$I(x) = \sum_{\text{VT}_i \in \Phi^{(a)} \setminus \{\text{VT}_0\}} H_{\text{VT}_i} (\tau |\text{VT}_i - x|)^{-\alpha} \rho_{\text{VT}} \mathbf{1}(\text{VT}_i \in \mathcal{A}^{(\text{AR}_0)}) \mathbf{1}(\text{VT}_i \in \mathbf{b}_x(d_{\text{max}})) \quad (\text{A.39})$$

donde $\Phi^{(a)}$, que es el proceso punto de los vehículos interferentes, sigue un PPP en el caso SLP y un HCPP en el caso MLP. Como el caso HCPP es intratable matemáticamente, se propone la siguiente suposición para hacer tratable el análisis:

Suposición: La interferencia en el caso MLP se puede modelar como sigue:

$$I(x) = \sum_{\text{VT}_i \in \Phi^{(a)}} H_{\text{VT}_i} (\tau |\text{VT}_i - x|)^{-\alpha} \rho_{\text{VT}} \mathbf{1}(\text{VT}_i \in \mathcal{A}^{(\text{RB}_0)}) \\ \times \mathbf{1}(|\text{VT}_i - x| > d_{\text{safe}}) \mathbf{1}(|\text{VT}_i - \text{VT}_0| > d_{\text{safe}}) \quad (\text{A.40})$$

donde $\Phi^{(a)}$ es un PPP con densidad λ_{LP_a} . La idea que hay detrás de esta asunción es que para modelar correctamente la interferencia, basta con imponer la condición de que no puede haber dos vehículos a menor distancia que d_{safe} , en las cercanías del transmisor y del receptor de prueba. Esta suposición resultará ser bastante precisa, tal y como se verá

con los resultados numéricos.

Además de la probabilidad de captura, en este trabajo son importantes el BR y la EE medios. No obstante, en este caso se considera por motivos de implementación que los vehículos transmiten con un MCS fijo. Por tanto el BR de los bits correctamente recibidos se expresa como sigue:

$$\text{BR}(x) = \mathbf{1}(\text{SINR}(x) > \gamma) \cdot b_{\text{AR}} \cdot \log_2(1 + \gamma) \quad (\text{A.41})$$

donde b_{AR} es el ancho de banda de cada AR. En el caso SLP, $b_{\text{AR}} = b_w/n_{\text{AR}}$, mientras que en el caso MLP, $b_{\text{AR}} = b_w/(n_{\text{AR}}n_L)$, siendo n_L el número de carriles. Para SLP, n_{AR} representa el número total de ARs, mientras que para MLP, n_{AR} representa el número de ARs por carril. Con el símbolo γ se representa el umbral asociado a la correcta decodificación de un mensaje transmitido con un MCS cuya SE es $\log_2(1 + \gamma)$. La EE se define como el cociente entre el BR y la potencia transmitida, y viene expresada en b/J. Su significado es cuánto cuesta en términos energéticos transmitir un bit que se reciba correctamente. Su expresión aparece a continuación:

$$\text{EE}(x) = \frac{\log_2(1 + \gamma)}{\rho_{\text{VT}}} \mathbf{1}(\text{SINR}(x) > \gamma) \quad (\text{A.42})$$

Se han considerado dos tipos de mensajes, periódicos y no periódicos. Los mensajes no periódicos se transmiten a causa de eventos que ocurren con cierta probabilidad. Esta probabilidad es un parámetro de la simulación que aquí se ha definido con el símbolo p_a . El caso periódico considera unos mensajes, de tamaño m_{bc} bits, que se transmiten cada t_{rep} segundos. Por tanto, aquí p_a no es un parámetro de simulación, sino una función que depende de los citados parámetros como sigue:

$$p_a = \frac{m_{\text{bc}}}{b_{\text{AR}} t_{\text{rep}} \log_2(1 + \gamma)} \quad (\text{A.43})$$

A.7.2 Resultados Teóricos

Los principales resultados teóricos aparecen recogidos en la siguiente tabla.

El significado de $c_1^{(\text{SLP})}$ y $c_1^{(\text{MLP})}$ es la probabilidad de captura que se tiene cuando la potencia de transmisión tiende a infinito para SLP y MLP, respectivamente.

Por otro lado, el problema de optimización resuelto se plantea como sigue:

Table A.1: Resumen de los principales resultados matemáticos en función de ρ_{VT}

Metric	$\bar{F}_{\text{SINR}}(\gamma)$	$\mathbb{E} [\text{BR}]$	$\mathbb{E} [\text{EE}]$
SLP	$c_1^{(\text{SLP})} e^{-\frac{c_2}{\rho_{VT}}}$	$\frac{b_w}{n_{\text{RB}}} \cdot \log_2(1 + \gamma) \cdot c_1^{(\text{SLP})} e^{-\frac{c_2}{\rho_{VT}}}$	$\frac{\log_2(1+\gamma)}{\rho_{VT}} \cdot c_1^{(\text{SLP})} e^{-\frac{c_2}{\rho_{VT}}}$
MLP	$c_1^{(\text{MLP})} e^{-\frac{c_2}{\rho_{VT}}}$	$\frac{b_w}{n_{\text{RB}} \cdot n_L} \cdot \log_2(1 + \gamma) \cdot c_1^{(\text{MLP})} e^{-\frac{c_2}{\rho_{VT}}}$	$\frac{\log_2(1+\gamma)}{\rho_{VT}} \cdot c_1^{(\text{MLP})} e^{-\frac{c_2}{\rho_{VT}}}$
	$c_2 = \gamma \sigma_n^2 (\tau r_{\text{bc}})^\alpha$	$c_1^{(\text{SLP})} = \frac{1}{d_A} \int_{v=-\frac{d_A}{2}}^{\frac{d_A}{2}} \mathcal{L}_{I(v+r_{\text{bc}})} \left(\frac{\gamma (\tau r_{\text{bc}})^\alpha}{\rho_{VT}} \right) dv$	
	$c_1^{(\text{MLP})} = \int_{v=-\frac{d_A}{2}}^{\frac{d_A}{2}} \frac{\mathbf{1}(v \notin \mathcal{B}_{v+r_{\text{bc}}}(d_{\text{safe}}))}{ \mathcal{D}(v+r_{\text{bc}}) } \mathcal{L}_{I(v+r_{\text{bc}})} \left(\frac{\gamma}{\rho_{VT}} (\tau r_{\text{bc}})^\alpha \right) \cdot dv$		

$$\begin{aligned}
& \underset{\rho_{VT}}{\text{maximize}} \mathbb{E} [\text{EE}] \\
& \text{subject to } \bar{F}_{\text{SINR}}(\gamma) \geq c_1^{(k)} \delta \\
& 0 < \delta < 1
\end{aligned} \tag{A.44}$$

donde $0 < \delta < 1$ sirve para expresar la probabilidad de captura, $\bar{F}_{\text{SINR}}(\gamma)$, como un porcentaje de la probabilidad de captura máxima $c_1^{(k)}$, siendo k una etiqueta para identificar a SLP o a MLP, $k = \{\text{SLP}, \text{MLP}\}$. La solución al problema es la potencia de transmisión óptima

$$\rho_{VT}^* = \begin{cases} c_2 & \text{if } 0 < \delta \leq e^{-1} \\ c_2 \ln^{-1}(1/\delta) & \text{if } 1 > \delta > e^{-1} \end{cases} \tag{A.45}$$

dicha potencia óptima de transmisión conduce a la máxima EE

$$\mathbb{E} [\text{EE}]^* = \begin{cases} \frac{c_1^{(k)}}{c_2} \log_2(1 + \gamma) e^{-1} & \text{if } 0 < \delta \leq e^{-1} \\ \frac{c_1^{(k)}}{c_2} \ln\left(\frac{1}{\delta}\right) \log_2(1 + \gamma) \delta & \text{if } 1 > \delta > e^{-1} \end{cases} \tag{A.46}$$

siendo la probabilidad de captura obtenida la que aparece a continuación

$$\bar{F}_{\text{SINR}}^*(\gamma) = \begin{cases} c_1^{(k)} e^{-1} & \text{if } 0 < \delta \leq e^{-1} \\ c_1^{(k)} \delta & \text{if } 1 > \delta > e^{-1} \end{cases} \tag{A.47}$$

donde de nuevo $k = \{\text{SLP}, \text{MLP}\}$.

Conclusiones teóricas: A partir de los resultados obtenidos se derivan las siguientes conclusiones teóricas:

1. En el caso MLP, el sistema para a estar limitado por ruido (no existe interferencia) si $d_{\text{safe}} > d_A$ y $n_{\text{AR}} > (2d_{\text{max}} + d_A)/d_A$; siendo d_{max} el rango máximo de comunicación.
2. La potencia óptima de transmisión es independiente del esquema considerado, SLP o MLP.

A.7.3 Resultados Numéricos

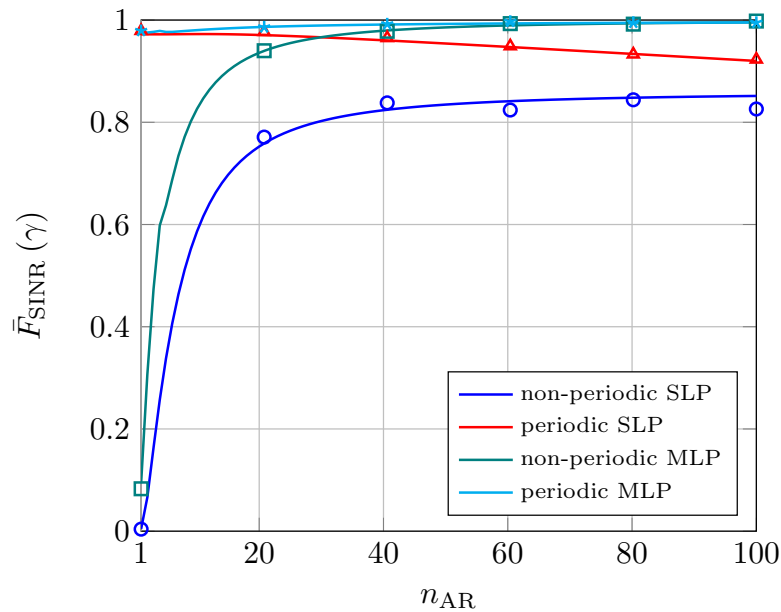


Figure A.14: Probabilidad de captura en función del número de ARs, n_{AR} , para SLP y MLP ($d_{\text{safe}} = 42$ m) con mensajes periódicos y no periódicos.

La Fig. A.14 ilustra la probabilidad de captura en función del número de ARs para SLP y MLP con mensajes periódicos y no periódicos. Se observa que para el caso de mensajes no periódicos, subir n_{AR} mejora mucho la probabilidad de captura. Esto se debe a que aumentar n_{AR} aumenta la distancia co-canal y disminuye por tanto la interferencia, ya que la densidad de vehículos interferentes es constante y depende de p_a . No obstante,

en el caso de mensajes periódicos, aumentar n_{AR} además de aumentar la distancia co-canal, también aumenta la densidad de vehículos interferentes, ya que aumenta p_a (véase la ecuación (A.43)). En el caso de MLP con mensajes periódicos, el efecto de aumentar la distancia co-canal domina al aumento de la densidad de interferentes y por ello, la probabilidad de captura crece con n_{AR} . No ocurre así para el caso SLP, donde domina el efecto del aumento de la densidad ya que existe en este caso interferencia de vehículos del mismo segmento que el transmisor de prueba. No obstante, los resultados de fiabilidad son bastante altos, en concreto con MLP se obtienen unas probabilidades de captura de 99.76% para mensajes periódicos y 99.55% para mensajes no periódicos con una alta densidad de vehículos interferentes ($p_a = 0.25$).

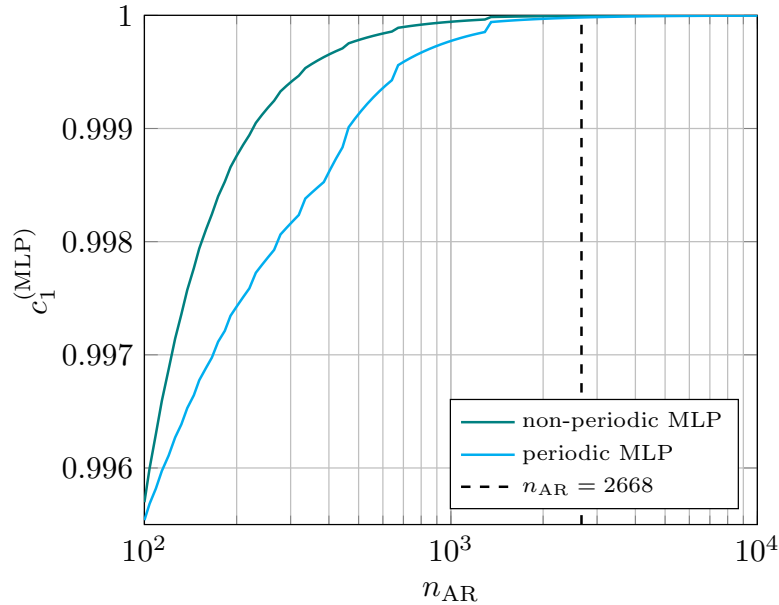


Figure A.15: Máxima probabilidad de captura, $c_1^{(MLP)}$, para n_{AR} de 10^2 a 10^4 , con MLP ($d_{safe} = 42$ m) para mensajes periódicos y no periódicos. $r_{bc} = 150$ m, $d_{max} = 56$ km y $\gamma = 5$ dB.

La Fig. A.15 ilustra la conclusión teórica obtenida acerca de la existencia de una región de funcionamiento limitada por ruido. En dicha figura se ilustra que para un número determinado de ARs, la probabilidad máxima $c_1^{(MLP)}$ alcanza el valor de 1. Por último la Fig. A.16 ilustra la EE en función de la potencia transmitida. Con una línea discontinua negra aparece la potencia óptima para $\delta = 0.3$ mientras que la línea naranja se

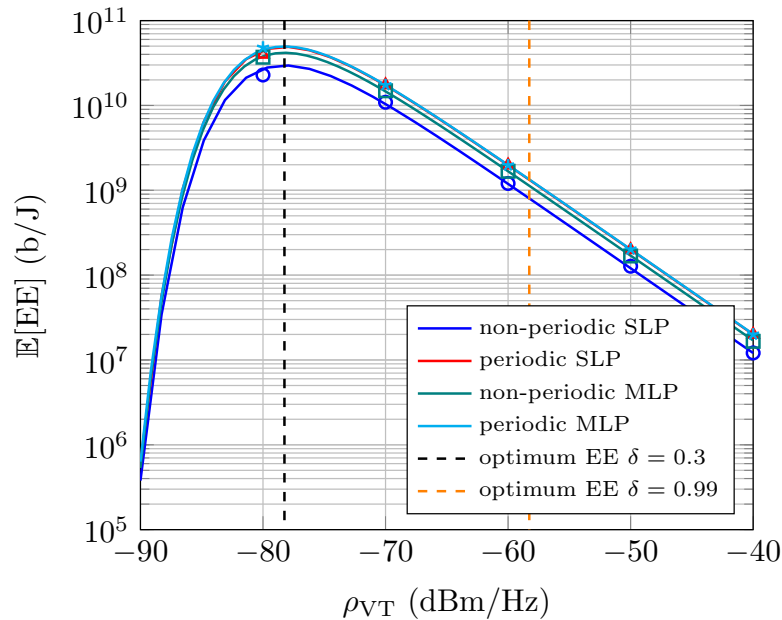


Figure A.16: EE media en función de la potencia de transmisión por Hz, ρ_{VT} , para SLP ($d_{\text{safe}} = 0$ m) y MLP ($d_{\text{safe}} = 42$ m) con mensajes periódicos y no periódicos.

asocia a $\delta = 0.99$. Se observa por tanto que aumentar la probabilidad de captura mínima requiere transmitir con mayor potencia, bajando la eficiencia energética.

A.8 Conclusiones

En esta tesis se ha llevado a cabo el modelado y análisis matemático de distintos mecanismos de mitigación de interferencias para sistemas celulares de nueva generación. El trabajo se ha centrado en primer lugar en el estudio de mecanismos donde, por medio del intercambio de información entre BSs, se consigue un conocimiento sobre la interferencia que permite limitarla, dando lugar a un aumento significativo de las prestaciones. Con respecto a este aspecto, se han propuesto y analizado dos mecanismos que limitan la interferencia generada en el sistema en dos niveles distintos, nivel físico y de acceso al medio, mediante un mecanismo de control de potencia y un algoritmo de planificación de recursos respectivamente. El mecanismo de planificación de recursos consiste en silenciar de forma inteligente aquellos usuarios en los instantes en los que causan mayor interferencia. Este silenciamiento lleva a una disminución necesaria de la justicia entre usuarios a la hora de

acceder a los recursos. Motivado por este aspecto, se ha desarrollado un modelo multi-usuario para evaluar la justicia entre usuarios en términos de probabilidad de cobertura. De esta manera se identifica la interacción que existe entre el control de potencia en el enlace ascendente y la justicia en cuanto a la probabilidad de cobertura. Para considerar condiciones de canal más severas que las que ofrece el canal Rayleigh, se ha llevado a cabo el análisis para un canal tipo Hoyt, que incluye a las distribuciones Rayleigh y Gaussiana unilateral como casos especiales.

Se ha propuesto un esquema basado en el acceso múltiple no ortogonal para redes cooperativas CRAN (Cloud Radio Access Networks). El esquema se ha modelado y analizado demostrando que se consigue mejorar las prestaciones de los usuarios de borde.

Finalmente, se ha analizado un mecanismo de acceso al medio distribuido para redes vehiculares, que está apoyado por la red celular, ya que ofrece la sincronización necesaria en tiempo y frecuencia. Se ha demostrado que dicho mecanismo permite alcanzar fiabilidades arbitrariamente altas con un diseño adecuado del número de recursos ortogonales y de la potencia de transmisión. Además, se ha obtenido la potencia de transmisión óptima que maximiza la eficiencia energética sujeta a una probabilidad de captura mínima.

El análisis de las mencionadas técnicas se ha realizado usando como herramienta matemática la geometría estocástica. No obstante ciertas correlaciones espaciales derivadas de los mecanismos de mitigación de la interferencia que se han estudiado complican el problema entre manos. Para realizar un análisis tratable y preciso se han desarrollado unos marcos matemáticos basados en una técnica conocida como *conditional thinning*. Gracias al análisis realizado ha sido posible ofrecer soluciones sencillas a problemas complejos. Dichas soluciones han derivado en numerosas conclusiones teóricas que conducen a un entendimiento profundo de las técnicas estudiadas.

Bibliography

- [1] Aguayo-Torres, M.C., et al.: WM-SIM LTE link simulator. Technical report, University of Malaga (2014). <http://riuma.uma.es/xmlui/handle/10630/7438>
- [2] Martin-Vega, F.J., Delgado-Luque, I.M., Blaquez-Casado, F., Gomez, G., Aguayo-Torres, M.C., Entrambasaguas, J.T.: LTE Performance over High Speed Railway Channel. In: Vehicular Technology Conference (VTC Fall), IEEE 78th (2013). doi:10.1109/VTCFall.2013.6692274
- [3] Ghosh, A., Mangalvedhe, N., Ratasuk, R., Mondal, B., Cudak, M., Visotsky, E., Thomas, T.A., Andrews, J.G., Xia, P., Jo, H.S., Dhillon, H.S., Novlan, T.D.: Heterogeneous cellular networks: From theory to practice. *Communications Magazine, IEEE* **50**(6), 54–64 (2012). doi:10.1109/MCOM.2012.6211486
- [4] Andrews, J.G., Singh, S., Ye, Q., Lin, X., Dhillon, H.S.: An overview of load balancing in hetnets: old myths and open problems. *IEEE Wireless Communications* **21**(2), 18–25 (2014). doi:10.1109/MWC.2014.6812287
- [5] Damnjanovic, A., Montojo, J., Wei, Y., Ji, T., Luo, T., Vajapeyam, M., Yoo, T., Song, O., Malladi, D.: A survey on 3GPP heterogeneous networks. *IEEE Wireless Communications* **18**(3), 10–21 (2011). doi:10.1109/MWC.2011.5876496
- [6] Singh, S., Andrews, J.G.: Joint Resource Partitioning and Offloading in Heterogeneous Cellular Networks. *Wireless Communications, IEEE Transactions on* **13**(2), 888–901 (2014). doi:10.1109/TWC.2013.120713.130548
- [7] Elshaer, H., Boccardi, F., Dohler, M., Irmer, R.: Downlink and Uplink Decoupling: A disruptive architectural design for 5G networks. In: 2014 IEEE Global Communications Conference, pp. 1798–1803 (2014). doi:10.1109/GLOCOM.2014.7037069

- [8] Liu, D., Wang, L., Chen, Y., El Kashlan, M., Wong, K.K., Schober, R., Hanzo, L.: User Association in 5G Networks: A Survey and an Outlook. *IEEE Communications Surveys Tutorials* **18**(2), 1018–1044 (2016). doi:10.1109/COMST.2016.2516538
- [9] Qi, Y., wang, H.: Interference-aware User Association under Cell Sleeping for Heterogeneous Cloud Cellular Networks. *IEEE Wireless Communications Letters* **PP**(99), 1–1 (2017). doi:10.1109/LWC.2017.2665556
- [10] Yang, C., Li, J., Ni, Q., Anpalagan, A., Guizani, M.: Interference-Aware Energy Efficiency Maximization in 5G Ultra-Dense Networks. *IEEE Transactions on Communications* **65**(2), 728–739 (2017). doi:10.1109/TCOMM.2016.2638906
- [11] Mahmood, N., Pedersen, K., Mogensen, P.: Interference Aware Inter-Cell Rank Coordination for 5G Systems. *IEEE Access* **PP**(99), 1–1 (2017). doi:10.1109/ACCESS.2017.2672799
- [12] Rost, P., et al.: Cloud technologies for flexible 5G radio access networks. *IEEE Commun. Mag.* **52**(5), 68–76 (2014). doi:10.1109/MCOM.2014.6898939
- [13] Wu, J., Zhang, Z., Hong, Y., Wen, Y.: Cloud radio access network (C-RAN): a primer. *IEEE Network* **29**(1), 35–41 (2015). doi:10.1109/MNET.2015.7018201
- [14] Simeone, O., et al.: Cloud radio access network: Virtualizing wireless access for dense heterogeneous systems. *Journal of Commun. and Net.* **18**(2), 135–149 (2016). doi:10.1109/JCN.2016.000023
- [15] Ding, Z., Yang, Z., Fan, P., Poor, H.V.: On the Performance of Non-Orthogonal Multiple Access in 5G Systems with Randomly Deployed Users. *IEEE Signal Processing Letters* **21**(12), 1501–1505 (2014). doi:10.1109/LSP.2014.2343971
- [16] Ding, Z., et al.: Application of Non-Orthogonal Multiple Access in LTE and 5G Networks. *IEEE Comm. Mag.* (2) (2017). doi:10.1109/MCOM.2017.1500657CM
- [17] Mir, A.H., Filali, F.: LTE and IEEE 802.11p for vehicular networking: a performance evaluation. *EURASIP Journal on Wireless Communications and Networking* (2014)

- [18] Lee, J., et al.: LTE-advanced in 3GPP Rel -13/14: an evolution toward 5G. *IEEE Comm. Mag.* **54**(3) (2016). doi:10.1109/MCOM.2016.7432169
- [19] Haenggi, M., Andrews, J.G., Baccelli, F., Dousse, O., Franceschetti, M.: Stochastic geometry and random graphs for the analysis and design of wireless networks. *IEEE Journal on Selected Areas in Communications* **27**(7), 1029–1046 (2009). doi:10.1109/JSAC.2009.090902
- [20] ElSawy, H., Hossain, E., Haenggi, M.: Stochastic Geometry for Modeling, Analysis, and Design of Multi-Tier and Cognitive Cellular Wireless Networks: A Survey. *Communications Surveys Tutorials, IEEE* **15**(3), 996–1019 (2013). doi:10.1109/SURV.2013.052213.00000
- [21] Andrews, J.G., Baccelli, F., Ganti, R.K.: A Tractable Approach to Coverage and Rate in Cellular Networks. *IEEE Transactions on Communications* **59**(11), 3122–3134 (2011). doi:10.1109/TCOMM.2011.100411.100541
- [22] Dhillon, H.S., Ganti, R.K., Baccelli, F., Andrews, J.G.: Modeling and Analysis of K-Tier Downlink Heterogeneous Cellular Networks. *Selected Areas in Communications, IEEE Journal on* **30**(3), 550–560 (2012). doi:10.1109/JSAC.2012.120405
- [23] Guo, A., Haenggi, M.: Spatial Stochastic Models and Metrics for the Structure of Base Stations in Cellular Networks. *Wireless Communications, IEEE Transactions on* **12**(11), 5800–5812 (2013). doi:10.1109/TWC.2013.100113.130220
- [24] Blaszczyszyn, B., Karray, M.K., Keeler, H.P.: Using Poisson processes to model lattice cellular networks. In: *INFOCOM, 2013 Proceedings IEEE*, pp. 773–781 (2013). doi:10.1109/INFCOM.2013.6566864
- [25] Xu, J., Zhang, J., Andrews, J.G.: On the Accuracy of the Wyner Model in Cellular Networks. *IEEE Transactions on Wireless Communications* **10**(9), 3098–3109 (2011). doi:10.1109/TWC.2011.062911.100481
- [26] Singh, S., Zhang, X., Andrews, J.G.: Joint Rate and SINR Coverage Analysis for Decoupled Uplink-Downlink Biased Cell Associations in HetNets. *IEEE Transactions on Wireless Communications* **14**(10), 5360–5373 (2015). doi:10.1109/TWC.2015.2437378

- [27] Singh, S., Baccelli, F., Andrews, J.G.: On Association Cells in Random Heterogeneous Networks. *Wireless Communications Letters, IEEE* **3**(1), 70–73 (2014). doi:10.1109/WCL.2013.111713.130707
- [28] Blaszczyzyn, B., Yogeshwaran, D.: Clustering comparison of point processes, with applications to random geometric models. *Stochastic Geometry, Spatial Statistics and Random Fields* **2120**, 31–71 (2015)
- [29] Novlan, T.D., Dhillon, H.S., Andrews, J.G.: Analytical Modeling of Uplink Cellular Networks. *Wireless Communications, IEEE Transactions on* **12**(6), 2669–2679 (2013). doi:10.1109/TWC.2013.050613.120325
- [30] Smiljkovikj, K., Popovski, P., Gavrilovska, L.: Analysis of the Decoupled Access for Downlink and Uplink in Wireless Heterogeneous Networks. *Wireless Communications Letters, IEEE* **4**(2), 173–176 (2015). doi:10.1109/LWC.2015.2388676
- [31] ElSawy, H., Hossain, E.: On Stochastic Geometry Modeling of Cellular Uplink Transmission With Truncated Channel Inversion Power Control. *Wireless Communications, IEEE Transactions on* **13**(8), 4454–4469 (2014). doi:10.1109/TWC.2014.2316519
- [32] Renzo, M.D., Guan, P.: Stochastic Geometry Modeling and System-Level Analysis of Uplink Heterogeneous Cellular Networks With Multi-Antenna Base Stations. *IEEE Trans. Communications* **64**(6), 2453–2476 (2016). doi:10.1109/TCOMM.2016.2552163
- [33] Ding, Z., et al.: The Use of Spatially Random Base Stations in Cloud Radio Access Networks. *IEEE Sig. Process. Lett.* (11) (2013). doi:10.1109/LSP.2013.2282157
- [34] Yang, Z., et al.: Performance Analysis of Cloud Radio Access Networks With Uniformly Distributed Base Stations. *IEEE Trans. on Vehic. Technology* **65**(1), 472–477 (2016). doi:10.1109/TVT.2015.2394458
- [35] Tian, Y., et al.: On the Performance of Opportunistic NOMA in Downlink CoMP Networks. *IEEE Comm. Lett.* (5) (2016). doi:10.1109/LCOMM.2016.2545672

- [36] Choi, J.: Non-Orthogonal Multiple Access in Downlink Coordinated Two-Point Systems. *IEEE Comm. Lett.* (2) (2014). doi:10.1109/LCOMM.2013.123113.132450
- [37] Nigam, G., Minero, P., Haenggi, M.: Coordinated Multipoint Joint Transmission in Heterogeneous Networks. *IEEE Transactions on Communications* **62**(11), 4134–4146 (2014). doi:10.1109/TCOMM.2014.2363660
- [38] Lee, N., Morales-Jimenez, D., Lozano, A., Heath, R.W.: Spectral Efficiency of Dynamic Coordinated Beamforming: A Stochastic Geometry Approach. *IEEE Transactions on Wireless Communications* **14**(1), 230–241 (2015). doi:10.1109/TWC.2014.2337305
- [39] Paris, J.F.: Nakagami-q (Hoyt) distribution function with applications. *Electronics Letters* **45**(4), 210–211 (2009). doi:10.1049/el:20093427
- [40] Renzo, M.D., Guan, P.: Stochastic Geometry Modeling of Coverage and Rate of Cellular Networks Using the Gil-Pelaez Inversion Theorem. *IEEE Communications Letters* **18**(9), 1575–1578 (2014). doi:10.1109/LCOMM.2014.2341251
- [41] Chun, Y.J., Cotton, S., Dhillon, H., Ghrayeb, A., Hasna, M.: A Stochastic Geometric Analysis of Device-to-Device Communications Operating over Generalized Fading Channels. *IEEE Transactions on Wireless Communications* **PP**(99), 1–1 (2017). doi:10.1109/TWC.2017.2689759
- [42] Blaszczyszyn, B., Mhlehler, P., Toor, Y.: Maximizing throughput of linear vehicular Ad-hoc NETWORKS (VANETs) - a stochastic approach. In: *Wireless Conference, 2009. EW 2009. European* (2009). doi:10.1109/EW.2009.5358011
- [43] Farooq, M., ElSawy, H., Alouini, M.S.: A Stochastic Geometry Model for Multi-hop Highway Vehicular Communication. *IEEE Transactions on Wireless Communications* **PP**(99), 1–1 (2015). doi:10.1109/TWC.2015.2501817
- [44] Jeong, Y., Chong, J.W., Shin, H., Win, M.Z.: Intervehicle Communication: Cox-Fox Modeling. *IEEE Journal on Selected Areas in Communications* **31**(9), 418–433 (2013). doi:10.1109/JSAC.2013.SUP.0513038

- [45] Wu, H., Fujimoto, R.M., Riley, G.F., Hunter, M.: Spatial Propagation of Information in Vehicular Networks. *IEEE Transactions on Vehicular Technology* **58**(1), 420–431 (2009). doi:10.1109/TVT.2008.923689
- [46] Tong, Z., et al.: A Stochastic Geometry Approach to the Modeling of DSRC for Vehicular Safety Communication. *IEEE Trans. on Intelligent Transp. Syst.* **17**(5) (2016). doi:10.1109/TITS.2015.2507939
- [47] Martin-Vega, F.J., Gomez, G., Aguayo-Torres, M.C., Renzo, M.D.: Analytical Modeling of Interference Aware Power Control for the Uplink of Heterogeneous Cellular Networks. *IEEE Transactions on Wireless Communications* **15**(10), 6742–6757 (2016). doi:10.1109/TWC.2016.2588469
- [48] Shin, H., Lee, J.H.: Channel reliability estimation for turbo decoding in rayleigh fading channels with imperfect channel estimates. *IEEE Communications Letters* **6**(11), 503–505 (2002). doi:10.1109/LCOMM.2002.804246
- [49] Zhang, H., Prasad, N., Rangarajan, S., Makhail, S., Said, S., Arnott, R.: Standards-compliant LTE and LTE-A uplink power control. In: *Communications (ICC), 2012 IEEE International Conference On*, pp. 5275–5279 (2012). doi:10.1109/ICC.2012.6364333
- [50] Martin-Vega, F.J., Aguayo-Torres, M.C., Gomez, G., Renzo, M.D.: Interference-Aware Muting for the Uplink of Heterogeneous Cellular Networks: A Stochastic Geometry Approach. Accepted for presentation in *International Conference on Communications (ICC) 2017*.
- [51] Martin-Vega, F.J., Aguayo-Torres, M.C., Gomez, G., Renzo, M.D.: On Muting Mobile Terminals for Uplink Interference Mitigation in HetNets System-Level Analysis via Stochastic Geometry (2017). Submitted to *IEEE Transactions on Communication*.
- [52] Martin-Vega, F.J., Lopez-Martinez, F.J., Gomez, G., Aguayo-Torres, M.C.: Multi-user coverage probability of uplink cellular systems: A stochastic geometry approach. In: *Global Communications Conference (GLOBECOM), 2014 IEEE* (2014). doi:10.1109/GLOCOM.2014.7037431

- [53] F. J. Martin-Vega, F.J.L.-M. G. Gomez, Aguayo, M.C.: A Closed-Form Expression for the Coverage of Cellular Systems under Hoyt (Nakagami-q) Fading (2017). submitted to IEEE Electronics Letters.
- [54] F. J. Martin-Vega, G.G.M.E. Y. Liu, Aguayo, M.C.: Modeling and Analysis of NOMA Enabled CRAN with Cluster Point Process (2017). submitted to IEEE Global Communications Conference (GLOBECOM) 2017.
- [55] Haenggi, M.: Mean Interference in Hard-Core Wireless Networks. *IEEE Commun. Lett.* **15**(8), 792–794 (2011). doi:10.1109/LCOMM.2011.061611.110960
- [56] 3rd Generation Partnership Project (3GPP): Study on LTE-based V2X Services
- [57] 3rd Generation Partnership Project (3GPP): Study on LTE Support for Vehicle to Everything (V2X) Services
- [58] Karedal, J., et al.: Path Loss Modeling for Vehicle-to-Vehicle Communications. *IEEE Trans. on Vehicular Tech.* **60** (2011). doi:10.1109/TVT.2010.2094632
- [59] Viriyasitavat, W., et al.: Vehicular Communications: Survey and Challenges of Channel and Propagation Models. *IEEE Vehicular Tech. Mag.* **10** (2015). doi:10.1109/MVT.2015.2410341
- [60] Fernández, H., et al.: Path Loss Modeling for Vehicular System Performance and Communication Protocols Evaluation. *Mobile Networks and App.* **18** (2013)
- [61] Haenggi, M.: *Stochastic Geometry for Wireless Networks*, (2013). Cambridge University Press
- [62] Martin-Vega, F.J., Aguayo-Torres, M.C., Gomez, G., Renzo, M.D.: On Stochastic Geometry Modeling of Distributed Location Access for Vehicular Ad Hoc Networks. Accepted for presentation in Vehicular Technology Conference (VTC spring) 2017.
- [63] Martin-Vega, F.J., Aguayo-Torres, M.C., Gomez, G., Renzo, M.D.: Geo-Location Based Access for Vehicular Ad Hoc Networks: Analysis and Optimization via Stochastic Geometry (2017). Under review (2nd round of reviews) for possible publication in *IEEE Transactions on Vehicular Technology*.

- [64] Martin-Vega, F.J., Liu, Y., Gomez, G., El Kashlan, M., Aguayo, M.C.: Coordinated Beamforming with Non Orthogonal Multiple Access for 5G Cloud Radio Access Networks. *IEEE Transactions on Wireless Communication* (2017). In elaboration.
- [65] 3GPP: Evolved Universal Terrestrial Radio Access (E-UTRA); Physical Layer Procedures
- [66] Castellanos, C.U., Villa, D.L., Rosa, C., Pedersen, K.I., Calabrese, F.D., Michaelsen, P.-H., Michel, J.: Performance of Uplink Fractional Power Control in UTRAN LTE. In: *Vehicular Technology Conference, 2008. VTC Spring 2008*. IEEE, pp. 2517–2521 (2008). doi:10.1109/VETECS.2008.554
- [67] Mullner, R., Ball, C.F., Ivanov, K., Lienhart, J., Hric, P.: Contrasting Open-Loop and Closed-Loop Power Control Performance in UTRAN LTE Uplink by UE Trace Analysis. In: *Communications, 2009. ICC '09. IEEE International Conference On*, pp. 1–6 (2009). doi:10.1109/ICC.2009.5198853
- [68] Simonsson, A., Furuskar, A.: Uplink Power Control in LTE - Overview and Performance, Subtitle: Principles and Benefits of Utilizing rather than Compensating for SINR Variations. In: *Vehicular Technology Conference, 2008. VTC 2008-Fall*. IEEE 68th, pp. 1–5 (2008). doi:10.1109/VETEFCF.2008.317
- [69] Goldsmith, A.J., Chua, S.-G.: Adaptive coded modulation for fading channels. *Communications, IEEE Transactions on* **46**(5), 595–602 (1998). doi:10.1109/26.668727
- [70] 3GPP: Evolved Universal Terrestrial Radio Access (E-UTRA); Physical channels and modulation. TS 36.211, 3rd Generation Partnership Project (3GPP) (September 2008). <http://www.3gpp.org/ftp/Specs/html-info/36211.htm>
- [71] Chan, P.W.C., Lo, E.S., Wang, R.R., Au, E.K.S., Lau, V.K.N., Cheng, R.S., Mow, W.H., Murch, R.D., Letaief, K.B.: The evolution path of 4G networks: FDD or TDD? *IEEE Communications Magazine* **44**(12), 42–50 (2006). doi:10.1109/MCOM.2006.273098
- [72] 3GPP: Evolved Universal Terrestrial Radio Access Network (E-UTRAN); X2 general aspects and principles. TS 36.420, 3rd Generation Partnership Project (3GPP) (December 2007). <http://www.3gpp.org/ftp/Specs/html-info/36420.htm>

- [73] Rao, A.M.: Reverse Link Power Control for Managing Inter-Cell Interference in Orthogonal Multiple Access Systems. In: Vehicular Technology Conference, 2007. VTC-2007 Fall. 2007 IEEE 66th, pp. 1837–1841 (2007). doi:10.1109/VETEFC.2007.387
- [74] Boussif, M., Quintero, N., Calabrese, F.D., Rosa, C., Wigard, J.: Interference Based Power Control Performance in LTE Uplink. In: Wireless Communication Systems. 2008. ISWCS '08. IEEE International Symposium On, pp. 698–702 (2008). doi:10.1109/ISWCS.2008.4726146
- [75] Guan, P., Renzo, M.D.: Stochastic geometry analysis of uplink cellular networks with multi-antenna base stations and interference-aware fractional power control. In: 2015 International Conference on Communications, Management and Telecommunications (ComManTel), pp. 13–17 (2015). doi:10.1109/ComManTel.2015.7394232
- [76] Hoehler, F.K.: Logistic equations in the analysis of S-shaped curves. *Computers in Biology and Medicine* **25**(3), 367–371 (1995). doi:10.1016/0010-4825(95)00013-T
- [77] Abramowitz, M., Stegun, I.: *Handbook of Mathematical Functions*, (1965). Dover Publications
- [78] Di Renzo, M., Guidotti, A., Corazza, G.E.: Average Rate of Downlink Heterogeneous Cellular Networks over Generalized Fading Channels: A Stochastic Geometry Approach. *Communications, IEEE Transactions on* **61**(7), 3050–3071 (2013). doi:10.1109/TCOMM.2013.050813.120883
- [79] Dhillon, H.S., Andrews, J.G.: Downlink Rate Distribution in Heterogeneous Cellular Networks under Generalized Cell Selection. *Wireless Communications Letters, IEEE* **3**(1), 42–45 (2014). doi:10.1109/WCL.2013.110713.130709
- [80] 3GPP: Evolved Universal Terrestrial Radio Access (E-UTRA); Radio Frequency (RF) System Scenarios
- [81] Rieger, E., Bijl, J.J., Rieger, M.: Two computer programs using logit transformation for the analysis of s-shaped curves. *Computers in Biology and Medicine* **23**(5), 389–397 (1993). doi:10.1016/0010-4825(93)90136-O

- [82] Menard, S.: Logistic Regression: From Introductory to Advanced Concepts and Applications, (2009). Sage Publications
- [83] Lin, Y., et al.: Optimizing User Association and Spectrum Allocation in Het-Nets: A Utility Perspective. *IEEE Jour. on Sel. Areas in Comm.* **33** (2015). doi:10.1109/JSAC.2015.2417011
- [84] Sesia, S., et al.: LTE, The UMTS Long Term Evolution: From Theory to Practice, (2009). Wiley Publishing
- [85] Renzo, M.D., et al.: The Intensity Matching Approach: A Tractable Stochastic Geometry Approximation to System-Level Analysis of Cellular Networks. *IEEE Transactions on Wireless Communications* **15**(9) (2016). doi:10.1109/TWC.2016.2574852
- [86] Ferenc, J.-S., Néda, Z.: On the size distribution of Poisson Voronoi cells. *Physica A: Statistical Mechanics and its Applications* **385**(2), 518–526 (2007)
- [87] 3GPP: Technical Specification Group Radio Access Network; Small cell enhancements for E-UTRA and E-UTRAN - Physical layer aspects. TR 36.872, 3rd Generation Partnership Project (3GPP) (April 2013)
- [88] Singh, S., Andrews, J.G.: Joint Resource Partitioning and Offloading in Heterogeneous Cellular Networks. *Wireless Communications, IEEE Transactions on* **13**(2), 888–901 (2014). doi:10.1109/TWC.2013.120713.130548
- [89] Himayat, N., Talwar, S., Rao, A., Soni, R.: Interference management for 4G cellular standards [WIMAX/LTE UPDATE]. *IEEE Communications Magazine* **48**(8), 86–92 (2010). doi:10.1109/MCOM.2010.5534591
- [90] Novlan, T.D., Andrews, J.G.: Analytical Evaluation of Uplink Fractional Frequency Reuse. *IEEE Transactions on Communications* **61**(5), 2098–2108 (2013). doi:10.1109/TCOMM.2013.031213.120260
- [91] Dhillon, H.S., Ganti, R.K., Andrews, J.G.: Modeling Non-Uniform UE Distributions in Downlink Cellular Networks. *IEEE Wireless Communications Letters* **2**(3), 339–342 (2013). doi:10.1109/WCL.2013.040513.120942

- [92] Dhillon, H.S., Ganti, R.K., Andrews, J.G.: Load Aware Modeling and Analysis of Heterogeneous Cellular Networks. *IEEE Transactions on Wireless Communications* **12**(4), 1666–1677 (2013). doi:10.1109/TWC.2013.13.120485
- [93] Chiu, S.N., Stoyan, D., Kendall, W.S., Mecke, J.: *Stochastic Geometry and Its Applications*, (2013). Wiley Series in Probability and Statistics
- [94] Haenggi, M.: On distances in uniformly random networks. *IEEE Transactions on Information Theory* **51**(10), 3584–3586 (2005). doi:10.1109/TIT.2005.855610
- [95] Romero-Jerez, J.M., Lopez-Martinez, F.J.: A New Framework for the Performance Analysis of Wireless Communications Under Hoyt (Nakagami- q) Fading. *IEEE Transactions on Information Theory* **63**(3), 1693–1702 (2017). doi:10.1109/TIT.2017.2655342
- [96] Liu, Y., et al.: Cooperative Non-orthogonal Multiple Access With Simultaneous Wireless Information and Power Transfer. *IEEE J. on Selected Areas in Comm.* **34**(4), 938–953 (2016). doi:10.1109/JSAC.2016.2549378
- [97] Chen, R., et al.: Broadcasting safety information in vehicular networks: issues and approaches. *IEEE Network* **24** (2010). doi:10.1109/MNET.2010.5395779
- [98] 3rd Generation Partnership Project (3GPP): Evolved Universal Terrestrial Radio Access (E-UTRA) and Evolved Universal Terrestrial Radio Access Network (E-UTRAN); Overall Description; Stage 2 (Release 14)
- [99] 5G Automotive Vision. 5G-PPP. <https://5g-ppp.eu/wp-content/uploads/2014/02/5G-PPP-White-Paper-on-Automotive-Vertical-Sectors.pdf>
- [100] Soret, B., Gatnau Sarret, M., Z. Kovacs, I., Martin-Vega, F., Berardinelli, G., Mahmood, N.H.: Radio resource management for V2V discovery. accepted in *Vehicular Technology Conference spring* (2017)
- [101] Hafeez, K.A., et al.: Performance Analysis and Enhancement of the DSRC for VANET’s Safety Applications. *IEEE Trans. on Vehicular Tech.* **62** (2013). doi:10.1109/TVT.2013.2251374

- [102] Chaabouni, N., Hafid, A., Sahu, P.K.: A collision-based beacon rate adaptation scheme(CBA) for VANETs. In: 2013 IEEE Internat. Conf. on Advanced Networks and Telecomm. Syst. (ANTS) (2013). doi:10.1109/ANTS.2013.6802861
- [103] Borgonovo, F., et al.: ADHOC MAC: New MAC Architecture for Ad Hoc Networks Providing Efficient and Reliable Point-to-Point and Broadcast Services. *Wireless Networks* **10** (2004)
- [104] Omar, H.A., Zhuang, W., Li, L.: VeMAC: A TDMA-Based MAC Protocol for Reliable Broadcast in VANETs. *IEEE Transactions on Mobile Computing* **12**(9), 1724–1736 (2013). doi:10.1109/TMC.2012.142
- [105] Su, H., Zhang, X.: Clustering-Based Multichannel MAC Protocols for QoS Provisionings Over Vehicular Ad Hoc Networks. *IEEE Transactions on Vehicular Technology* **56** (2007). doi:10.1109/TVT.2007.907233
- [106] Bi, Y., et al.: A multi-channel token ring protocol for QoS provisioning in inter-vehicle communications. *IEEE Trans. on Wireless Comm.* **8** (2009). doi:10.1109/TWC.2009.081651
- [107] Bana, S.V., Varaiya, P.: Space division multiple access (SDMA) for robust ad hoc vehicle communication networks. In: *IEEE Intelligent Transportation Systems*. (2001). doi:10.1109/ITSC.2001.948791
- [108] Katragadda, S., et al.: A decentralized location-based channel access protocol for inter-vehicle communication. In: *Vehicular Technology Conference* (2003). doi:10.1109/VETECS.2003.1207140
- [109] Blum, J.J., Eskandarian, A.: A Reliable Link-Layer Protocol for Robust and Scalable Intervehicle Communications. *IEEE Transactions on Intelligent Transportation Systems* **8** (2007). doi:10.1109/TITS.2006.889441
- [110] Ismail, M., et al.: Network cooperation for energy saving in green radio communications. *IEEE Wireless Comm.* **18** (2011). doi:10.1109/MWC.2011.6056695
- [111] Gearhart, C., Breitenbach, A.: Connectivity and Convergence: Transportation for the 21st Century. *IEEE Elect. Mag.* **2** (2014). doi:10.1109/MELE.2014.2314498

- [112] Feng, W., et al.: Green information and communication technology: energy efficiency in a motorway model. *IET Comm.* **4** (2010). doi:10.1049/iet-com.2009.0153
- [113] Yang, C., et al.: Energy-Efficient Hybrid Spectrum Access Scheme in Cognitive Vehicular Ad hoc Networks. *IEEE Comm. Lett.* **17** (2013). doi:10.1109/LCOMM.2012.122012.122341
- [114] Dua, A., et al.: An Energy Efficient Data Dissemination and Information Retrieval Scheme for VANET. In: *IEEE Intern. Conf. on Data Sci. and Data Int. Syst.* (2015). doi:10.1109/DSDIS.2015.99
- [115] Dong, P., et al.: Energy-efficient cluster management in heterogeneous vehicular networks. In: *IEEE Conf. on Computer Comm. Workshops (INFOCOM WKSHPs)* (2016). doi:10.1109/INFCOMW.2016.7562156
- [116] Chen, L.W., et al.: Finding Lane Positions of Vehicles: Infrastructure-Less Cooperative Lane Positioning Based on Vehicular Sensor Networks. *IEEE Vehic. Tech. Mag.* **10** (2015). doi:10.1109/MVT.2015.2479249
- [117] Cheung, W.C., Quek, T.Q.S., Kountouris, M.: Throughput Optimization, Spectrum Allocation, and Access Control in Two-Tier Femtocell Networks. *IEEE Journal on Selected Areas in Communications* **30**(3), 561–574 (2012). doi:10.1109/JSAC.2012.120406
- [118] 5G Automotive Association: The Case for Cellular V2X for Safety and Cooperative Driving. <http://www.5gaa.org/pdfs/5GAA-whitepaper-23-Nov-2016.pdf>
- [119] Martin-Vega, F.J., Blanquez-Casado, F., Lopez-Martinez, F.J., Gomez, G., Entrambasaguas, J.T.: Further Improvements in SOVA for High-Throughput Parallel Turbo Decoding. *Communications Letters, IEEE* **19**(1), 6–9 (2015). doi:10.1109/LCOMM.2014.2371041